THE MECHANISM OF CORROSION-EROSION IN STEAM EXTRACTION LINES OF POWER STATIONS

BY

Luis Efrain Sanchez-Caldera

B. S. Universidad Autonoma Metropolitana, Mexico (1978)

M. Sc. Imperial College of Science and Technology
University of London, England (1981)

Submitted to the Department of Mechanical Engineering in Partial Fulfillment of the Requirements for the Degree of

Doctor of Philosophy

at the

MASSACHUSETTS INSTITUTE OF TECHNOLOGY

June 1984

Signature of Author _____
Department of Mechanical Engineering
April 19, 1984

Certified by _____
Prof. P. Griffith
Thesis Supervisor

Certified by _____
Prof. E. Rabinowicz
Thesis Supervisor

Certified by _____
Prof. W. Unkel
Thesis Supervisor

Accepted by _____
Prof. Warren M. Rohsenow,
Chairman Departamental Committee on Graduate Studies
Department of Mechanical Engineering

THE MECHANISM OF CORROSION-EROSION IN STEAM EXTRACTION LINES OF POWER STATIONS

BY

LUIS EFRAIN SANCHEZ-CALDERA

Submitted to the Department of Mechanical Engineering on April 19, 1984 in partial fulfillment of the requirements for the Degree of Doctor of Philosophy in Mechanical Engineering

ABSTRACT

This study deals with one of the mechanisms of wear by which a low carbon steel pipe loses metal in a steam-water flow, namely, the removal of iron corrosion products by mass transfer phenomena into a liquid water film. To investigate this phenomenon, a high temperature and high pressure water loop was constructed. In this rig a material typical of that used in steam extraction lines was tested under conditions representative of the secondary water of a boiling water reactor. Wear rates were computed from weight change measurements at different temperatures (250-350 F) and velocities (1-10 ft/s). These data agreed with previous published results showing that there exists a temperature for which the wear rate is maximum (approximately 300 F). To predict wear rates, a phenomenological model based on thermodynamics, chemical kinetics and mass transfer aspects of the corrosion of steel under no-flow conditions was developed. The model, which is capable of estimating wear rates as a function of temperature, geometry, pH and velocity, agrees well with the experimental data, both in predicting the rate of wear and in establishing the temperature for maximum material loss.

Thesis Supervisor: Dr. Peter Griffith

Title: Professor of Mechanical Engineering

ACKNOWLEDGEMENTS

Special gratitude is expressed to Professor Peter Griffith for suggesting the subject of this thesis and for his constant advice and encouragement throughout its development.

I also wish to convey my thanks and appreciation to Professor Ernest Rabinowicz for his numerous comments and suggestions, many of which will not be forgotten, and to Professor William Unkel, whose guidance was essential in the development of this work.

I am indebted to the Mechanical Engineering Department technicians, Mr. J. (Tiny) Caloggero and Mr. A. Riggby, for their ideas and comments which were always of great value. I am also grateful to Mr. F. Johnson who not only offered important suggestions, but also bore with me through the task of stopping the leaks of the "mummy" (the experimental rig).

The financial assistance provided by the Mexican people through CONACYT and Banco de Mexico, S.A. (I.I.E.) is greatly acknowledged.

I would also like to express sincere thanks to Marita Erebia for her encouragement during the last months of the program and for assisting me on numerous occasions, often leaving her work aside, in preparing this report.

During the course of the work I was fortunate to

have had the support and help of A. Jackobek, T. Pappas, and Benito Fernandez. Deep appreciation is expressed to Luis Sanchez R., Ramon Balado, and Rafael Camacho who provided the initial encouragement for entering this program. Lastly, special thanks are in order for my officemates, Hung, Jonathan , Byong and Richard, and for others (too many to mention here) whose friendship will always be remembered.

To my Parents, my Brothers

and my Sister

TABLE OF CONTENTS

ABSTRACT

ACKNOWLEDGEMENTS

CHAPTER 1 INTRODUCTION 10

1.1 DESCRIPTION OF THE PROBLEM 10
1.2 PREVIOUS WORK 16
1.2.1 Droplet Impingement 16
1.2.2 Corrosion and Corrosion-Erosion 16
1.3 OBJECTIVES OF THE INVESTIGATION 17
1.4 OUTLINE OF THE REMAINDER OF THE REPORT 18

CHAPTER 2 CORROSION AND CORROSION-EROSION BACKGROUND . . 20

2.1 GENERAL ASPECTS ABOUT CORROSION 21
2.1.1 Definition 21
2.1.2 Electromechanical Reactions 22
2.1.3 Polarization 29
2.1.3.1 Polarization Curves 29
2.1.3.2 Polarization Curves Used In Determining The Corrosion Rate 35
2.1.4 Passivity 37
2.1.5 Influence of Environmental Factors On The Corrosion of Metals 38
2.1.5.1 Effect of Oxidizers 38
2.1.5.2 Effect of Temperature And H^+ Concentration. 42
2.1.5.3 Effect of Velocity 42
2.1.6 Types of Corrosion 42
2.1.7 Corrosion Rate Laws 44
2.2 THE CORROSION OF STEEL IN WATER 47
2.2.1 Early Research 48
2.2.2 Electrochemical Aspects 50
2.2.3 Sweeton and Baes Work 56
2.2.4 Mechanism By Which Iron Diffuses Across Oxide Layers 56
2.3 CORROSION-EROSION OF STEEL 60
2.3.1 Recent Work On Corrosion-Erosion 60
2.3.2 Variables Influencing Corrosion-Erosion Rate 64
2.3.2.1 Oxygen Contents 64
2.3.2.2 Temperature 64
2.3.2.3 Velocity 66
2.3.2.4 Hydrogen Ion Concentration (pH) 67

2.3.2.5 Material Composition 68
2.4 RECAPITULATION 69

CHAPTER 3 DERIVATION OF A MODEL FOR CORROSION-EROSION 71

3.1 INTRODUCTION 71
3.2 INITIAL STEPS IN THE DEVELOPMENT OF THE MODEL 75
3.3 THE SIMPLEST MODEL $C_1 = C_e$ 78
3.4 CONSIDERATION OF MASS DIFFUSION THROUGH THE OXIDE. 79
3.5 PROPOSED MODEL FOR CORROSION-EROSION 82
3.5.1 Description Of The Model 82
3.5.2 Model Equations 84
3.5.3 Characteristics Of The Model 92
3.5.3.1 Diffusion Controlled 92
3.5.3.2 Kinetically Controlled 93

CHAPTER 4 EXPERIMENTAL STUDIES 94

4.1 GENERAL FEATURES REQUIRED FROM THE EXPERIMENT 94
4.1.1 Steam Extraction Line Characterization . . 94
4.1.2 Experimental Work Aimed At Developing The Corrosion-Erosion Model 96
4.2 DESCRIPTION OF THE EXPERIMENTAL APPARUTUS . 96
4.3 THE CORROSION-EROSION EQUIPMENT 101
4.3.1 Specimen Preparation 101
4.3.1.1 The Machining Process 103
4.3.1.2 The Cleaning Process 104
4.3.2 The Test 104
4.4 POST TEST DETERMINATIONS 106
4.4.1 Descaled Weight Change Determination . . . 106
4.4.2 Scanning Electron Microscope Examination . 109
4.4.3 Determination Of The Chemical Compostion Of The Oxide 110

CHAPTER 5 EXPERIMENTAL RESULTS 112

5.1 INITIAL REGION 114
5.2 PRELIMINARY CALCULATIONS 114
5.2.1 Velocity Calculations 115
5.2.2 First Estimate Of The Wear Rate 116
5.3 OXIDATION RATE CALCULATION 117
5.4 S.E.M. OBSERVATIONS 120
5.5 X-RAY PHOTOELECTRON SPECTROMETER 129

CHAPTER 6 DISCUSSION OF RESULTS 135

6.1 ANALYSIS OF EXPERIMENTAL RESULTS 135
6.1.1 Accuracy Of The Results 135
6.1.1.1 Errors In The Determination Of Testing Conditions 136
6.1.1.2 Error In Determining The Wear Rate . . . 138
6.1.1.3 Comparisons Of Experimental Results with Other Wear Rates 143
6.1.2 Velocity Behaviour 145
6.1.3 Comments On The S.E.M. And X-Ray Photo-Electron Spectrometer 146
6.2 THE CORROSION-EROSION MODEL 149
6.2.1 Relations Used to Determine The Value Of The Parameters In Eq. 49 150
6.2.1.1 Method To Calculate Iron Species Diffusion 150
6.2.1.2 Mass Transfer Coefficient 151
6.2.1.3 Determination Of The Equilibrium Concentration C_e 153
6.2.1.4. Values Given to θ and δ 155
6.2.2 Reduction Of Data - Calculation of K . . . 156
6.2.3 Plot Of Ln K Vs 1/T 159
6.2.4 Procedure To Determine Corrosion-Erosion Rates 165
6.2.4.1 Comparison Between Experimental And Theoretical Results 165
6.2.4.2 Description Of The Procedure To Determine Corrosion-Erosion Rates 165
6.2.5 Possible Uses For The Results Presented In This Report 169
6.2.5.1 The Corrosion-Erosion Model 169
6.2.5.2 The Information Gathered - List Of Solutions To Corrosive-Erosive Wear . . 170
6.2.5.3 The Description Of The Experimental Rig 177
6.3 FUTURE WORK 177
6.3.1 Suggestions For Future Work On Subjects Related To Corrosion-Erosion 177
6.3.2 Suggestions For Future Work On Corrosion-Erosion 178
6.3.3 Modification Suggestions To The Experimental Procedure And Apparatus 179
6.3.3.1 Experimental Rig - Modifications 179
6.3.3.2 Experimental Procedure - Modifications . 180

CHAPTER 7 SUMMARY AND CONCLUSIONS 183

REFERENCES 186

APPENDICES

A WEAR RATE BY DROPLET IMPINGEMENT 196

B DERIVATION OF THE CORROSION-EROSION MODEL . 209

C DESCRIPTION OF THE COMPONENTS OF THE SYSTEM 220

D MACHINING PROCESS FOR MAKING SPECIMENS . . . 235

E GUIDELINES FOR THE OPERATION OF THE CORROSION-EROSION RIG 238

F RAW DATA USED IN THE CALCULATION OF THE WEAR RATE 251

G COMPUTER PROGRAMS WEARR4 AND CORERO 256

CHAPTER 1

INTRODUCTION

Corrosion-erosion is now considered responsible for many of the failures in the equipment used for steam generation, such as tubes of condensers, lines for the extraction of steam, and casings of turbines. The wide range for potential failure sites and the increase in expense of unscheduled power plant outages, especially in the nuclear power industry, have led to an increasing interest in the study of corrosion-erosion.

1.1 DESCRIPTION OF THE PROBLEM

Steam extraction lines made of low carbon steel operating under ordinary temperature and pressure conditions, e.g., 90 % quality at 60 psia, have experienced wear of the order of 1 mm/y (in this thesis the word wear is used as a synonym of removal rate of material). In some stations elbows that have an expected lifetime of 30 years have been replaced after 8

years, (Griffith et al., 1981)

Initial work on this project, reported by Vu (1981), showed wall thickness measurements taken at different locations of Boston Edison Pilgrim Unit-1 piping system. The wall thickness obtained from ultrasound technique measurements showed an unexpected wear pattern. As a typical example, the wall thickness measurements of the last elbow of the low pressure steam extraction line (also named line E103-A) is shown here. Figure 1 shows how the elbow was sectioned. Figure 2 shows the actual wear pattern of the elbow. The numbers in Fig. 2 refer to the remaining pipe thickness so that locations of minimum thickness correspond to locations of maximum wear. The figure shows that there are two distinct regions of high wear, one on the outside and one on the inside of the elbow.

To get insight into how that pattern of wear is developed, a two-phase flow (air-water) visual experiment was constructed. The facility made out of 2" diameter pipe with glass elbows represented the piping arrangement around the last bend of the E103-A steam extraction line.

The flow pattern in the elbow showed that the bend acts to separate the phases and further, that the presence of the secondary flow within the bend brings the fluid that inpinges on the outside of the elbow towards the inside of the bend. As a result, a film of

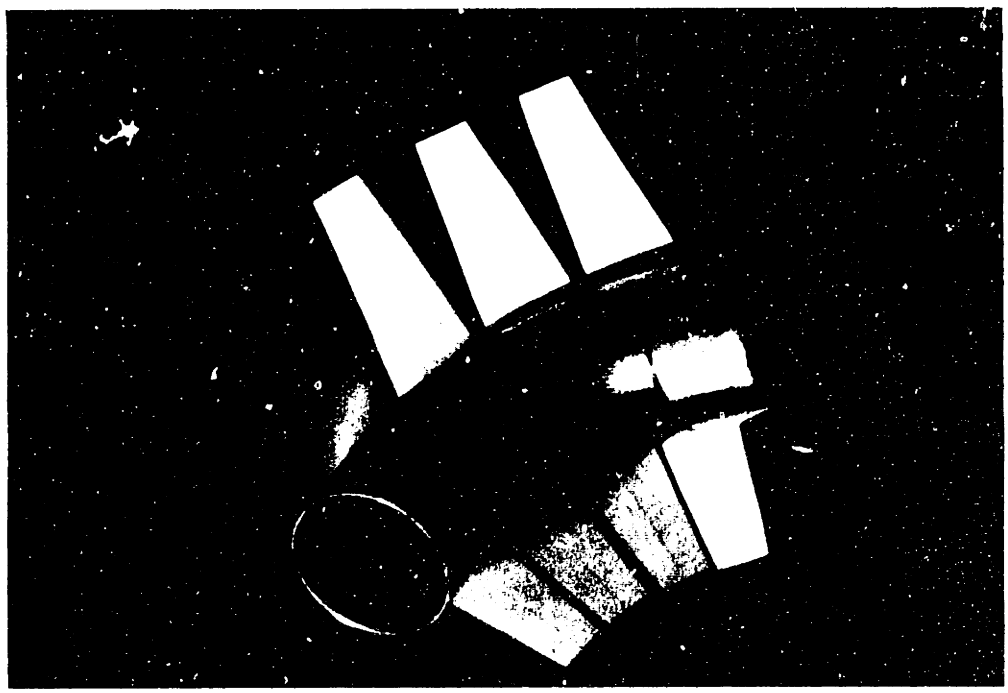

Fig. !. Development of surface of a 90° elbow (Vu, 1982).

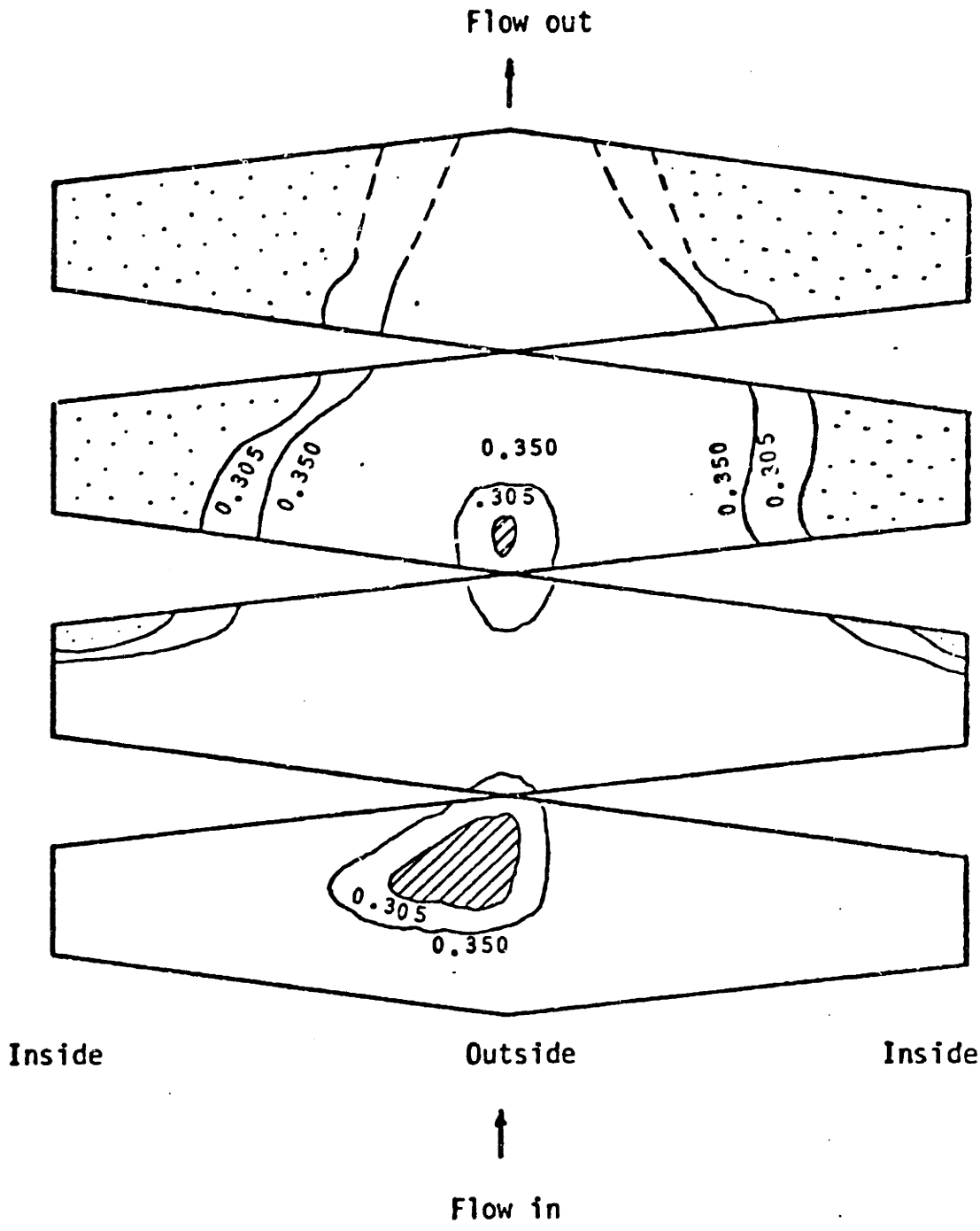

Fig. 2. Wear pattern in last elbow of steam line E-103A after 9 years in service (Vu, 1982)

water forms in the inner radius of curvature of the bend, as shown in Fig. 3.

The above results and the study of the corrosion of steels in water linked the wear pattern of Fig. 2 to two distinct mechanisms of wear, namely, a) fracture of the protective oxide layer because of droplet impingement for the outside of the bend, and b) removal of iron ions by mass transfer into the liquid water film for the inside of the bend. From here on this last mechanism of material removal will be termed oxide dissolution.

In Appendix A our understanding of the phenomena of liquid impingement is presented. The work in this report deals mainly with the wear produced by oxide dissolution. To understand the phenomena involved, it is necessary to define the variables that influence this type of wear. Once this influence is known, means of predicting the wear rate must be developed. Completing this task provides power station personnel and designers of plants with alternative solutions by which failure of pipes can be detected, prevented or eliminated.

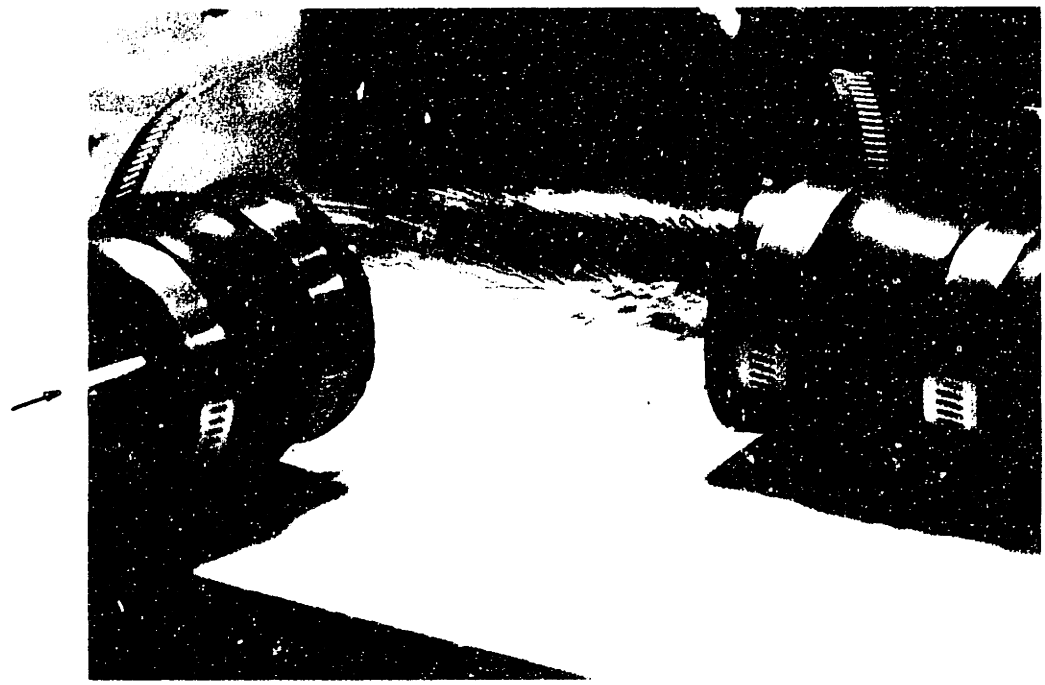

(3a)

(3b)

Fig. 3. Photograph of first elbow (horizontal) showing local turbulence and distribution of drops and water film: (a) inside, (b) outside (Vu, 1982).

1.2 PREVIOUS WORK

1.2.1 Droplet Impingement

In the initial stages of the research, the work was focused on the damage to the material caused by droplet impact. To predict the wear rate in a steam extraction line through this mechanism, it is necessary to integrate elements from two-phase flow, corrosion, and fatigue by droplet impingement. Appendix A summarizes the initial steps that were taken towards obtaining a relation to evaluate wear rates.

It is important to mention here that there exist in the literature empirical relations for estimating rates by droplet impingement for specific materials, (Heymann, 1969,1979; Adler 1980). However, what is needed is a general relation that allows the wear rate to be calculated from target and droplet properties (Springer, 1976). In our research we have sought to obtain this type of expression.

1.2.2 Corrosion And Corrosion-Erosion

The studies related to the oxidation of steel and, specifically, to corrosion-erosion are reviewed in Chapter 2. The reason for assigning more importance to this material and describing it separately is that obtaining a clear understanding of how iron and steel corrode is one of the objectives of this thesis.

Researchers working in the areas of fluid mechanics and two-phase flow know relatively little about corrosion and chemical kinetics. Chapter 2, although not an exhaustive review, highlights the major findings about the oxidation of steel and also identifies the controversies that need to be resolved.

1.3 OBJECTIVES OF THE INVESTIGATION

In this thesis, the initial activities of the M.I.T. corrosion-erosion group in the field of droplet impingement and oxide dissolution are reported.

In order to study oxide dissolution it is necessary to investigate the chemical aspects linked to the phenomenon of corrosion-erosion in single phase (water). This is important, since the regions of high wear are those regions where the liquid film was found, and those regions are only in contact with liquid water. This investigation deals only with single phase corrosion-erosion. Once this is well understood, it will be possible to deal properly with problems of wear in two-phase (steam-water) systems.

To fulfill this objective the specific goals of the research have been:

1. To characterize the wear, under a common range of operating conditions, of a typical material from which steam extraction lines are made, A155 Gr. C, (Griffith et al. 1981) and

2. To propose a method for estimating the wear rate as a function of important variables (velocity,temperature, pH).

To achieve the above goals, a high temperature and high pressure loop was designed and constructed. Its operation has aided the characterization of a specific material for different temperatures (100 to 320 F) and different velocities (up to 30 ft/s). It also provides in-house experience about the corrosion-erosion phenomenon.

1.4 OUTLINE OF THE REMAINDER OF THE REPORT

The rest of the report is divided into the following 6 chapters.

Chapter 2 provides a literature review on the oxidation of steel. In this chapter, the behaviour of the variables that influence the wear rate (temperature, velocity, pH and material composition) is described.

In Chapter 3, the assumptions used in developing a model to predict wear rates are stated; and an equation is then derived. Because the fundamental constants are unknown, their value needs to be determined from the

experimental wear rate data; this is done in Chapter 6.

Chapter 4 describes the experimental work. The most important decisions in the design and operation of the laboratory rig are included in this chapter, whereas more specific details about the apparatus have been left for Appendix C.

Chapter 5 presents the results gathered from the experimental work.

The discussion and analysis of results are found in Chapter 6. This chapter includes the reduction of the data to yield the value of unknown constants of the model derived in Chapter 3, and summarizes the procedure for estimating the wear rate. The chapter also includes a list of solutions for alleviating the corrosion-erosion in plants. It concludes with recommendations for future work on the subject of corrosion-erosion and for modifications on the corrosion-erosion rig.

The final chapter (Chapter 7) reviews the work done. After Chapter 7, the appendices are found. They provide additional information like the study of wear by droplet impingement, listing of the computer programs to evaluate wear rates, and tables with raw data from the experiments.

CHAPTER 2

CORROSION AND CORROSION-EROSION BACKGROUND

There is considerable work in the corrosion-erosion field and in particular for the corrosion of steel. In this chapter the fundamentals of corrosion and corrosion-erosion, will be reviewed. It is of interest here to identify the term corrosion-erosion as one of many forms of corrosion.

The continuous removal of protective oxide layers either by mechanical damage (abrasion, solid particle or droplet impact) or by convective effects of fluid turbulence is termed corrosion-erosion wear (Heitman, 1981). There are two different types of corrosive-erosive wear. The first type, as implied by the above definition, is produced when there is mechanical attack i.e., the cohesive forces of the material are broken and macroscopic portions of the material are removed by force. This type of material removal is discussed in Appendix A for the

case of droplet impingement on an oxide or on a metal. In the second type of corrosion-erosion a dissolution process transforms the iron into soluble iron compounds which are carried away into the flow by convection mass transport phenomena. In the remainder of this report, the term corrosion-erosion will be used as a synonym of this second type of wear, i.e., the removal of the protective oxide layer in the absence of mechanical attack, also called flow- assisted corrosion, (Bignold, 1981).

As mentioned above, this chapter will give a background of corrosion and corrosion-erosion. The first sections will give the general aspects about the theory of corrosion of metals; the second part deals specifically with the corrosion of steel, while the final sections of the chapter present the recent work on corrosion-erosion.

2.1 GENERAL ASPECTS ABOUT CORROSION

The next section is a summary of the general aspects of corrosion. The information here provided is based on the material found in corrosion textbooks (Fontana and Greene, 1978; Evans, 1960; Uhlig, 1963).

2.1.1 Definition

Corrosion denotes the destruction of a metal or an alloy by chemical change, electromechanical change or physical dissolution, i.e., the formation of ions which

incorporate homogeneously into the corrosion environment, that is, without forming a different phase (Evans, 1960). This definition of corrosion is general and accounts for metal transformation into a combined state (oxides, hydroxides, salts) as well as the passage of solid metal into the solution of another metal in liquid or molten state.

2.1.2 Electromechanical Reactions

Corrosion processes are mostly electromechanical because most of the reactions that occur on the metal surface can be divided into two (or more) partial reactions of oxidation and reduction.

In oxidation reactions, also called anodic reactions, there is a production of electrons or an increase in the valence of the element. In a reduction or cathodic reaction, there is a consumption of electrons or a decrease in the valence of the element occurs.

The most general anodic reaction is the dissolution of the metal (M),

$$M \rightarrow M^{z+} + ze^{-} , \qquad (1)$$

into a metal ion and free electrons. Some specific examples are

$$Fe \rightarrow Fe^{+2} + 2e^{-},$$

or

$$Al \rightarrow Al^{+3} + 3e^{-}.$$

There are various cathodic reactions, the most important ones for this work are the evolution of hydrogen, in the reaction

$$2H^{+} + 2e^{-} \rightarrow H_2, \qquad (2)$$

and the reduction of oxygen in neutral or basic solutions, according to the reaction

$$O_2 + 2H_2O + 4e^{-} \rightarrow 4OH^{-}. \qquad (3)$$

The overall corrosion reaction of zinc (Zn) in hydrochloric acid (HCl), can be expressed as

$$Zn + 2HCl \rightarrow ZnCl_2 + H_2. \qquad (4)$$

which can be written as:

$$Zn + 2H^{+} + 2Cl^{-} \quad Zn^{++} + 2Cl^{-} + H2$$

Noting that the valance of chlorine is 1, both in the reactants and in the products, it is clear that chlorine has not taken part in the reaction. Therefore, Eq. 4 is equivalent to a two step reaction

$$Zn \rightarrow Zn^{2+} + 2e^{-}, \quad \text{anodic reaction} \qquad (4a)$$

together with

$$2H^{+} + 2e^{-} \rightarrow H_2, \quad \text{cathodic reaction} \qquad (4b)$$

Accepting the two step anode/cathode reaction process, it is clear that there must be anodic regions (anodes) and cathodic regions (cathodes) for the corrosion process to occur. However, the cathode and anode do not have to be macroscopically separated. Reactions 4a and 4b can occur at the same point on the metal surface, and in fact, this is the cause of the corrosion of metals exposed to water, salt, acid or alkaline solutions.

Corrosion in aqueous media is similar to the electrode phenomenon that takes place in a flash light. As shown in Figure 4, the battery contains a centered carbon electrode, a zinc cup, a resistance and an electrolyte (NH_4Cl solution) and can be used to drive a load such as a light bulb.

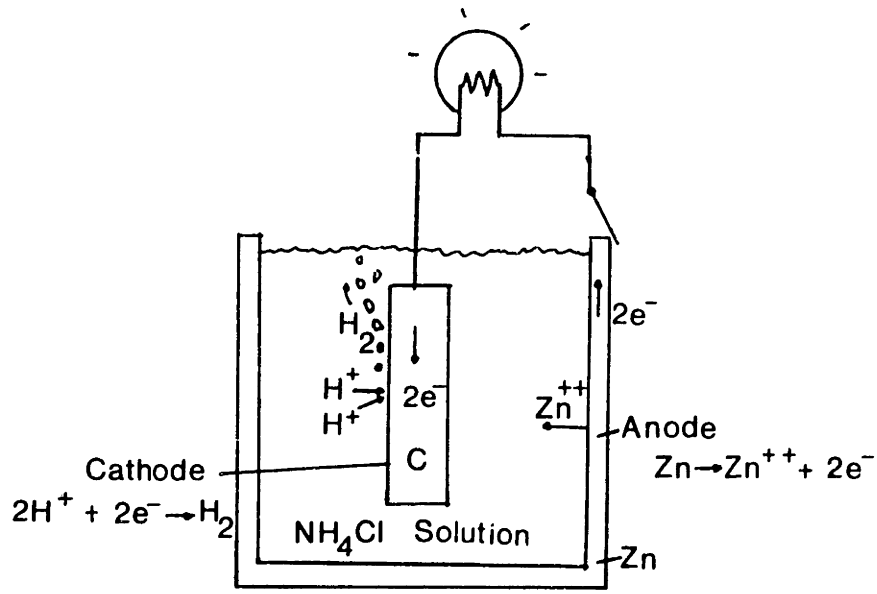

Figure 4. Elements that make up a flashlight.

Upon closing of the external circuit, zinc ions go into the solution in accordance to Eq. 4a; at the same time, electrons from the zinc move through the connecting wires and into the carbon electrode. The arriving electrons are consumed by the reduction reaction of Eq. 4b. The driving potential for the current comes from the different electrode potential of the two materials. The overall process results in the corrosion of zinc into solution to replace the hydrogen ions removed from the electrolyte by the release of hydrogen at the cathode.

As mentioned previously, the anode and cathode do not have to exist as macroscopically separate as in the case

of the flashlight. On the contrary, they exist on the same metal and their positions shift continuously.

There are several reasons for local chemical potential differences that lead to closely (microscopically) spaced anodic and cathodic regions to arise. For example, anodic and cathodic regions are established a) between cold worked metal in contact with annealed metal, b) at grain boundaries in contact with grains, c) at a single metal crystal of definite orientation, d) at phase change boundaries, e) at regions where the metal contains electrical conducting impurities, and f) at regions where identical electrodes are in contact with a solution of different composition or temperature (Uhlig, 1963).

From the knowledge of electromotive forces of electrolytic cells, when no current flows through a sensitive galvanometer, the free energy change (ΔG) that accompanies an electromechanical reaction can be calculated as:

$$\Delta G = -nFE_{cell} \qquad (5)$$

where: n = the numbers of electrons being transferred,

F = the Faraday constant (96,490 coul/equiv) and

E_{cell} = the cell potential.

The sign of the change of free energy is important to determine whether a reaction occurs spontaneously or not. If the final energy of the products is less than the energy of the reactants ($\Delta G<0$), then the reaction is spontaneous.

To make use of Eq. 5, the cell potential needs to be determined. Based on thermodynamic reasoning, an equation can be derived to express the e.m.f. of a cell in terms of concentration (or partial pressures) of reactants and products. This equation is called the Nernst Equation,

$$E_{cell} = E^{o} - \frac{RT}{nF} \ln \frac{\Pi Ap_i^{\alpha_i}}{\Pi Ar_i^{\alpha_i}}, \qquad (6)$$

where: E_{cell} = cell potential

E = standard hydrogen potential

R = gas constant

T = temperature K

n = number of electrons in the transfer

F = Faraday constant

Ap, Ar = activity (related to concentration) of

products and reactants

α_i = stoichometric coefficients of the reaction

Further information on corrosion including examples of the use of Eq. 6 may be obtained in one of the standard textbooks on corrosion (Fontana and Greene, 1978; Uhlig, 1963; Sully, 1966). In section 2.2 of this paper, Eq. 6 will be used to aid the explanation of the corrosion of steel.

To sum up this section, it is important to realize that the electrolytic cells that are made under the controlled conditions of a laboratory are analagous to what occurs during the corrosion of a metal. The triggers of corrosion on the same metal can be chemical, metallurgicical or mechanical in nature (oxides, mill scales, grain orientation, dislocation arrays, precipitated phases, localized stresses, scratches, impurities of the metal). These features are more chemically active and require less activation energy to react; thus, they become the anodes of the local action cells, while more flat and smooth regions on the metal become cathodes.

2.1.3 Polarization

Up to this point, we have only mentioned the free energy change of a reaction as an indication of whether corrosion takes place. However, the most important consideration in our study is corrosion rates and not corrosion tendencies.

2.1.3.1 Polarization Curves -

A tool often used by corrosion scientists to describe corrosion systems is a polarization curve. Figure 5a shows a polarization curve for the hydrogen electrode. Figure 5b provides the set up that could be used to obtain such a plot. Since hydrogen is a gas, platinum (Pt), which does not intervene in the reaction is used to provide a surface at which reactions can occur. The electrolitic cell of Fig. 5b is composed of following elements: two electrodes, and two external circuits, one connected to a power supply and an ampmeter, another, connected to a voltmeter.

When the system in Fig. 5b lies in an open circuit condition, the current i is zero and the potential E will also be zero (the hydrogen provides a standard to which electropotential of other metals is compared, thus, by convention, E is defined as zero for the hydrogen electrode).

If net current through the circuit is zero the oxidation ($H_2 \rightarrow 2H^+ + 2e^-$) and reduction ($2H^+ + 2e \rightarrow H_2$)

reaction rates at each electrode are the same (i.e., the number of hydrogen molecules being formed is the same as the number of hydrogen molecules being dissociated into hydrogen ions).

The polarization curve (Fig. 5a) is a plot of potential vs. log of the reaction rate for one electrode. The units chosen for the reaction rate are not moles reacted per unit area per unit time, but they are units of current density (amperes per unit area of electrode). These units are a convenient way to represent reaction rates as will become evident in the following paragraphs. Corrosion rates are converted to current density units by multiplying the reaction rate (r_o) by the Faraday constant and the number of electrons transfered (for the case of $2H^+ + 2e^- \rightarrow H_2$, the number of electrons transfered is 2).

In Fig. 5a the point at coordinates (i_o,0) corresponds to the open circuit potential condition, i.e. the equilibrium condition. Note that the location of the equilibrium condition will depend on the particular oxidation-reduction process that takes place at the electrode. Now, the condition when the power supply provides electrons to one of the electrodes is analyzed.

If the power supply in Fig. 5b starts to provide elctrons to electrode 1, the forward reaction ($H2 \rightarrow H^+ + 2e^-$) would be favored at electrode 1. If the power supply instead provides electrons to electrode 2, the reverse reaction ($H_2 \rightarrow H^+ + 2e^-$) would then be favored at electrode

1.

When a net current flows to or from an electrode, its potential E is no longer the equilibrium potential E_{cell} (Eq. 6). The current causes a potential change which tries to oppose the shift in equilibrium. The potential change, or overpotential, caused by the net current to or from an electrode is measured in volts. This departure from the equilibrium potential ($E-E_{cell}$) is called polarization (Uhlig, 1963).

It has been found experimentally that the relation between reaction rate and overpotential follows a logarithmic law. The Taffel equation which provides a relation between reaction rate (expressed in units of current density) and overpotential is

$$\eta \equiv E - E_{cell} = \pm b \log \frac{i}{i_o} , \qquad (7)$$

where: η = overpotential

+ = the possitive sign is used for the oxidation reaction

- = the negative sign is used for the reduction reaction

b = a constant

i = the rate of oxidation or reduction reaction in units of current density

i_o = the rate of the oxidation reaction at equilibrium (which is the same as the

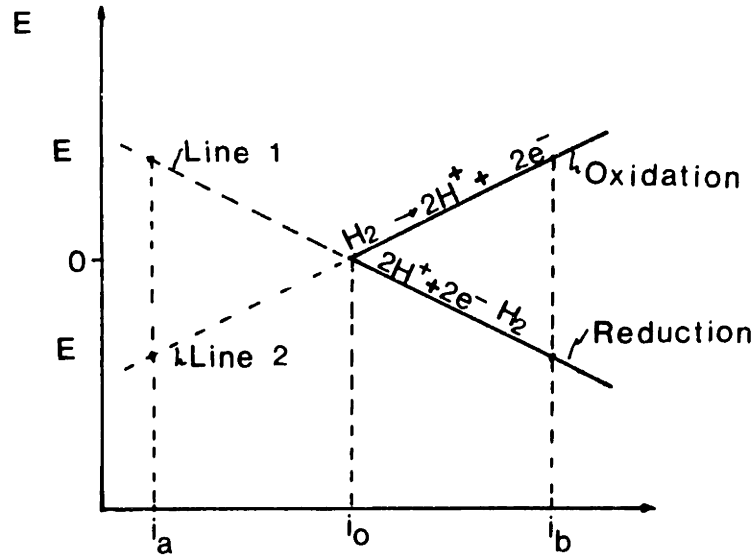

Log Current Density (Reaction Rate)

a) Polarization Curve.

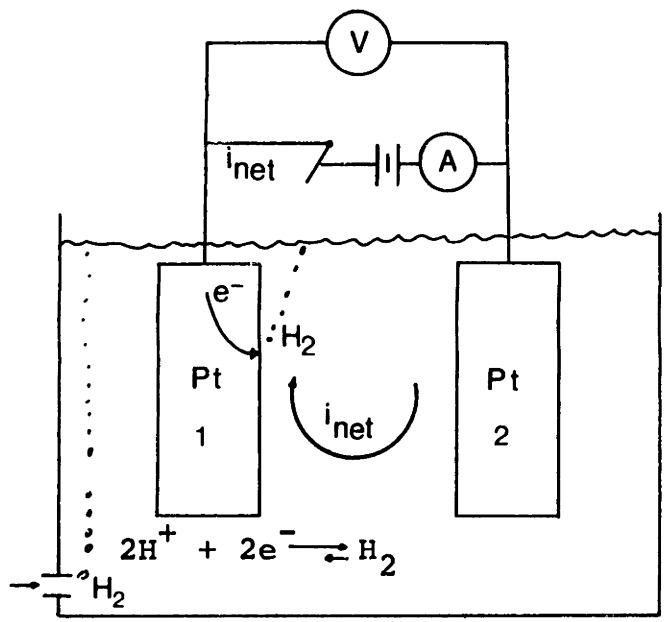

b) Electrolitic cell in conditions where the power supply provides electrons to electrode 1.

Figure 5. Corrosion studies through polarization curves

reduction reaction)

Equation 7 is graphically ilustrated in Fig. 5a (line 1 is representative of Eq. 7 using the negative sign and line 2 is with positive sign). On a semilogarithmic plot of potential vs. current density, the relations of current density and potential are linear functions as shown in Fig. 5a. It is now necessary to relate the current measured by the ampmeter in Fig. 5b with the associated value of current density in Fig. 5a.

As the power supply of figure 5b starts to send electrons to electrode 1, the net rate of the reaction $2H^+ + 2e^- \rightleftarrows H_2$ (equals the forward minus the reverse reaction rates) must consume the same number of electrons as those being sent by the power supply. In equation form this is:

$$|i_{net}| = |i_{red} - i_{ox}| \quad . \qquad (8)$$

This condition is necessary to satisfy the principle that there may not be accumulation of electrical charge during a electrochemical reaction process.

Being compatible with the condition of the power supply sending electrons to electrode 1, a potential at which the reduction reaction on the electrode is favored in Fig. 5a is analyzed. As an example of this condition potential E_1 in Fig. 5a was chosen. For this case Eq. 8 is modified to

$$i_{net} = i_a - i_b \quad . \qquad (8a)$$

Since the current is in a logarithmic scale, it is found that i_{net} is approximately equal to i_b; that is, the actual current through the circuit of Fig. 5b is considered equal to the value of the current density for the reduction reaction. The same considerations as above can be taken for the condition of the power supply providing electrons to electrode 2. The counterpart case in Fig. 5a would correspond to a condition of $E = E_2$. In this case, Eq. 8 would also become

$$i_{net} = i_b \quad , \qquad (8b)$$

which in this case corresponds to the oxidation reaction rate.

From this explanation it becomes evident that the dashed section of lines 1 and 2 in Fig. 5a are of no importance in determining the net current and as can be seen in Fig. 6 they are in general omitted. At this point the polarization curve for a specific electrode has been explained, similar type of curves have been derived for other metals and other metal combinations. In the following section the plots are used to describe the corrosion of a metal. It is worthy to remember that the polarization curves provide the actual value of the net

current for conditions in which the oxidation or reduction process are not at equilibrium and that at equilibrium conditions (i.e., no net current) the value of current density is representative of the rate at which the oxidation reaction is taking place, which is the same as the rate at which the reduction reaction is proceeding.

2.1.3.2 Polarization Curves Used In Determining The Corrosion Rate -

Having explained the general method by which polarization curves can be obtained, they can now be used to explain the behaviour of metals in corrosive environments. Figure 6a shows the case of zinc immersed in hydrochloric acid. In Figure 6b polarization curves of each individual electrode (hydrogen and zinc) are provided.

In the open circuit condition, the voltage determined by voltmeter V is $E_{cell} = E_1 - E_2$ (Eq. 6). In this condition the net current through the circuit is zero and the conditions i_{o_1} and i_{o_2} are equilibrium conditions.

Now consider the case when the circuit is closed and the resistance R is decreased. Due to the potential difference $E_1 - E_2$ the oxidation reaction is favored at electrode 1 (Eq. 4a) while the reduction reaction (Eq. 4b) is favored at electrode 2. At the limit when the short circuit condition is reached, both electrons are at the same potential. Through all this sequence the

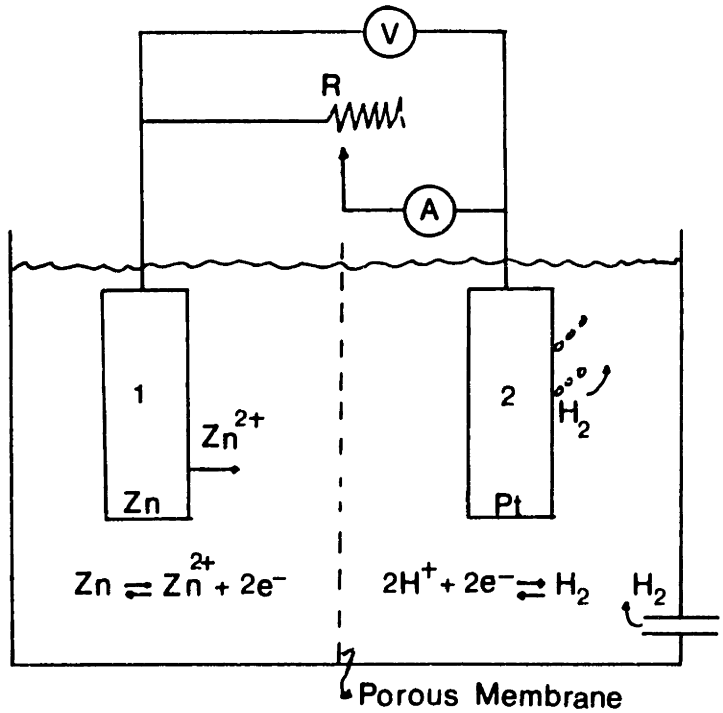

6a) Electrolitic cell from which polarization curves are obtained.

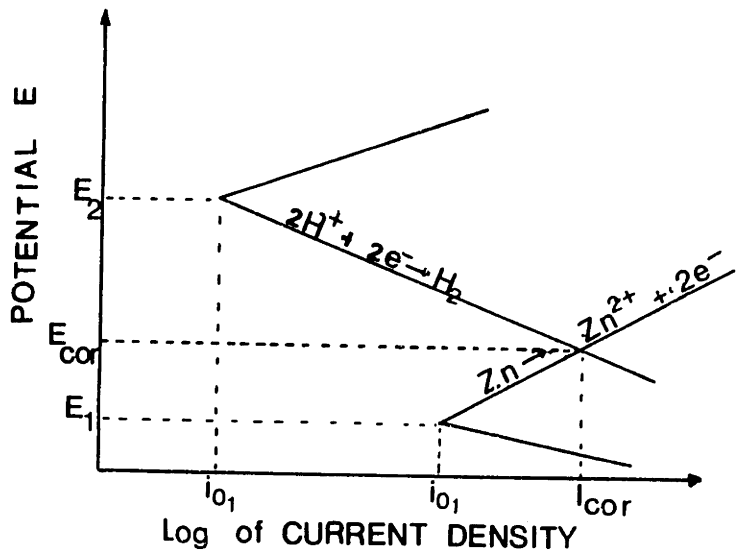

6b) Polarization Curve.

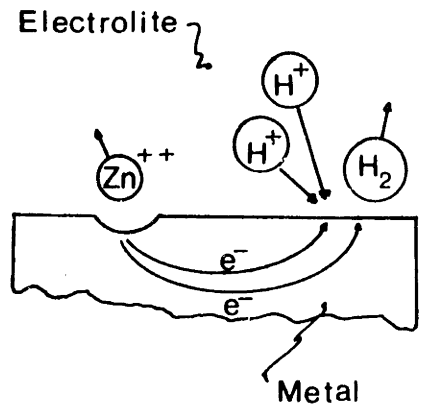

6c) Actual corrosion process.

Figure 6. Polarization curves used to determine corrosion rates

principle of no accumulation of charges is maintained, so that the same total number of electrons being consumed at the electrode 2 in the formation of hydrogen is the same as those generated during the formation of zinc ions.

The final state corresponding to the short circuited condition is representative of the corrosion rate. Indeed as explained previously, for a metal in a corrosive environment the anode and cathode locations lie in the same metal, see Fig. 6c. Thus a representative rate at which corrosion is taking place is given by the intersection of the polarization curves of the reduction and oxidation processes (Fig. 6b). This intersection corresponds to the situation at which the total oxidation rate is equal to the total reduction rate.

Diagrams like the one presented in Fig. 6b will be used in the following section to explain the phenomenon of passivity and the influence of oxygen in the corrosion rate.

2.1.4 Passivity

One of the interesting phenomena within corrosion science is the passivity of metals. This condition is the state in which a metal or an alloy resists corrosion in an environment where thermodynamically the reaction ought to occur (Uhlig, 1948; Scneir, 1963).

There is no agreement on a theory to explain passivity. While Faraday in 1844 suggested that

passivation is caused by a film, not necessarily an oxide, on the metal surface that prevents contact between the metal and the solution, others (Russel et al., 1925) suggest that electrical fields caused by different electron configurations near the metal are responsible for impeding the flow of metal ions and/or oxidizers. The book by Uhlig (1948) is recommended for further details.

Although the causes of passivity may be difficult to define, it can be qualitatively described by characterizing the behaviour of metals which show this effect. A polarization diagram for a passive system is shown in Fig. 7. As the oxidizing power increases (the overpotential increases), the corrosion rate increases; but, at a certain critical potential the corrosion rate sharply decreases entering the passivated state, where the corrosion rate is independent of potential over a considerable potential region. Further increase in potential, eventually leads to higher corrosion rates.

2.1.5 Influence Of Environmental Factors On The Corrosion Of Metals

2.1.5.1 Effect Of Oxidizers -

Figure 6 shows the case of hydrogen as the only cathodic reaction. If in a system there is an addition of oxidizers such as oxygen, which through a reaction like Eq. 3 can be a consumer of electrons, the reaction rate in general tends to increase; see Figure 8(a). The

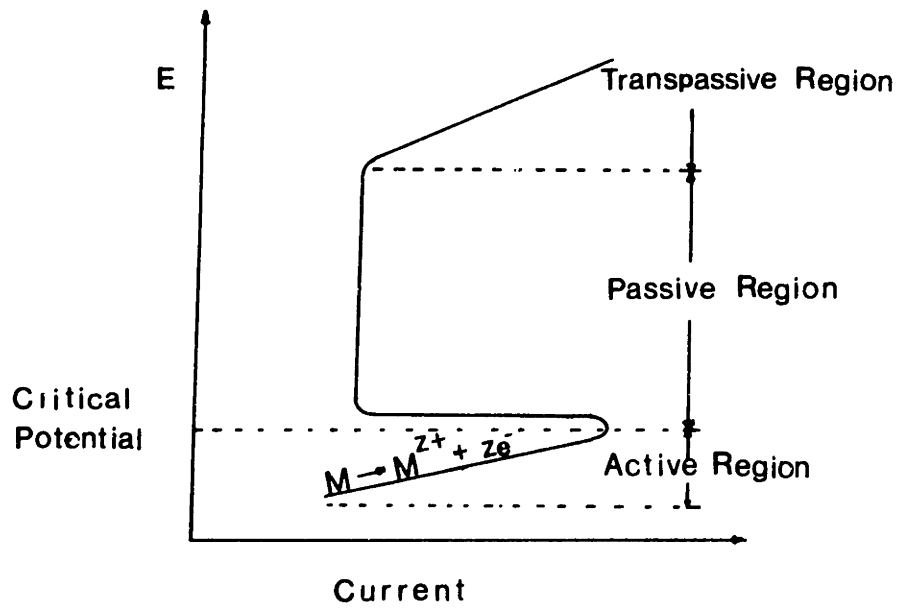

Figure 7. Polarization curve for a metal that can be passivated (Uhlig, 1963)

figure shows that, bearing in mind that the total oxidation rate has to be equal to the total reduction rate, the point of intersection of the lines describing the total cathodic and anodic process shifts location from the corrosion rate by only one oxidizer (i_1 or i_2 to i_3). With the exception of passivating systems, the shift will always tend towards a higher corrosion rate. In a passivated system it is possible that an increase in the

oxidizer would yield a lower corrosion rate, see Fig. 8(b) (i_1 to i_2).

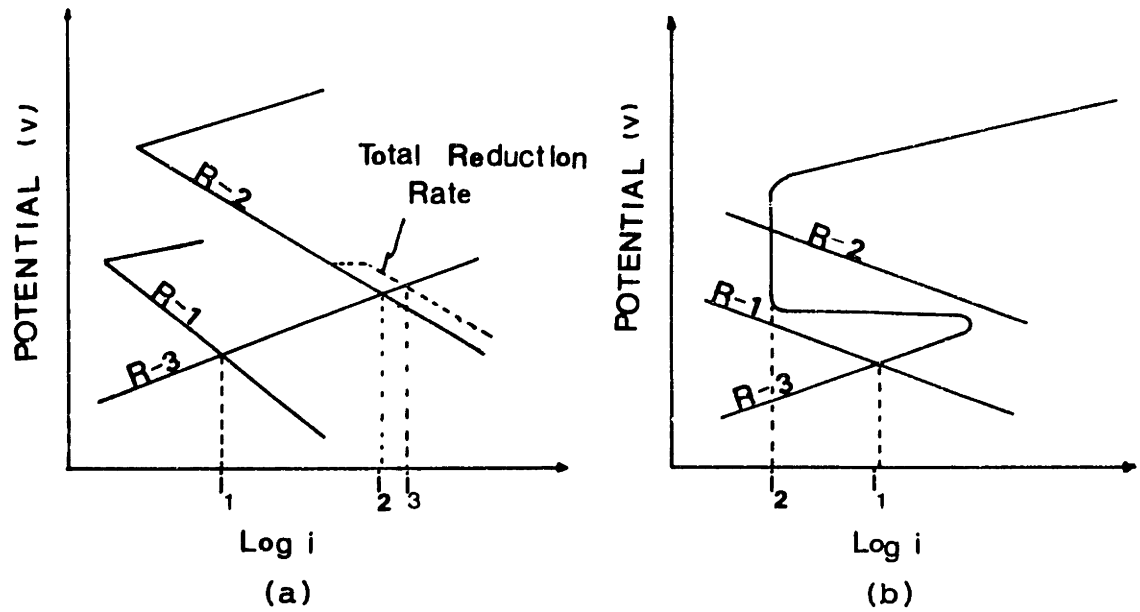

OXIDATION REACTIONS

R-1: $2H^+ + 2e^- \rightarrow H_2$

R-2: $O_2 + H_2O + 4e^- \rightarrow 4OH^-$

REDUCTION REACTION

R-3: $M \rightarrow M^{z+} + ze^-$

Figure 8. Polarization curves for a) non-passive system, and b) passive system showing the influence of additional oxidizer (Fontana and Greene, 1978).

As an example, iron can passivate depending on the overvoltages caused by the dissolved oxygen concentration. In this case, passivation is related to the fact that more oxygen yields a more protective film, that is, a film with low ion conductivity and chemical solubility.

The critical value of oxygen that causes a decrease in oxidation rates for distilled water is about 12 ml /l , see Fig. 9. For some environments the passivated state cannot be reached because the solubility of oxygen in water is limited and it is insufficient to produce a passive state. Also, protecting a surface through passivation by oxygen is dangerous because in the case the film breaks, such a breakdown would be accompanied by severe corrosion at very localized regions of the surface, i.e., pitting, (Uhlig, 1963).

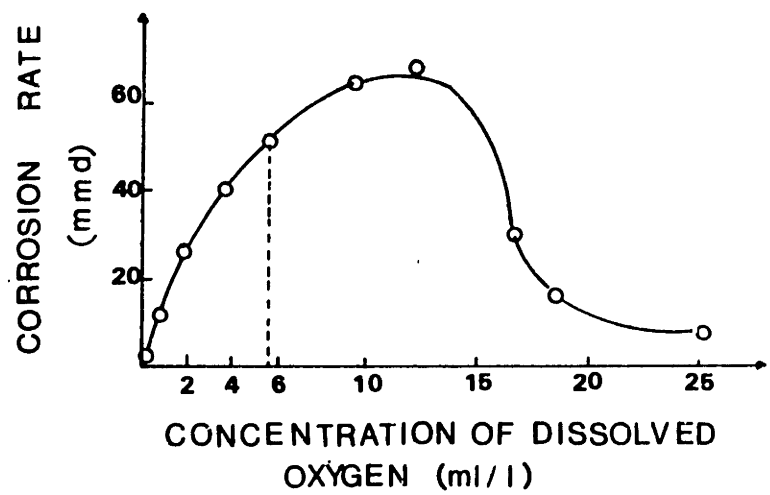

Figure 9. Passivation of mild steel through oxygen concentration in slowly moving distilled water, 48 h test, 25°C, (Uhlig, 1963, p. 82).

2.1.5.2 Effect Of Temperature And H^+ Concentration -

Increasing temperature, in general, tends to accelerate the corrosion rate. Temperature provides more energy to the system and allows for the chemical and diffusion rates to increase.

For the case of steel at temperatures close to 150 C (300 F), the influence of temperature is opposite to what is expected. This strange behaviour will be explained in the next section. The influence of $[H^+]$ is directly linked to an increase in oxidizing power as described previously. Thus, an increase in the hydrogen ion concentration in general increases the corrosion rate.

2.1.5.3 Effect Of Velocity -

The velocity of the solution increases the corrosion rate only when the corrosion process is controlled by cathodic diffusion. But even under these circumstances, corrosion rates may become independent of the velocity at very high speeds.

2.1.6 Types Of Corrosion

There are different ways to classify the corrosion phenomena. One alternative is to consider the extension of the damaged region. If a large portion of the metallic

surface is corroded, this is referred to as General Corrosion. If small areas are the only ones damaged, this is called Localized Corrosion; and when only small holes appear, this is called Pitting (Evans, 1948)

In Uhlig's (1948) book the following forms of corrosion are mentioned:

1. Direct Attack: This form of corrosion leads to General Corrosion. It involves a direct reaction with the metal to produce corrosion products; these products may be immediately soluble in the liquid present.

2. Two Stages Attack: At times the metal reacts with its environment to form a corrosion product which is somewhat soluble. In this case, of which iron is an example, metal may enter the liquid as an oxide or a hydroxide and may precipitate as a less soluble oxide or hydroxide at a distance from the metal.

3. Electrochemical Attack: The term electrochemical corrosion is often used to denote the attack when the anode and the cathode are spatially separated and thus there are electric currents flowing through perceptible distances. The combination of structures with two different metals may often lead to this type of corrosion. Some examples are iron and copper in sodium chloride solutions.

4. Conjoint Action Attack: Often, corrosion and erosion operate simultaneously and the damage produced is frequently greater than the effect of corrosion or erosion alone. The combination of the two agents is called Conjoint Action (Evans, 1960). Forms of conjoint action include: corrosion cracking, corrosion fatigue, and corrosion-erosion.

The book by Fontana and Green (1978) is recommended for a good review of the different types of corrosion.

2.1.7 Corrosion Rate Laws

Reviewing the corrosion rate laws is the final section of the general background on corrosion. Learning about the different corrosion rate laws, allows us to be aware of some of the phenomena that can occur when corrosion takes place.

The existing types of oxidation rate laws are: the parabolic, the cubic, the logarithmic, the asymptotic, the inverse logarithmic, the rectilinear and the paralinear. These laws are theoretical models that were derived from phenomena that are assumed to occur inside the oxide layer. Although the laws have been found to adequately represent the behaviour of the oxidation of metals, sometimes, corrosion data follows rates which do not conform with any of the above laws and at other times, for

the same metal, several laws may be followed during different ranges of temperature.

For the purpose of completeness, some of these laws will be briefly reviewed. A more complete study can be found in Evans (1960), and Kubashewski (1965).

1. The Parabolic Law: A protective oxide layer forms a continuous barrier between reactants and thus inhibits the reaction. The simplest and natural assumption that can be made about the effectiveness of this barrier is that its protective power is directly proportional to its thickness:

$$\frac{d\delta}{dt} = \frac{k}{\delta} \quad ,$$

$$\delta^2 - \delta_o^2 = kt \quad , \qquad (9)$$

where δ_o, k = are constants functions of temperature but not of time

δ = thickness of the oxide layer at time t.

The parabolic law implies that i) an oxide layer is compact and adherent, ii) the slow step in the process of corrosion is the diffusion of a reacting material through the oxide layer, and

iii) the oxide is regarded as electrically neutral (Shreir, 1963).

2. Logarithmic and Asymptotic Laws: In both the asymptotic and logarithmic laws, it is assumed that the diffusion of species is through a porous film. In the logarithmic law,

$$W = K_a + K_b \log(at+1), \quad (10)$$

where W = weight change per unit area

K's, a = constants functions of temperature

The logarithmic law is obtained when it is considered that the diffusion through the pores is considered to be accompanied by the blocking of neighbouring pores as a result of compressional forces in the oxide. For the asymtotic law, the diffusion through the pores is accompanied by blockage of the same pores by material formed within it. The asymtotic law has the equation:

$$W = K_c(1-\exp(-K_d t)). \quad (11)$$

3. Rectilinear Law : The equation that describes this law is

$$W = K_g t + K_h \quad . \qquad (12)$$

This type of law corresponds to a porous layer that constantly breaks off and maintains a constant resistance to the diffusion of the oxidizing species. The actual wear rate will depend on the temperature, the hydrodynamic conditions, the chemistry of the environment and the properties of the material being oxidized. These conditions will determine the rate at which the layer is thickening, which is equal to the rate at which the layer is flaking off. The corrosion-erosion of low carbon steel follows this type of law.

2.2 THE CORROSION OF STEEL IN WATER

The material of which steam extraction lines are made is a low carbon steel. For this reason this study concentrates on the corrosion of this particular material.

2.2.1 Early Research

Cataldi et al. (1958) studied several materials under a wide range of conditions and in tests lasting from 1000 to 2000 hours.

These authors found that carbon steel has little resistance to corrosion when compared to stainless steels.

Early researchers who described the oxidation of low carbon steels in the range of 300 to 500 C were Potter and Mann (1963). Their experimental results showed that the corrosion of steel in stagnant conditions leads to the formation of a double layer of magnetite, each of which contains the same amount of iron; however, the outer layer is poorly adherent. These findings suggested that the inner corrosion layer grows towards the metal and the outer macrocrystaline layer grows towards the solution.

Potter and Mann considered that the inner layer was non-porous. This conclusion led them to assume that the mechanism of corrosion was a double migration process, through solid films of magnetite, in which oxygen moves towards the metal and the iron ions diffuse towards the solution.

Later Pearl and Wozaldo (1965) tested carbon steel specimens in water, steam-water and saturated steam evironments at temperatures close to 300 C. They found that their descaled weight loss data, after the initial start up period of 500 hours followed a linear rate law,

$$\Delta W = \Delta W_o + St, \qquad (13)$$

where; ΔW = weight change

ΔW_o = a constant that accounts for non-linear kinetics during the initial period

S = a constant a function of temperature.

Until then, work had mainly been empirical, and there was no actual research aimed at finding out what was the actual mechanism by which corrosion took place.

In 1966, Castle and Masterson, through their static experiments at 300 C proposed that the corrosion of steel occurs via a counter diffusion of species through a porous oxide, not a solid film as proposed by Potter and Mann. Castle and Mastersom were the first to suggest that the physical-chemical properties of the solution and thus the hydrodynamics around a steel specimen influences the rate of oxidation. In other words, mass transfer to the solution is an important step in the corrosion of steels. Several mechanisms have been suggested for explaining the way in which iron diffuses across the oxide layers. Some of these mechanisms will be briefly described. Before doing so, it is necessary to review the electrochemical aspects involved in the corrosion of steel.

2.2.2 Electrochemical Aspects

Iron corroding in an aqueous environment can form three different types of oxides with the outermost part of the layer being the richest in oxygen and the innermost being the poorest. The oxides are Wustite (FeO), Haematite (Fe_2O_3) and Magnetite (Fe_3O_4).

The conditions in a power station are such that the dissolved oxygen concentration is very low (100 ppb); thus, the discussion in this section is focused on oxygenless water.

The oxidation of steel in an aqueous oxygenless environment forms, as a final product, a porous oxide layer of magnetite (Castle and Thomson, 1967). The pores in these films are associated with the dissolution of iron at the metal oxide interface and its transport into solution in the ferrous form.

Experiments with carbon steel in water at a temperature above 150 C have shown that the first step in the oxidation of steel is the formation of the hydroxide of iron $Fe(OH)_2$. The following reactions, which take place at the metal-oxide interface, account for the generation of this hydroxide (Berge [1972],Gadiyar [1979], Heitmann [1981]):

$$Fe \rightarrow Fe^{2+} + 2e^{-} \quad , \qquad (14)$$

$$2H_2O \rightarrow 2H^{+} + 2OH \quad , \qquad (15)$$

$$2H^{+} + 2e^{-} \rightarrow H_2 \quad , \qquad (16)$$

$$Fe + 2H_2O \rightarrow Fe(OH)_2 + H_2 \quad . \qquad (17)$$

Heitman (1982) uses Fig. 10 to represent the corrosion of steel in oxygenless water under static conditions.

The graph is a representation of the Nernst Equation (Eq. 6) for the iron-water system.

When the anodic reaction is Eq. 14 and the cathodic reaction is Eq. 16, the Nernst Equation becomes:

$$E_{cell} = E_o - \frac{RT}{nF} \text{Log} \frac{\{ a_{Fe^{++}} \}\{ a_{H_2} \}}{\{a_{H^+}\}} \qquad (18)$$

here E_o is the standard oxidation-reduction potential for iron (0.44v).

Equation 18 can be rearranged as follows when T is 298 K and the concentration of species are low enough for the activities to be equivalent to concentrations:

$$E_{cell} = E_o - \frac{RT}{nF} \log[Fe^{++}] + \log[H_2] - 2\log(H^{-}) \quad . \qquad (19)$$

From the definition of pH and with the partial pressure of hydrogen assumed to be one, Eq. 19 becomes:

$$E_{cell}=E_o-\frac{RT}{nF}\log[Fe^{++}] - \frac{2RT}{nF}pH \quad . \qquad (20)$$

Substituting numbers we obtain,

$$E_{cell} = 0.44 - 0.059\log[Fe^{++}] - 0.059pH, \qquad (21)$$

$$E_{cell} = L - 0.059pH \quad , \qquad (22)$$

where L can be evaluated if the concentration of Fe is known ($L = 0.44 - 0.059*\mathrm{Log}[Fe^{++}]$).

The line with potential,

$$E = -0.059pH \quad , \qquad (23)$$

in Fig. 10 describes the cathodic reaction involving H_2 formation.

For a given Fe^{++} concentration and pH, an electric potential difference between the local voltaic couple (anode and cathode) on the iron surface is set. If the initial condition is the horizontal line at $[Fe^{++}] = 1.0x10^{-8}$ mol/Kg and pH = 7, the production of ferrous hydroxide (Eq. 17) leads to an increase in the concentration of iron ions (Eq. 14) and a decrease in the

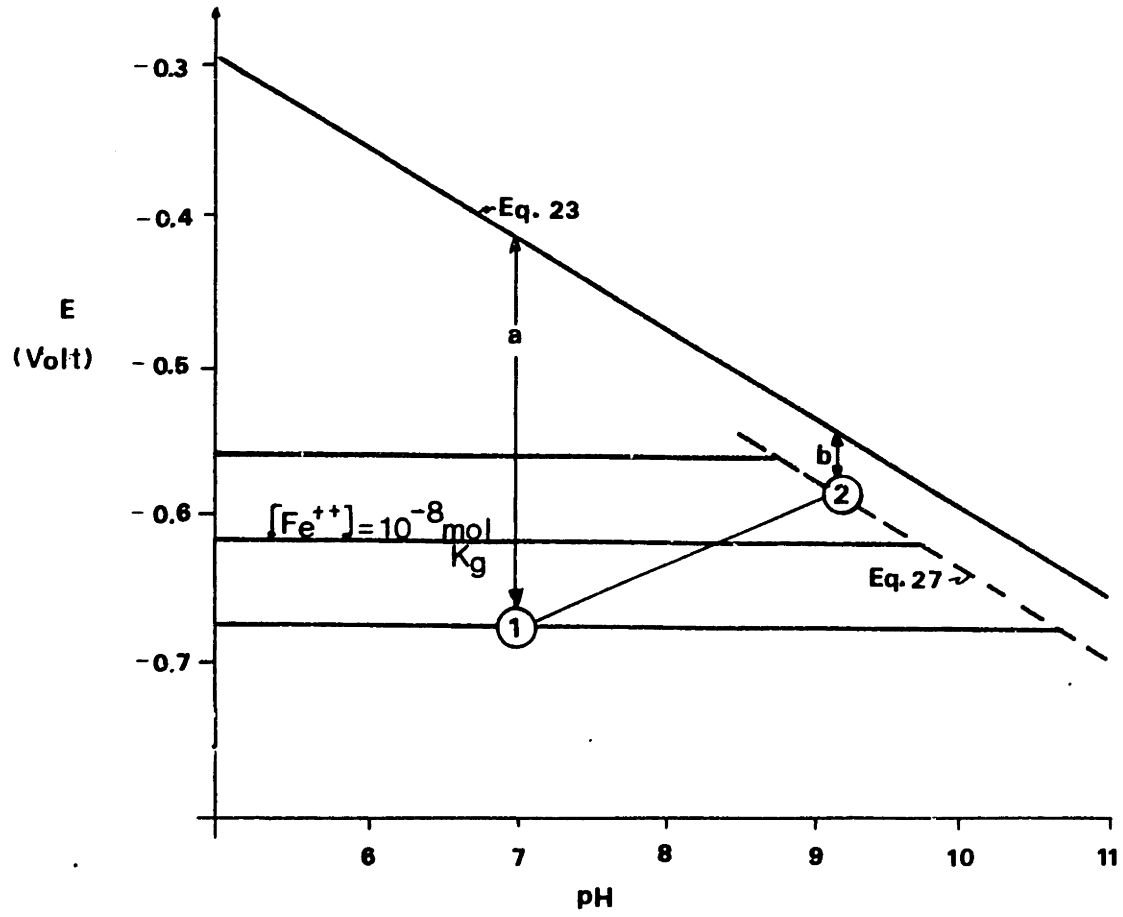

Figure 10. Diagram for steady state corrosion of iron in water (Heitman and Kastner, 1982).

concentration of H^+ (Eq. 16), i.e., an increase in pH. Under static conditions, the ferrous hydroxide production proceeds up to the moment when the hydroxide reaches the saturated concentration. This in turn causes the potential difference "a" to be reduced to "b". In order for the reaction to stop, E_{cell} from Eq. 6, would have to be zero ($\Delta G = 0$ from Eq. 5) but this condition is not reached because the maximum concentration of iron ions allowed is given by the solution product of $Fe(OH)_2$. This is now explained.

In accordance to the solubility reaction

$$Fe(OH)_2 \rightarrow Fe^{++} + 2(OH)^-, \qquad (24)$$

the concentration of Fe cannot exceed the value given by

$$[Fe^{++}]_{max} = \frac{K_{Fe(OH)_2}}{|OH^-|^2} , \qquad (25)$$

where $K_{Fe(OH)_2}$ is the solubility product constant for $Fe(OH)_2$.

Extra hydroxide formation would precipitate as a white film on the surface of the metal.

The concentration of OH^- has to comply also with the deionization product for water (K_W)

$$|OH^-| = \frac{K_W}{|H^+|} , \qquad (26)$$

Equation 26 in 25 yields the following relation

$$[Fe^{++}]_{max} = \frac{H^{+2} \; K_{Fe(OH)_2}}{K_W^2} , \qquad (27)$$

This expression is also shown in Fig. 10 and marks the maximum Fe^{++} concentration for a given pH.

Since the system has not reached equilibrium ($\Delta G \neq 0$) ferrous hydroxide keeps being formed, and thus, having reached the solubility limit, precipitates on the metal. The protective film of hydroxide suppresses all electrode

processes, and thus the corrosion stops in the steady state condition.

In a dynamic system, the flow removes iron ions, and because of this, the line in Fig. 10 corresponding to Eq. 27 is never reached.

The hydroxide produced during the first step of the oxidation of iron can form magnetite through the Schikorr reaction (Castle and Thomson, 1967)

$$3Fe(OH)_2 \rightarrow Fe_3O_4 + H_2 + 2H_2O \quad , \quad (28)$$

The rate of this reaction becomes very fast at temperatures close to 200 C, (Heitman, 1982).

To account for the double layer of magnetite under static water experiments, it is necessary that Eq. 28 takes place at the metal and at the oxide-water film interface.

To explain the flow of ferrous ions through the oxide layer during static flow conditions, several hypothesis have been made (see table 1). There is no agreement among researchers, the explanation by Berge et al. (1976) is supported by some experimental work, and it is based on the work of magnetite solubility carried by Sweeton and Baes (1970). Before discussing the theory of Berge et al. it is necessary to review briefly the work of Sweeton and Baes.

2.2.3 Sweeton And Baes Work

The research carried on by these investigators showed that the oxide magnetite can lead to the formation of hydroxide type compounds (Fe^{++}, $Fe(OH)^{+}$, $Fe(OH)_2$, $Fe(OH)_3^{-}$) which are soluble in water (1.0×10^{-14} Kg/Kg_{H_2O}). Their experimental data on the solubility of magenetite as a function of temperature and pH (see Fig. 11) allowed them to compute themodynamic data ($\Delta S, \Delta H$) for calculating the equilibrium constant for the following reaction:

$$Fe_3O_4 + 3(2-b)H^{+} + H_2(g) \rightarrow Fe(OH)_b^{(2-b)+} + (4-3b)H_2O \quad , \quad (29)$$

where b = 0, 1, 2, and 3.

The work of Sweeton and Baes is useful since it suggests that the hydroxides of iron are the compounds by which iron is lost in a dynamic test, and that the solubility of magnetite influences how much of these species can exist at equilibrium.

2.2.4 Mechanism By Which Iron Diffuses Across Oxide Layers

As was previously mentioned, the double migration process through the oxide layer is responsible for the formation of two oxide layers on the static corrosion

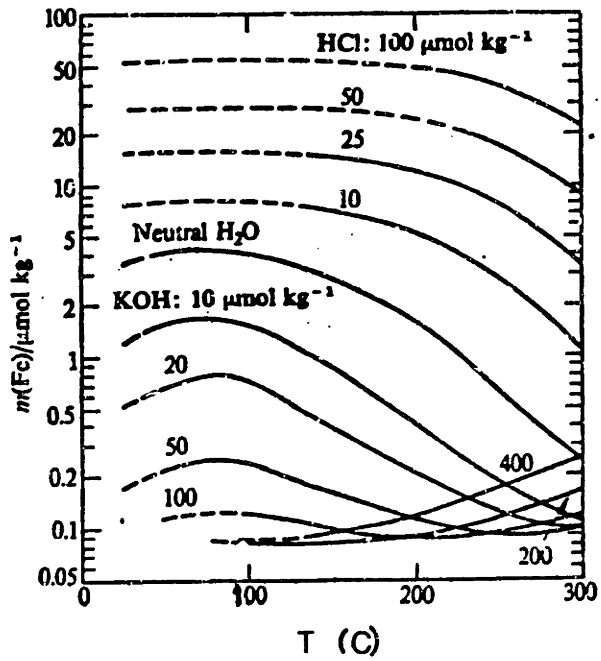

Figure 11. Solubility of Fe_3O_4 in aqueous solutions saturated with H_2 at 1 atm and 25 C (Sweeton and Baes, 1970).

tests. Table 1 summarized various mechanisms which have been proposed in order to explain how the iron ions diffuse, without precipitating, through the pores of the magnetite layers.

The model of Berge (1976) supported by experimental evidence, presents an explanation for describing the flow of iron through the oxide. Berge suggests that a gradient of hydrogen is developed wihtin the oxide layer and that in accordance with Eq. 29 a complementary equilibrium of soluble iron concentration gradient is also formed. This soluble iron gradient is the driving force for the ferrous ions to move across the oxide layer.

Table 1. Mechanism by which iron diffuses towards solution.

Author	Proposed mechanism for diffusion through layer	Comments
Castle & Mann (1966)	A thin layer of ferrous hydroxide exists at the metal oxide interface (below the porous layer). The difference in solubility between the hydroxide layer and the magnetite is responible for the soluble iron gradient.	This theory leads to supersaturation of soluble iron through the pores of the oxide layer. The experimental results were 15 times larger than the corrosion rate values predicted by this theory.
Bignold, Garnsey, and Mann. (1972)	The concentration gradient is caused by stoichometry variation in magnetite, i.e., the oxide is not only magnetite, it varies through the layer (FeO_n where $1<n<1.5$).	This theory does not present the problem of supersaturation, but it has not been proven through experiment.
Berge, Ribon and Saint Paul (1976)	The formation of magnetite at the metal interface generates hydrogen: $3Fe+4H_2O \rightarrow Fe_3O_4+H_2$. (a) The dissolution reaction equation is (Sweeton and Baes): $Fe_3O_4+3OH^-+H_2+H_2O \rightarrow 3Fe(OH)_3^-$. (b) A hydrogen concentration gradient can be established through the layer, which in turn, by the equilibrium suggested in Eq. b, generates a gradient of iron species.	Bignold (1972) showed the electrochemical potential in the oxide layer is constant (thus there should not be an H_2 gradient). Berge contradicts him and gives experimental evidence.

In this theory it is considered that the H_2 gradient is the result of the magnetite generation at the metal oxide interface via the combined effect of Eq. 17 and 29:

$$3Fe + 4H_2O \rightarrow Fe_3O_4 + H_2 \quad , \quad (30)$$

This magnetite generation produces H_2 which elevates its concentration at the metal oxide interface relative to the concentration of H_2 in the free stream and thus, produces the H_2 and the ferrous ion gradients.

With the ferrous ion species (Fe^{++}, $Fe(OH)^{+}$, $Fe(OH)_2$ and $Fe(OH)^{-}_3$) having diffused to the oxide water interface, in a static experiment the ferrous ions can be precipitated into magnetite by Eq. 28, and thus form a second layer.

Under dynamic conditions, the mechanism of corrosion is somewhat different than in static corrosion. The iron hydroxides that diffuse through the pores from the metal-oxide water interface do not have time to precipitate as magnetite on the oxide-water interface; therefore, the outside oxide layer often does not form. Water removes the iron hydroxides from the dissolution of the magnetite (Eq. 29) at the oxide water interface. The net removal rate will depend on the concentration of soluble iron species at the oxide-water interface and on the physical chemical characteristics of the water. This phenomenon, which is now described is the

corrosion-erosion wear of steel.

2.3 CORROSION-EROSION OF STEEL

Having reviewed some of the theories on the mechanisms by which steel is corroded, we now examine the important literature on corrosion-erosion.

2.3.1 Recent Work On Corrosion-Erosion

Various reports have appeared since 1974 on the phenomenon of corrosion-erosion. It was from the knowledge gathered from these reports that the behaviour of the variables that influence the wear was understood.

In order to study the phenomenon of corrosion-erosion, researchers have made use of laboratory rigs or have inserted their specimens inside the pipes of the power plants. Table 2 lists some of these investigations, and it gives brief information about the characteristics of the experiments used.

The table shows that some of the investigators have tried to obtain a model for estimating corrosion-erosion damage. The model of Keller (1974) is empirical and has the big disadvantage of not including the influence of the chemistry of the water (pH, oxygen concentration).

The models of Bignold et al. (1981) and Berge (1982) fail to provide the value of the essential constants needed to estimate the wear from their relations.

Table 2. Corrosion-Erosion Studies.

Reference	Equipment	Two-phases present	Temperature	Velocity range	Material Composition	Range of Wear Rate	Comments (Model)
Keller (1974)	In power stations	Yes	50 - 150 C	?	Low carbon steel to 13 % Cr.	0.4 - 5 $\frac{mm}{y}$	Keller (1974) proposed a model. His relation was derived empirically. He was able to predict for his experimental data, wear rates within a factor of 5. His model disregards the chemistry of the water (pH, O_2).
Coulon & Thauvin (1979)	Laboratory rig.	Yes	?	?	A wide range of steels	?	Coulon and Thauvin's work deals mainly with droplet impingement.
Berge et al. (1972, 1980, 1982)	Laboratory impinging jet	No	225 - 300 C	0 - 18 $\frac{m}{s}$	-	5.58×10^{-3} 0.067 $\frac{mm}{y}$	Berge et al proposed a model: $\dot{m}'' = 2K\lambda(C_e-C_o)/(2K+\lambda)$ where: $\dot{m}''$ = wear rate, λ = mass transfer coefficient, K = a reaction rate constant, C_e and C_o = equilibrium and bulk fluid iron ion concentration. Berge et al. fail to give a method to evaluate K.
Bignold et al. (1980, 1981)	Laboratory mainly flow through orifices.	No	up to 350 C	up to 208 Kg/h	Mild steels	0.04 - 3 mm/y	Bignold et al. derived a model which shows the wear rate to be dependent on the third power of the mass transfer coefficient. Their model is not completely validated (specifically, the behaviour of temperature is not explicitly considered), several constants in their equation lack values and a procedure to evaluate them is not given.

Table 2 continued. . .

Reference	Equipment	Two-phase flow	Temperature	Velocity range	Material Composition	Range of Wear Rate	Comments (Model)
Kunse (1981)	Laboratory rig.	Yes	185 - 200 C	Up to 180 m/s.	C22.8 15Mo 3 10Cr Mo $\frac{9}{10}$	up to 0.4 mm/y.	Kunse (1981) is the only researcher that considers that the corrosion-erosion wear rate was not a constant. He fitted his data to a parabolic function of time.
Faber (1982)	In power plants Test bars in drain of turbine.	Yes	≈ 135 C	≈ 52.6 $\frac{m}{s}$	0.2C 0.15C .5 Mo 0.15C .8 Cr &.7 Cu 0.15C 2,2 $\frac{Cr}{Mo}$ 0.15C 5 Cr	0 - 2.6 mm/y	
Heitman and Kastner	Laboratory rig.	No	50 -250 C	5 - 40 $\frac{m}{s}$	St 37.2 15 Mo3 15 NiCuMoNb5 13 CrMo44 10 CrMo910	0.001 - 33 mm/y.	

Furthermore, the model of Berge, which is based on the explanation given in Section 2.2.4 as the mechanism by which iron diffuses across oxide layer, assumes that there is equilibrium concentration of hydroxides through the oxide layer; this condition will be analyzed in Chapter 3 to show that such a model would not be able to explain the experimental findings of corrosion-erosion; specifically, it would not be able to predict the behaviour of wear rate as a function of temperature.

A reason for not having obtained a workable expression is the lack of physically realistic model that expresses clearly the influence of both the hydrodynamics and the kinetics of the chemical reactions involved. This in turn is linked to the fact that experimental work has made use of very complicated geometries (bends, impinging plates, orifices). In these cases the hydrodynamics by themselves are difficult to establish; and, it makes it even more difficult to determine the way in which the hydrodynamics influences the reaction kinetics.

In general, experimental data of corrosion-erosion wear rates follow a rectilinear law and thus the wear rate is a constant. As explained in Section 2.1.6 a constant rate implies that the oxide layer provides constant resistant to corrosion by maintaining constant thickness and porosity.

2.3.2 Variables Influencing Corrosion-Erosion Rate

In this section, the influence of oxygen, temperature, velocity, pH and material composition are reviewed.

Another variable that influences the wear rate is the state of the surface. Little has been done on this subject. Berge (1972) reports of an experiment where polishing the surface electrolytically vs. polishing it mechanically with 600 sand paper, causes the wear to increse by a factor of 4. Results on the influence of surface finish are inconclusive.

2.3.2.1 Oxygen Contents -

The investigation of Brush and Pearl (1972) on low carbon steel on temperatures between 10 and 200 C, showed that an increase in the O_2 contents from 20 to 200 ppb decreases the wear by up to a factor of 10. The reason for this decrease in wear rate has been explained in Section 2.1.5.1. The concentration of the oxidizer causes the metal to passivate by achieving a more protective oxide layer.

2.3.2.2 Temperature -

Temperature is perhaps the variable that influences the wear in the most unexpected manner.

Since Keller's work (1974), several authors, among them Bignold et al. (1981) and Heitman (1982), have shown

that for the steel specimens from their tests, there exists a temperature at which the wear rate is maximum, see Fig. 12. The critical temperature usually lies close to 150 C (300 F).

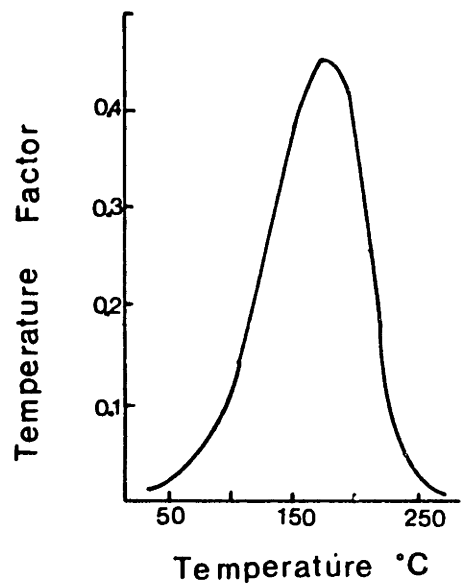

Figure 12. Temperature dependence of corrosion-erosion losses under two-phase flow conditions (Keller, 1974).

The critical temperature has been explained as the result of a very quick transformation of ferrous ions into magnetite (Eq. 28) as the temperature is increased (>200 C).

It appears that at a low temperature the generation of ferrous ions from Eq. 17 is slow. As the temperature increases, more ferrous ions are generated (thus there are more ferrous ions that can be carried away into the flow).

When T increases considerably (T > 150 C) the conversion into magnetite is very fast (Eq. 28), and it tends to form a more protective film (less porous) which leaves only a few ferrous ions to be removed by the flow.

The influence of temperature on wear rates is important from the point of view of controlling corrosion-erosion. In order to provide a fix for the steam extraction lines of power stations it is necessary to test the material of interest and observe its behavior for the range of temperatures between 100 C to 190 C. This is part of the experimental work that will be described in future sections.

2.3.2.3 Velocity -

Corrosion-erosion has in general been observed at points of hydrodynamic disturbances in the fluid flow (orifices, valves, bends). This fact points to the idea that a mass transfer process at the oxide-water interface must be the final important step in a chain of physical-chemical phenomena.

Attempts have been made to relate wear rates to local mass transfer rates.

Until now there is no strong correlation between the mass transfer coefficients and the experimental values of the wear rates. In fact it is possible to find experimental results where wear rates are proportional to h_d (Berge, 1980). There are cases where the wear rate is

proportional to $h_d^{8/7}$ (Heitman and Kastner, 1982) and cases where the wear rate has been found to be dependent on h_d^3 (Bignold, 1981). All this suggests that the wear rate may be a complicated function of velocity which may take different forms depending on the range of operating temperatures or hydrodynamic conditions. It also suggests that in order to study the phenomenon, well defined hydrodynamic conditions are important.

In any case, the controlling aspect for corrosion-erosion wear is the elimination of places of high turbulence, where mass transfer rates are likely to increase.

2.3.2.4 Hydrogen Ion Concentration (pH) -

A considerable reduction of the wear rate by corrosion-erosion is achieved by increasing the pH from a value of 7 to 9.5.

This phenomenon is understandable from the information given in Section 2.1.5.2. The formation rate of ferrous hydroxide (Eq. 17) decreases as the concentration of hydrogen ions decreases (pH increases) because the oxidizing power of the environment decreases.

As in the case of velocity, the dependence of the wear rate on pH has not been well correlated, but, in general it is expected that the wear rate will be close to a linear dependence with the hydrogen ion concentration (Bignold, 1980).

2.3.2.5 Material Composition -

Material composition has a very strong influence on the wear rates of steel. Some work has been done in this field (Heitman and Kastner, 1982; Faber, 1981). An example of this experimental work is shown in Fig. 13.

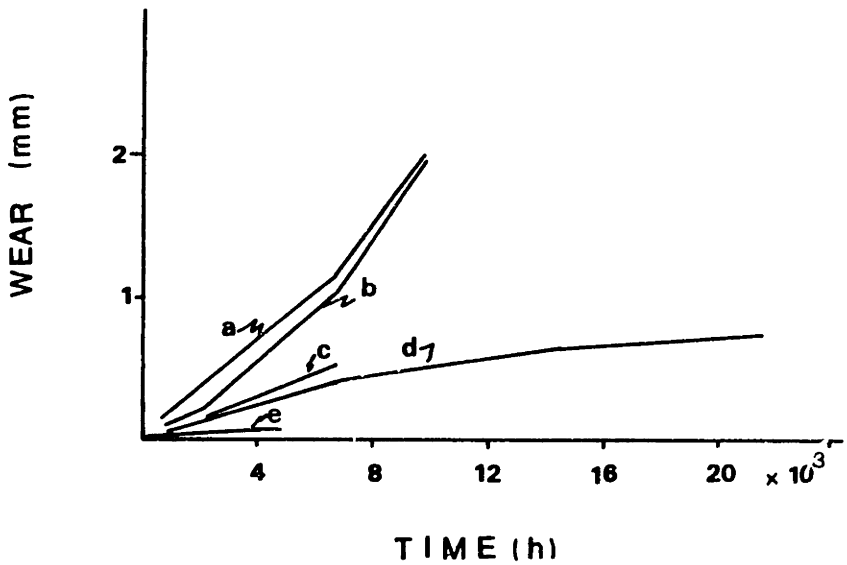

Figure 13. Corrosion-erosion of low alloyed steel, PWR environment: a) 0.15C 0.5Mo; b) 0.2C; c) 0.15C 0.8Cr 0.7Cu; d) 0.15C 2.2Cr/Mo; e) 0.15C 5Cr, (Faber et al., 1982)

As expected, the stainless steels are very corrosion resistant. This is mainly a result from having in their composition chromium (sometimes molybdenum and copper have also proved beneficial (Berge, 1982)). When Cr is present in the material, the inner layer of magnetite is a chromium-rich spinel structure. This layer has good protective characteristics against corrosive-erosive wear.

It is considered that the selection of appropriate materials, like the utilization of 13% Cr, could completely alleviate corrosion-erosion wear, but, in many

cases, the use of 2.5% Cr offers sufficient resitance to wear.

2.4 RECAPITULATION

With the literature survey of the previous sections the reader must have a general knowledge of the way in which steel corrodes.

It is worth keeping in mind that in corrosion-erosion a corrosion layer of constant thickness covers the metal. The layer acts as a constant resistance and tends to yield a linear law for the wear rate. It is also important to recall that there is a critical temperature for which wear rates are maximum and that in order to correlate the influence of velocity with wear rate, very well defined hydrodynamic conditions are required during experimentation.

Finally, it is also worthwhile to remember that in the literature no model was found which could estimate wear rates from physical-chemical properties of the water, nor is there particular experience with the low carbon steel A155 Gr C55.

A complete model to describe the wear rate should be capable of incorporating the influence of temperature, pH, oxygen concentration, velocity and material composition on the wear rate.

There was no reason to believe that the influence of the above variables on the wear rate of A155 Gr. C55 was

to be different than explained previously. The experiments described in the following chapters show that, indeed, the wear rate for the material of interest behaved as described above.

CHAPTER 3

DERIVATION OF A MODEL FOR CORROSION-EROSION

In this chapter, the model of corrosion-erosion is derived from the background information provided in previous chapters.

3.1 INTRODUCTION

As shown in previous sections, the removal of material by corrosive-erosive wear is the result of several phenomena that include, among others, the initial reaction of pure iron with water and the final step of mass transport of hydroxides into the bulk flow of water. The oxide layer, formed on the iron plays an important role, by restricting the flow of water to the metal and the flow of hydroxides by diffusion from the iron surface to the main water flow; this in turn affects the hydroxide concentration at the iron-oxide and oxide-water interfaces. Figure 14 has been developed in order to organize and help quantify these

individual effects. This figure is now explained.

The first step is to consider a porous oxide layer, the pores being filled with water. It is through these pores that the different species diffuse.

Process A. At the metal-oxide interface in the regions where the pure metal is in contact with the water the iron is converted into hydroxides, (Eqs. 17,18, and 19). During this conversion hydrogen molecules are produced and hydrogen ions are consumed (the pH and the hydrogen concentration near the metal surface increase with respect to the conditions in the bulk of the water). The consumption of hydrogen ions activates water dissociation to maintain the ionic product of $[H^+][OH^-]$ constant.

Process B. The high concentration of hydroxides at the metal oxide interface favors the transformation of hydroxides into magnetite (the Schikorr reaction, Eq. 28); part of the dissolved iron from process B becomes oxide and is deposited on the porous layer.

Process C. The fraction of iron not converted into oxide diffuses to the outside by concentration gradient (the diffusion rate is controlled by Ficks Law). The hydrogen concentration at the metal-oxide interface is also higher than at the metal-water interface causing a net diffusion of

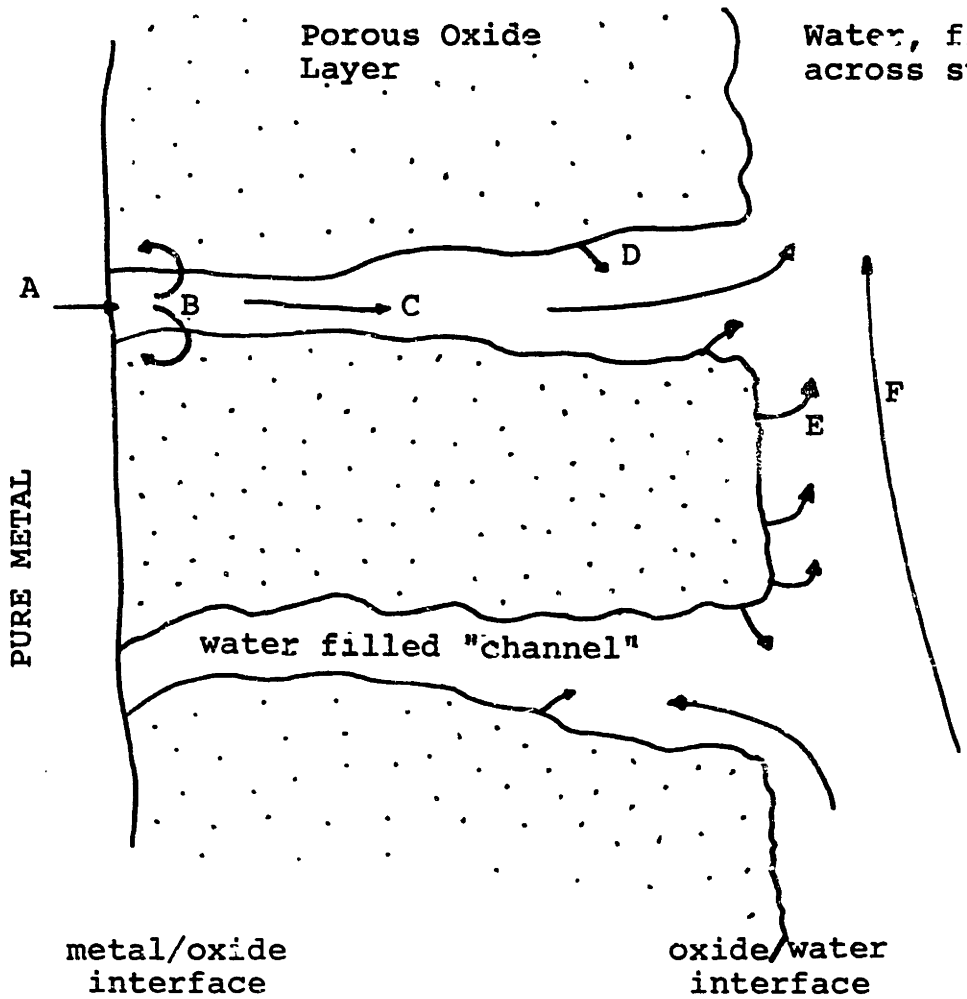

A. Iron hydroxides are generated:

$$Fe + H_2O \rightarrow Fe(OH)_2 + H_2$$

B. Magnetite is formed according to the Schikorr reaction:

$$3Fe(OH)_2 \rightarrow Fe_3O_4 + H_2 + 2H_2O$$

C. A fraction of the hydroxides formed in step B and H_2 generated in steps A and B diffuse through the oxide.

D. Magnetite can dissolve in the pore.

E. Magnetite dissolves at the oxide-water interface.

F. Water flow removes the different species by a convection mass transfer mechanism.

Figure 14. The different phenomena occurring during corrosion-erosion.

hydrogen towards the water interface.

Process D. Through the pores the concentration of the hydroxides is lower than the saturation concentration; therefore, some oxide dissolution takes place inside the pore.

Process E. At the oxide water interface, the concentration of hydrogen ions is the highest; this favors the transformation of the magnetite into hydroxides (Eq. 29).

Process F. Water removes iron hydroxides by a forced convection mass transfer porcess.

Other Processes. 1) Since reactions ten towards equilibrium at any point in the pore the magnetite can dissolve, in accordance to Eq. 32, to yield other hydroxide species besides $Fe(OH)_2$.

2) If the oxygen content is high, other oxides besides magnetite can form, namely haematite (Fe_2O_3). This formation would also be accompanied by the diffusion of oxygen to the metal-oxide interface and therefore provide for an additional path for electrons to be consumed (i.e., another cathodic reaction, Eq. 3).

The complicated picture of processes involved during corrosion-erosion (see Fig. 14) implies that rates of hydroxide formation, magnetite dissolution water dissociation and mass transport mechanisms of diffusion through the layer and to the water, all have

to be considered for an accurate simulation of the phenomena.

Through the knowledge of reaction rates, it would be possible to indentify the limiting processes which determine wear rates, and also make transient analysis of the initial wear period which is responsible for the final thickness and porosity of the oxide layer.

Unfortunately, the reaction rate expressions for the different chemical equations are unknown. A general expression for reaction rates involves the products of the concentration of the reactants to different powers. The unknowns would be numerous and to carry out experimental work to obtain the value of unknown variables was beyond the scope of this work especially if more than one hydroxide species were taken. A different approach was considered. The model presented in this chapter was built up from a simple set of ideas.

3.2 INITIAL STEPS IN THE DEVELOPMENT OF THE MODEL

The starting point for the derivation of the model comes from considering three important experimental findings. These are:

1. The wear is a linear function of time.

2. The wear rate is maximum at a temperature between 250 to 350 F.

3. The wear increases with velocity.

Any model must be consistent with all three of these experimental observations.

The last consideration suggests that if hydrodynamic conditions are important and, there is no mechanical attack on the metal, the mass transfer from the oxide water interface is the final step for the removal of the soluble species.

This rate of mass transfer can be modeled as a diffusion process, whereby the relevant equation is, (Bignold, 1981):

$$\frac{dm}{dt} = h_d(C_1 - C_\infty) \quad , \qquad (31)$$

where dm/dt = wear rate

h_d = coefficient of mass transfer

C_1 = soluble iron species concentration at water-oxide interface.

C_∞ = soluble iron species concentration far from the oxide-water interface.

Equation 31 was the foundation from which the model of corrosion-erosion was based.

The difficulty in using Eq. 31 lies in determining

the correct mass transfer coefficient and the correct concentration at the interface oxide-water.

Expressions for the mass transfer coefficients as a function of Reynolds and Schmidt numbers are of the form (Rohsenow and Choi, 1961)

$$\frac{h_d d}{D} = \alpha Re^{\beta} Sc^{\gamma} \quad , \qquad (32)$$

where V = velocity

ν = kinematic viscosity

d = characteristic dimension,

Re = Reynolds number ($= Vd/\nu$)

D = coefficient of diffusivity

Sc = Schmidt number ($= \nu/D$)

α, β, γ = constants, typically $\beta = 7/8$, and $\gamma = 1/3$.

The actual value of the constants and the definition of a characteristic dimension depend on the geometry of the material being damaged. Only for simple flow conditions, such as for a flow inside a tube or over a flat plate, are the characteristic dimension and the value of the constants α, β, and γ well known.

For the case of a thin film of water in the inside of a bend of a steam extraction line an expression for h_d needs to be sought.

This thesis has focused on obtaining a relation

for C_1, the concentration of the diffusing species at the oxide water interface. This relation must be a function of temperature, pH, material composition, and velocity.

In the following sections, 3 different relations to determine the wear rate by corrosion-erosion are discussed. The relations provide, implicitly or explicitly, a relation for C_1. The first two expressions are only intermediate steps in the derivation of the model of corrosion-erosion, Section 3.5.

3.3 THE SIMPLEST MODEL $C_1 = C_e$.

The simplest alternative is to consider that the concentration of soluble iron species at the oxide-water interface is the concentration obtained when the reaction of magnetite solubility (Eq. 29) is in equilibrium (C_e).

Assuming this model the mass transfer rate would be given by

$$\frac{dm}{dt} = h_d(C_e - C_\infty) \quad , \qquad (33)$$

where h_d = mass transfer coefficient

C_e = equilibrium iron concentration for magnetite solubility

C_∞ = iron species concentration far from the oxide/water interface.

Although the above equation is simple to implement for a geometry where the mass transfer coefficient, h_d, is known, the relation lacks consistency with the experimental findings. As can be seen in Fig. 11 for the range of temperatures between 100 and 200 C (200 to 370 F) the solubility of magnetite (equilibrium concentration of soluble iron species) does not have a maximum; as a consequence wear rates would not peak around 150 C and thus this relation, by itself is insufficient.

3.4 CONSIDERATION OF MASS DIFFUSION THROUGH THE OXIDE

A second step in complexity of the model adds in the resistance to diffusion of species through the oxide layer, Ficks Law of diffusion, Eq. 34 below.

In this case, the model would assume that the concentration at equilibrium (C_e) exists at the metal-oxide interface and that the active species diffuse through the pores in the film of thickness δ. Figure 15 gives a sketch of this model.

Since the wear rate should be linear and the thickness of the oxide constant, there is no possibility of accumulation of species inside the oxide layer.

The oxide layer must be porous to allow the species to diffuse to the oxide-water interface. In the pores

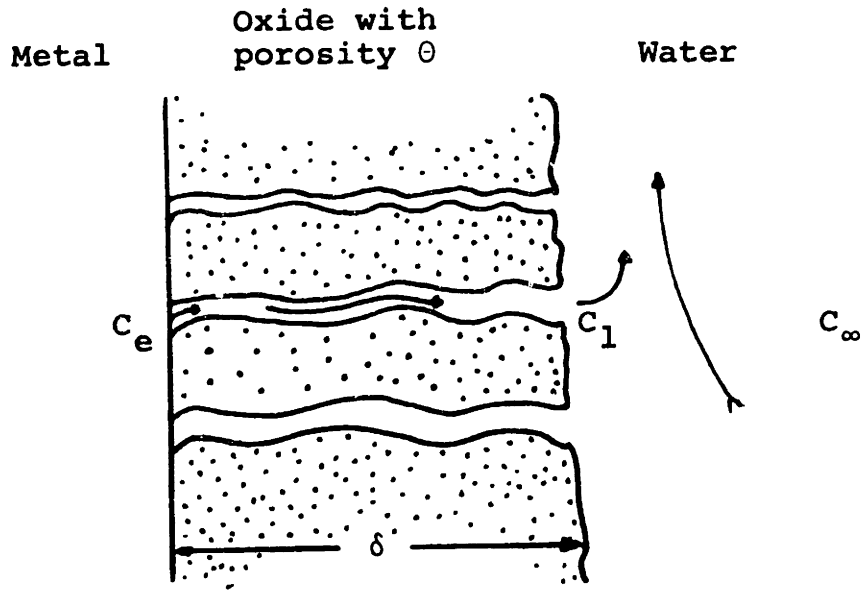

Figure 15. Model of corrosion-erosion including diffusion of iron species through the layer.

the concentration of hydroxides is below saturation level so there is no possibility of clogging, but some dissolution may take place. This model disregards this dissolution process. Equation 33 needs to be modified to account for the wear per unit area of metal per unit time, by considering the porosity Θ. The porosity is regarded as the porous space per unit volume of oxide, as well as the available corrosion area per unit area of metal.

The diffusion in the oxide layer occurs only through the pores. On the oxide surface the mass transfer process is approximated by assuming that the concentration C_1, exists only at the pores. The next

step in the derivation of the model is obtained by considering the following two equations:

$$\dot{m}'' = \frac{D\Theta}{\delta}(C_e - C_1) \quad , \qquad (34a)$$

$$\dot{m}'' = h_d (C_1 - C_\infty) \quad , \qquad (34b)$$

where $m = dm/dt$ = wear rate per unit area of metal

D = diffusion coefficient of iron species

Θ = porosity

δ = oxide thickness

h_d = mass transfer coefficient

C_e, C_1, C_∞ = iron hydroxide concentration at equilibrium at oxide water interface and in the bulk of the fluid respectively.

To reveal the important features of this model, let us assume that the concentration of the diffusing iron species at infinity is zero.

By eliminating C_1 from Eq. 34 a and b, the wear rate becomes:

$$\dot{m}'' = \frac{\Theta C_e}{\frac{1}{h_d} + \frac{D}{\delta}} \quad , \qquad (35)$$

Equation 35 still fails to model the wear peak as a function of temperature. It includes the variation of

C_1 with velocity to a non fixed power, a feature which agrees better with the experimental findings. Furthermore, the equation allows for the evaluation of the resistance $1/h_d$ and D/δ. The calculation, which was done with values of D, and h_d given in a later section, showed that the resistances are of comparable magnitude and that both should be included in the model.

What equations 33 and 34 have not done is to account in some meaningful way for the reaction kinetics that occur at the metal-oxide interface. So far these kinetics have been lumped into C_e.

In order to overcome the above difficulty, the information provided in the section "Corrosion of Steel in Water" will be used to incorporate the reaction rate kinetics within the model.

3.5 PROPOSED MODEL FOR CORROSION-EROSION

3.5.1 Description Of The Model

The model presented here is based on the explanation given for the corrosion of steel in section 2.2.2.

The first step that was considered in the oxidation of steel is the formation of iron hydroxide. In oxygenless water the hydroxide is converted into magnetite (Heitman and Kastner, 1982). Equations 17 and 28 describe these steps.

$$Fe + H_2O \rightarrow Fe(OH)_2 + H_2 \quad , \qquad (17)$$

$$3Fe(OH)_2 \rightarrow Fe_3O_4 + 2H_2O + H_2 \quad , \qquad (28)$$

Making reference to Fig. 10, recalling that in static corrosion the reactions tend to stop when the concentration of hydroxides reaches the solubility limit, the major assumption of the model is made. This is the consideration that the reaction at the metal-oxide interface takes place at a rate which is proportional to the difference between the concentration given by the solubility limit i.e., the "equilibrium" of iron species and the actual concentration of iron species at the metal-oxide interface ($C_e - C_o$).

The solubility limit of iron species is here taken as the equilibrium concetration of species for the reaction in Eq. 29 i.e.,

$$Fe(OH)_2 + (4-3b)H_2O \rightarrow Fe_3O_4 + 3(2-b)H^+ + H_2(g) \quad , \qquad (29)$$

The reaction rate at the metal oxide interface will be considered a first order reaction, as:

$$\dot{m}'' = K(C_e - C_o) \quad , \qquad (36)$$

where K is a reaction rate constant specific for each material. Assuming an Arrhenius expression for K (K.=.AlExp(-El/RT), Eq. 37 becomes:

$$\dot{m}'' = \{A_1 \mathrm{Exp}(\frac{-E_1}{RT})\}(C_e - C_o) \quad , \qquad (37)$$

where A_1 = pre-exponential factor

E_1 = activation energy

R = universal gas constant

T = temperature

C_e = equilibrium concentration of iron species at the metal oxide interface.

C_o = concentration of iron species at the metal oxide interface.

The choice of a first order reaction will be justified or disproved by the results below, but the expectation was that, together with the rest of the assumptions, Eq. 37 represents a minimum model to explain the major features of the results.

3.5.2 Model Equations

The picture presented in Fig. 14 is now modified as shown in Fig. 16; this is the picture used to derive the model of corrosion-erosion.

It is convenient in this section to recapitulate and list all the assumptions that yield the model of

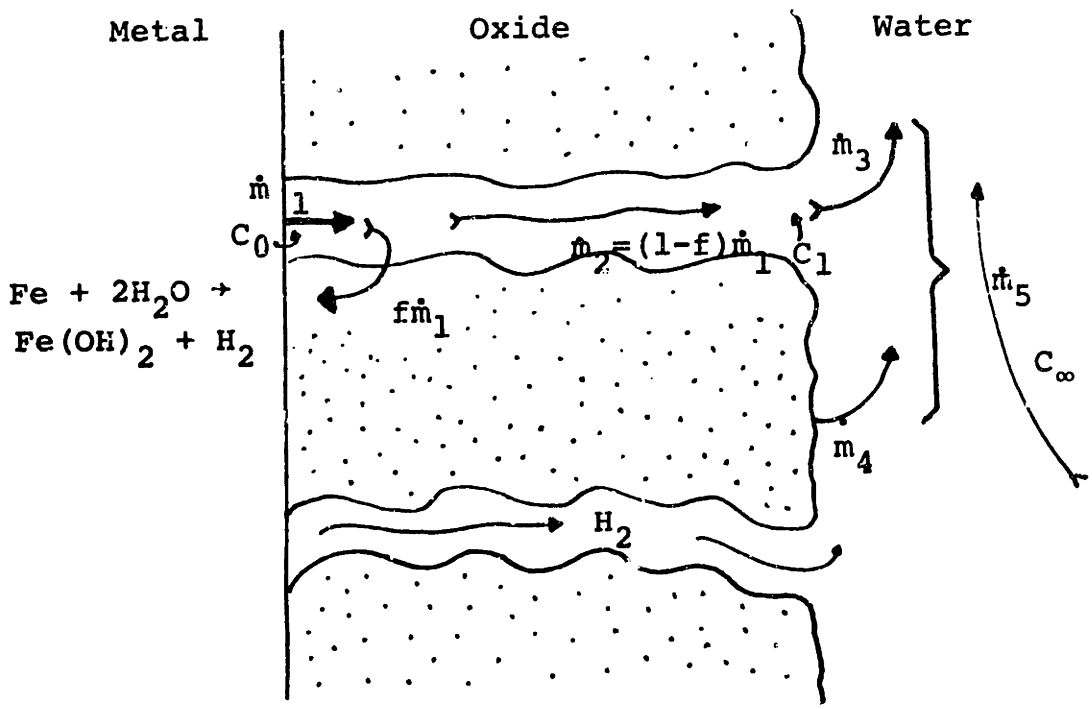

$\dot{m}_1$ = oxidation rate
$\dot{m}_2$ = diffusion through porous oxide
$\dot{m}_3$ = mass transfer to the water
$\dot{m}_4$ = oxide dissolution.

Figure 16. Processes included in the corrosion-erosion model.

corrosion-erosion.

Assumption 1.- Only steady state is considered The oxide layer has been developed and its thickness (δ) and porosity (θ) have a constant values. This first hypothesis assumes that corrosion brings about the formation of magnetite with a subsequent oxide fracture that leaves the layer with a constant porosity. Simultaneously, the layer is assumed to remain at a constant thickness by producing magnetite on the metal oxide

interface at the same rate that oxide dissolves at the oxide-water interface. This assumption also makes reference to the amount of hydroxides being formed in the pore. If the resistance to corrosion is constant, neither the porosity nor the layer thickness can change as a function of time. The amount of magnetite formed at the metal base has to be the same as that being dissolved in the pore and on the oxide-water interface. The assumption in the model is that the major part of the dissolution takes place on the oxide surface, where the H^+ concentration is the greatest; as a result, the diffusion through the pore remains unaffected.

Assumption 2.- Of the amount of iron oxidized at the metal-oxide interface a fraction f is converted into magnetite and this is the same amount being removed at the oxide-water surface. It has been assumed that f has a fixed value of 0.5, this is based on the static experiments of the corrosion of steel, where in general the outside oxide layer had the same amount of iron as the inner layer.

Assumption 3.- There is no net circulation or flow of water inside the oxide layer; therefore the simulation of the transport of species inside the layer can be considered as a concentration diffusion problem.

Assumption 4.- The water is oxygen free, and the

only oxide present is the magnetite.

Assumption 5.- The reaction rate at the metal-oxide interface proceeds at the rate $\dot{m}_1'' = K(C_e - C_o)$ where $K = A_1 EXP(-E_1/RT)$.

Assumption 6.- The hydroxides diffuse through the pores due to differences in concentration from the metal to the water. The diffusion path length is considered to be equal to the oxide thickness.

Assumption 7.- At the oxide-water interface, the concentration at the pores is C_1, but everywhere else, it is different. The mass transfer from the pores to the water is considered to be equal to $h_d(C_1 - C_\infty)$, and the mass transfer from the non-porous oxide is equal to the amount of oxide formed at the metal-oxide interface, see Fig. 16.

The list above permits the use of the following equations to represent the wear rate ($\dot{m}''$):

$$\dot{m}_1'' = K\Theta(C_e - C_0) \quad , \quad (38)$$

$$\dot{m}_2'' = (0.5)\dot{m}_1'' = \frac{D\Theta}{\delta}(C_0 - C_1), \quad (39)$$

$$\dot{m}_3'' = (0.5)\dot{m}_1'' = h_d\Theta(C_1 - C_\infty), \quad (40)$$

This system of 3 equations with three unknowns (m_1, C_o, and C_1) can be solved for $\dot{m}_1''$. A complete derivation

of the solution can be found in Appendix B; here to reveal the important characteristics of the model, we assume that C_∞, the concentration of iron species in the bulk of the fluid, is zero.

The resulting equation is:

$$\dot{m}_1'' = \frac{C_e \Theta}{\frac{1}{K} + (0.5)\{\frac{1}{h_d} + \frac{\delta}{D}\}} \qquad (41)$$

where: $\dot{m}_1''$ = wear rate ($mol/cm^2 s$)

C_e = equilibrium concentration of iron species obtained from Fig. 11 (mol/cm^3)

Θ = porosity (cm^2 open area/cm^2 metal, $cm^3 H_2O/cm^3$)

h_d = mass transfer coefficient

$K = A_1 Exp(-E_1/RT)$ = reaction rate constant (cm/s)

f = fraction of oxidized metal converted into magnetite at the metal-oxide interface (a constant with value 1/2)

D = diffusion coefficient of iron species in water (cm^2/s)

δ = oxide thickness (cm)

C_∞ = 0. = iron species concentration in bulk of the fluid (mol/cm^3)

The suggested value for each of the constants and

for each variable that appears in the equation is given in Section 6.2.4.2, where the method to calculate the wear rate from Eq. 41 is reviewed. In this section general comments about the method to obtain each variable are made.

Temperature, pH and hydrogen ion concentration in the bulk of the fluid are assumed to be known.

There are a number of relations that can be used to determine the diffusion and the mass transfer coefficients. The relation for diffusion coefficient used in this study was found in Rohsenow and Choi (1961), and the expression used to calculate the mass transfer coefficient was given by Berger et al.(1977). These relations are given in section 6.2.1.

A range for the values of porosity ($0.001 < \Theta < 0.1$), was suggested by Surman and Castle (1969).

Values of the thickness of the oxide layer, can be determined experimentally by measuring it under a scanning electron microscope, results will show that δ is of the order of 1 μm.

The equilibrium concentration of iron species at the metal-oxide interface, C_e, depends on the pH and the hydrogen concentration at the metal-oxide interface. In accordance to equation 16 and 17 two hydrogen ions are consumed and one hydrogen molecule produced for each Fe(OH)2 that is formed. It is hence possible to write conservation equations for hydrogen and to arrive at the

following equations that describes the hydrogen concentration at the metal-oxide interface

$$H_{2_0} = \dot{m}_1'' RT\left\{\frac{}{D_H^{\Theta}}\left(1 + \frac{1}{3}f\right) + \frac{1}{h_{d_{H_2}}}\right\} + H_{2_\infty} \quad , \quad (42)$$

where H_{2_0} = hydrogen concentration at metal-oxide interface (atm)

$h_{d_{H_2}}$ = mass transfer coefficient for hydrogen (cm/s)

D_H = diffusion coefficient of hydrogen in water (cm^2/s)

R = universal gas constant ($atm*cm^3/mol\ K$)

T = temperature (K)

$\dot{m}_1''$ = the wear rate, Eq. 41

H_{2_∞} = concentration of hydrogen in the bulk of the fluid (atm)

For the hydrogen ion, it is assumed that the dissociation of water is fast enough so that the concentration of H^+ at the metal-oxide interface always satisfies the ionization product for water, K_W. The equation for hydrogen ion concentration at the metal oxide interface becomes

$$H_0^+ = H_\infty^+ - 2C_0 + \frac{-A + (A^2 - B)^{\frac{1}{2}}}{2} \qquad (43)$$

where: H^+_∞ = hydrogen ion concentration in the bulk of the fluid (mol/cm^3)

$C_o = C_e - \frac{m_1}{h_d \theta}$ = iron hydroxides at the metal-oxide interface (mol/cm^3)

K = Dissociation product of water at the temperature of operation (mol^2/cm^6)

$A = H^+_\infty - 2C_o + K_w/H^+_\infty (mol/cm^3)$

$B = 4[(H^+_\infty - 2C_o)K_w/H^+_\infty - K_w]$ (mol^2/cm^6)

The derivation of Eq. 42 and 43 are given in Appendix B.

Equations 41, 42, and 43 represent a system of 3 equations with 3 unknowns $\dot{m}''_1$, H_{2_o} and H^+_o. The three equations constitute the model of corrosion-erosion.

At this stage the only unknown parameters are constant A_1 and E_1, which determine the value of the reaction rate constant K.

With experimental values of $\dot{m}''$ for a well controlled experiment (h_d, T known) it is possible to obtain K for different temperatures and velocities by using Eq. 41.

If the model is correct a plot of ln K vs 1/T should yield a straight line whose slope will be the activation energy E_1 and the intercept with the y-axis will be A_1. With E_1 and A_1 known, a procedure to estimate wear rates is available.

3.5.3 Characteristics Of The Model

The model has two parameters which have opposite effects with rising temperature. As the temperature increases, K increases exponentially, in contrast to C_e which decreases also exponentially. These opposing influences were expected to yield the wear rate peak as a function of temperature.

The model also includes variation of wear rate with velocity. The variation is not explicit since besides h_d, C_e also depends on velocity through Eq. 42.

At this point it is convenient to test the model and verify that it satisfies the conditions for very high or very low velocities.

3.5.3.1 Diffusion Controlled -

In this case, the value of the reaction rate constant K would be much greater than the value of the resistances related to h_d and D. With very large K, Eq. 41 reduces to:

$$\dot{m}_1'' = \frac{C_e \, \Theta}{(0.5)\{\frac{1}{h_d} + \frac{\delta}{D}\}} \cdot \qquad (44)$$

This is an adequate result which indicates that the concentration at the metal-oxide interface would reach C_e and that the controlling mechanism is the diffusion of species through the layer (δ) and into the water (h_d).

3.5.3.2 Kinetically Controlled -

In this case h_d and D would be large compared to K. In this case Eq. 41 would be modified to

$$\dot{m}''_1 = K\Theta C_e \quad . \quad (45)$$

This equation expresses the maximum rate at which the reaction proceeds under conditions of extremely rapid removal of iron species.

The results in these sections provide some assurance that the model has the correct characteristics.

A final screening test is whether or not a straight line can be obtained when plotting ln K vs. 1/T. For this purpose it is necessary to obtain wear rate data. The experimental work that was needed to accomplish this task is now discussed.

CHAPTER 4

EXPERIMENTAL STUDIES

This chapter describes the main features of the design and operation of the corrosion-erosion loop. It also reviews the procedures for preparing a sample and for determining wear rate data.

4.1 GENERAL FEATURES REQUIRED FROM THE EXPERIMENT.

The experimental work served two purposes: it provided detailed data of corrosion-erosion rates for the material of a steam extraction line under a range of actual operating conditions, and it was used to guide development of the corrosion-erosion model.

4.1.1 Steam Extraction Line Characterization

In order for the corrosion-erosion loop to simulate adequately the conditions of steam extraction lines and for the information gathered to be readily applied to power stations, it was desired for the rig to have the

following characteristics:

1. The testing material should be the same as that found in power stations steam extraction lines.

2. The temperature range of operation should be from 220 to 370 F.

3. The pH of operation should be between 5 and 10.

4. The oxygen contents should be low (200 ppb) and the hydrogen concentration should be around 20 ppb.

5. The velocity of the water in the loop should be comparable to the velocity of the water film in the steam extraction line (30 ft/s).

It is worth remembering that the present study deals with the mechanism of mass transfer of iron species from the oxide to liquid water. The regions where the wear takes place in the inside of a bend are those where a liquid film is present. For this reason, the experimental apparatus is a single phase liquid water system. The model developed in the previous section is in accordance with this situation.

4.1.2 Experimental Work Aimed At Developing The Corrosion-Erosion Model

The experimental work must provide well defined hydrodynamic conditions. A simple geometry that permits mass transfer coefficients to be estimated from expressions in the literature is preferred. Although impinging flow on plates and flow through orifices may cause considerable weight loss, which makes it easier to measure, the hydrodynamics related to these geometries are complicated. For example Bentrcia (1982) conducted experiments of wear by solid particles through an orifice. His results showed that the pattern of wear was non-symmetrical. In this report, therefore, the decision was made to consider flow through an annulus, with the inside wall of the annulus being the material tested. Figure 17 shows the specimen assembly.

A geometry as simple as an annulus allows the mass transfer coefficient to be determined and makes it possible to use Eq. 41 to obtain the values of K.

4.2 DESCRIPTION OF THE EXPERIMENTAL APPARATUS.

Having defined what was needed for the wear test loop to yield useful information, it was designed and constructed accordingly. In this section only the major decisions in the design of the rig are included. The interested reader may find some of the design guidelines

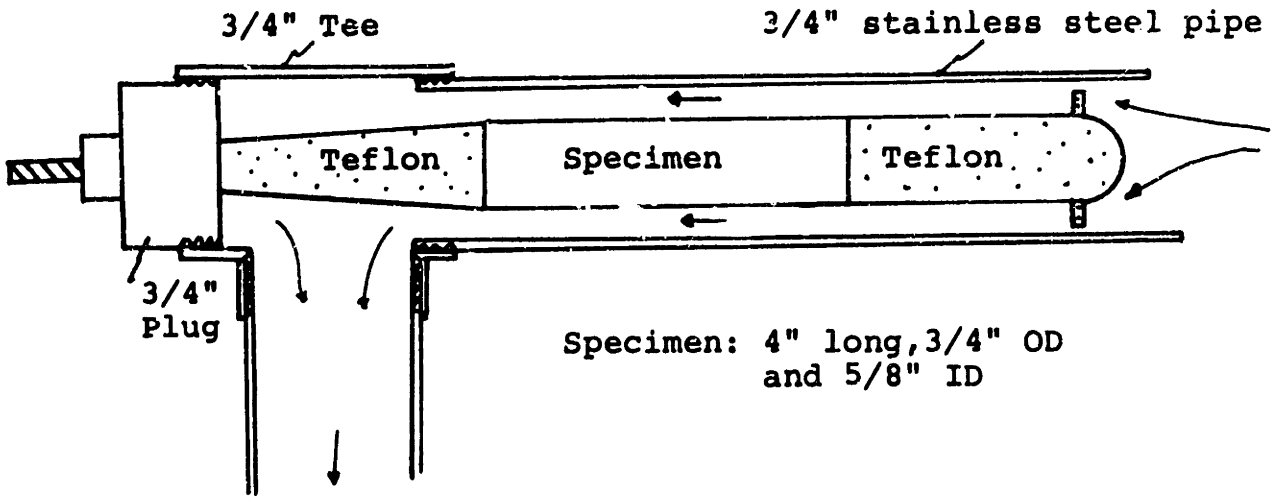

Figure 17. Specimen assembley.

in Appendix C.

The easiest method by which wear rates can be determined is by measuring the weight change produced by corrosion-erosion on a fixed area during a certain period. The longer the period, the less the error in the determination of the wear rates. A period of more than 200 hours was believed to be necessary for a constant wear rate to be developed (Heitman, 1982, Berge, 1980).

During this time, a specimen was subjected to a constant flow of water with fixed values of temperature and pH.

To heat distilled water at 320 F, to pass it

through the specimen, and to throw it away is a very costly and therefore unwise alternative. Recirculation of the water was necessary. In order to accomplish this task, a pump and a pressure vessel were used. The pump recirculated high pressure and high temperature water. The vessel, in turn, served as a reservoir of water; in it the pressure was kept constant and the fluctuation from the pump or any other part of the system were damped.

The loop was made of stainless steel. This prevented high wear rates everywhere except at the place where the material was tested.

To keep the water clean, it was necessary to include as part of the rig a purification system that could return the water to the original condition. In pursuing the above purification, it was discovered that the resins that are used during the cleaning process only work with low temperature water, that is, below a temperature of 120 F. It was therefore necessary to cool the water before the ion exchanger and then raise it up to the original temperature level. The heat requirements to do the above cooling and heating would be of the order of 90 KW, an excessive amount. A recuperator could be used to avoid having to waste all that heat; but, the price of such a recuperator would be very high because temperature gradients across walls would be small and the heat transfer area requirement

would be excessive. For example, for a calculation of a 1/2" pipe in a 1" pipe counter-flow heat exchanger, the area requirements would be such that the total length of the recuperator would be about 110 ft.

In order to reduce the cost of the purification system, calculations were performed to estimate the influence that smaller percentages of purification would have on the total amount of mass removed by corrosion-erosion. The calculations were made according to Eq. 33 for an area of one square foot that was worn according to a mass transfer coefficient of 0.2 ft/h (Mahato, 1968) and an equilibrium concentration C_e at the oxide-water boundary. These assumptions were considered an upper limit to the amount of material removed (C_e was taken at a neutral pH and at saturated H_2 pressure conditions, Fig. 11).

The calculation was performed as follows. A time period Δt was defined as the ratio of the volume of the loop to the volumetric flow rate through the test section. For a given percentage of purification, the amount of material removed was obtained by calculating the concentration of iron species in the water for each cycle. A numerical procedure was used to calculate the total mass removed when only a part of the flow was purified. The result was then compared to the values of total mass removed obtained with 100% purification. The results showed that after 2 days, the "percentage of

agreement" between the two values gave a good idea of the final agreement at the 10th day. Table 3 gives the values of percentage agreement for different conditions of purification.

Table 3.

Removal mass in the abscence of total purification (two days).

Percent Purification	Agreement with 100% purification
0 %	4.6 %
5 %	90.2 %
10 %	95.1 %
15 %	96.7 %
20 %	98.0 %

The table shows that important improvements are reached from 0 to 10% purification. Purification of 10% of the water was equivalent to only 10% of the heat requirements, i.e., 9 KW. This was the design value chosen.

At this point, the elements of the corrosion-erosion loop have been established Figure 18 shows a flow diagram that includes the major components of the rig.

Although the design and construction of the corrosion-erosion rig were important achievements in the

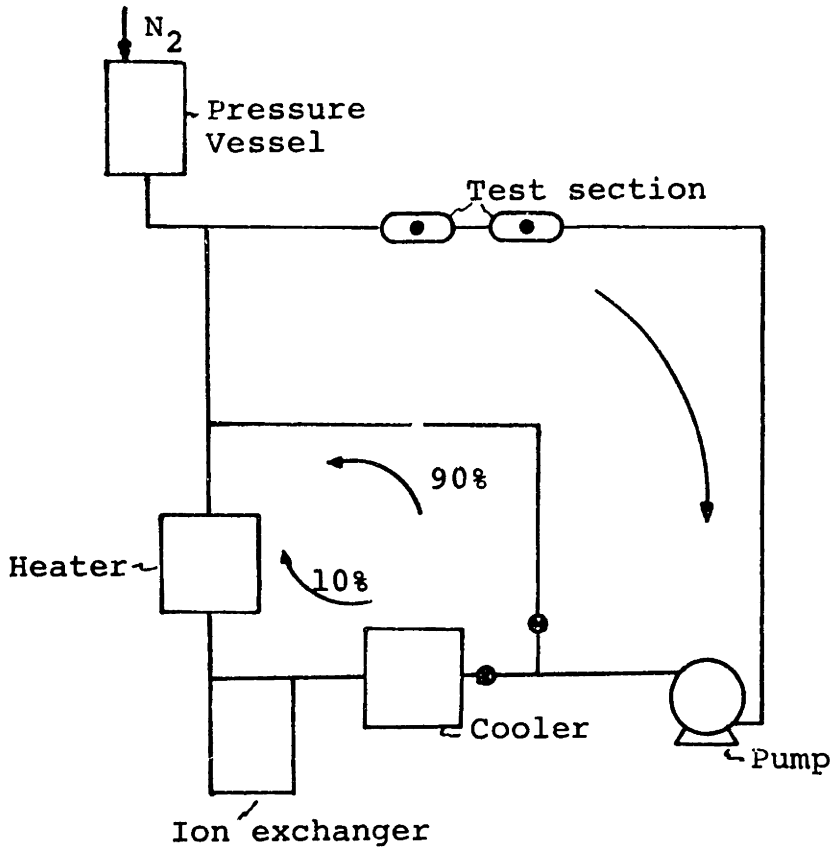

Figure 18. The components of the corrosion-erosion rig.

present work, for the purpose of continuity, the description of each component has been left for Appendix C. Figure 19 gives an idea of the dimensions and arrangement of the different components of the system.

4.3 THE CORROSION-EROSION EQUIPMENT.

4.3.1 Specimen Preparation.

The material from which the specimens were made was A155 Gr C55. This material is equivalent to SA285 Gr C and is part of the steam extraction lines of Boston Edison Pilgrim Power Station. The material is a low

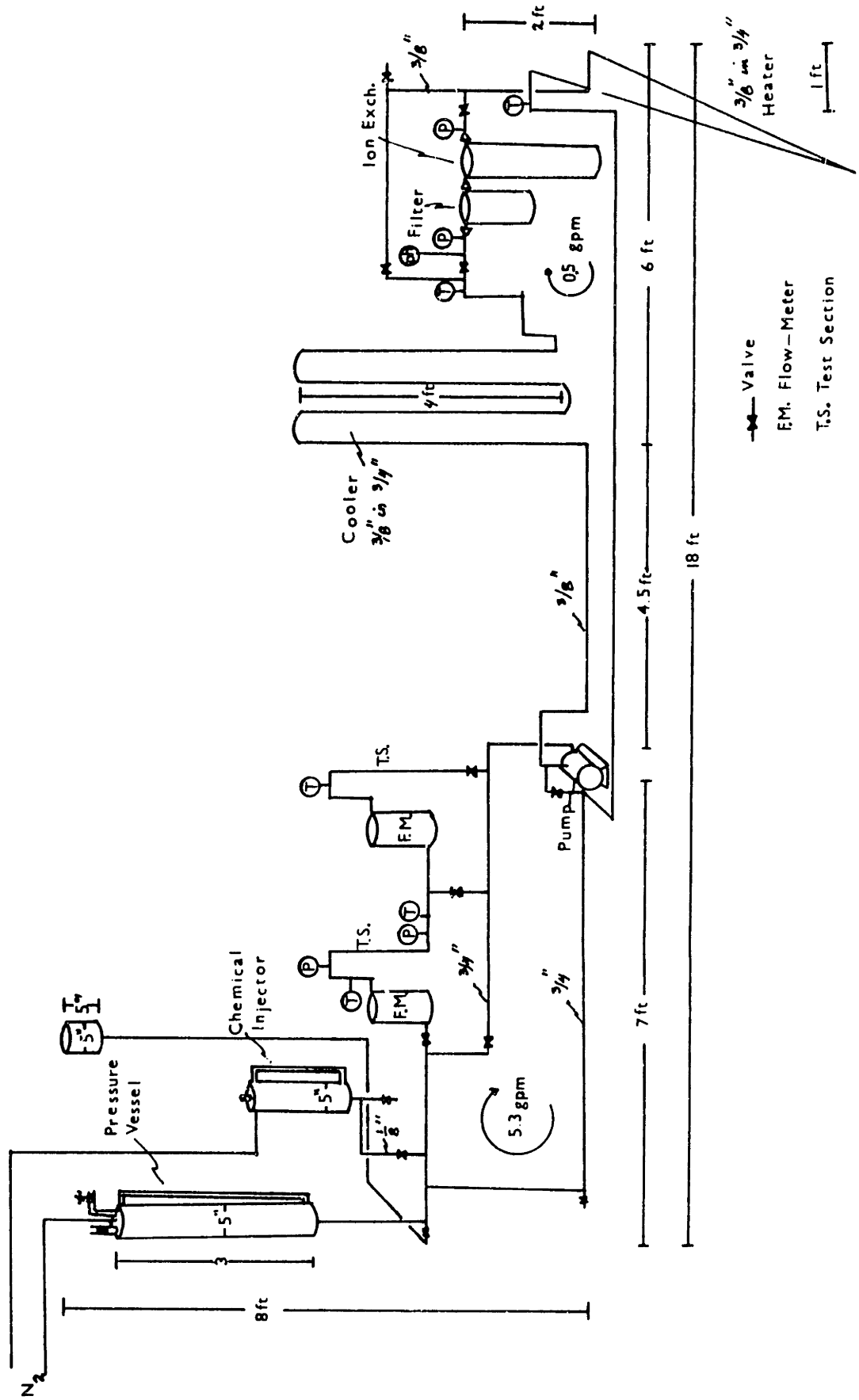

Figure 19. Dimensions and arrangements of the corrosion-erosion rig.

carbon steel of the following composition (ASME, 1974; Metals Handbook, 1961):

ELEMENT	COMPOSITION (%)	
	Limits	Average
Carbon	0.11 to 0.28	.17
Manganese	0.28 to 0.90	.45
Phosphorous	0.00 to 0.035	-
Sulfur	0.00 to 0.045	-

Preparation of the sample includes a machining and cleaning process; these procsses are now reviewed.

4.3.1.1 The Machining Process -

The specimen (Fig. 17) was made from a 2" plate A155 Gr C55. The plate is cut into a 1" x 1" x 4" square bar. The specimen is then machined , using the lathe, to the dimensions of Fig. 17 (OD = 3/4", ID = 5/8", with tolerance ±0.005"). The machining procedure as well as the cleaning technique are recommended to be the same for all specimens. The machining procedure which was followed is described in Appendix D.

4.3.1.2 Cleaning Process. -

Before the specimen was weighed, adequate cleaning to remove all grease and oxide on the surface was performed. The procedure used was obtained from ASME, 1981.

The specimens were first cleaned with propylalcohol. Once they were dry (with air or a clean cloth), they were put into a solution of one part hydrochloric acid to three parts of distilled water for 1/2 hour. After this period, the specimen was quickly rinsed in 3 baths of water, dried with air, and placed in a desiccator. The initial weight was then recorded.

It is worth mentioning that once the specimen is cleaned, it should not be touched, either by bare hands or gloves.

4.3.2 The Test.

Having recorded the initial weight of the specimen, the test section was assembled by threading the pieces of teflon on the ends of the specimen. With the specimens assembly ready, it was put inside the rig, which by that time was full of hot distilled water and had been venting for about 15 minutes.

The test started at the moment that the temperature in the loop was close (±20 F) to the desired condition. At that moment the valves of the test section were opened During the first transient period while

reaching the conditions of interest, the velocity and temperature through the test section were recorded every 5 to 10 minutes. After an hour or two, the system stabilized and only required that the external variations of the city water flow rate to the heater, and the decrease in pressure because of small leaks, be compensated by the appropriate movement of valves. In this manner, the test is run for a period of 10 to 15 days. During the test, recordings of the flow rate and temperature conditions at the test section were done at least 3 times a day. Often, external influences to the system, (electrical shut-off, city water or steam restrictions) caused transients which influenced conditions considerably.

A detailed procedure for the operation of the loop has been left for Appendix E. The information in this appendix should be useful to the next person who will operate the rig.

In the final day of the operation the pump was stopped, the pressure was released and the specimen was taken out of the loop; it was then allowed to cool for about 5 minutes in air before disassembling the test section. The specimen was then rinsed in distilled water, dried with air, and its final weight was recorded.

4.4 POST TEST DETERMINATIONS.

From the weight change measurements, the surface area available for wear, and the period of the test, the wear rate was calculated.

More information from the experiment was obtained by performing three further tests: descaled weight change determination, scanning electron microscope examination (SEM) and the determination of the chemical composition of the oxide by using the X-Ray Photoelectron Spectrometer (XPS).

4.4.1 Descaled Weight Change Determination.

In an effort to correct a limitation linked to the geometry of the test section, it was decided to obtain the final weight loss by removing the oxide left on the specimen at the end of the test.

The limitation needing correction was the water leakage to the inside of the specimen during the course of the experiment. An unexpected oxide layer was formed in the inside. It was thought that the determination of the weight of the inside oxide layer would give more accurate data of the wear rate. The decision to remove the oxide layers from the inside as well as the outside of the specimen was taken, and, in so doing, an average rate at which the metal was oxidized was calculated. The method of calculation of how the weight of the

outside and inside oxide layers were determined and how these results influence the wear rates are explained in the discussion section. Here we simply describe the procedure that was followed to descale the specimens.

The method by which specimens were descaled was by submerging the specimen in Clark Solution (ASME, 1981). This solution consists of mixing 20g of antimonium trioxide and 50 g of stannous chloride in one liter of hydrochloric acid. Since descaling takes place very quickly, it was preferred to maintain the solution cool (≈4 C).

To prepare the specimen for this determination, it was first cut roughly in half,this allowed for some evidence to be left of how the specimen looked with the oxide layer.

The half of specimen to be descaled was rinsed in water, dried, weighed and its ends were plugged to prevent leakage of the solution to the inside. By using this method, it was possible to descale first the outside oxide layer. The determination of the amount of oxide on the outside consisted of submerging the piece of the plugged specimen in Clark Solution for several seconds (1 to 3 seconds). After the submersion, the piece was quickly rinsed, dried, and weighed. Repeating the same procedure yielded a curve of weight change vs. time such as the one shown in Fig. 20. the drastic change of slope caused by the slower rate at which metal

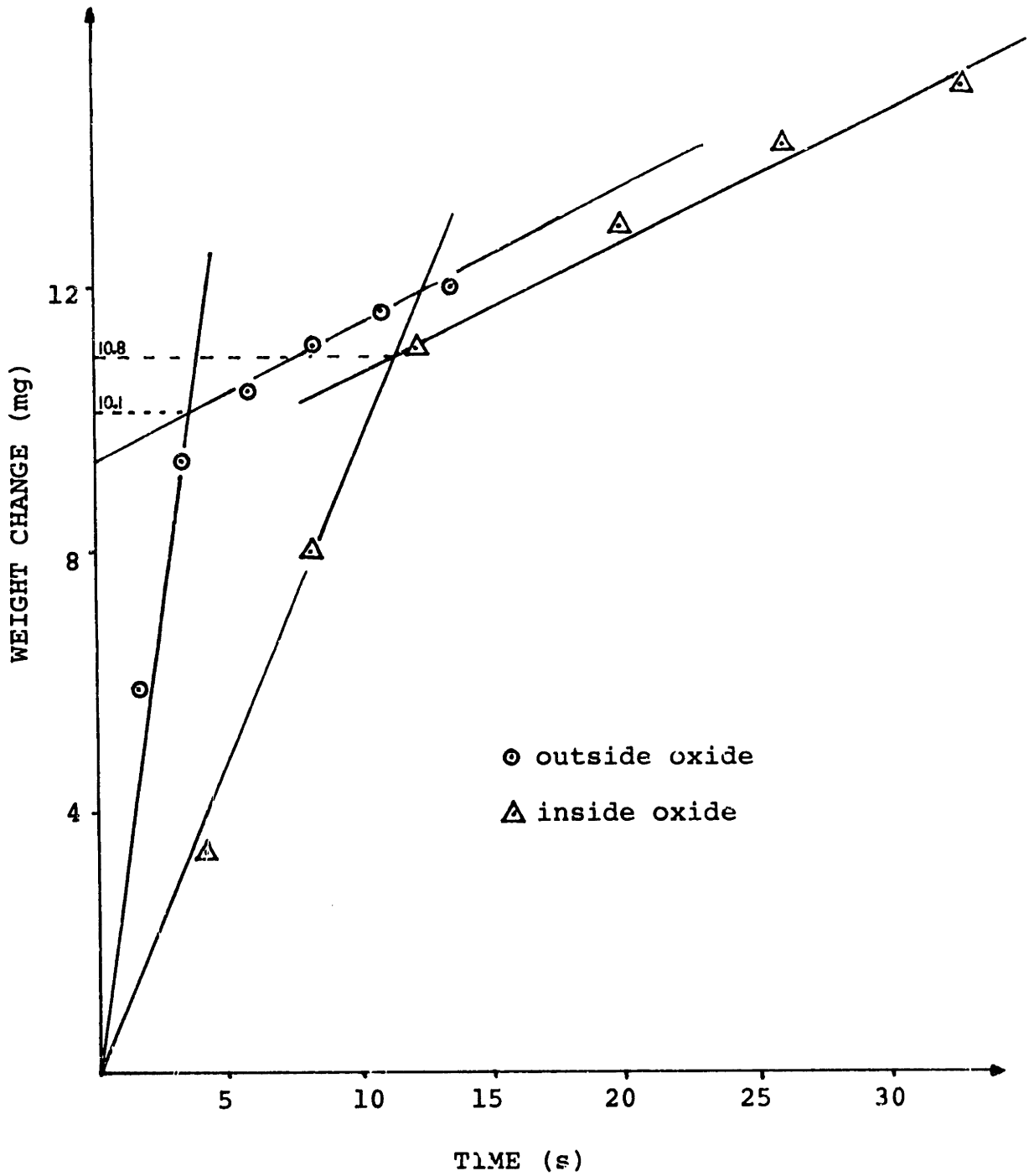

Figure 20. Curve of weight change vs. time during the descaling test.

is removed when compared to the oxide removal rate was used to determine the weight of the oxide layer.

Determining the weight of the inside layer required the same procedure as for the outside except that the specimen piece was plugged on one side only and the Clark Solution was poured inside.

4.4.2 Scanning Electron Microscope Examination.

Some of the specimens were cut to produce a sample of half the cylinder, 1" in length, as sketched in Fig. 21. This piece was then molded in bakelite according to standard techniques which involve heat and pressure (Gregor, 1983). The molded piece was then polished with successively finer sand papers (50, 120, 200, 320, 600) and finally on cloth with 0.3 and 0.05 μm alumina particles. The scratchless surface, a cross-section view of the specimen, was then etched with 2% nitric acid, coated with gold and then observed under the scanning electron microscope. Thickness and structure of the oxide layers were determined. Some of the pictures taken during these examinations are included in the results section.

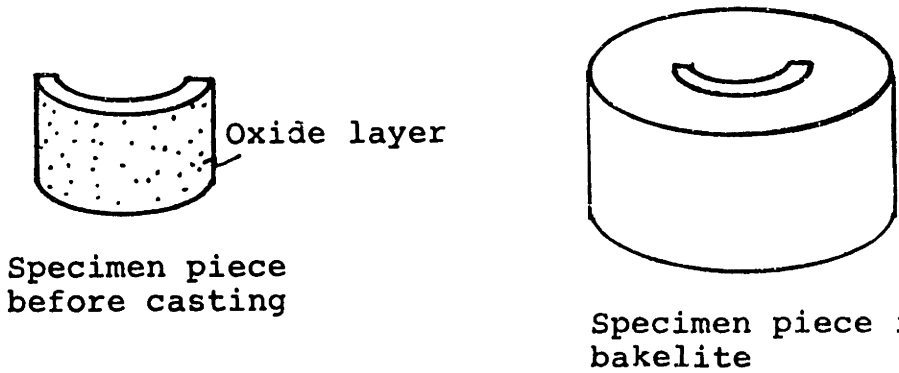

Figure 21. Geometry of the specimen piece that was observed under the scanning electron microscope.

4.4.3 Determination Of The Chemical Composition Of The Oxide.

This test was only performed on a couple of specimens. The idea was to verify that the black substance that remained on the specimens after the corrosion-erosion test was an iron oxide and, specifically, it was desired to determine which iron oxide it was, magnetite (Fe_3O_4) or Haematite (Fe_2O_3).

The results of these tests were inconclusive and excessive testing was not possible due to the busy schedule and the high cost of using the X-Ray Photoelectron Spectrometer.

Nevertheless, the information gathered is reported

in the results section and thus the procedure followed is here briefly described. The piece of the specimen to be examined had an area of 1 x 1 cm . It was sonically washed in methanol, dried, and placed in the spectrometer. In order to have a standard with which to compare, pure magnetite as well as haematite powder were bought from a local supplier. The magnetite powder was 95 % pure, while the haematite was 99 % pure. The powders were compressed into a small cylinder of 5 mm diameter and 4 mm length.

The technicians operating the spectrometer produced graphs of number of electrons counted vs. the energy spectrum. Depending on the position of the peaks where most of the electrons were collected, it is possible to determine the compounds which are present in the samples. The graphs that the spectrometer produced for the samples of interest together with the wear rate data are included in the following section.

It is important to note at this stage that the corrosion-erosion rig is a useful tool for testing materials subjected to corrosion. Its construction allows for different materials, different water environments and different geometries to be tested.

CHAPTER 5

EXPERIMENTAL RESULTS

In this chapter, the results from the corrosion-erosion test are shown together with the information gathered from the scanning electron microscope and from the X-Ray Photoelectron Spectrometer. The results are only presented here, whereas the detailed discussion of the same is left for next chapter.

The results which are about to be described were generated from wearing down a specimen of material A155 Gr C55 in the corrosion-erosion rig (see Section 4.3.1).

The tests were about 10 to 15 days long and they took place at 6 different temperatures ranging from 250 to 350 F, two different velocities and at a value of pH from 5.5 to 6.0 (this was the original pH of the Belmont Co. distilled water, our local supplier of distilled water).

The velocities for which tests were carried out were approximately 2 and 10 ft/s. The decision to

operate at these velocity conditions was the result of an unwanted restriction to the test section during the initial tests. The problem was corrected, but in order to make use of all the data, the tests that followed were still carried out at the same velocity conditions.

To determine representative values of the conditions of a test, the recorded values of temperature and flow rate at the test section were averaged in time. The value of temperature and flow rate at the test section at a given time were considered representative of conditions of the last period of the test (i.e., since the previous recording of the conditions).

One of the major concerns of the tests is related to the amount of dissolved oxygen that remained in the system. Degassing for 10 to 20 minutes was part of the standard startup procedure, and thus, there is reason to believe that oxygen conditions were similar for all tests. During some tests a Beckman 715 Oxygen Analyzer was used. Although this system is not recommended for measuring very low oxygen concentrations, estimates by using the instrument suggest that concentrations as low as 50 ppb were possible, but probably the average concentration of oxygen throughout the test was 200 ppb.

The experimental results are now described.

5.1 INITIAL REGION

To obtain information about the wear rates as a function of time, the specimens at 250 F were taken out of the loop several times during the course of the experiment. Weight changes at every period were recorded.

Figure 22 shows the weight loss for specimens at high and low velocities, 250 F and pH of 5.5. It is important to notice that the weight loss is calculated as the initial weight minus the weight at a particular time. A negative weight loss therefore stands as an increase in weight from its original value.

The figure shows that during a period of 50 hours after the beginning of a test, the weight of the specimen increases. After that, the specimen starts losing weight and it reaches its original weight at around 125 hours. The figure also shows that at around 150 hours (6 days) the wear rate becomes linear and that the high velocity test experiences, indeed, a higher wear rate than the low velocity.

5.2 PRELIMINARY CALCULATIONS

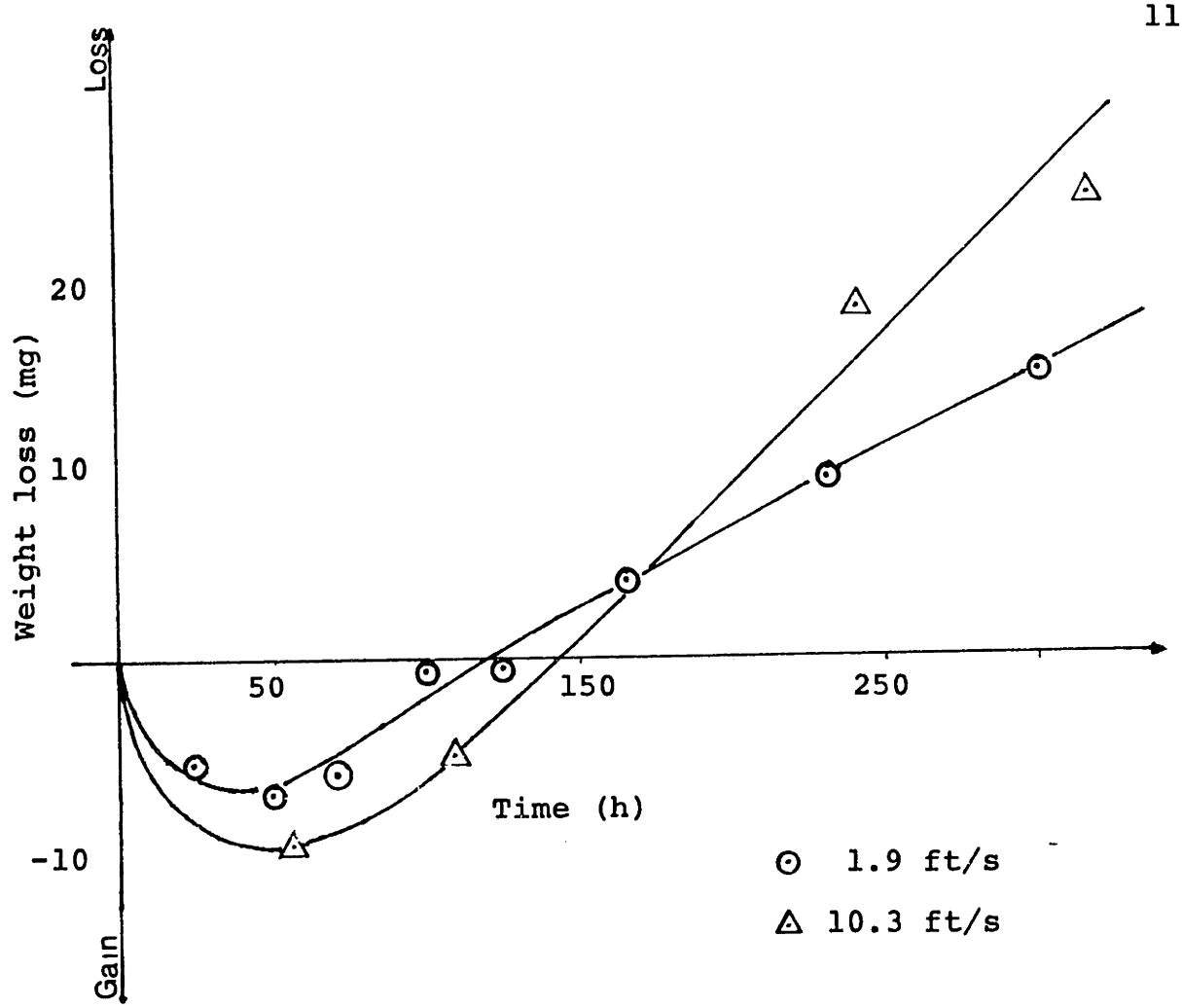

Figure 22. Weight change as a function of time, specimens at 250 F, pH=5.5.

5.2.1 Velocity Calculations

As mentioned previously, temperature and flow rate through the test section were averaged over time. With the averaged flow rate the velocity was calculated for the specific specimen by accounting for the area available for flow and a correction factor for changes in density due to temperatue; these changes affect the value determined for the flow through the flow meter.

The relation used to calculate the velocity is:

$$V = \frac{2.22 \times 10^{-3} QR}{A_f} \quad , \quad (46)$$

where: V = velocity in ft/s

Q = flow rate (gpm)

R = ratio of water density at the temperature of the test to standard water density

A_f = area of flow (area of an annulus in ft^2) given by the space between the specimen and the pipe wall, see Fig. 17.

2.22×10^{-3} = constant required to make the equation dimensionally exact.

5.2.2 First Estimate Of The Wear Rate

With the specimen weighed at the beginning and at the end of a test, the wear rate was first estimated as the total weight loss divided by the time of the test. The relation used to calculate the estimate of the wear rate is

$$\dot{\delta} = \frac{87600 \, \Delta W}{\rho_{met} t A_w} \quad , \quad (47)$$

where: $\dot{\delta}$ = wear rate expressed in mm/y

ΔW = weight change in g

ρ_{met} = metal density in g/cm

t = duration of the test in h

A_w = area available for wear in cm (πDL, D outside diameter of specimen, L its length).

87600 = constant required to make the equation dimensionally exact.

The raw data used in the calculations is provided in Appendix F; the results of using Eq. 47 are plotted in Fig. 23. The figure shows the wear rate for different temperatures at two different velocities.

From the figure it is evident that the wear rates of the specimens at low velocity are less than those at high velocity, and that there is a temperature for which the wear rate is maximum.

The error bars of each experimental value are a measure of the accuracy with which temperature and weight changes were determined.

5.3 OXIDATION RATE CALCULATION

As mentioned in section 4.4.1, a portion of the specimen was descaled and a correction for an inside oxide layer which should have not been formed was also made. The raw data used in calculating the total amount of oxidized iron is part of Appendix F. The raw data in the appendix consists of length of specimen used in the descaling test, the weight of the inside and outside

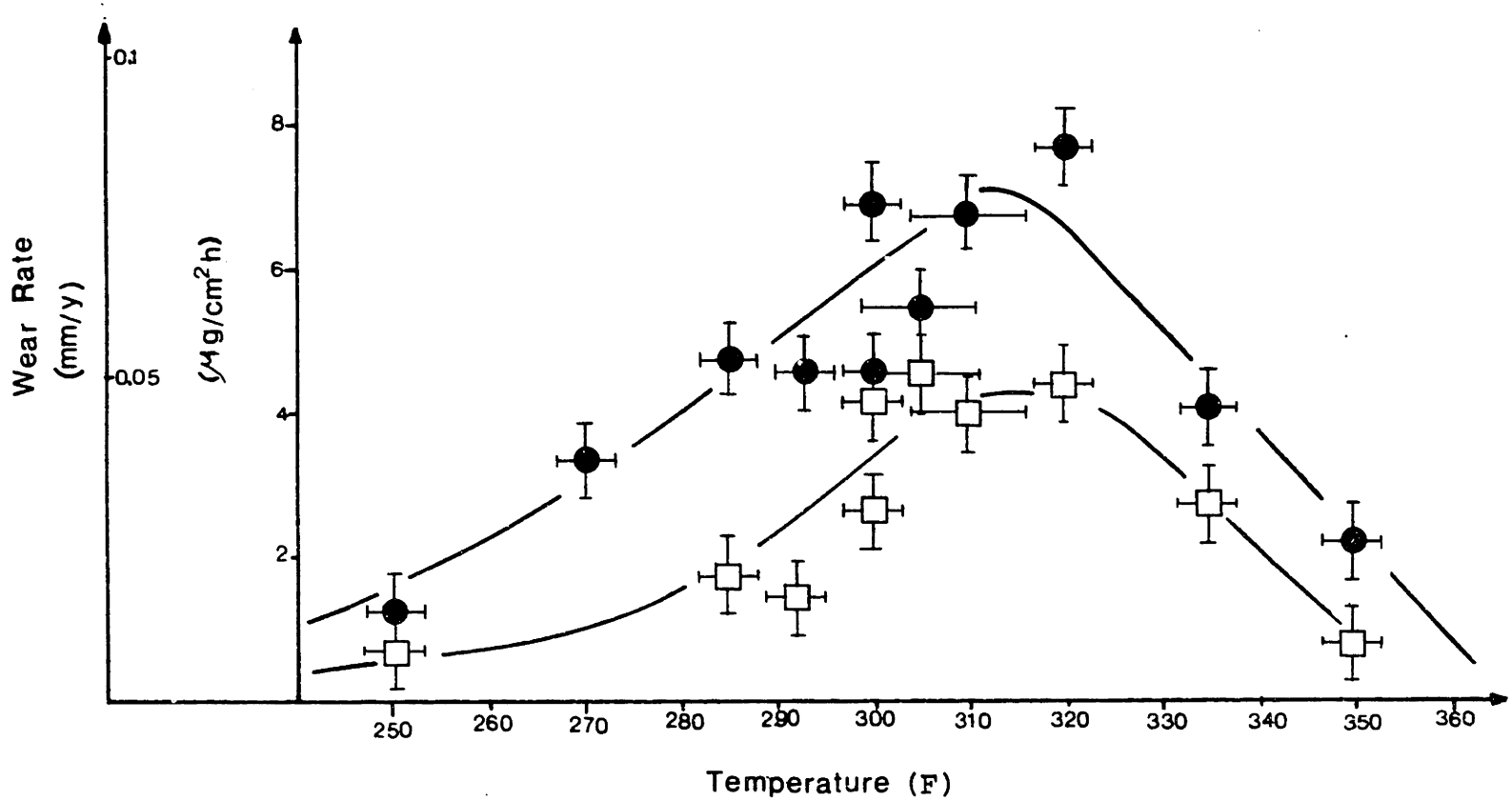

Figure 23. Wear rate (according to Eq. 47) vs. temperature experimental data for high (9.5 ft/s) and low (1.7 ft/s velocity, pH = 5.6.

oxide, the original weight change from begining to end of the test, and the length of the test to calculate the oxidation rate. The following equation was used to calculate this rate:

$$\dot{m}_1'' = (\Delta W + \{\Delta W_o + \Delta W_i * .276\} * \frac{L}{L_s}) * \frac{10^6}{A_w t} \quad , \qquad (48)$$

where:
$\dot{m}_1''$ = wear rate (g/cm h)
ΔW = original weight loss from the experiment (g)
ΔW_o = weight of the outside oxide (g)
ΔW_i = weight of the inside oxide (g)
L_s = length of the piece of specimen taken to be descaled (cm)
L = original length of the whole specimen (cm)
A_w = area available for wear (cm)
t = duration of the test (h)

Equation 48 suggests that the oxide on the outside should be considered as part of the total weight change, since it is iron that has been oxidized and it does not provide any strength to the material.

The third term in Eq. 48 corresponds to the correction of the wear rate for the oxide which should have not been formed in the inside of the specimen. Assuming that the oxide is magnetite ($Fe_3 O_4$), the

fraction of weight that corresponds to the oxygen (0.276) is the amount of material by which the specimen weight change is corrected. The iron in the oxide should not have reacted; and therefore, it does not enter into the correction. The descaled wear rates calculated from Eq. 48 are plotted in Fig. 24 for the high velocity points and in Fig. 25 for the low velocity points. The curves in the figures show the same characteristics as those in Fig. 23.

5.4 S.E.M. OBSERVATIONS

The techniques used to look at specimens under the scanning-electron microscope were not well developed. In some cases part of the oxide was removed, making it difficult to make measurements of oxide thickness. Gaps and extraneous materials were sometimes present and thus the pictures in this section only give an idea of the characteristics of the oxide. In the discussion section, under the heading of "Experimental Technique Improvements" ideas for making the procedure more representative are suggested.

The photographs in Figures 26 to 29 show a cross-section of different specimens.

The figures reveal that the oxide is a single layer of thickness 0.5 to 8 microns; there was no consistant trend of thickness vs. temperature or velocity.

Figures 30 and 31 shows the appearance of the

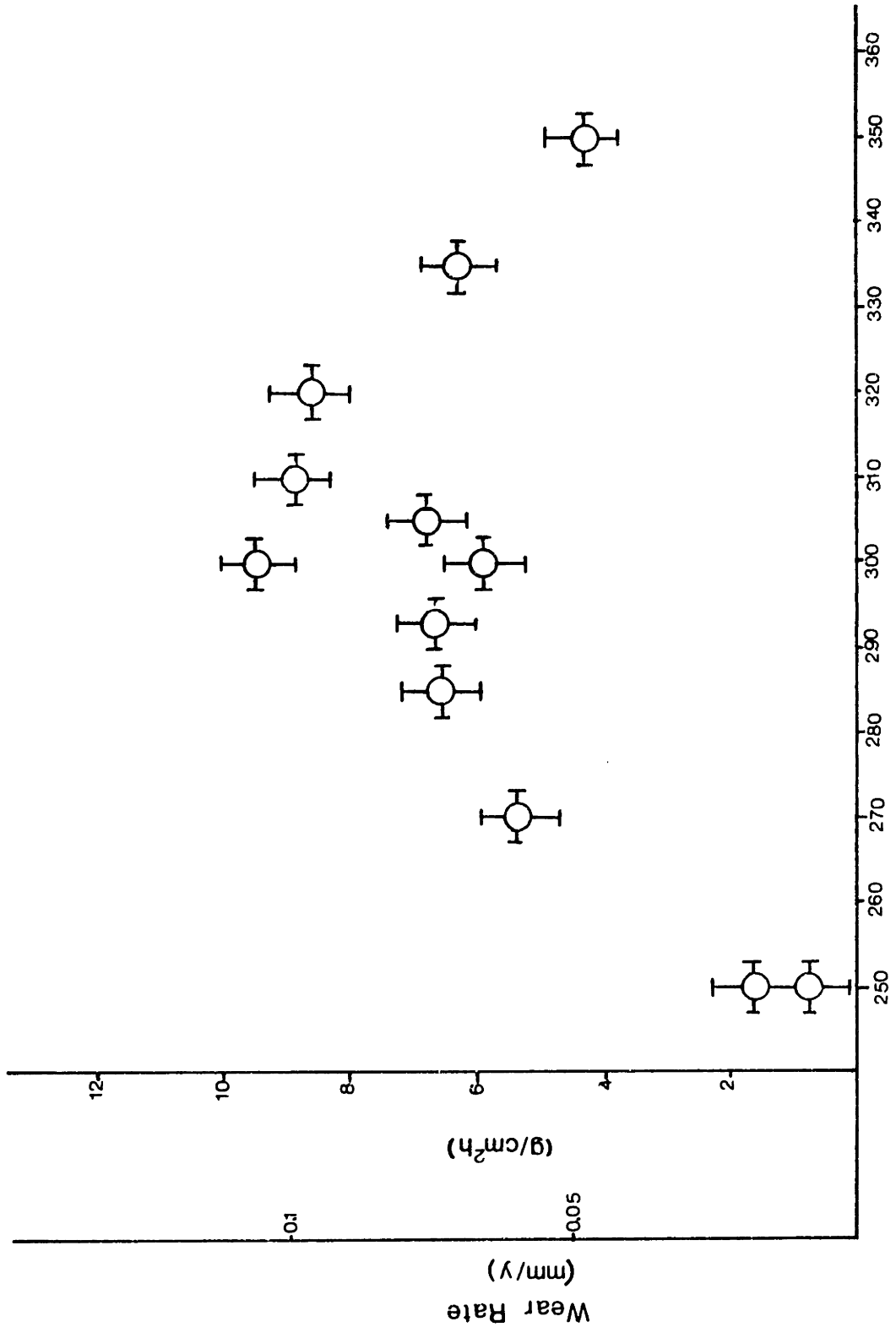

Figure 24. Descaled wear rate (Eq. 48) vs. temperature for high velocity specimens (9.5 ft/s), pH 5.6.

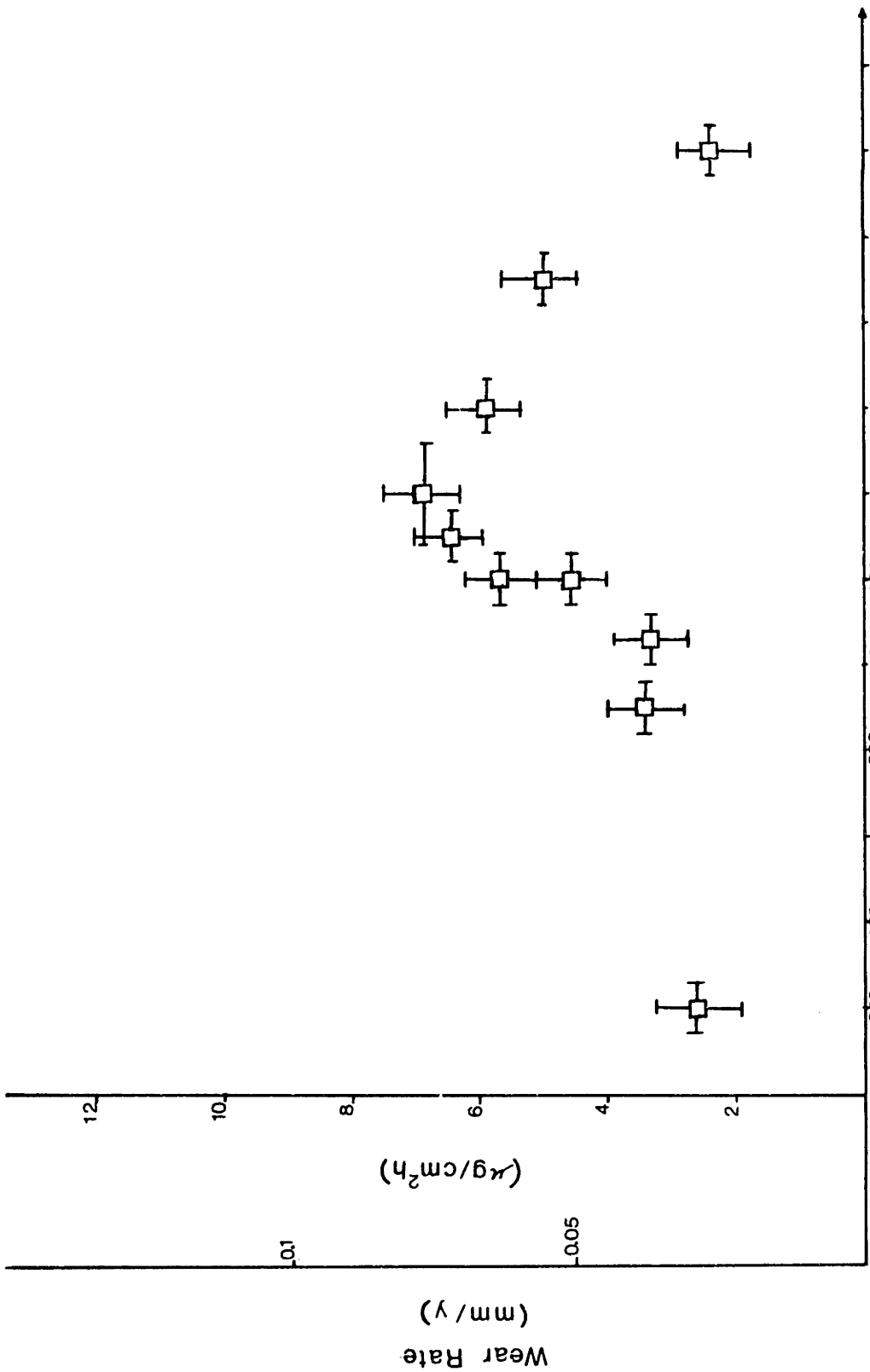

Figure 25. Descaled wear rate (Eq. 48) vs. temperature for low velocity specimens (1.7 ft/s), pH = 5.6.

X-1000

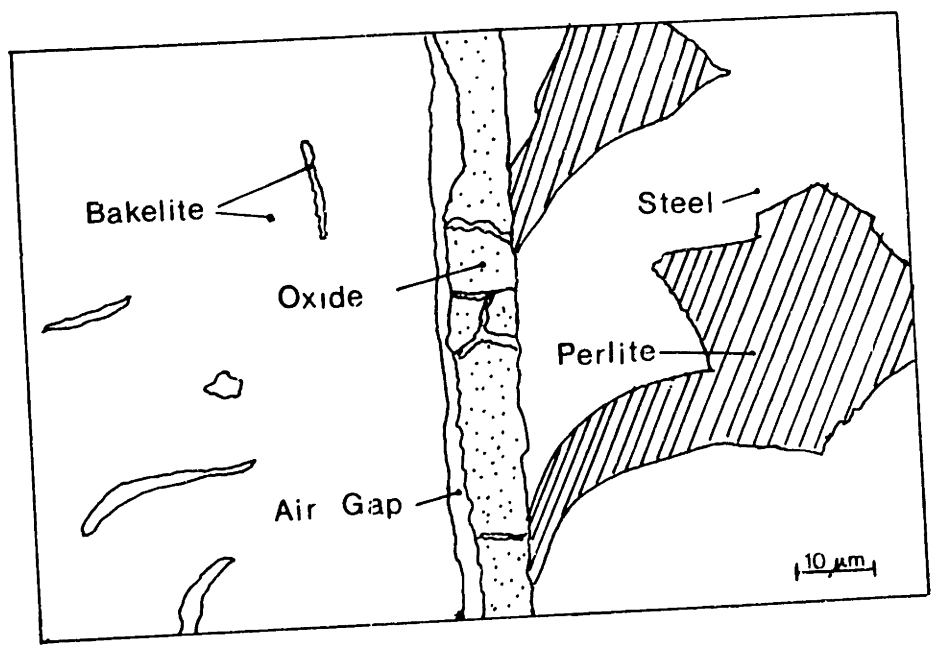

Figure 26. Oxide layer thickness δ for high velocity specimen (9.5 ft/s) at 270 F, δ = 8μm.

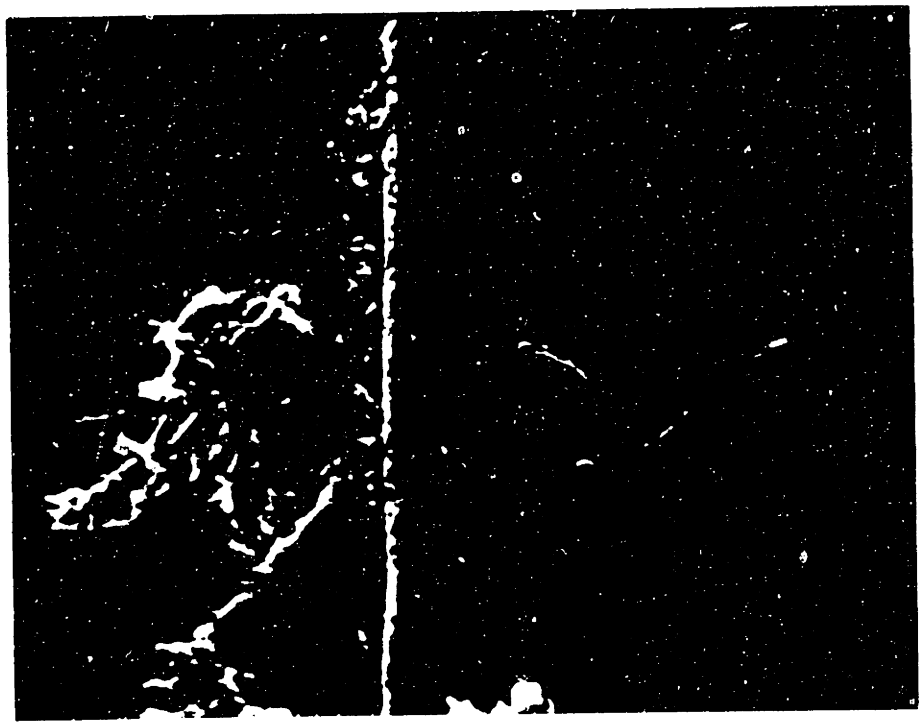

X-4500

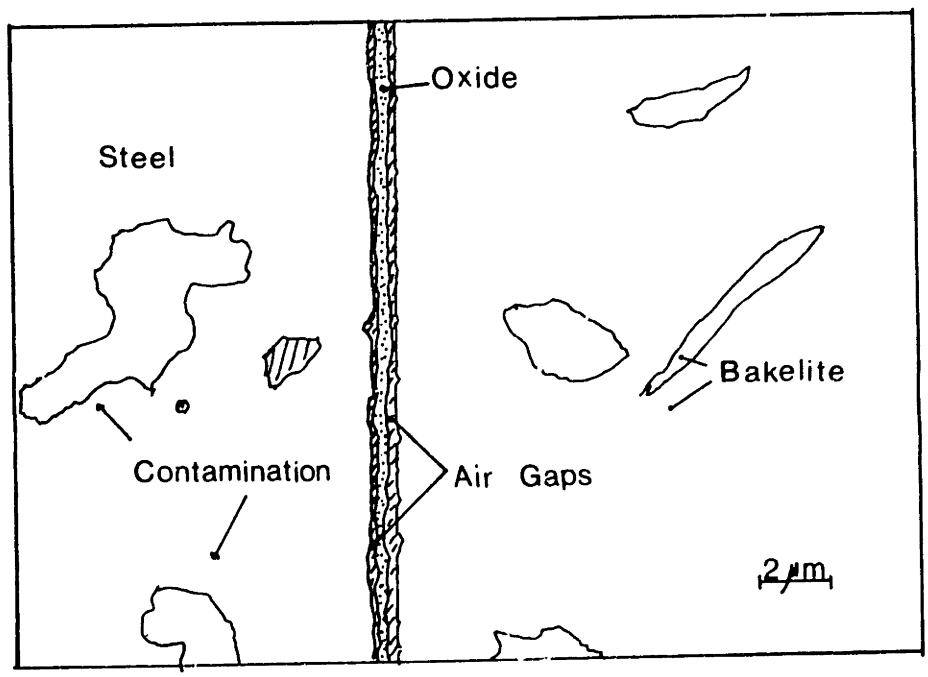

Figure 27. Oxide layer thickness δ for high velocity specimen (9.5 ft/s) at 285 F, δ = 0.4μm.

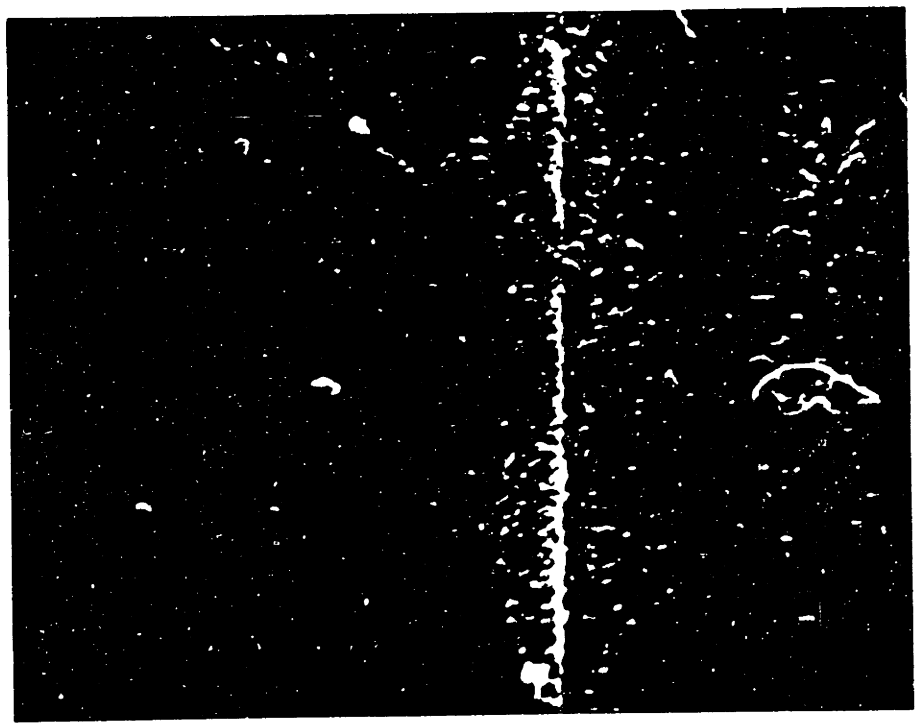

X-9400

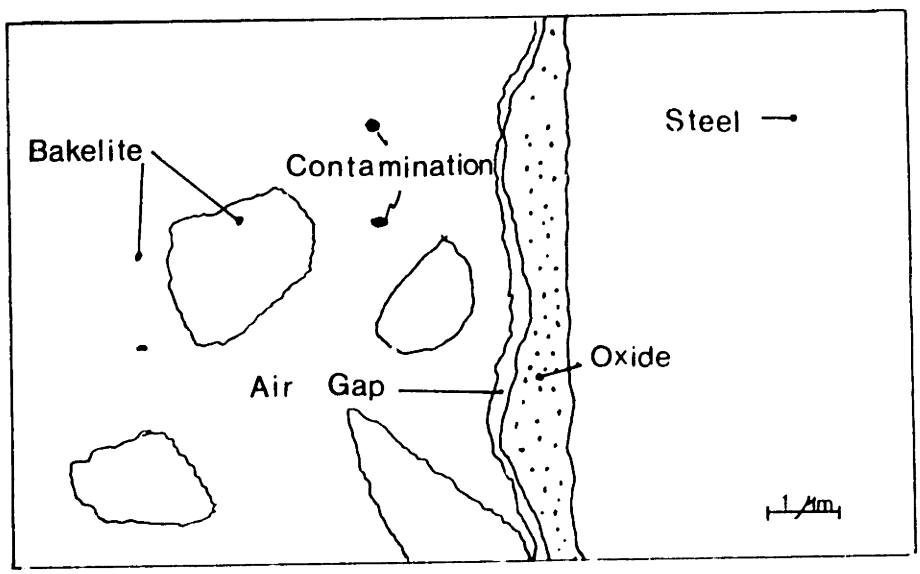

Figure 28. Oxide layer thickness δ for high velocity specimen (9.5 ft/s) at 293 F, δ = 0.8μm.

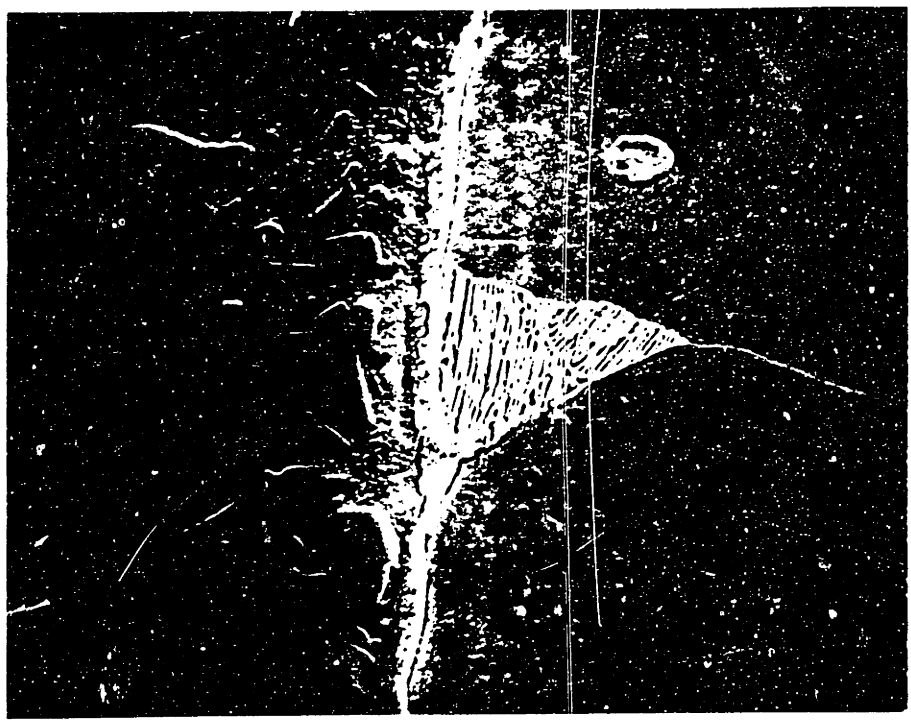

X-1800

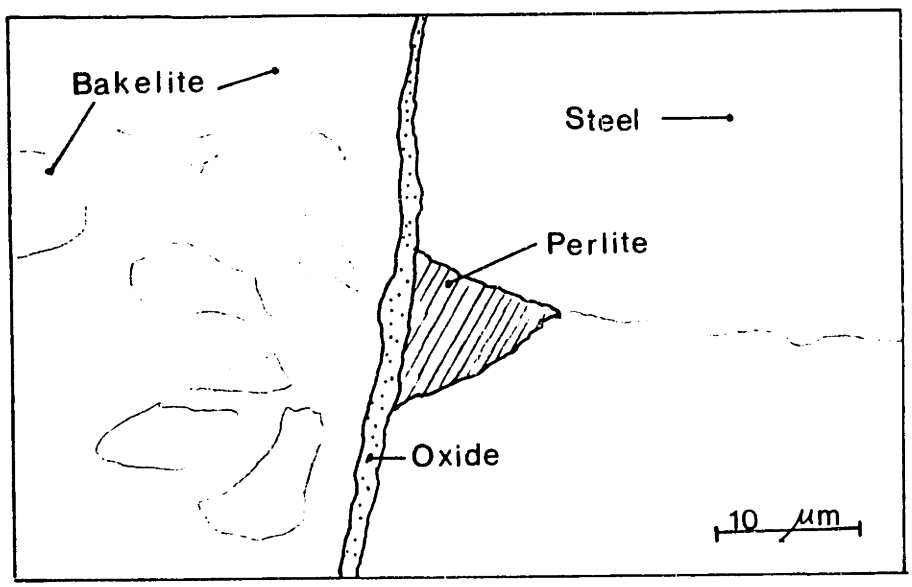

Figure 29. Oxide layer thickness δ, for high velocity specimen (9.5 ft/s) at 320 F, δ = 1.8μm.

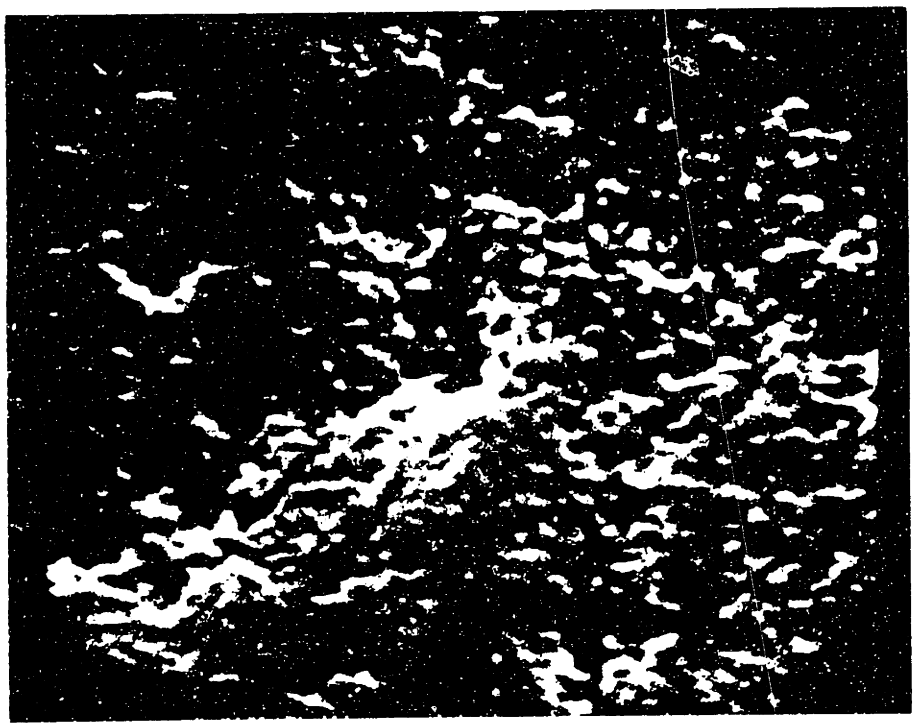

X-20,000

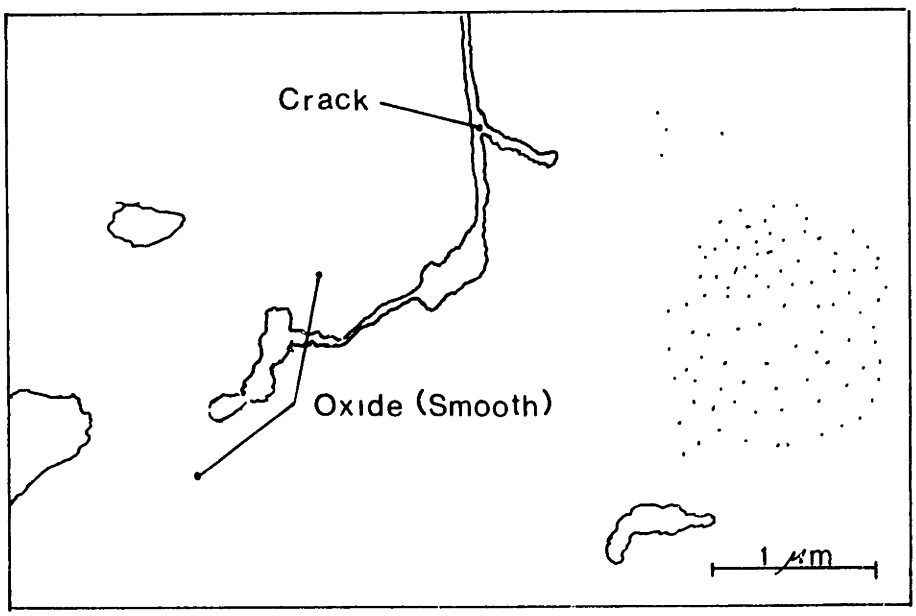

Figure 30. Frontal view of oxide on high velocity specimen (9.5 ft/s) at 300 F.

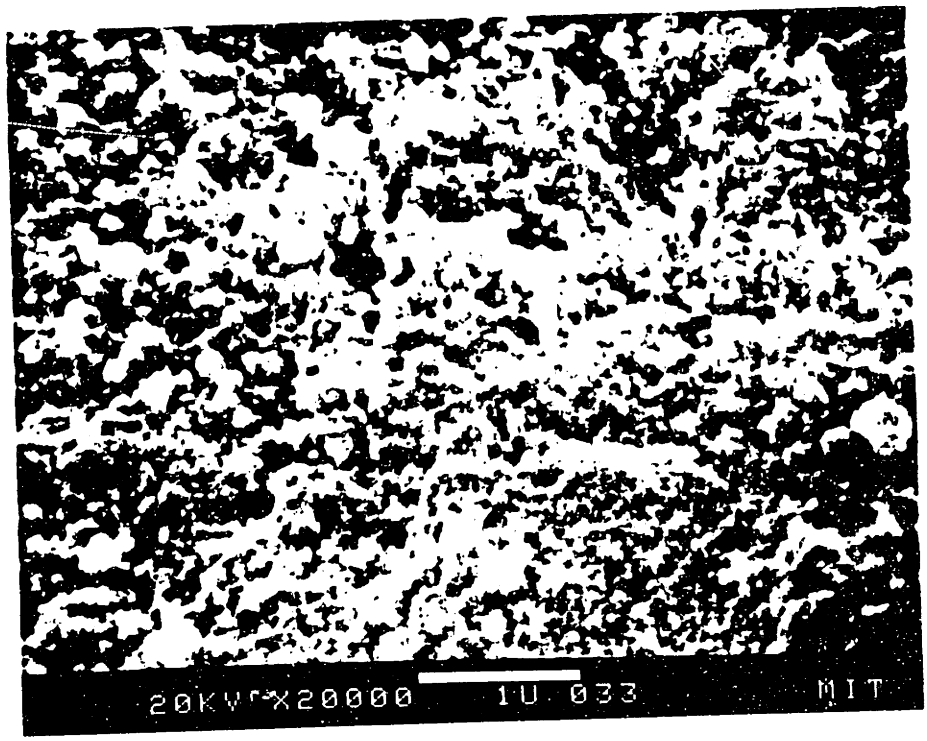

X-20,000

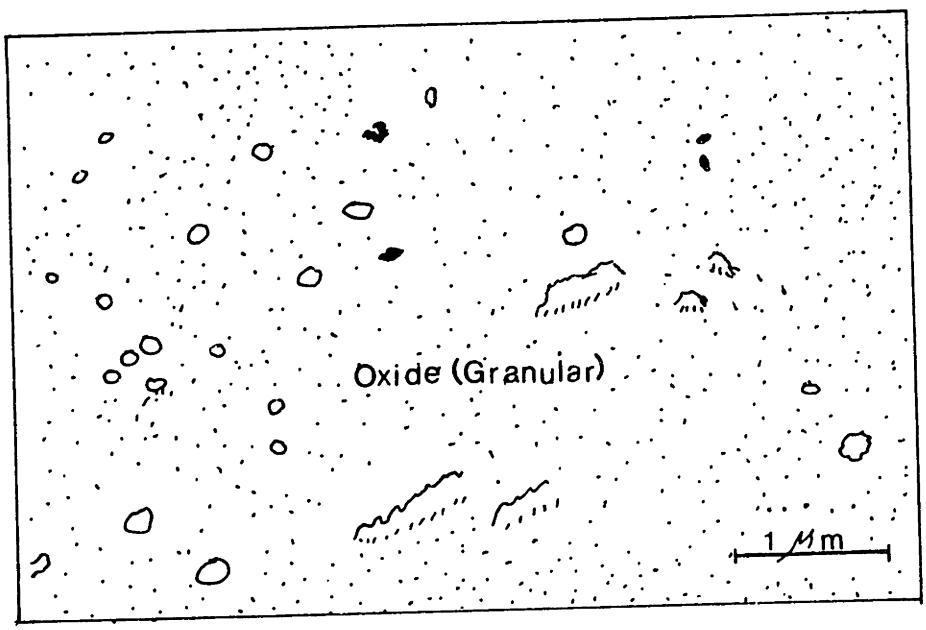

Figure 31. Frontal view if oxide on high velocity specimen (9.5 ft/s) at 310 F.

exterior oxide. In the case of the specimen at 300 F, this appearance is smooth while at 335 F it appears to be formed from packed particles. The pictures do not permit making any serious conclusion about the porosity of the film.

The X-Ray analyzer of the S.E.M. can determine large molecular weight elements, it cannot detect light elements like oxygen. The x-ray detector can only provide information about the elements that are present and not about the compounds of which they form part. Differentiating the various iron oxides is not possible with this technique.

5.5 X-RAY PHOTOELECTRON SPECTROMETER

As mentioned previously, it is possible to detect compounds through this system.

The system detects the electrons taken out of their orbits by impinging X-rays. The energy of each electron is linked to the orbital to which it belonged and thus to a specific compound. According to the electron energies, a compound can be recognized by locating the energies where the greatest number of electrons were collected.

The energy spectrum for all specimens looks qualitatively like the one presented in Figs. 32-34 for the magnetite powder. As can be seen the peaks around 730 and 530 ev are the locations of maximum collection.

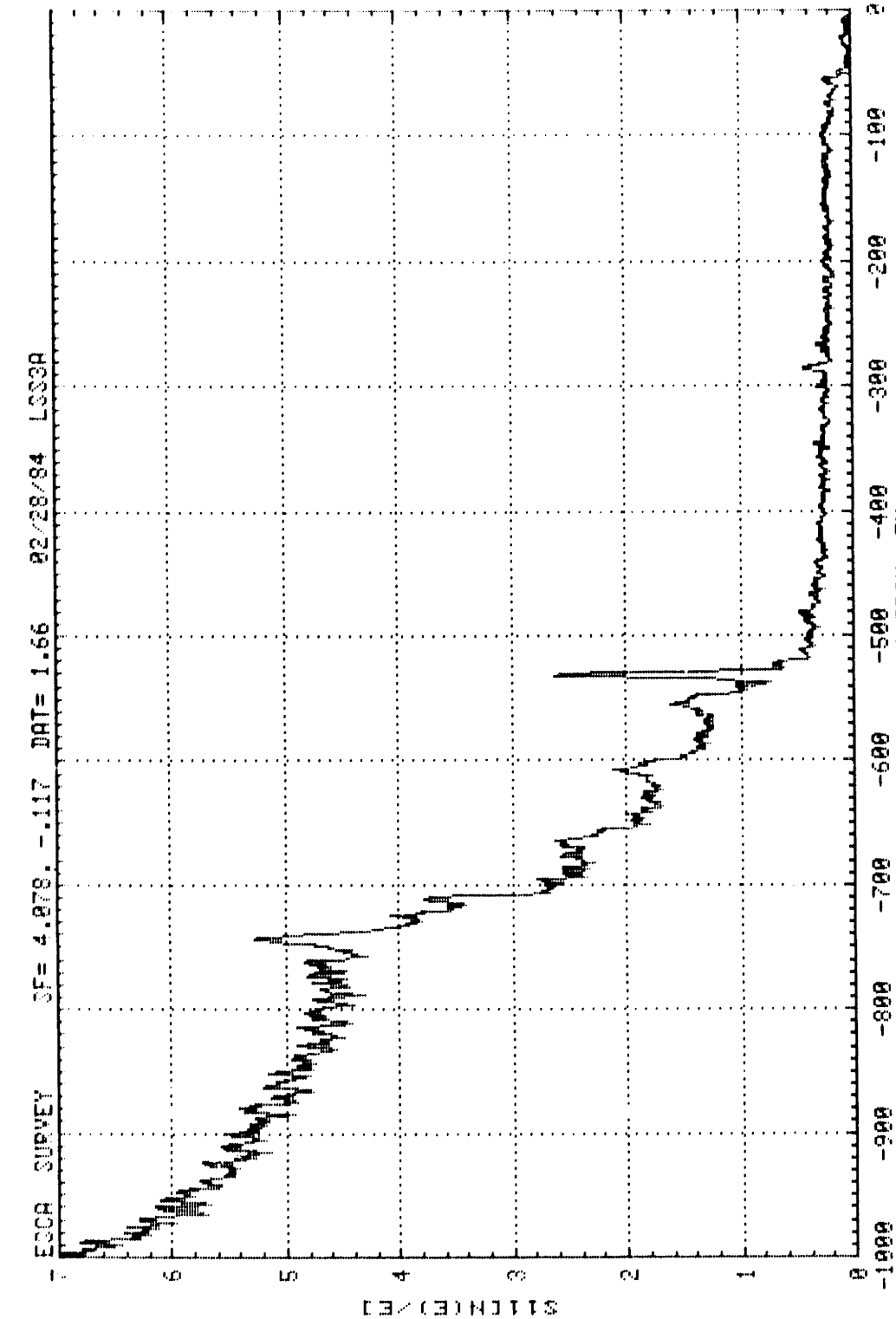

Figure 32. Survey of electrons collected vs. energy for magnetite powder (presputtered). The peaks at 720 ev correspond to the iron peaks, while the peak at 530 corresponds to the oxygen peak.

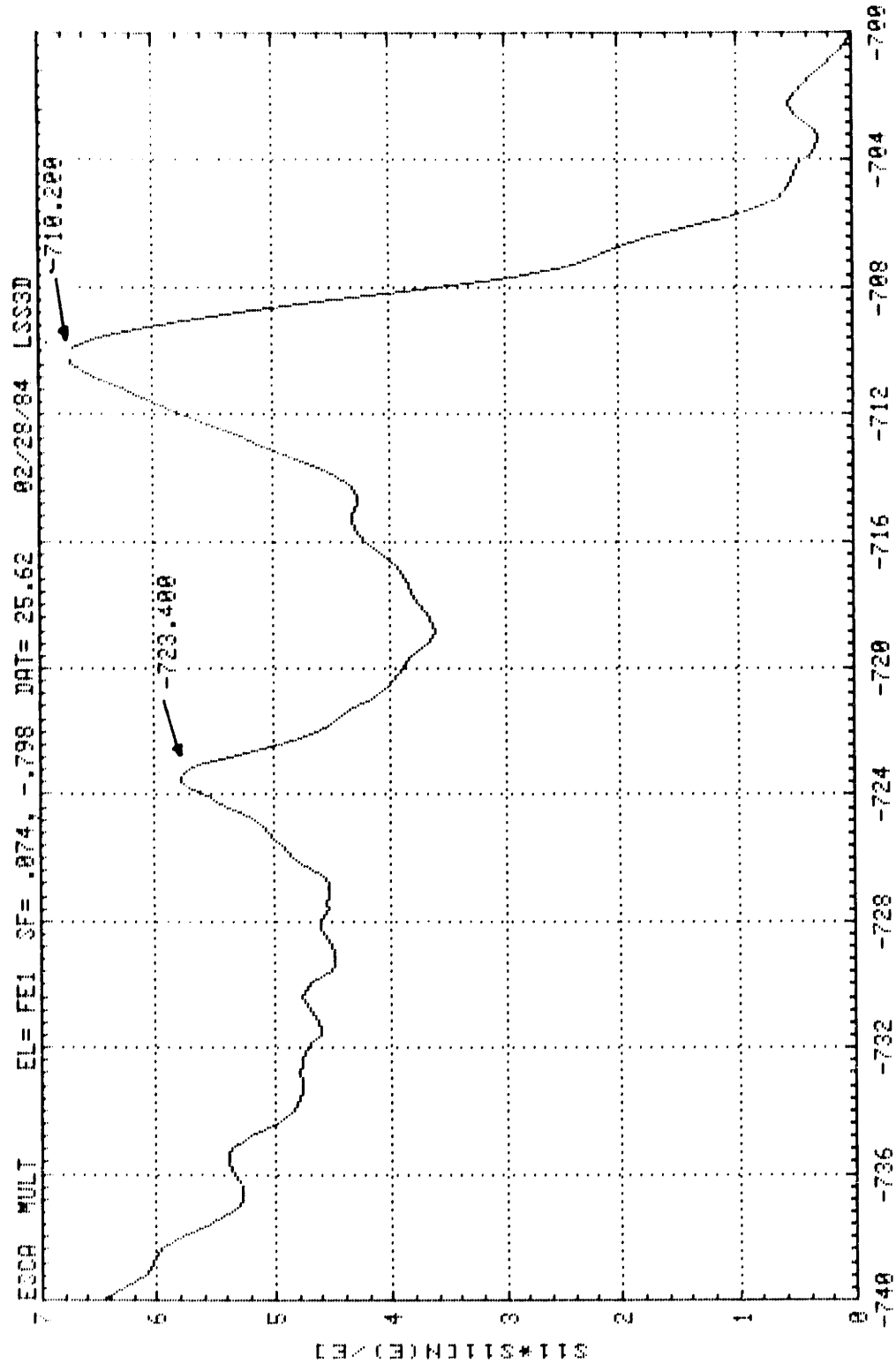

Number of Collected Electrons at specific energy

Figure 33. Location of iron peaks 723 and 710.2 ev for magnetite powder, 4m sputtered with argon and in a neutralized electron field to avoid charging.

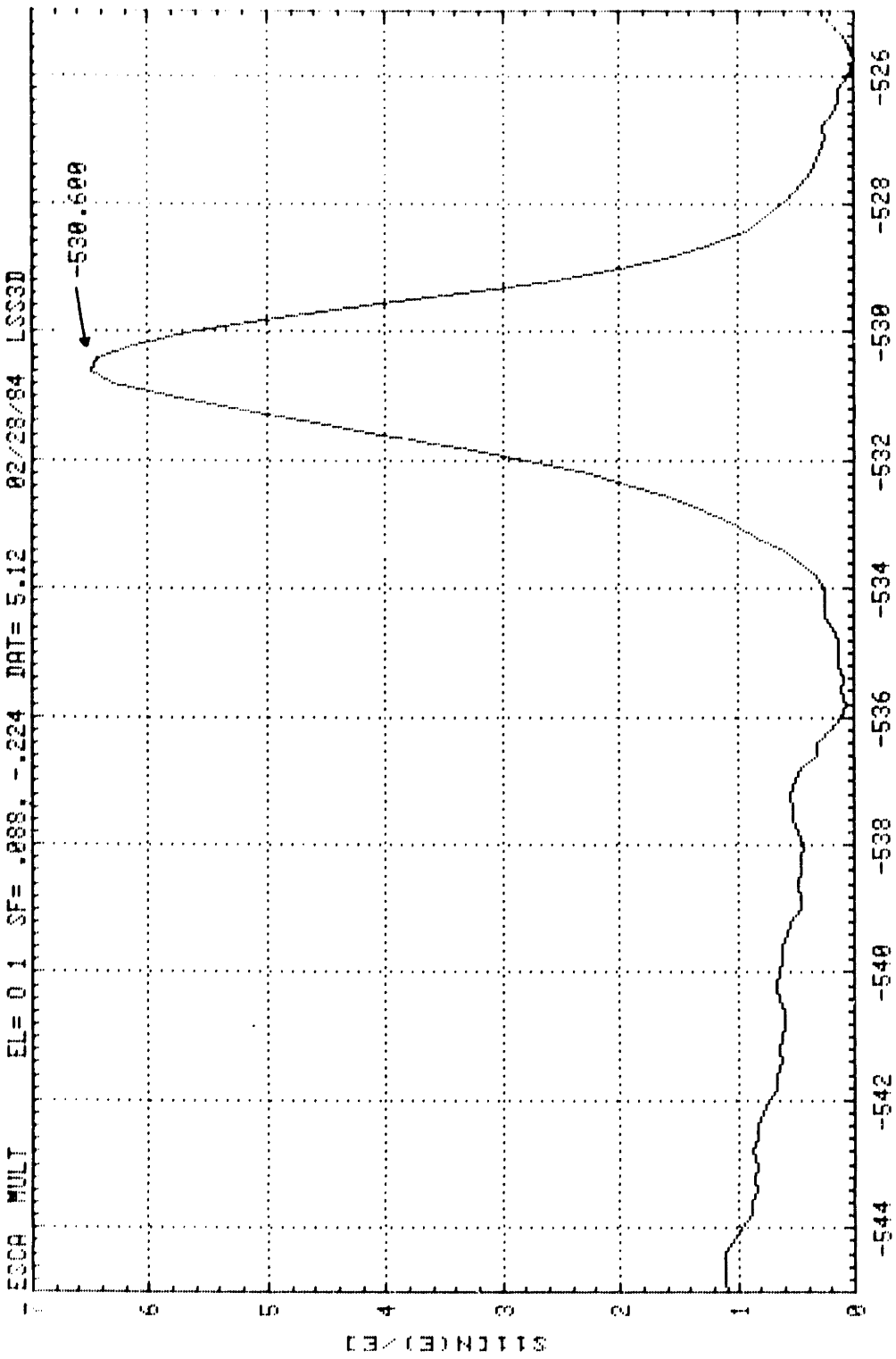

Number of Collected Electrons at Specific Energy

Figure 34. Location of oxygen peak 530.6 ev for magnetite powder, sputtered 4m in argon and in a neutralizing election field to avoid charging.

These locations correspond to the iron and oxygen peaks and it is the position of the maximum heights which are used to make comparisons between the pure magnetite, haematite and the corrosion-erosion specimens. Plots which were similar to those of magnetite were obtained for the haematite powder and the high velocity specimens at 305 and 320 F. Table 4 presents the location where the iron peaks and the oxygen peaks were found for each material tested.

Table 4. Energy location of iron and oxygen peaks for the different materials tested in the XPS.

Material Tested	Iron Peaks Location (ev)	Oxygen Peaks Location (ev)
Magnetite	723.4, 710.2	530.6
Haematite	723.6, 710.0	529.6
HV 305 F *	723.8, 710.4	530.6
HV 320 F *	724.2, 710.4	530.6

* HV stands for high velocity specimen (9.5 ft/s)

The table shows a very good agreement between the oxygen peaks of the magnetite and the specimens. No such clear distinction exists when comparing the iron

peaks. At this stage the wear data from the experiment has been presented and its oxide has been analyzed. In the next chapter all these results are discussed in detail.

CHAPTER 6

DISCUSSION OF RESULTS

This chapter describes the uncertainty associated with the results of last section; it also discusses the implications of the results, their reduction to obtain the value of the constant K for the model developed in Chapter 3; and most important, it provides the procedure to estimate wear rates, a list of solutions to avoid corrosion-erosion wear and suggestions for future work.

6.1 ANALYSIS OF EXPERIMENTAL RESULTS

6.1.1 Accuracy Of The Results

This section comments on the experimental errors linked to the results presented in Chapter 5.

6.1.1.1 Errors In The Determination Of Testing Conditions - -

The first consideration in this regard concerns the evaluation of the errors in obtaining the value of temperature, pH, velocity, oxygen content, and material coposition. It is important to comment on the methods used in determining the conditions of an experiment and on whether the values of such conditions were close enough to the set point values.

1. Temperature: This was the variable that was the least difficult to determine. Three thermocouples mounted around the test section measured the temperature of the test. At first, the thermocouple junctions were actually inside the water. The temperature difference among the thermocouples was 1 F, and since the junction was inside the water, it is likely that the actual temperature was very close to the one registered. The error bars in Figs. 27 through 29, pertaining to the temperature, are an estimate of the mean error from the averaged time value ($\pm$3 F). The bars are not related to the individual temperature measurements where the error would only be of the order of $\pm$0.5 F.

2. Velocity: With an accurate determination of the temperature (which allows for a good estimate of the water density) and knowing the dimensions of the test section (that was measured with a micrometer) the calculation of velocity for a given time was determined. The error associated with the variations of the flow rate through the test section over time are estimated at 10% of the averaged velocity.

3. Material Composition: During the present research no variation of the material composition was considered. All specimens were fabricated from the same 2", A155 Gr C 55 plate.

   In regard to the differences in conditions of the surface, they were considered minimal. As was discussed previously, the machining and cleaning procedures were standardized (see Section 4.3.1). As a result, small errors associated to material composition and surface finish are expected.

4. pH: The distilled water used in the tests had a pH of 5.2 to 5.7. The measurement was obtained by making use of a Beckman pH-Meter analyzer (Model 900) as well as pH meter colorimetric paper. As the test proceeded, the

value of pH often rose to 6 but it was never above it. The low pH of the water may be caused by the presence of carbon dioxide which may yield carbonic acid.

5. Oxygen Contents: The amount of oxygen in the sampling line water was estimated, by making use of an old oxygen analyzer, to range from 200 to 1000 ppb. The error in the determination is not felt to be representative of the actual oxygen content in the loop. This conclusion is derived from two observations. One is the fact that the loop was in all cases degassed for about 20 minutes prior to the beginning of a test; and second is that for tests carried at the same temperature while keeping pH and velocity constant, the wear rate values came out to be similar, see runs near 300 F in Figs. 23 to 25. Errors in evaluating the wear rate are discussed in the following sections.

6.1.1.2 Error In Determining The Wear Rate. -

a) The error inherent in a single wear rate measurement.

A question often asked is whether the measured amount of material lost represents the actual wear

caused by corrosion-erosion or whether it is only a result of weight loss while assembling and disassembling the test section. Experience shows that when the assembly components in a system such as this one are screwed and unscrewed, a weight loss of around 0.3 mg occurs, (Rabinowicz, 1983). The weight losses which are related to the wear rates presented in the previous chapter, are of the order of 40 to 200 mg, and thus suggest that the measurements are, in fact, representative of the wear phenomenon.

The next point to discuss is the assessment of the adequacy of the method used for calculating the wear rate.

Figure 35 recalls the general way in which a specimen loses weight (the figure is similar to Fig. 22). The initial weight increase is caused by the formation of an oxide layer which achieves constant thickness after about 150 h.

The above figure shows that by taking the wear rate as the total weight loss divided by the duration of a test (slope 1) a rather close approximation to the actual wear rate (slope 2) is achieved. In this case, the actual slope is underestimated and the error can be evaluated at 0.6 mg/cm^2h (0.005 mm/y). The error bars in Figures 23 through 25 are representative of this value.

The other method used to estimate the wear rate

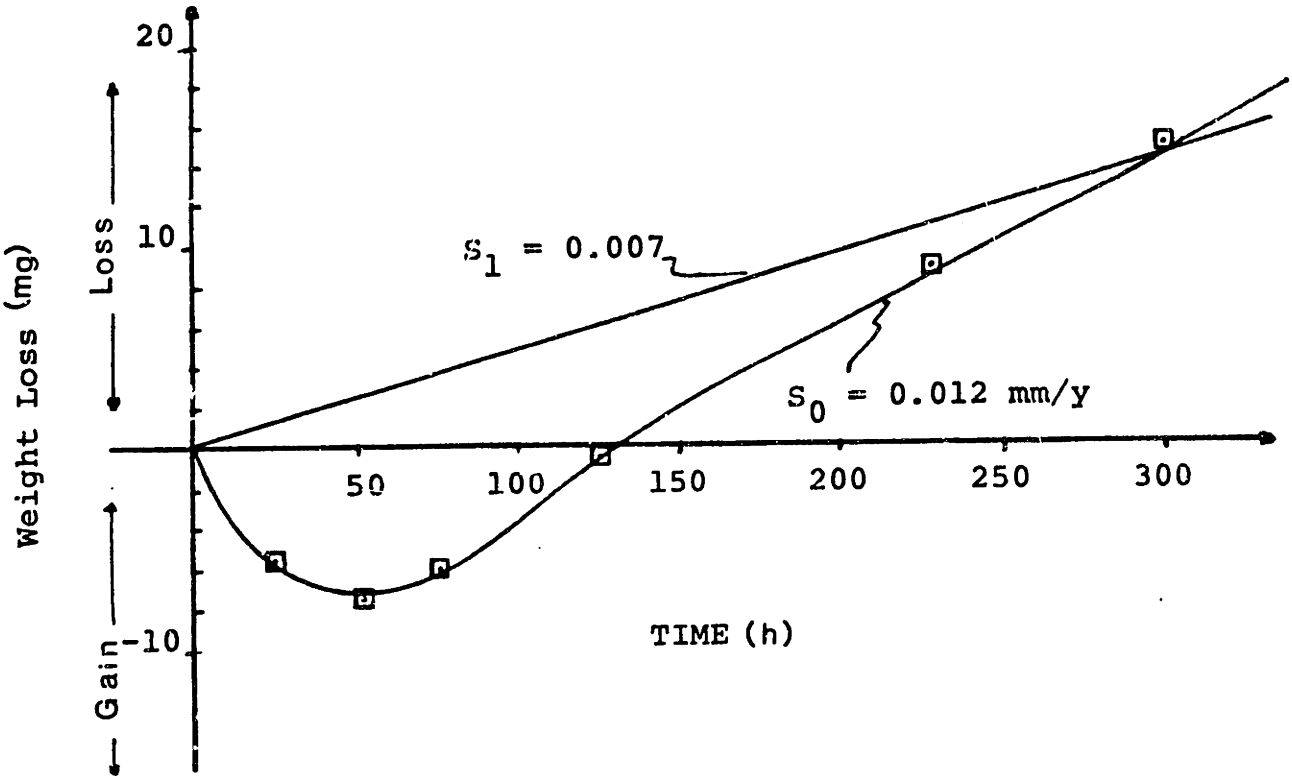

Figure 35. Weight loss as a function of time: low velocity specimen (250 F).

makes use of the descaled weight loss. If a plot of descaled weight loss as a function of time were to be made, Fig. 36 would probably be obtained. We observe that estimating the wear rate by dividing the total descaled weight loss by the duration of the test overestimates the wear rate. This is the reason why the wear rate values of Fig. 23 are different from those of 24 and 25.

An important fact to point out is that a more accurate determination of the wear rate would be obtained by having a longer test period or recording the

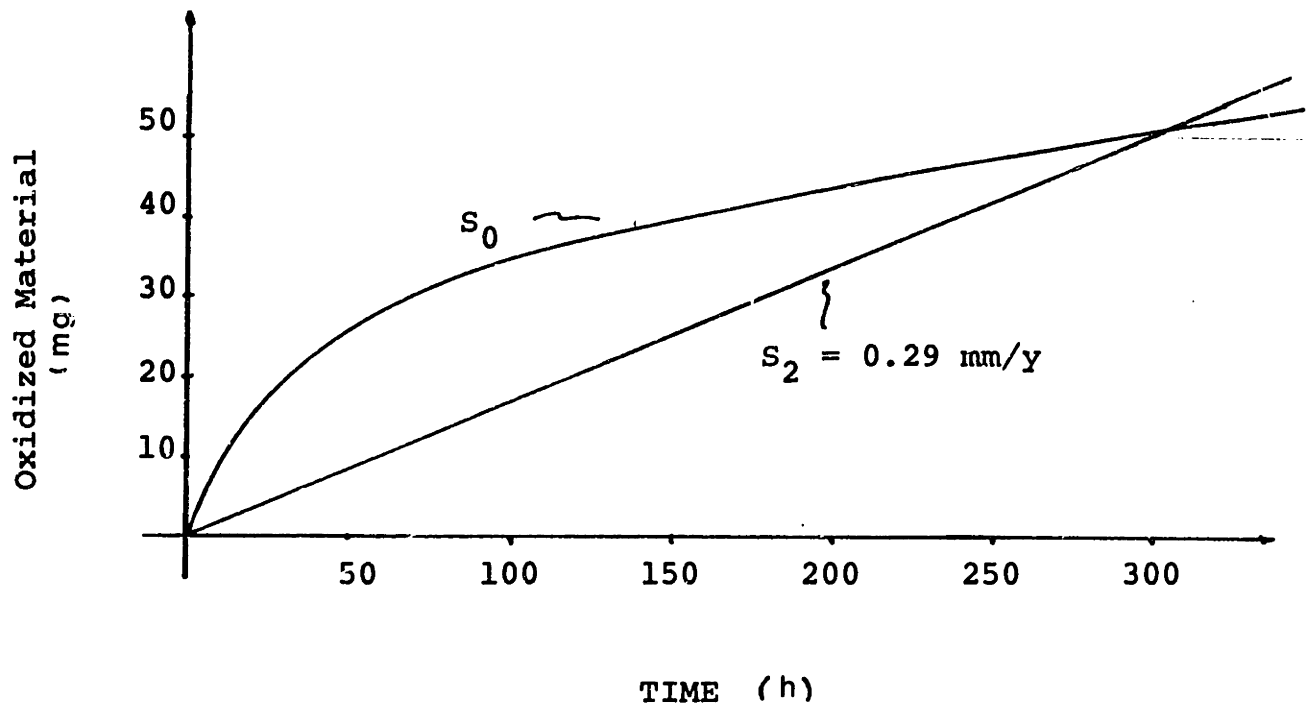

Figure 36. Expected curve for the amount of material oxidized as a function of time (low velocity specimen 250 F).

weight loss after the 10th and 13th day. While the first alternative implies test periods of over half a month (a long time), the second method poses the risk of contamination every time the specimen is taken out of the loop; none of these methods were therefore adopted.

The above discussion leads to the conclusion that the results reported in Figures 23 through 25 provide limiting values for the wear rate, and that comparisons can be made since in reporting the data on a specific figure the same technique for the calculation of wear rates was used for all the points plotted.

b) Repeatability of the Result.

To check for consistency and reliability of the wear rate data, the experimental rig ran 3 times at a temperataure close to 300 F and twice near 250 F, under the same velocity and pH conditions

The results in Figures 23 through 25 show that the wear rates for these cases agree fairly well. An error bar on the wear rate, representative of the reproducibility error of the experiment, would be on the order of 0.6 g/cm h. This value is considerably less than the variations of wear rate produced by temperature variations and is the same as the error in the calculation of the wear rate (as explained in part (a) of this section).

Another reason to consider the repeatability of the results adequate is the fact that one of the tests around 300 F (305 F) was run with the low velocity section placed before the high velocity section. This was opposite to the usual way of running the tests, where, with the test chambers in series, the high velocity chamber was placed before the low velocity one. With the positions for the high and low velocity specimens interchanged and with the wear rate values around 300 F being close to each other, the results suggest that a) positioning the specimens in series does

not appreciably affect the determination of the wear rate; and, b) the results are reliable. First order trends can therefore be obtained from looking at the results of the Figures 23, 24 and 25. Second order effects caused by the non-controllability of some of the variables, e.g., oxygen and hydrogen contents, will influence our quantitative results.

6.1.1.3 Comparisons Of Experimental Results With Other Wear Rate - Experiments.

In this section some values of corrosion-erosion rates found in the literature are compared with our results. Table 5 lists the results of several authors and includes the results of this work.

The values of wear rates obtained in this work agree with the values of other researchers when considering the temperature conditions and the low velocity of operation. Even better is the comparison of the band width and the location of the maximum wear rate in a wear rate vs. temperature curve. In all cases the mean band width was 50 C and as shown in previous table the peak for all cases occurs near 150 C. These results suggest that the regions most likely to suffer damage by corrosion-erosion are those pipes where the temperature is around 150 C (300 F).

Table 5
Comparison of Wear Rate Values

Research	Conditions	Wear Rates ($\mu g/cm^2 h$)	Temp at Maximum Wear (F)
Berge et al. (1980)	Low alloyed Mn steel T = 300 C, 5 m/s impinging jet.	0.1	-
Keller (1974)	Low carbon steel to 13% Cr steel Data from different power stations.	35 - 500	150
Bignold et al. (1980)	Carbon steel 100<T<170 C, 40 m/s post orifice specimen pH=9.05	40 - 180	136
Heitman (1982)	Several materials 120<T<175 C, 38 m/s	0.5 - 3000	150
This work	Low carbon steel 120<T≤180 C, 3 m/s flow through an annulus pH=5.6.	1 - 9	155

Although our results apply mainly to conditions of BWR water, it is considered that the behaviour with respect to temperature (i.e., finding a temperature for which wear is maximum) would be similar in the case PWR environments (pH = 9.0) for low carbon steels of similar compositions as that of the material tested here (see Section 4.3.1).

The above considerations lead to the conclusions that the experimental rig has indeed captured the phenomenon of corrosion-erosion, and has provided

representative wear rate data of low carbon steel A155 Gr C55.

6.1.2 Velocity Behaviour

The fact that all low velocity specimens came with a smaller wear rate than the high velocity specimen supports the idea that the wear is partially diffusion controlled. It therefore makes it evident that regions of high mass transfer coefficients accompany high wear rates by corrosion-erosion.

This is of interest to designers and construction personnel of power stations. Features that enhance the mass transfer coefficient, e.g., sharp bends and unfinished welds, can create regions of recirculation and separation where mass transfer rates can be enlarged, (Pak, 1984, Berkow, 1984).

From the data reported in Fig. 23, the point at a temperature of 250 F is noteworthy. For this run the wear rate of the high velocity specimen is very similar to the one at the low velocity. This suggests, as discussed earlier, that when temperature is low, the process becomes independent of fluid dynamics and more dependent on the kinetics of the chemical reactions (activation controlled), the model developed in Chapter 3 agrees well with these findings.

In general, in corrosion-erosion the experimental facts indicate that both hydrodynamics and chemical

kinetics influence the wear rate.

6.1.3 Comments On The S.E.M. And X-Ray Photoelectron Spectrometer

The information gathered from these instruments is of limited use.

The cutting and polishing techniques used to examine the specimens under the scanning electron microscope (S.E.M.) require some improvement. As shown in the pictures taken by the S.E.M., air gaps and contamination of specimens makes it difficult to determine the structure of the oxide layer.

In any case, observing the oxide thickness does not provide very useful information, since the area under examination is very small and the sample is poor. Although the place where the microscope scans is chosen at random, the area of this examination is diminutive compared to the size of the area that was worn. Many more places would have to be analyzed in the microscope to have a representative magnitude of the oxide thickness of a particular run.

From all the S.E.M. observations, the conclusions obtained are that the oxide thickness varies from 0.5 to 8 microns, and that porosity changes of the oxide layer as a function of temperature were not evident when looking at the surface of the oxide. The results of a maximum wear rate at 150 C (300 F) suggest that

passivation is taking place. Since one of the theories of passivation makes reference to a protective film, the fact that the wear decreases with temperature could mean that a more protective film exists at high temperature. This in turn can be associated to changes in the porosity of the film. Although this is a valid explanation for the decrease in wear rate after 300 F, there was no direct physical evidence of this from the pictures that have been taken. This is felt to be a reflection of the crude experimental techniques.

The information gathered from the XPS is of some value, but again many more samples are needed to provide a representative reading.

The preparation of the specimen requires that the specimens be kept in a corrosion-free atmosphere, so that when they are examined with the spectrometer, the outermost oxide layer, which is the scanned area, is the actual oxide formed during the corrosion-erosion test.

To draw conclusions about the data collected from using the spectrometer, two conditions must be met:

1. The scanning must be made on the actual oxide formed during the corrosion-erosion test, and

2. There must be good standards with which comparisons can be made.

To satisfy the first requirement, it is necessary to take great care of the specimen from the moment it is

removed from the corrosion-erosion chamber, to when it is "sputtered" (cleaned by bombardment of argon) for the removal of the first oxide layers (this step takes place inside the spectrometer). If several layers of oxide are removed during the sputtering the first condition above will be met.

In regards to the second condition, it is essential to have good standards in order to achieve accurate determination of which components are present in the oxide.

Standards from which comparisons can be made do not exist. A single analysis on the magnetite and haematite powder may not be adequate standards; this is the reason why the conclusions that can be obtained from Table 4 are not completely reliable. From looking at the iron peaks it is difficult to draw any final conclusion. A clear difference arises when looking at the oxygen peaks; as can be seen in Table 4, their location agrees exactly with the oxygen peak for the standard magnetite powder. This is a clear distinction since there is 1 ev difference between the locations of oxygen peaks of standard magnetite and haematite. This evidence points out that the oxide on the specimens is indeed magnetite and that the concentration of oxygen was low enough so that haematite was not able to form.

7.2 THE CORROSION-EROSION MODEL

In Chapter 3 a series of hypotheses was made about the mechanisms of corrosion-erosion. These hypotheses resulted in the derivation of Eq. 41 i.e.,

$$\dot{m}_1'' = \frac{C_e \Theta}{\frac{1}{K} + (1-f)\{\frac{1}{h_d} + \frac{\delta}{D}\}} \qquad (41)$$

where $K = A_1 \mathrm{Exp}(-E_1/RT)$ and $f = 0.5$ (49)

By rearranging Eq. 41 it is possible to obtain an expression for K,

$$K = \frac{1}{\frac{C_e \Theta}{\dot{m}_1''} - (1-f)\{\frac{1}{h_d} + \frac{\delta}{D}\}},$$

To employ this equation, the values of D, h_d, Θ, δ, C_e and $\dot{m}_1''$ must be determined.

The wear rate data of Chapter 5 directly provides the values of $\dot{m}_1$. The rest of the parameters are evaluated by making use of the methods described in the following sections.

Obtaining the values of K for the different experimental conditions allows a graph of ln K vs 1/T to be constructed. If in such plot the derived values of K are aligned on a straight line, it will prove that the assumptions made in the derivation of the model were adequate, and it will also allow the values of A_1 and E_1

in the expression $K=A_1 Exp(-E_1/RT)$ to be obtained (E_1 will be the slope of the line multiplied by R, while A_1 will be the inv. log of the value at which the line intercepts the y-axis).

The methods to calculate the value of the parameters of Eq. 49 and the computational method used in obtaining the value of K are given in the following sections. It is in section 6.2.2 where the plot of ln K vs 1/T is shown.

6.2.1 Relations Used To Determine The Value Of The Parameters In Eq. 49

6.2.1.1 Method To Calculate Iron Species Diffusion - Coefficient -

The corrosion-erosion model takes into account the diffusion of solubilized iron hydroxide compounds; therefore, the diffusion coefficients which require evaluation are the ones pertaining to the compounds Fe^{++}, $Fe(OH)^{+}$, $Fe(OH)_2$ and $Fe(OH)^{-}_3$. Lapukhov (1966) reports an experimental diffusion coefficient of Fe in water at 150 C of 4.041×10^{-5} cm /s. This value agrees pretty well with the value of 7×10^{-5} at 300 C given by Castle and Mann (1966).

To have a relation to calculate the diffusion coefficient at different temperatures the expression used was the one given by Rohsenow and Choi (1961):

$$D = \frac{4.0 \times 10^{-7} T}{\mu (\tilde{V}^{1/3} - 2)} \quad , \qquad (50)$$

where: T = temperature (R)

μ = viscosity (lb/hrft)

$\tilde{V}$ = atomic volume of the compound (cm^3/g_{mol})

Knowing the value of the diffusion coefficient for Fe^{++} at one temperature (Lapukhov, 1966), from Eq. 50 the atomic volume of Fe^{++} was obtained ($\tilde{V} = 270 \frac{cm^3}{g_{mol}}$). By considering that the volume of a compound is increased by 7.4 for every oxygen atom and by 3.7 for every hydrogen atom present, the atomic volumes of the rest of the hydroxide species were determined. With $\tilde{V}$ known for each specie, Eq. 50 was used to determine diffusion coefficient with variations of temperature. The actual value of the diffusion coefficient used in the mass transfer equation was obtained by a weighted average over the diffusion coefficient of each iron species, see Section 6.2.4.2 numbers 8 and 9 for further details on this calculations.

6.2.1.2 Mass Transfer Coefficient Calculation -

In order to obtain the value of the mass transfer coeffiecient, h_d , use was made of the following expression given by Berger and Hau (1977):

$$Nu = \frac{h_d D_e}{D} = 2 + cRe^a Sc^{1/3}, \qquad (51)$$

where: h_d = mass transfer coefficient

D_e = characteristic dimension (in our case taken as the equivalent diameter)

D = diffusion coefficient of the iron species

Re = Reynolds number

Sc = Schmidt number

$c = 0.0165 + 0.011 ScExp(-Sc)$

$a = 0.86 - 10/(4.7 + Sc)^3$

The above equation, is valid over the range $0.6 < Sc < 10^4$ and $10^4 < Re < 10^6$. The reasons for choosing Eq. 51 as the key equation to obtain the mass transfer coefficient were this wide range of applicability and the broad experimental data on which it was based.

It is important here to notice that due to the fact that the wear specimen had a simple geometry, an equivalent diameter can easily be calculated. The test section used in the experiment was an annulus; therefore, the equivalent diameter becomes:

$$D_e = \frac{D_1^2 - D_2^2}{D_1} \qquad (52)$$

where: D_1 = annulus outer radius

D_2 = annulus inner radius

The data for the high velocity specimen (9.5 ft/s)

in a test at 175 C (350 F) is given as an example of the typical values used in the calculation procedure: equivalent diameter, De, 0.36 cm, diffusion coefficient, D, 4.9×10^{-5} cm^2/s, mass transfer coefficient h_d = 0.098 cm/s, Schmidt number, Sc, 35.

6.2.1.3 Determination Of The Equilibrium Concentration C_e - -

To obtain the equilibrium concentration of iron species, the thermodynamic data of Sweeton and Baes (1970) is used. Their results already shown in Fig. 11, provided equilibrium values of soluble iron hydroxide species as a function of pH and temperature. To make use of the information provided in Fig. 11 use is made of additional data given by Sweeton and Baes (1970)

The equilibrium constant for reaction in Eq. 29 was defined as:

$$K_{e_b} = \frac{[Fe(OH)_b^{(2-b)}]}{[H^+]^{2-b}\,[H_2]^{1/3}}\,, \qquad (53)$$

where the square brackets stand for the concentration of species and b can take the values of 0, 1, 2, and 3.

Equation 53 allows the value of the equilibrium concentration of iron to be obtained when the values of K_{e_b}, $[H^+]$, and $[H_2]$ are known. The same authors from

their experimental work provided an expression to calculate K as a function of temperature. The expression used is:

$$K_{e_b} = \mathrm{Exp}\{\frac{-A_b}{T} + B_b(\mathrm{Ln}(T) - 1) + D_b)/R\}\ , \qquad (54)$$

where: A_b, B_b, D_b = constants with known values

T = temperature (K)

R = universal gas constant

The values of the constants A_b , B_b , and D_b are specific for each compound of iron. These values are included in Appendix G, as part of the computer program WEARR4.FOR.

To calculate the concentration of iron species at the metal-oxide boundary from Eq. 53, the concentration of hydrogen and hydrogen ions at the metal-oxide interface are required. Section 3.5.2 provided the necessary relations, Eqs. 42 and 43, to calculate the required concentrations. Equations 42 and 43 require the value of the concentration of hydrogen ions and hydrogen gas in the bulk of the fluid. The concentration of hydrogen ion at infinity has been taken to be the original pH of the water modified to the temperature of operation. While the hydrogen concentration at infinity has been considered 0.05% of the saturation value. This value was taken from

Bignold, et al. (1980) who considers that the partial pressure of hydrogen in nuclear reactors is approximately 1 to 5 g/Kg, while saturation is 1585 g/Kg.

6.2.1.4 Values Given To Θ And δ

The only parameters missing to make use of Eqs. 41, 42, and 43 are the porosity and the oxide layer thickness.

Surman and Castle (1969) gave a range of values of porosity between 0.001 and 0.1 . In the computational procedure to calculate the value of K (next section) the porosity value used was 0.0005, this value gave better agreement between the model and the experimental results. It is important to mention that in the actual calculation procedure for the wear rates, the porosity is not kept constant, see section 6.2.4.2)

In regards to oxide thickness, the pictures taken by the scanning electron microscope suggest that the range for δ was from 0.5 to 9 microns. Values of 0.3 to 1.5 were obtained from the weight of the outside oxide i.e., by considering the weight of the oxide to be distributed on the surface of the specimen as a uniform layer. In the computational procedure the value of 1 micron was used for δ.

6.2.2 Reduction Of Data - Calculation Of K

A computational procedure was developed to calculate the value of $[H_c^+]$ and $[H_{2_o}]$ at the metal oxide interface. With the values obtained, Eq. 49 was used to obtain the value of K.

A flow diagram of the computational procedure is shown in Fig. 37. The program WEARR4.FOR, used in the actual calculation and included in Appendix G, follows the flow diagram of Fig. 37.

The only further comment required is that in the computational procedure the concentration at equilibrium, C_e, for each iron species (Fe^{++}, $Fe(OH)^+$, $Fe(OH)_2$, $Fe(OH)^-_3$) was obtained from Eq. 53 by using values of b equal to 0, 1, 2, and 3. Also, a diffusion coefficient for each compound was calculated. Having obtained the ratio of individual concentration to total concentration of iron species, an average diffusion coefficient, D_{av}, was calculated. It was the value of D_{av} that was used in the calculation for the average mass transfer coefficient, h_d.

The final output of the program are the values of K and ln K obtained from Eq. 52. The values of K and ln K are also shown in Appendix G. In the following section, the plot ln K vs 1/T is discussed.

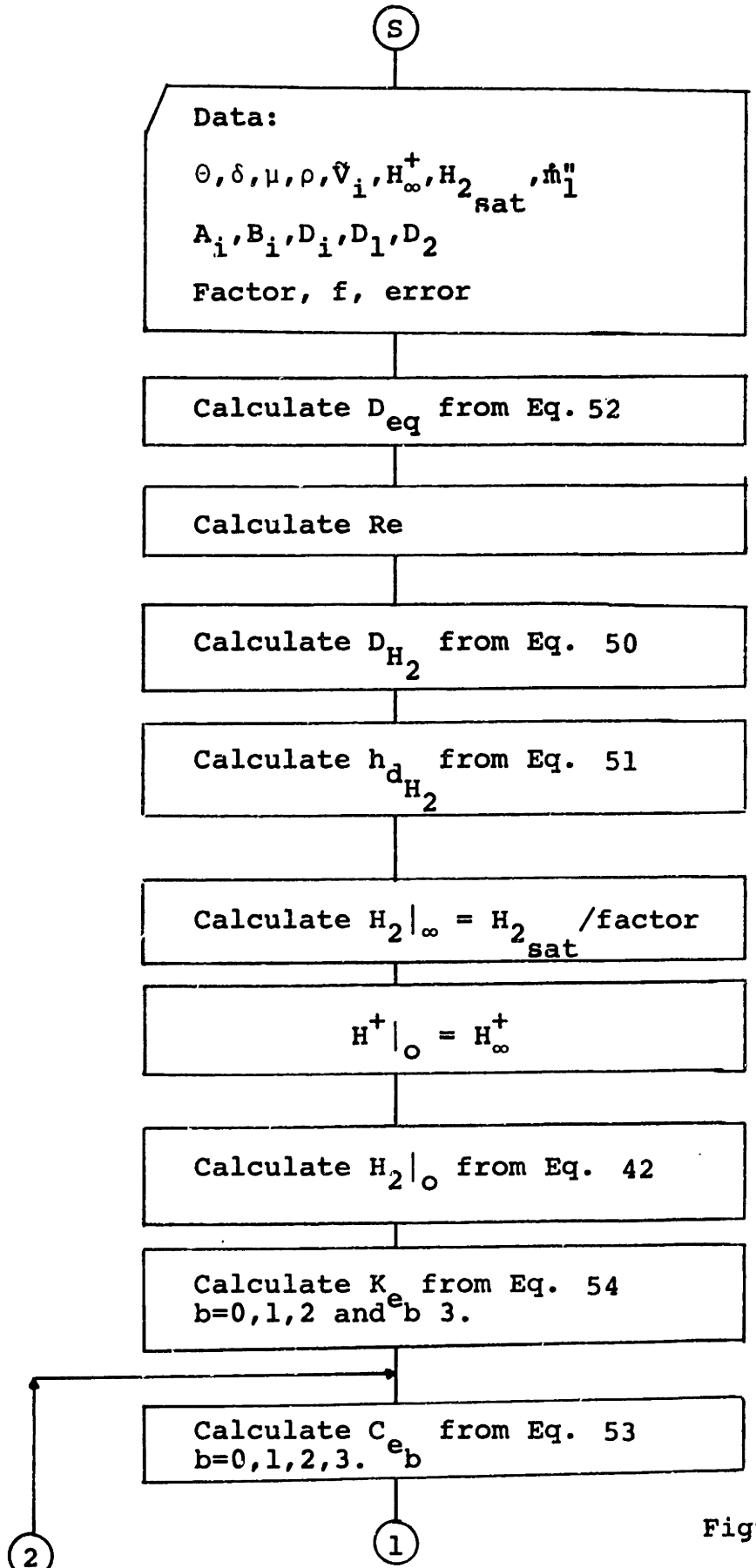

Figure 37, continued

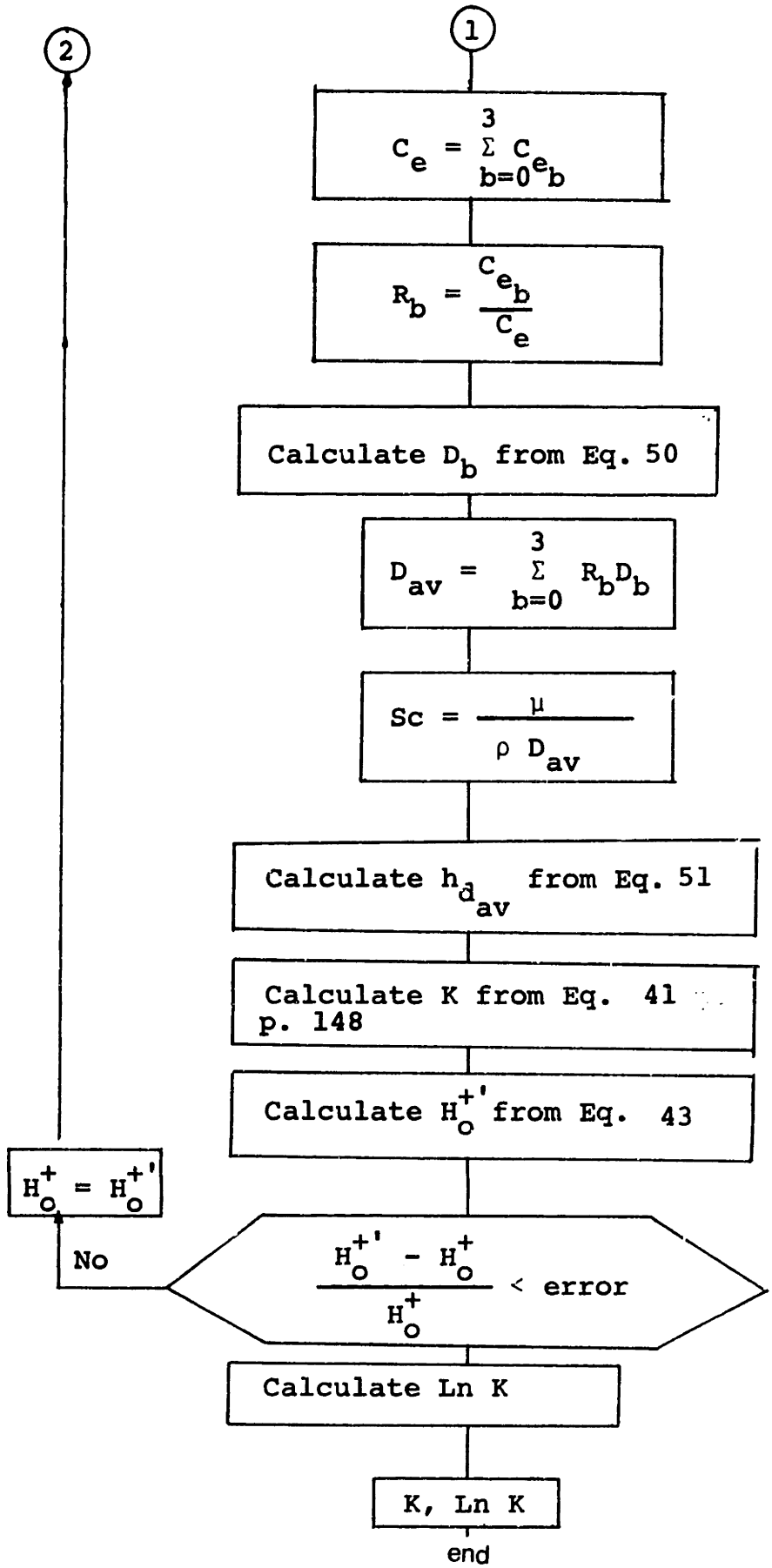

Figure 37. Flow diagram of the computational Procedure for obtaining K.

6.2.3 Plot Of Ln K Vs 1/T

Figure 38 shows the plot of ln K vs. 1/T. In the figure the points align fairly well on a straight line. Furthermore, the slope of the curve, obtained from a least square error fit to all, minus the two points at 350 F, of the data provided in Fig. 38, is equal to 17,990 K, which yields a value of 35,620 cal/g_{mol} for the activation energy. This value is found to agree well with the values of activation energy of steel corroding in steam reported by Surman (1973).

The fit shown in Fig. 38 is not perfect, especially at a high temperature where higher values of K would be required for a better fit. This means that the decrease of equilibrium concentration of soluble iron with increase in temperature is not enough to explain the decrease in corrosion rate.

Several ideas were analyzed in order to find a better fit for the wear rate data of Fig. 38. The factor f (the fraction of hydroxides transformed to magnetite at the metal-oxide interface) was varied from 0.0 to 0.5 and no fundamental change was appreciated (i.e., the behaviour of the results of Fig. 38 remained practically unchanged). This result is encouraging since it shows that the value of f equal to 0.5 is of no fundamental importance.

Another alternative analyzed was the assumption that the reaction rate constant in its pre-exponential

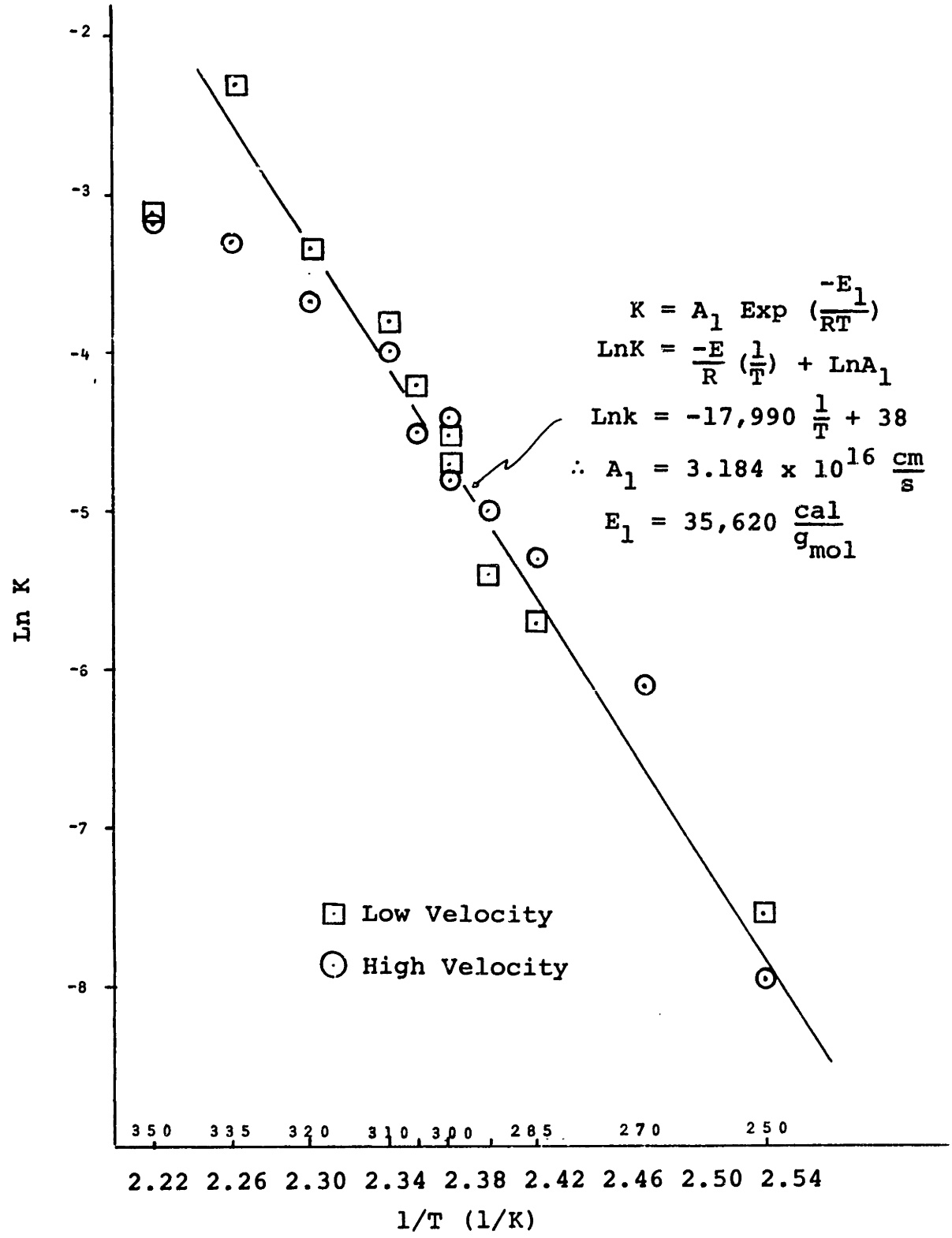

Figure 38. Logarithm of the reaction rate constant vs. 1/T. PH = 5.6, f = 0.1, Factor 2,000.

term had a dependence of temperature, $K = AT^{n}Exp(-E/RT)$. The effect needed was the reduction of the rate at which K increases as the temperature is raised; this would be achieved by using negative values for the exponent n. The range of values examined for n was from 0 to -2. The improvement (measured as better alignment of the data of Fig. 38 to a straight line) was very small.

The above exercises led to postulate that in the model developed we can only account for such fast decrease in the corrosion-erosion rate as a function of temperature by considering that the structure of the oxide layer is changing as a function of temperature and therefore it is necessary to assume some variations of porosity with temperatures, in line with Kubashewski and Hopkins (1967) which report porosity decreases as a function of temperature for oxides of niobdium. In our case, it needs to be experimentally verified that porosity changes are the reason for the variation in oxidation rate of low carbon steel. In this report the porosity of the layer was assumed to decrease linearly from 0.0005 to 0.0001 in the range of temperatures between 300 and 350 F. Figure 39 shows the assumed behaviour for porosity.

Nevertheless, the results of Fig. 38 are very encouraging. The figure shows that velocity effects have been adequately decoupled (high velocity points at one temperature sometimes have higher K-values than the

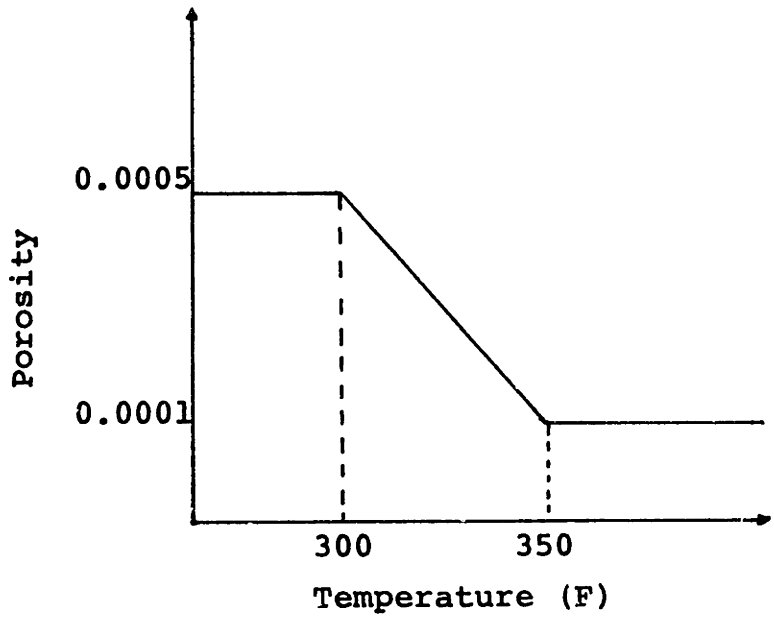

Figure 39. Variation of porosity with temperature assumed in calculation procedure.

low velocity points, but in other cases, it is the low velocity points that have high K values.

The figure also provided the method with which to estimate the value of the reaction rate constant K. From the slope and the y-intercept of the line in Fig. 38, K (in cm/s) becomes:

$$K = 3.184 \times 10^{16} \, EXP(35.620 / RT). \quad (55)$$

With this last equation a procedure to estimate the wear rate is now available.

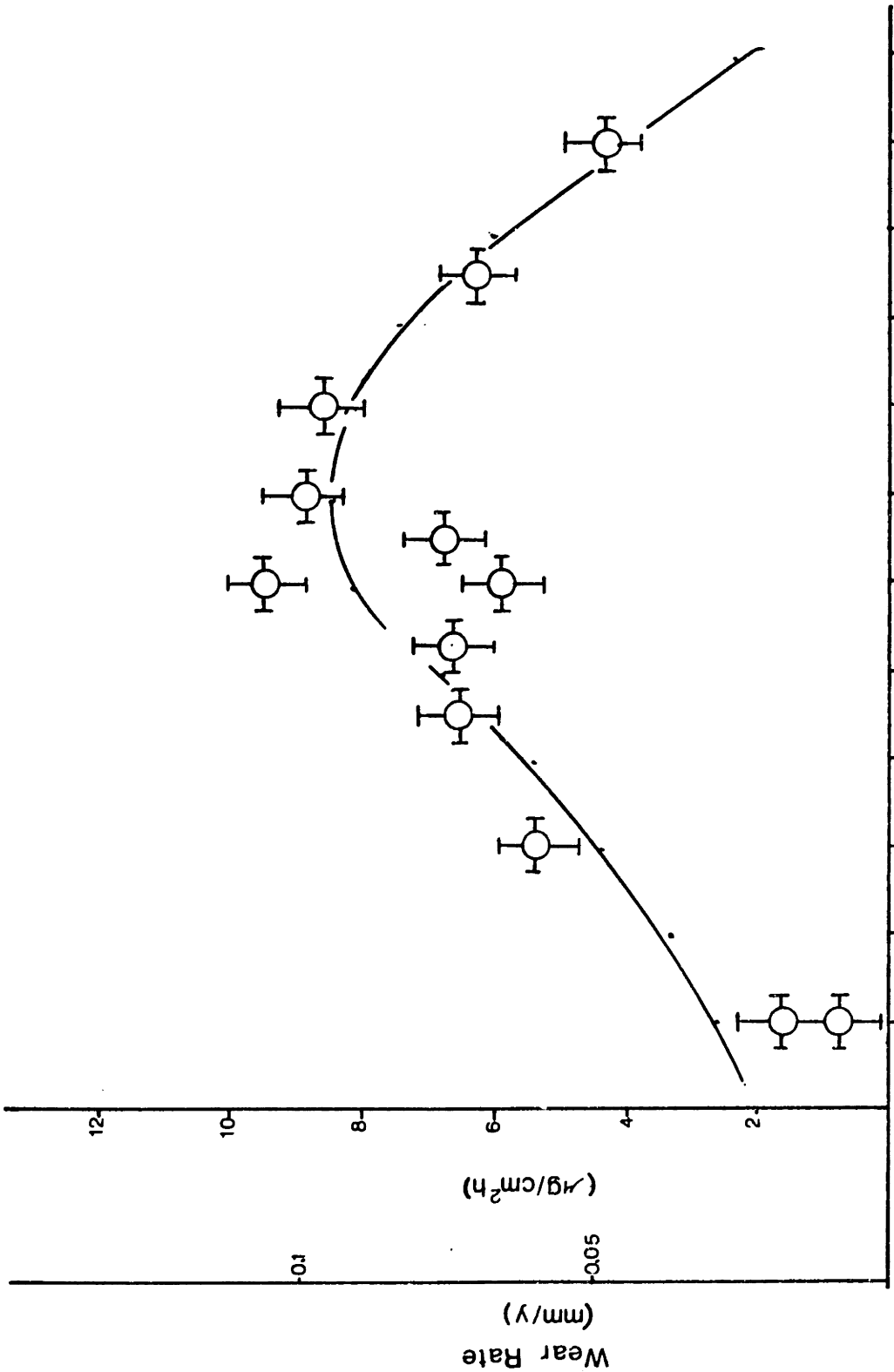

Figure 40. Comparison between the wear rate data and the results of the corrosion-erosion model for the high velocity specimens with f = 0.5, Factor = 2,000, pH = 5.6.

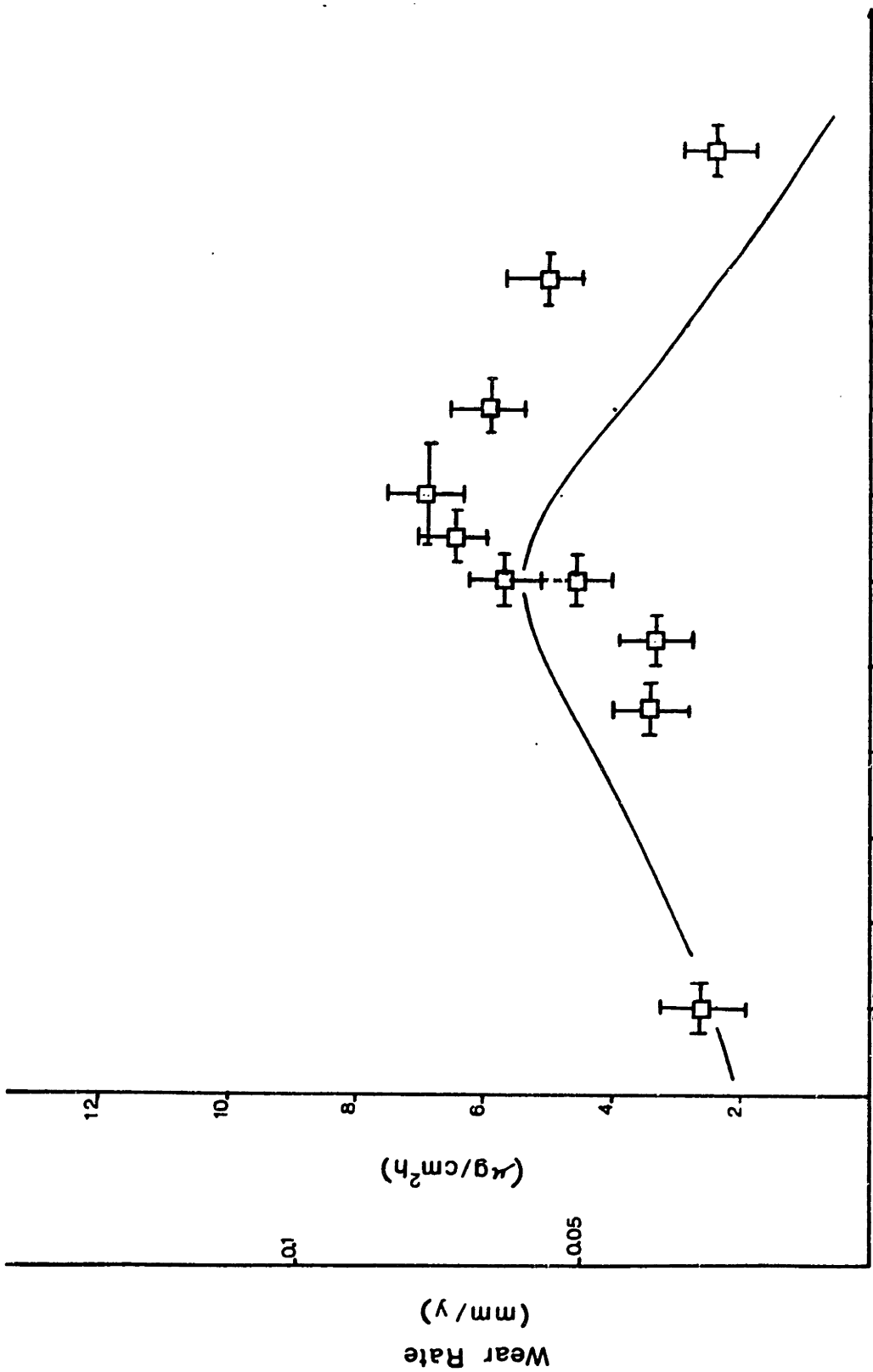

Figure 41. Comparison between the wear rate data and the results of the corrosion-erosion model, low velocity specimens, f = 0.5, Factor = 2,000, pH = 5.6.

6.2.4 Procedure To Determine Corrosion-Erosion Rates

6.2.4.1 Comparison Between Experimental And Theoretical Results -

The computer program CORERO.FOR was created. This program calculates wear rates in the range of temperatures between 250 and 360 F (120-175 C). The program was applied to the case of pH=5.6,δ=1μm and velocity of 9.5 ft/s and 1.7 ft/s (0.6 and 3 m/s). The results obtained were compared to the original experimental data.

Figures 40 and 41 show the results of the model together with the experimental data.

The results show good trends in regards to velocity and temperature and suggest that the wear rate can be predicted within a factor of 2. Since the data is not perfect the model is considered the best what can be done with the information gathered, but room for improvement through further experimentation is available.

6.2.4.2 Description of the Procedure to Determine Corrosion-Erosion Rates

The procedure which is the basis of the computer program CORERO.FOR is now described; see Appendix G for the listing of the program and the results from which Figs. 40 and 41 were obtained. The following list outlines the procedure to evaluate the corrosion-erosion

rate of low carbon steel of composition similar to that of steel A155 Gr C55. The procedure is the basis of the CORERO.FOR computer program.

1. Values of δ, pH, H_{2_∞}, temperature, velocity, geometric dimensions and thermodynamic properties must be provided.

2. The values of the equilibrium constant for each of the species are obtained from Eq. 54:

$$K_{e_b} = \text{EXP}[-\frac{A_b}{T} + B_b(\ln(T) - 1) + D_b)/R], \quad (54)$$

Values of A_b, B_b and D_b for b = 0, 1, 2, and 3 are provided in Appendix G.

3. The value of the concentration of hydrogen in the bulk of the fluid was considered to be the saturation value at the temperature of operation divided by FACTOR. Factor was chosen to be 2000.

4. Porosity is calculated as a function of temperature. In the calculation procedure it was assumed that $\Theta = 0.0005$ for $T < 300$ and that it decreases linearly to 0.0001 from 300 to 350 F, see Fig. 39.

5. The fraction of material oxidized that becomes magnetite at the metal-oxide interface, f (which is the same amount of material dissolved at the oxide-water interface), was considered to be 50%.

6. Diffusion coefficients for the iron species and for hydrogen are computed. The equation to be used is:

$$D = \frac{4.0 \times 10^{-7} T}{\mu (\tilde{V}^{1/3} - 2)} , \qquad (50)$$

At this stage the mass transfer coefficient for hydrogen can be computed from Eq. 51.

7. To start the calculation the hydrogen gas and hydrogen ion concentrations at metal-oxide interface are assumed to be the same as those in the bulk of the fluid.

8. The total concentration of iron species at equilibrium is computed by obtaining the individual concentration of each species, from Eq. 53,

$$[Fe(OH)_b^{(2-b)+}] = K_{e_b} [H^+]_o \; [H_2]_o , \qquad (53)$$

for b = 0, 1, 2, and 3 (the subindex o stands for the concentration of H^+ and H_2 at the metal-oxide interface) and then obtain the total concentration by adding the individual concentrations.

9. An average diffusion coefficient is obtained by calculating the ratio of the concentration of iron from each species to the total iron concentration. Then, the sum of these ratios multiplied by the respective diffusion coefficient of each hydroxide species yields an average diffusion coefficient.

10. An average mass transfer coefficient for iron species is obtained by making use of Eq. 51,

$$Nu = \frac{h_d D_e}{D} = 2 + cRe^a Sc^{1/3}, \qquad (51)$$

with $a = 0.86 - 10/(4.7 + Sc)^3$,

and $c = 0.0165 + 0.011ScExp(-Sc)$.

11. The wear rate is finally estimated from Eq. 41,

$$\dot{m}_1'' = \frac{C_e^{\Theta}}{\frac{1}{K} + (0.5)\{\frac{1}{h_d} + \frac{\delta}{D}\}} \qquad (41)$$

where $K = 3.184 \times 10^{16} \exp(35{,}620 / RT)$, (55)

12. Having calculated $\dot{m}_1''$, improved values of the concentrations of hydrogen and hydrogen ions can be obtained from Eqs. 42 and 43,

$$H_{2_0} = \dot{m}_1'' RT \left\{ \frac{\delta}{D_H \Theta} \left(1 + \frac{1}{3} f\right) + \frac{1}{h_{d_{H_2}}} \right\} + H_{2_\infty} \quad , (42)$$

$$H_0^+ = H_\infty^+ - 2C_0 + \frac{-A + (A^2 - B)^{\frac{1}{2}}}{2} \qquad (43)$$

13. With the improved values of H_0^+ and H_{2_0} an iterative procedure is followed by repeating steps 6 through 10 until an adequate convergence criterion for the concentration of H_0^+ and H_{2_0} is achieved.

6.2.5 Possible Uses For The Results Presented In This Report

6.2.5.1 The Corrosion-Erosion Model -

The major achievement in this thesis is to have derived an equation that can be used to estimate corrosion-erosion rates. The equation was derived for a specific material and it is expected that the value of the reaction rate constant obtained should change for other material compositions.

6.2.5.2 The Information Gathered - List Of Solutions To Corrosive-Erosive Wear

One of the required tasks during this work was to gain information about corrosion and, specifically, on the corrosion-erosion process. It is considered that the required knowledge was obtained and that the report provides an adequate review of the important variables that influence the corrosion-erosion rate. Understanding this behavior not only guided us towards deriving a model, but it also provided ideas on how to control high corrosion-erosion rates. A summary of these controlling measures is now listed.

1. Steam Quality.- Corrosion-erosion is a phenomenon generated as a result of the motion of fluid. The fluid provides a thermodynamically favorable environment for the corrosion to take place and the velocity provides a means with which to remove corrosion products. In dry steam conditions, dissolution cannot take place, and although corrosion proceeds following a parabolic rate law, (Surman, 1970), the wear rate is smaller than in a wet steam or water environment. The above results suggest that corrosive-erosive wear is proportional to the amount of liquid water in the pipe and thus adequate separation of the

liquid water can alleviate the wear problem.

2. Geometry.- Our experimental results and data from power stations clearly show that the regions where maximum wear is expected are the regions where high levels of turbulence are present. The turbulence arises either as a result of high fluid velocity or due to the presence of some fitting such as an orifice, a valve, or a branching of the flow.

   Although reducing the number of places where high local turbulence occurs can only be adequately addressed at the design stage (for example, by use of longer radius elbows), the use of inserts or straightners for plants already in operation may alleviate the problem by eliminating recirculation flow regions. A first step was taken by Berkow (1984) to evaluate the use of inserts.

3. Temperature.- The critical temperature around 150 C (300 F), at which maximum corrosion-erosion occurs is an important factor to consider. The mean width of the wear rate vs temperature curves is about 50 C. This is a rather small temperature range which might suggest that future design of steam extraction lines made of low carbon steel should avoid to

operate under temperatures close to 150 C.

4. Hydrogen Ion Concentration (pH).- The mechanism presented for the corrosion of steel in oxygenless water showed that, in this case, the principal oxidizer is the hydrogen ion. Providing more hydrogen ions (decrease in pH) increases the potential and thus the rate of metal dissolution. Sweeton and Baes (1970), Berge (1981) and Bignold (1981) have experimental data that shows that the wear rate decreases when the pH is raised (hydrogen ion concentration lowered) to a value of 9.5. From these results the recommendation is towards the use of pH of 7 or higher (9.75).

5. Oxygen.- The concentration of dissolved oxygen in the water is of great importance. Although oxygen in general increases corrosion rates it can passivate metals like iron, and induce a decrease in wear rate as shown by Brush and Pearl (1972), and Nesmeyanova (1970).

   Considerable decreases in the wear rate occur from 1 to 200 ppb of oxygen, sometimes by a factor of 100. Nevertheless, the high values of oxygen that account for the lower wear rates have the risk of pitting the material drastically if oxide layers are fractured. All

of the above results suggest the need for accurate control of oxygen contents to minimize corrosion-erosion or pitting corrosion.

6. Alloy for Use in Bends.- Low carbon steels are known to be only slightly corrosion resistant. There are data that suggest that, while corrosion-erosion wear can be in may cases alleviated by using alloyed steel with as little as 2.5 % Cr, a 13% Cr pipe is considered corrosion-erosion free, (Keller, 1974, Fontana and Green, 1978, Farber, 1982, Kunze, 1981, Berge, 1982).

Other elements that also provide corrosion-erosion resistance are copper and molybdenum. Results quoted by Berge (1982) show that these elements decrease the wear rate; two relations have been empirically derived for the influence of percentage of Cu and Mo in the wear rate. The data behind the relations is not extensive.

Implementing material changes is certainly a design alternative for reducing corrosion-erosion wear, but it may also be adequate to implement material changes during the maintenance period of an already operating plant.

An important consideration to keep in mind

is that joining two dissimilar metals leads to an increase in the risk of galvanic corrosion. Although an oxidation-reduction potential would be generated when a low carbon steel comes in contact with a 2.5% Cr steel, this potential may be small enough to be of no concern. Even if the potential is not small the corrosion rate might be so slow that galvanic corrosion is of no concern. Only corrosion tests can determine the actual rate of galvanic corrosion for a specific combination of materials, and therefore further experimental work on material combinations is recommended.

7. Workmanship.- This last point is related to the geometry considerations already discussed above. Good design consideration in regards to geometry (i.e., long radius elbows, no sharp turns etc.) may prove ineffective if the final alignment of the pipe and fitting or if the weld to join them is improperly done. Care must be taken to leave nice and smooth connections which will avoid regions of recirculation and separation, which enhance mass transfer rates, and as a consequence wear rates.

The equation is expected to predict wear rates within a factor of 10 of the actual wear rate, and faithfully predict parametric trends.

Improvements will come after further validation by the future experimental work that is proposed in Section 6.3.

A very important aspect to remember at this stage is the difference that exists between the actual conditions in a steam extraction line elbow and the experimental working conditions of the corrosion-erosion rig in our laboratory.

A simple geometry subjected to conditions of single-phase liquid water was used in the rig. In the power station the flow pattern is annular dispersed flow, and under certain conditions the film of water in the inside radius of curvature of a bend detaches from the surface creating a region of intense recirculation.

The geometric conditions are very different and therefore a linkage is required between the experimental work and the plant's actual problem. This linkage refers to the calculation of the mass transfer coefficient h_d. This coefficient will be determined by the characteristics of the film (flow rate, dimensions), which in turn depend on the geometry of the pipe and on the behavior of the two-phase flow. At present it seems that mass transfer rates would have to be increased considerably beyond those found in the experiments (a

factor of a 100 or more on the mass transfer rate) to achieve the high wear rate values found in the power station. Perhaps under actual conditions, the oxide layers formed are of greater porosity or smaller thickness; and therefore yielding the high wear rate values obtained in power plants.

The model developed here can be used to obtain the wear rates of steam extraction lines due to a water film. To be able to use the model the film's mass transfer coefficient needs to be estimated. Knowing the chemical conditions of the water it is possible to use the procedure in the previous section to obtain an estimate of the wear rate. The value of wear rate obtained might be increased by a factor of 4 if roughness is present and or by a factor of 2 if recirculation and separation are present.

From the above discussion, the need to study mass transfer rates in annular flows must be evident. A first step towards the necessary linkage between the results in this report and the actual wear rates in plants was taken by Pak (1984), who investigated the wear pattern on glue coated elbows for different qualities, velocities, and piping conditions.

6.2.5.3 The Description Of The Experimental Rig

The report includes the procedure for operating the corrosion-erosion rig. Nevertheless, certain deficiencies in the design have been observed through the results. These deficiencies, which will be discussed in the next section, and the operating procedure, constitute important information to the next person that carries on with the work on corrosion-erosion.

The rig as it stands can be used to test different materials, different environments, and different combination of materials (to check for galvanic corrosion); it may prove to be a useful system in future corrosion-erosion research.

6.3 FUTURE WORK

In this section a list of ideas for future work is provided. The ideas are aimed at validating the model developed here, and at determining explicit solutions for the alleviation of corrosive-erosive wear.

6.3.1 Suggestions For Future Work On Subjects Related To Corrosion-Erosion

From the discussion about the corrosion-erosion in steam extraction lines, a number of subjects requiring further work arose. One important need is to determine

local mass transfer coefficients for complicated geometries. It is necessary to evaluate mass transfer coefficients for water films that separate from the wall, as well as for impinging droplets travelling at low speed (i.e., unable to cause mechanical wear). Knowledge of the characteristics of the water film is important in the determination of mass transfer coefficients.

The above ideas are aimed at making the model here developed more trustworhty for power station application. Also they would help to identify potentially high wear rate locations in a piping system.

6.3.2 Suggestions For Future Work On Corrosion-Erosion

The corrosion-erosion apparatus in the laboratory can be used for further experimentation of corrosion-erosion. The experimentation would validate the developed model and would allow to obtain solutions related to material composition, pH and oxygen cocentration.

The rig is capable of operating at different velocities, up to 30 ft/s, at different ph's. Time constraints have prevented us from continuing with this experimentation, but the information gathered from such proposed work is thought to be important in further validating the model developed in Chapter 3.

Inserting different materials and different

combinations of materials (to test for galvanic corrosion) would provide the basis for selecting the most adequate and least expensive material that could be used in actual practice. This is an important activity in which to engage since material composition is a definite solution to the problem of corrosion-erosion.

Testing specimens with a specified roughness can also provide information about the important, but little known, aspect of how the surface finish affects corrosion-erosion.

The final and most important investigation must include the examination of an actual specimen from a failed pipe. Examination under the scanning electron microscope and in the X-Ray Photoelectron spectrometer would provide useful knowledge about oxide thickness and porosity of steam extraction lines. The wear pattern and surface finish on the oxide can provide some insight into the mechanism of the wear.

6.3.3 Modification Suggestions To The Experimental Procedure And Apparatus

6.3.3.1 Experimental Rig - Modifications - -

The additions that are now proposed to the corrosion rig are aimed at achieving more controllability of the oxygen content which is the variable not adequately controlled during our tests.

The loop requires a sampling line where vacuum can be created, and where oxygen and pH probes, which do not stand pressures greater than 100 psi, can be used. The line should prevent leakage which may change the oxygen concentration.

In order to be able to modify oxygen contents in the loop the water must be boiled before filling the system, argon must bubbled through and, if very low levels of oxygen are required, hydrazine should be injected (Bailinger, 1984). All this can be done with little modification. The pressure vessel already in operation needs to be modified to allow for a connection to an argon tank and to the hydrazine injector, and for impeding water from passing through to the rest of the loop until oxygen conditions are well established (this last requirement can easily be satisfied by fitting a valve at the bottom of the pressure vessel). A suitable oxygen analyzer is required for monitoring this important variable.

6.3.3.2 Experimental Procedure Modifications -

The method of running the test and obtaining wear data seems adequate. Nevertheless, room for improvement exists especially with regards to the techniques used in preparing samples for the S.E.M. and the XPS.

The first modification required is linked to the design of the test section. The general geometry used

has proven to be acceptable, but it is necessary to eliminate completely the possibility of water leaking through to the inside of the specimen. A possible alternative to the specimen assembly is given in Fig. 41. A test assembly as suggested in Fig. 41 not only would prevent leakage, but it would also ease the assembling and disassembling process.

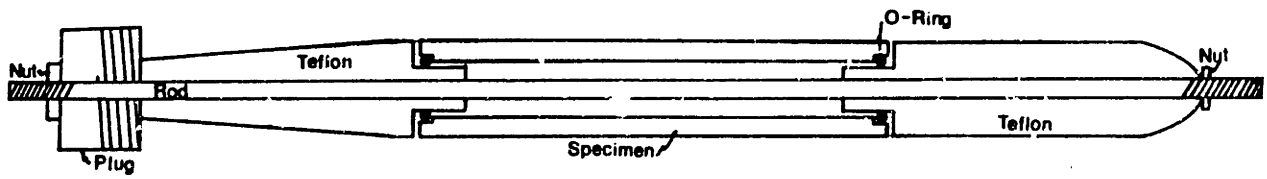

Figure 41. Improved design of the specimen assembly for the prevention of oxidation in the inside of the specimen. Compare with Figure C1, Appendix C.

In regards to the techniques used in the preparation of the specimen to be observed under the S.E.M., the suggestion refers to a first step that may be worth taking after the specimen is cut to 1/2 of its final size.

To protect friable corrosion products from damage due to shock and to define accurately oxide boundaries, vacuum impregnation with an epoxy resin is strongly recommended. The equipment required is a vacuum chamber with a rotatable table (Buehler, 1983). The cutting, mounting and polishing techniques can then be completed.

A suitable etchant should be applied before placing the specimen under the S.E.M.. In the past, the etchant used was nital (2% nitric acid). This is believed to be a strong etchant since the pictures show that corrosion products were somewhat dissolved. It is therefore recommended to use more gentle etchants; see Buehler (1983) for specific suggestions.

Finally through all the process of analysis by S.E.M. and spectrometer care must be taken to work under clean and safe conditions. The use of gloves, sample tongs and safety glasses is strongly recommended.

Two major achievements of this work were discussed in this chapter the first was a procedure for the estimation of wear rates (Section 6.2.4.2); the second was a list of solutions for the alleviation of corrosive-erosive wear (Section 6.2.5.2).

CHAPTER 7

SUMMARY AND CONCLUSIONS

Systematic measurements were performed concerning material wear due to corrosion-erosion of specimens in single-phase liquid water with a pH of 5.5 and at two different velocities. In particular, the effects of the fluid temperature on a low carbon steel, A155 Gr C55, were analyzed.

The results showed that there exists a temperature at which the wear rate is a maximum (150 C) and that specimens subjected to a high velocity systematically experience higher wear rates than those at low velocity.

During the work two goals were pursued.

The first goal was to present the state of our knowledge regarding the phenomenon of corrosion-erosion. This information is of great interest to personnel working with this sort of problem.

Fulfilling the above objective led to the conclusion that the problems occurring from corrosive-erosive wear can be considerably diminished or

even eliminated if the systems are properly designed and constructed. This includes the use of chrome alloy materials, a reduction in flow velocity, an increase in the pH value or the oxygen content and good workmanship when the connections of pipe fittings are made.

Since the improvement of material composition is an expensive design solution, it may be only adopted for the critical temperature range. Further work to suggest inexpensive protective material combinations with low risk of galvanic corrosion is necessary for plants already in operation and experiencing corrosion-erosion problems.

The second goal, the development of a model to estimate wear rates, can be considered 80% achieved. The model developed was based on the description of the corrosion of iron given by Heitman (1981). What is now required is to further validate the model by obtaining wear rate data for different velocities, oxygen contents and pH's.

A list of steps to follow in order to evaluate wear rates is included in Section 6.2.4.2

A specimen with a well-defined geometry, used in the experimental work, allowed for mass transfer coefficients to be determined. This geometry also proved that the method in which the kinetics and hydrodynamics were treated was adequate. An energy activation value of close to 30,000 cal/gmol was related

tc the kinetics of the corrosion-erosion. This value, which is typical of activation energies of steel corroding in steam is an encouraging result and gives credibility to the model.

Future work on topics related to corrosion-erosion is necessary, particularly in the area of mass transfer coefficient of films and sprays over curved walls. In addition, further work is needed to develop a procedure to estimate film and spray characteristics of annular flow in large diameter piping systems containing two-phase flow.

With the knowledge gathered from the proposed research it would be possible to employ with more confidence the model developed here. This would make it possible to identify high wear locations, and consequently take suitable measures to prevent plant shut downs or accidents. This last point should be sufficient to warrant further studies on the subject.

REFERENCES

Adler, W. F.
"The Mechanism of Liquid Impact", Treatise on Material Science and Technology (New York: Academic Press, 1980) pp. 15-19.

ASME Standards
Annual Book of Standards. Section II (1974) part H.

ASME Standards
Annual Book of Standards. Part 10-G1 (1981)

Ballinger, Ronald
"Discussion on Testing Equipment for Corrosion", Private Communication (January, 1984)

Bentrcia, Mohamed
"Erosion Distribution in the Vicinity of an Obstruction", M. Sc. Thesis, M.I.T. Mech. Eng. (1982)

Berge, Ph.
"Mecanisme de L'Oxydation des Aciers dans L'eau a Haute Temperature et de la Formation des Depots d'Oxydes", Congress d'Ermenoville (Ermenoville, France: March, 1972)

Berge, Ph., C. Ribon and P. Saint Paul
"Effect of Hydrogen on the Corrosion of Steels in High Temperature Water", Corrosion-NACE, V. 32, No. 6 (June, 1976) pp.223-228.

Berge, Ph., J. Ducreux and P. Saint Paul
"Effects of Chemistry on Corrosion-Erosion of Steel in Water and Wet Steam", Water Chemistry of Nuclear Reactor Systems BNES (Bournemouth: October, 1980) pp. 15-19.

Berge, Ph. and F. Khan
"Corrosion-Erosion of Steels in High Temperature Water and Wet Steam", Reunion E.D.F. (Les Renardiers: May, 1982).

Berger, F. P. and K. Hau
Heat and Mass Transfer, V. 20, (1977) p. 1185.

Berkow, M. Jonathan.
"The Use of Novel Bend Geometries to Reduce or Eliminate Erosive-Corrosive Wear in Steam Extraction Lines", M. Sc. Thesis M.I.T. Mech. Eng. (1984).

Bignold, G., J. R. Garnsey and G. M. W. Mann
"High Temperature Aqueous Corrosion of Iron Development of Theories of Equilibrium Solution Phase Transport through a Porous Oxide", Corrosion Science V. 1 (1972) pp. 325-332.

Bignold, G. J. and I. S. Woolsey

"Hysterisis Effects in Response of Mild Steel Circuits to Changes in Water Chemistry", Water Chemistry II. BNES (Bournemouth, 1980) pp. 25-29.

Bignold, G. J., K. Garbett, R. Garnsey and I. S. Woolsey
"Erosion-Corrosion in Nuclear Steam Generators", Water Chemistry II. BNES, (Bounemouth, 1980)

Bignold, G. J., K. Garbett, R. Garnsey and I. S. Woolsey
"Tackling Erosion-Corrosion in Nuclear Steam Generating Plants", Nuclear Engineering International, V. 26, No. 314 (June, 1981)

Bignold, G. J., C. H. de Whaley, K. Garbett, K. Garnsey, I. S. Woolsey, D. F. Libaert and R. Sale
"Erosion Corrosion of Mild Steel in Amoniated Water", Met. Corrs. Proc. International Congress on Metallic Corrosion 8th (1981).

Bradbury, D. and M. A. Dhil
"Water Chemistry of Nuclear Reactor Systems Second International Conference, 1980", Nuclear Energy, V. 20, No. 1 (1981) pp. 13-14.

Brush, E. G. and W. L. Pearl
"Corrosion and Corrosion Product Realease in Neutral Feedwater", Corrosion NACE, V. 28, No. 4, (April, 1972) pp. 129-136.

Buehler
"Metallographic Preparation for Corrosion Studies", Metal Digest, V. 22, No. 2 (1983).

Castle, E. and G. M. Mann
"The Mechanism of Formation of a Porous Oxide Film on Steel", Corrosion Science, V. 6, (1966) pp. 253-262.

Castle, J. E. and H. G. Masterson
"The Role of Diffusion in the Oxidation of Mild Steel in High Temperature Aqueous Solution", Corrosion Science, V. 6 (1966) pp. 93-104.

Castle, J. E. and R. G. Thompson
"Stability of Ferrous Hydroxide in Aqueous Suspension at 300 C", J. Appl. Chem. V. 17 (June, 1967) pp. 177,178.

Cataldi, H. A., C. F. Cheng and V. S. Musick
"Investigation of Erosion and Corrosion of Turbine Materials in Wet Oxygenated Steam", Transactions of the ASME (October, 1958) pp.1465-1478.

Faber, G., A. Hausermann, and R. Svoboda
"Ten Years of Experience with Erosion-Corrosion in a PWR and a BWR Plant", ASME Paper No. 82-JPGC-PWR-46 (1982).

Fitzsimmons, W. L. Pearl, and M. Siegler
"Simulated Boiling Water Reactor and Superheat Reactor Corrosion Facility", Nuclear Science and

Engineering, V. 17, (1963) pp. 18-29.

Fontana, Mars G. and N. D. Greene
Corrosion Engineering (New York: Mc. Graw Hill, 1978).

Gadiyar H. S. and N. S. D. Elayathu
"Corrosion and Magnetite Growth on Carbon Steels in Water at 310 C- Effect of Dissolved Oxygen, pH and EDTA Addition , Corrosion-NACE, V. 36, No. 6 (June 1980) pp. 306-312.

Garnsey, R.
"Boiler Corrosion and the Requirement for Feed-Water and Boiler-Water Chemical Control in Nuclear Steam Generators", Water Chemistry of Nuclear Reactor Systems, BNES (London: 1978) pp. 1-10.

Garnsey, R.
"Corrosion of PWR Steam Generators", Nuclear Energy, V. 18, No. 2 (April, 1979) pp.117-132.

Gregor, Arthur
"Techniques for Mounting Specimens for Observation in SEM", Private Communication (August, 1983).

Griffith, P., E. Rabinowicz, Hung Vu and Luis E. Sanchez-C
"Erosive-Corrosive Wear in Steam Extraction Lines", Progress Reports, M.I.T. Mechanical Engineering (August 1981 - October 1982).

Heitman H. G. and W. Kastner
"Erosionskorrosion in Wasser Damfkreislaufen-Urschen und Gegenmaznahmen", (Erosion-Corrosion in Water-Steam Cycles-Causes and Counter Measures), V.G.B. Kraftwerkstechnik, V. 62, Heft 3 (March 1982) pp. 211 - 219.

Henry, George
"Density Variations in Water Flowing over a Flat Plate with Surface Boiling", M. Sc. Thesis M.I.T. Mech. Eng. Dept. (1952).

Heymann, F. J.
"High Speed Impact Between a Liquid Drop and a Solid Surface", Journal of Applied Physics, V. 40 No. 13, (December, 1969) pp. 5113 - 5122.

Heymann, F. J.
"Conclusions from the ASTM Interlaboratory Test Program With Liquid Impact Erosion Facilities", Proc. 5th Int. Conf. on Erosion by Solid and Liquid Impact (1979) pp. 1-10.

Hutchings, I. M.
"A Model for the Erosion of Metals by Spherical Particles at Normal Incidence", Wear, V. 70 (1981) pp. 269 - 281.

Ishii, M. and M. A. Grolmes
"Inception Criteria for Droplet Entrainment in

Two-Phase Concurrent Film Flow", A.I.Ch.E. Journal, V. 21, No. 2 (March, 1975) pp. 308 - 318.

Ishii, M., I. Kataoka and G. Kocamastafaogullari
"Phenomenological Modeling of Two Phase Flow in Water Reactor at ANL (Two Fluid Model, Interfacial Area, Droplet Entrainment and Droplet Size)", NRC 9th Water Reactor Safety Research Information Meeting (October 30, 1981).

Jones, Bob (Beckman Instruments)
"pH Measurement in High Purity Water", Technical Information (Representatives Memorandum) for Instrument Line No. E - Chem 81-4, (April, 1981).

Keller, H.
"Erosionskorrosion an Nabdampturbinen" (Erosion-Corrosion in Wet Steam Turbines), V.G.B Kraftwerkstechnick, V. 54, Heft 5 (May, 1974) pp. 292 - 295.

Kubaschewski, O. and B. Hopkins
Oxidation of Metals and Alloys (New York: Academic Press, 1979).

Kunze, E.
"Erosion-Corrosion in Power Plants", Met. Corros. Proc. Int. Congress on Metallic Corrosion 8th (1981) pp. 1555 - 1560.

Lambert, I., J. Montel and P. Courvoisier
"Influence of Hydrogen Pressure on the Solubility of Magnetite in Aqueous Solutions", Water Chemistry II BNES (1980) pp. 31 - 35.

Lapukhov, A. S.
"On Diffusion Transportation of Substance in Fissure Faces and Through Intergranular Space of Water-Saturated Rocks", Geologia i Geofizika (in Russian), No. 12 (1966).

Maddock, C., P. M. C. Lacey and M. A. Patrick
"The Structure of Two Phase Flow in A Curved Pipe", Conference in Multiphase Flow Systems, The Inst. of Chem Eng. Symp Series No. 3 (1974) pp. 12 -21.

Metal Handbook
8th Edision, V. 1, Properties and Selection of Metals (Ohio: American Society for Metals, 1961) p. 66.

Mohato B. K. and L. W. Shemilt
"Effect of Surface Roughness on Mass Transfer", Chemical Engineering Science, V. 23 (1968) pp. 183 - 185.

Mc. Manus, H. N.
"Local Liquid Distribution", ASME Tech. Paper No. 61-Hyd-20 (1961).

Nesmeyanova, K. A.

"Effect of Oxygen on Steel Corrosion in Steam-Water Flows at a Temperature of 280 C", Soviet Atomic Energy Research, V. 29 (1970) pp. 781 - 785.

Pack, Byong G.
"Prediction of Maximum Wear Location in Steam-Extraction Lines of Power Plants", M. Sc. Thesis M.I.T. Mech. Eng. Dept. (1984).

Pearl, W. and G. Wozaldo
"Corrosion of Carbon Steel in Simulated Boiling Water and Superheated Reactor Environments", Corrosion-NACE, V. 21 (August, 1965) pp. 260 - 267.

Potter, E. and G. Mann
"Mechanism of Magnetite Growth on Low-Carbon Steel in Steam and Aqueous Solution up to 550 C", 1st International Congress of Metal Corrosion (London: 1962).

Rabinowicz, E. and K. Chakravarthy
"Erosive-Corrosive Wear of Copper", Journal of Lubrication Technology (Technical Briefs), Transactions of the ASME (April 1977) pp. 302 - 303.

Rabinowicz, E.
"Experimental Errors", Private Communication (September, 1983)

Rohsenow, Warren
"Condensation in Forced Convection", Class Notes, M.I.T. Course Number 2.57 (Spring 1982).

Rohsenow, Warren and H. Choi
Heat, Mass and Momentum Transfer, (Eleglewood Cliff, N. J.: Prentice Hall, 1961).

Sanchez-Caldera, L. E.
"Review of the Phenomenon of Erosion-Corrosion in Steam Extraction Lines of Power Stations", Congress on Two-Phase Gas Liquid Flow in Pipes, Instituto de Investigaciones Electricas (Mexico: August, 1983)

Scully, J. C.
Fundamentals of Corrosion (New York: Pergamon Press, 1966)

Shreirer, L.
Corrosion, V. 1 and V. 2 (London: Georg Newness Ltd., 1963).

Sprague, P. J, S. Wilkin and M. Coney
"Effects of Two Phase Flow on Wall to Fluid Mass-Transfer in Bends and and Straight Pipes", 1983 European Two Phase Flow Group Meeting (Zurich, 1983) pp. 1 - 13.

Springer, George
Erosion by Liquid Impact (New York: John Wiley and Sons, 1976).

Surman, P. L.

"The Oxidation of Iron at Controlled Oxygen Partial Pressures- I. Hydrogen/Water Vapor", Corrosion Science, V. 13 (1973) pp. 113 - 124.

Surman, P. L.
"The Oxidation of Iron at Controlled Oxygen Partial Pressures- II. Carbon Monoxide-Carbon Dioxide", Corrosion Science, V. 13 (1973) pp. 825 - 832.

Surman, P. L. and J. E. Calstle
"Gas Phase Transport in the Oxidation of Fe and Steel", Corrosion Science, V. 9, (1969) pp. 771 - 777.

Sweeton, F. H. and C. F. Baes, Jr.
"The Solubility of Magnetite and Hydrolisis of Ferrous Ion in Aqueous Solutions at Elevated Temperatures", J. Chem. Thermodynamics, V. 2 (1970) pp. 479 - 500.

Tabor, D.
The Hardness of Metals (Oxford: Clarendon, 1951).

Uhlig, H. Herbert
The Corrosion Handbook (New York: John Wiley and Sons, Inc., 1948).

Uhlig, H. Herbert
Corrosion and Corrosion Control and Introduction to Corrosion Science and Engineering (New York: John Wiley and Sons, Inc., 1963).

Evans, Ulick
The Corrosion and Oxidation of Metals: Scientific Principles and Practical Applications (London: Edward Arnold LTD., 1960).

Vu, Hung V.
Erosive-Corrosive Wear in Steam-Extraction Lines of Power Plants, M.I.T., Mech. Eng. M. Sc. Thesis (June, 1982) pp. 1 -50.

Wallis, G. B.
"Annular Two Phase Flow. Part I Simple Theory", Journal of Basic Engineering, Transactions of the ASME (March, 1970) pp. 59 - 72.

Wallis, G. B.
"Annular Two Phase Flow. Part II Additional Effects", Journal of Basic Engineering, Transactions of the ASME (March, 1970) pp. 73 - 82.

White, M. Frank
Fluid Mechanics (New York: Mc Graw Hill Book Co., 1979) pp. 311 - 313.

Other References Used, But Not Cited

Adler, W. F.
"Assessment of the State Knowledge Pertaining to Solid Particle Erosion", Contract No. DAAG29-77-C-039 U.S. Army Research Office (June, 1979).

Allen, P. and H. A. Hampson
"The Effect of Electrical Potential on the Dissolution of Iron Oxide Crystals I. A Review of Selected Relevant Literature", Surface Technology, V. 7, (1978) pp. 273-287.

Allen, P., N. A. Hampson and J. F. Tyson
"The Differential Capacitance of Magnetite", Surface Technology, V. 9 (1979) pp. 395-400.

Allen, P., N. A. Hampson and G. J. Bignold
"The Effect of the Potential on the Dissolution of Magnetite", Surface Technology, V. 12 (1981) pp. 199-204.

Anderson, G. and P. D. Hills
"Two Phase Annular Flow in Tube Bends", Conference in Multiphase Flow Systems Session B-1, pp. J1 (1974).

Arden, T. V.
"The Solubility Products of Ferrous and Ferrosic Hydroxides", J. Chem. Soc. (1950) pp. 882-885.

Bechtel, S. E., D. Bogy and F. E. Talke
"Impact of a Liquid Drop Against a Flat Surface", I.B.M. J. Res. Develop., V. 25, No. 6 (November, 1981) pp. 963-971.

Beck, T. R., D. W. Mahaffey and J. H. Olsen
"Pitting and Deposits with Organic Fluid by Electrolysis and by Fluid Flow", J. Electrochem. Soc. Electrochemical Science and Technology, (February, 1972) pp. 155-160.

Beck, T. R., D. W. Mahaffey and J. H. Olsen
"Wear Small Orifices by Streaming Current Driven Corrosion", Transactions of the A E Journal of Basic Engineering (December, 1970) pp. 782-791.

Belton, G. R. and F. D. Richardson
"A Volatile Iron Hydroxide", Trans. Faraday Society, V. 58 (1962) pp. 1562-1572.

Beslu,P., G. Frejaville and Lalet
"A Computer Code Pactole to Predict Activation and Transport of Corrosion Products in a PWR", Water Chemistry of Nuclear Reactor Systems, BNES (London, 1978) pp. 195-201.

Comley, G. C. W.
"Some Aspects of System Chemistry of BWR's"

Progress in Nuclear Energy, V. 2 (1978) pp. 153-181.

Cordovi, M. A.
"Corrosion Considerations in Light Water-Cooled Nuclear Power Plants", Int. Nickel Power Conference (Kyoto, Japan: 1972) pp. 1-34.

Dawson, David and Olev Trass
"Mass Transfer at Rough Surfaces", J. Mass Transfer, V. 15, (1972) pp. 1317-1336.

Evans, A. G., Y. M. Ito and M. Rosenblatt
"Impact Damage Thresholds in Brittle Materials Impacted by Water Drops", J. Appl. Phys., V. 51, No. 5 (May, 1980) pp. 2473-2482.

Eisenberg, M., C. W. Tobias and C. R. Wilkie
"Ionic Mass Transfer and Concentration Polarization at Rotating Electrodes", J. Electrochemical Soc. V. 101, No. 6 (1954) pp. 306-319.

Godfrey, Douglas
"Diagnosis of Wear Caused by Liquid Flowing over Metals", Wear Diagnosis Seminar ASME/ASLE Int. Lubric. Conference (August, 1980) pp. 1-12.

Harvis, F. R.
"SGHWR Steam Turbine for the 100 MW(e) Prototype", Nuclear Engineering, (June, 1967) pp. 440 - 443.

Humphrey, J. and Sheng Chang
"Measurement and Calculation of Developing Turbulent Flow in a U-Bend and Downstream Tangent of Square Cross-Section", Second Annual Technical Report Turbulent Flow and Heat Transfer in Passage around 180 Bend, An Experimental and Numerical Study (September, 1981)

Hussey, R. J., G. I. Sproule, D. Caplan and M. J. Graham
"The Growth and Structure of Oxide Films Formed on Fe in Oxygen and Carbon Dioxide at 550 C", Oxidation of Metals, V. 11, No. 2 (1977) pp. 65 - 79.

Klein, I. E., J. Sharon and A. E. Yaniv
"A Mechanism of Oxidation of Ferrous Alloys by Superheated Steam", Scripta Metallurgica, V. 15 (1981) pp. 141 - 144.

Krzyzanowsky J. and Z. Szprengiel
"The Influence of Droplet Size on the Turbine Blading Erosion Hazard", J. of Engineering for Power, V. 100 (October, 1978) pp. 561 - 565.

Lesser, M. B.
"Analytic Solutions of Liquid-Drop Impact Problems", Proc. R. Soc. Lond. A, V. 377 (1981) pp. 289 - 302.

Linton, W. H. and T. K. Sherwwod
"Mass Transfer from Solid Shapes to Water in Stream

Line and Turbulent Flow", Chemical Engineering Progress (May 1950) pp. 258 - 264.

Lister, D. H.
"The Transport of Radioactive Corrosion Products in High Temperature Water. II The Activation of Isothermal Steel Surfaces", Nuclear Science and Engineering, V. 59 (1976) pp. 406 - 426.

Mijering, J. L. and M. L. Verheijke
"Oxidation Kinetics in the Case of Aging Oxide Films", Acta Metallurgica, V. 7 (May, 1959) pp. 331 - 338.

Orna, Miloslav and Zdenek Ruml
"A Contribution to the Erosion Resistance of Turbine Blade Materials", Proc. 5th Int. Conf. on Erosion by Solid and Liquid Impact (1979) pp. 23.1 - 23.9.

Pallev, I. and B. S. Filippovich
"Phenomena of Liquid Transfer in Two-Phase Dispersed Annular Flow" Int. J. Heat and Mass Transfer, V. 9 (1966) pp. 1089 - 1093.

Pocock F. J., J. A. Lux and R. V. Seibel
"Control of Iron Pickup in Cycles Utilizing Carbon Steel Feedwater Heaters", Proc. Amer. Power Conf., V. 28 (1966) pp. 758 - 771.

Rao, Veerabhadra and B. C. Syamala Rao
"Similarities in Different Experiments of Erosion Caused by Cavitation and Liquid Impingement", Journal of Testing and Evaluation, V. 9, No. 3 (May, 1981) pp. 179 - 138.

Rickerby, D. G., B. N. Pramila Bai and N. H. Macmillan
"The Effect of Crystallographic Orientation on Damage in MgO due to Spherical Particle Impact", Journal of Material Science, V. 14 (1979) pp. 1807 - 1816.

Rickerby, D. G. and N. H. Macmillan
"The Erosion of Aluminum by Solid Particle Impingement at Normal Incidence", Wear, V. 60, (1980) pp. 369 - 382.

Sleicher, C. A.
"Maximum Stable Drop ize in Turbulent Flow", A.I.Ch.E. Journal, V. 8, No. 4 (September, 1962) pp. 471 - 475.

Tabakoff, W., J. Ramachandran and A. Hamed
"Temperature Effects on the Erosion of Metals Used in Turbomachinery", Proc. 5th Int. Conference on Erosion by Solid and Liquid Impact (1975) pp. 47.1 - 47.5.

Troyanovskii, B. M.
"Influence of Wetness on Efficiency of Steam Turbines", Teploenergetika, V. 25, No. 10 (1978)

pp. 28 - 33.

Uhlig, H. Herbert
"Initial Oxidation Rate of Metals and the Logarithmic Equation", Acta Metallurgica, V. 4, (September, 1956) pp. 541 - 554.

Uhlig, H. and Anton de S. Brasunas
"Effect of Magnetic transformation at the Curie Temperatures on Oxidation Rates of Chromium-Iron Alloys", Journal of the Electrochemical Society, V. 97, No. 12 (December, 1950) pp. 498 - 452.

Yehudah, Taitel, Naugab Lee and A. Dukler
"Transient Gas Liquid Flow in Horizontal Pipes: Modeling the Flow Pattern Transitions", A.I.Ch.E. Journal, V. 24, No. 5 (September, 1978) pp. 920 - 933.

Yehudah, Taitel, Dvora Bornea and A. E. Dukler
"Modelling Flow Pattern Transitions for Steady Upward Gas-Liquid Flow in Vertical Tubes", A.I.Ch.E. Journal, V. 26, No. 3 (May, 1980) pp. 345 - 354.

APPENDIX A

WEAR RATE BY DROPLET IMPINGEMENT

In the initial stages of the corrosion-erosion research most of the work was focused on the damage of the material caused by droplet impact.

To predict the wear rate by impinging droplets it is necessary to put together elements from two-phase flow, corrosion, and fatigue by droplet impingement. The first steps toward this integration, in the case of steam extraction lines, are briefly reviewed in this appendix.

A.1 EQUATION FOR THE WEAR BY DROPLET IMPINGEMENT

In searching for an equation where wear rates could be obtained from droplet and target characteristics, the first step was to abandon the idea of obtaining an empirical relation as those were already available in the literature, (Heymann, 1969, 1979).

The second step was to examine the amount of material removed during the impact of a high velocity droplet. The

analysis used to obtain the wear rate expression was similar to the one reported by Hutchings et al. (1980) for the wear of solid spherical particles.

In deriving the wear equation the following important assumptions were made (Griffith et al., 1981-1982):

1. The velocity of the droplet is high enough for the pressure resulting from impact to cause plastic deformation.

2. All the energy of the droplet is used in deforming the material plastically.

3. The criterion for failure is one of critical strain, i.e. the fracture occurs when the material undergoes a maximum strain.

4. The strain at a point after N impacts is related to the strain produced by one impact through random walk theory i.e. the strain produced by each impact is radially directed in all directions, see Fig. A1.

It is noteworthy to point out that the first of the above assumptions poses a limitation on the cases where the derived equation can be used. The equation can only be used in cases where the velocity of droplets is high enough for the yield stress of the material to be reached. A limit of applicability for the size and velocity of droplets must therefore, be obtained (The Best Number may be useful in this respect, [Tabor, 1931]).

From assumptions 1 through 4 the expressions for the number of impacts required to cause failure (incubation

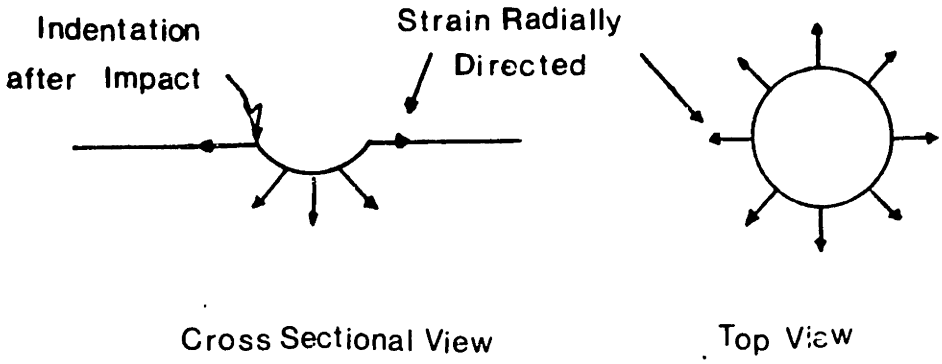

Figure A1. The strain produced by a droplet impact is considered to be radially directed in all directions.

period) and the following relation for the volumed removed per droplet impact, were derived;

$$\dot{v}' = \frac{k\rho_{drop} m_{drop} V^4}{\varepsilon_c^2 P^2} \qquad (A1)$$

where $\dot{v}'$ = the volume removed per droplet impact

k = the wear coefficient

ρ_{drop} = drop densitiy

V = velocity

ε_c = critical strain of target

P = hardness

m_{drop} = mass of a droplet

The interested reader can find the detailed derivation of this relation in Griffith et al. (1981-1982).

It is important to emphasize the characteristics of Eq. A1. The main assumption under which this equation was based is that the mechanism by which wear takes place is direct deformation of the material. Other effects, such as wave propagation, lateral outflow jetting, and hydraulic penetration (Adler, 1979), have not been considered.

Equation 1 has three very attractive characteristics:

a) the wear is related to target and droplet properties,

b) the equation shows that the wear is proportional to a high power of velocity. This agrees well with experimental data, see Heymann (1979), Springer (1976), Adler (1980), and

c) the equation is dimensionally exact.

The most challenging task in employing Eq. A1 is to determine the appropriate values for the hardness P, and the critical strain ε_c for the target, and the constant k

A.2 TWO PHASE FLOW CONSIDERATIONS

For the case of the steam extraction lines mentioned in Figure 2 of the text where the velocity and quality (x) were 130 ft/s and 93 % respectively, annular flow is the dominant flow pattern for this conditions.

To obtain the mass velocity of droplets impacting on an elbow or a tee, we first obtain the amount of liquid that

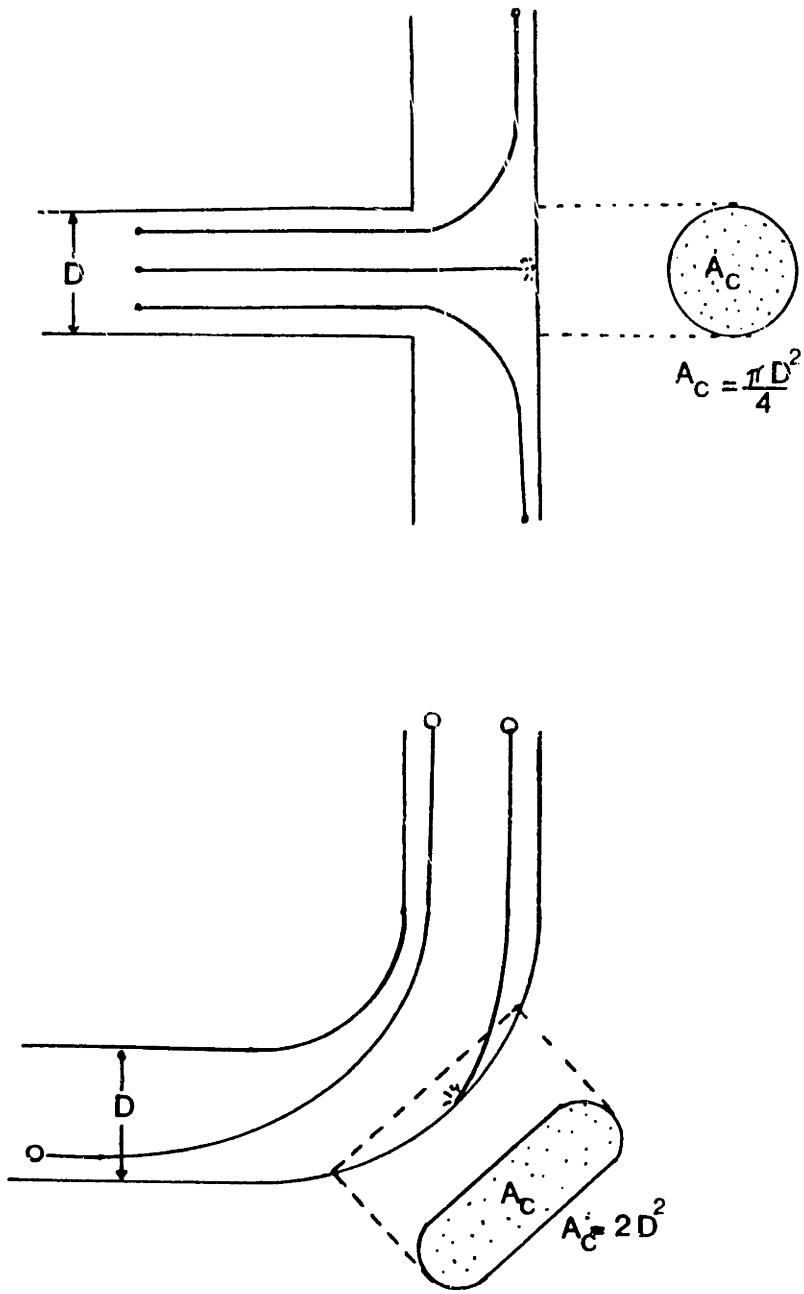

Figure A2. Characteristic areas for a Tee and an elbow.

becomes droplets, F_e. The fraction F_e, known as the entrainment, can be estimated through the use of empirical relations like those of Wallis (1969) and Ishii (1981). These correlation tend, in general, to provide an upper bound for the wear rate since they represent equilibrium entrainment conditions; it takes considerable distance for an entrainment percentage to obtain its fully developed value.

Not all of the droplets traveling in the pipe will impact the characteristic area, A_c, see Fig. A2. The fraction of droplets that hit the pipe, F_h, is influenced considerably by the secondary flow. The factor F_h can be estimated through the numerical integration of the equation of motion of a droplet traveling in a two-dimensional flow.

The above considerations lead to the following expression for the number of droplets arriving per unit area per unit time:

$$N_i = \frac{\dot{m}(1-x)F_e F_h}{\rho_{drop} V A_c} \quad , \qquad (A2)$$

where N_i = number of impacts per unit area per unit time,

$\dot{m}$ = total mass flow rate in steam extraction line.

Equation A1 multiplied by equation A2 yields:

$$\dot{v} = \frac{kV^4 \rho_{drop} \dot{m}(1-x) F_e F_h}{\varepsilon_c{}^2 P^2 A_c} , \qquad (A3)$$

which is the relation expressing the amount of material removed per unit area per unit time.

A.3 CORROSION CONSIDERATIONS

Discussion of the corrosion of steel in liquid water was included in Chapter 2. In this section, we only analyze the different possibilities from which to estimate the wear rate by droplets that impinge on a metal that is subjected to corrosion.

For our analysis, we have assumed that an oxide layer forms on the metal and that it tends to grow as a function of time following a parabolic or logarithmic law, $\delta(t)$,(see Chapter 2); under static conditions (no flow) the oxides formed on steel in aqueous solutions do tend to follow such laws, (Scully, 1966, Surman, 1969).

Figure A3 shows the decision making process as well as the alternatives to estimate the wear rate by droplet impingement. The figure is now further explained.

First it is necessary to determine whether the droplet has enough energy to cause erosion, either in the metal or in its oxide. The possibility of a droplet having enough energy to cause mechanical damage is first analyzed.

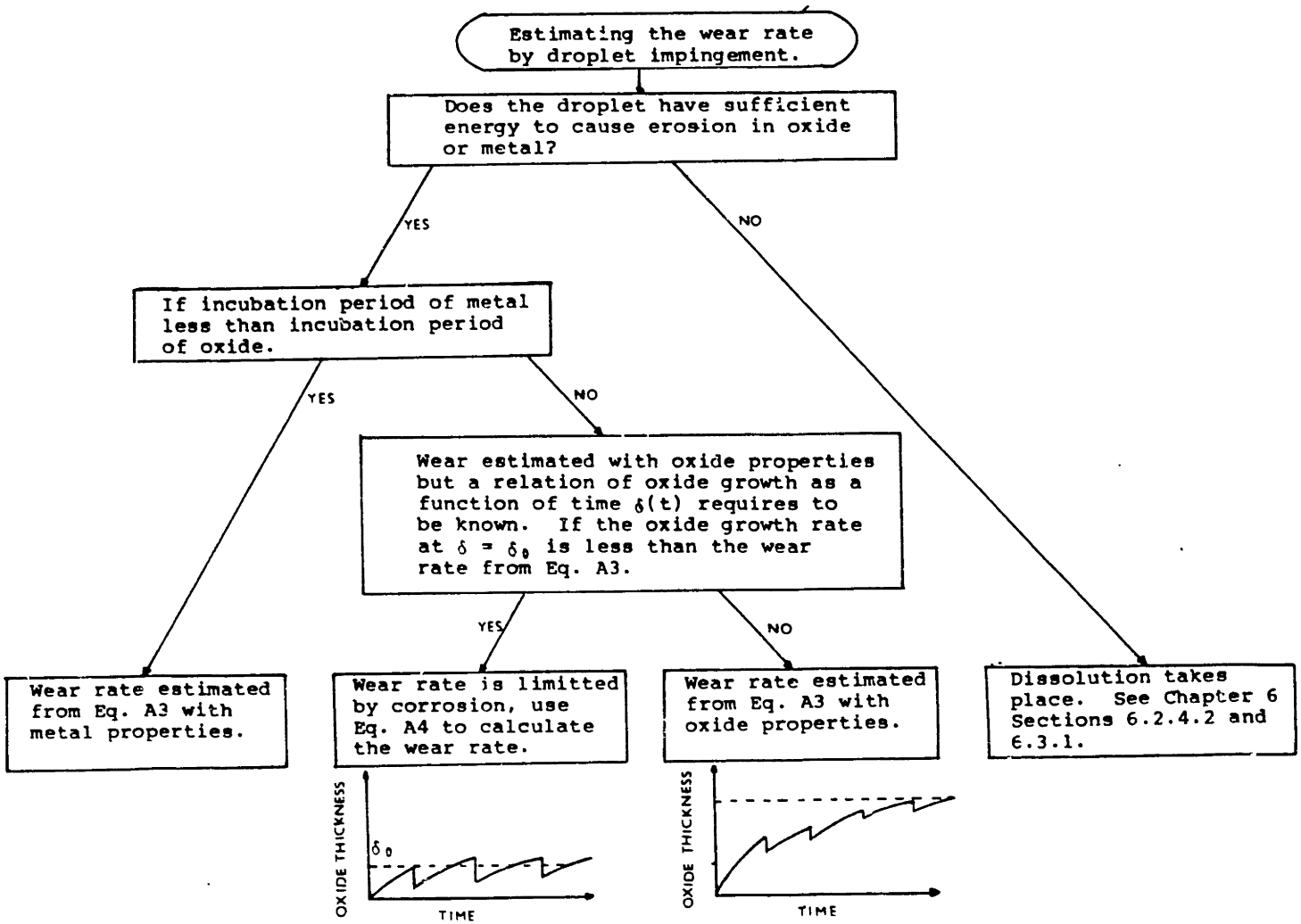

Figure A3. Alternatives to estimate the wear rate in a corrosion environment.

In Eq. A3 it is necessary to determine whether the target material is an oxide or a metal.

If the incubation period for the metal (the number of impacts required for the metal to fail) is less than the incubation period for the oxide, metal properties (P and ε_c) would be used in Eq. A3. This is the case, for example, of chromium oxide, (Faber, 1982).

When the incubation period of the corrosion layer is less than that of the metal, the properties to be considered in determining the wear rate are those of the corrosion layer.

The author believes that in order for the oxide to be removed, it must grow in thickness, as is shown in Fig. A4(a). If we assume, as mentioned previously, that the thickness of the oxide follows a known function of time $\delta(t)$, we can idealize the phenomenon by considering that the oxide must reach thickness δ_o for oxide wear to occur, see Fig. A4(b). The value of δ_o has been taken as the depth necessary for the plastic deformation of one droplet impact to remain confined in the oxide; see Griffith et al., Final Report (1982) for further details.

At this stage in the decision making process two possibilities arise when a comparison is made between the wear rate obtained from Eq. A3 (with oxide properties) and the growth rate of the oxide layer ($\dot{\delta}$) at the moment when the oxide thickness reaches the thickness δ_o. The two possibilities are:

The metal is damaged but not removed (within incubation period for metal).

The oxide begins to grow. The metal does not reach ε_c

The oxide film thickness greater than δ_o The metal does not experience further damage.

Oxide removal

(a)

Mechanism of oxide removal (incubation period of metal greater than incubation period of oxide)

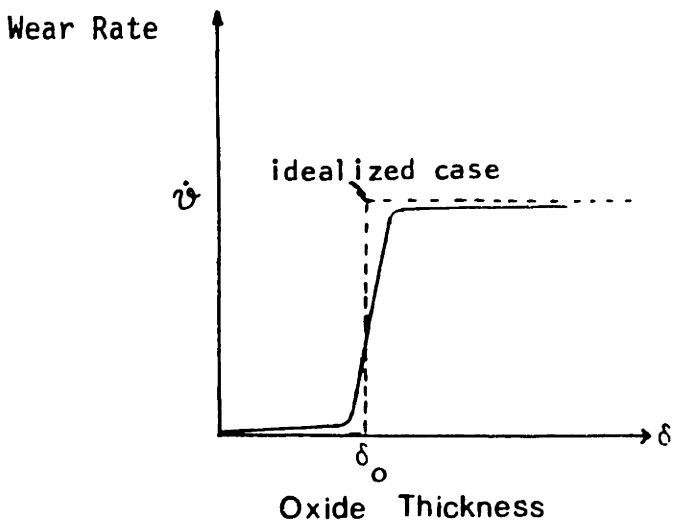

(b)

Figure A4. Assumed mechanism of oxide removal by droplet impingement.
a) Description of the mechanism.
b) Graph representing the assumption that oxide wear rate is considered zero if oxide thickness, δ, is less than δ_o and $\dot{v}$ (Eq. A3) if δ is greater than δ_o.

a) If the oxide growth rate at $\delta = \delta_o$ is larger than the wear rate from Eq. A3, the oxide layer can continue to grow until an equilibrium is reached, see Fig. A3. In this case the wear rate can be predicted directly from Eq. A3.

b) If the oxide growth rate at $\delta = \delta_o$ is smaller than the wear rate from Eq. A3, the oxide layer will be reduced almost to zero thickness. In this possibility it will be necessary to wait for the oxide thickness to reach again δ_o so that further removal by droplet impingement can take place. This possibility suggests that the limiting mechanism is the corrosion rate and that the metal lost can be evaluated by considering the amount of iron that is removed when the thickness of the oxide is reduced from δ_o to zero in a time period t_1. The following relation expresses this rate of removal:

$$\text{wear rate} = \frac{k_2 \rho A_c \delta_o}{t_1} , \quad \text{(A4)}$$

where k_2 = the ratio of iron weight in the oxide.

ρ = oxide densitiy

A_c = characteristic area

δ_o = the parabolic or logarithmic assumed known relation for the oxide growth as a function of time, oxide thickness at time t_1.

t_1 = time for δ to reach δ_o.

A final alternative to calculate the wear rate is the possibility that the droplet may not have enough energy to cause wear by impingement.

If the droplet is traveling at a low velocity or if the material is so resistant that erosion can not take place, low carbon steel can still be worn down by the removal of iron ions by a convection mass transfer process. This is the principal mechanism that has been considered in the report.

In the case where this dissolution process exists, the impingement phenomenon increases the wear rate of corrosion alone by providing high mass transfer coefficients, i.e., high mass transfer rates, of iron ions to the film of water formed by the impinged droplets. The study of mass transfer coefficients provides the information necessary to employ the model which was developed in Chapter 3, see Section 3.1.1.

A.4 FUTURE WORK

The above notes show the introductory work on corrosion-erosion by liquid impact. Further work is necessary to obtain a criterion for the energy requirements for the droplets to cause erosion. Experimental work of the type where a metal is first oxidized and subsequently

impinged by droplets is also needed. The experimental data would determine the wear coefficient of Eq. A3. This equation may then be further validated through the use of more experimental data. A procedure for calculating erosive-corrosive wear in different systems may then be established.

APPENDIX B

DERIVATION OF THE CORROSION-EROSION MODEL

In this appendix the derivation of the main relations of the model are briefly described.

B.1. The Corrosion-Erosion Rate Equation

In the model it is assumed that steady state conditions have been reached, Figure B1 shows the processes that the model takes into account.

All the assumptions that led to the model of corrosion-erosion have been discussed in the text. For the purpose of deriving the equations only some of them are explicitly reviewed.

1. The transformation of iron into hydroxides occurs from the overall reaction:

$$Fe + 2H_2O \rightarrow Fe(OH)_2 + 2H_2 \,. \qquad (B1)$$

The net rate of hydroxide formation at the metal interface is assumed to be given by:

$$\dot{m}_1'' = K\Theta(C_e - C_o). \qquad (B2)$$

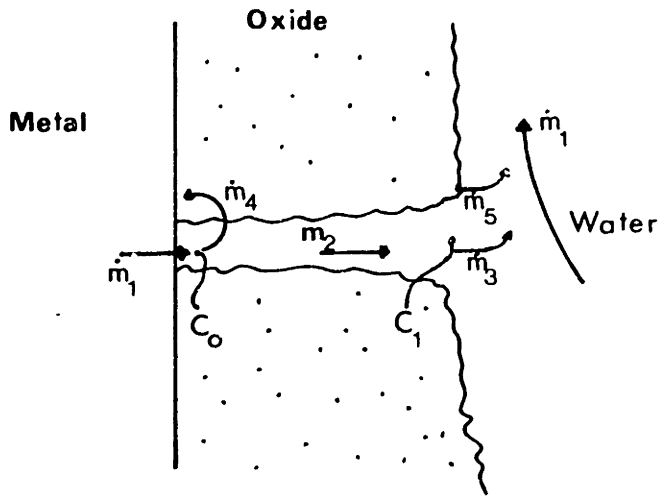

$$\dot{m}_1'' = \dot{m}_2'' + \dot{m}_4''$$
$$\dot{m}_2'' = \dot{m}_3'', \quad \dot{m}_2'' = (1-f)\dot{m}_1''$$
$$\dot{m}_4'' = \dot{m}_5''$$
$$\dot{m}_1'' = \dot{m}_3'' + \dot{m}_5''$$

Figure B1. Processes considered in the model of corrosion-erosion: $\dot{m}_1''$ = iron dissolution, $\dot{m}_2''$ = iron hydroxide diffusion through the oxide layer, $\dot{m}_3''$ = removal of iron hydroxide by water, $\dot{m}_4''$ = conversion of hydroxides to magnetite, $\dot{m}_5''$ = dissolution of magnetite.

where: K = a function that depends on temperature only.

Θ = porosity (available area per unit area of metal).

C_e = equilibrium concentration of iron hydroxide at temperature, H^+ and H_2 conditions of the metal-oxide interface.

C_o = the actual concentration of hydroxides at the metal-oxide interface.

2. There is a diffusion of the iron species through the oxide layer. The diffusion rate accounts for the removal of hydroxides that do not become magnetite at the metal interface, i.e. the fraction (1-f). The diffusion through the layer is expressed as:

$$\dot{m}_2'' = (1-f)\dot{m}_1'' \qquad \text{(B3a)}$$

$$\dot{m}_2'' = \frac{D\Theta}{\delta}(C_o - C_1), \qquad \text{(B3b)}$$

where: D = diffusion coefficient of iron species

Θ = porosity (volume of water per unit volume of oxide)

C_o, C_1 = iron hydroxide concentration at the metal-oxide interface and at the oxide-water interface respectively.

$(1-f)$ = fraction of hydroxides not converted into magnetite at the metal-oxide interface.

3. By forced convection mass transfer the hydroxides

leave the pores and are mixed into the water according to:

$$\dot{m}_3'' = (1-f)\dot{m}_1'' , \qquad \text{(B4a)}$$

$$\dot{m}_3'' = h_d\Theta(C_1 - C_\infty), \qquad \text{(B4b)}$$

where: h_d = mass transfer coefficient

C_∞ = iron concentration in the bulk of the fluid.

Equations B2, B3, and B4 represent a system of 3 equations with 3 unknowns $\dot{m}_1''$, C_o, and C_1. The following steps lead to the model of corrosion-erosion.

From Eqs. B3 and B4, and solving for C_1:

$$\frac{D\Theta}{\delta(1-f)}(C_o - C_1) = \Theta h_d(C_1 - C_\infty),$$

$$C_1 = \frac{DC_o + \delta h_d C_\infty}{D + (1-f)K\delta} , \qquad \text{(B6)}$$

From B3 and B1 and solving for C_o:

$$(1-f)KC_e - (1-f)KC_o = \frac{DC_o}{\delta} - \frac{DC_1}{\delta}$$

$$C_o = \frac{\delta(1-f)KC_e + DC_1}{D + (1-f)K\delta} , \qquad \text{(B7)}$$

Equation B6 in Eq. B5 yields an expression for C_1:

$$C_1 = \frac{D\delta(1-f)KC_e}{(D+h_d\delta)(D+(1-f)K\delta-D^2} - \frac{h_d\delta C_\infty(D+(1-f)K\delta)}{(D+h_d\delta)(D+(1-f)K\delta)-D^2} , \quad (B7)$$

From Eq. B7 in B4 an expression for the oxidation rate is obtained:

$$\dot{m}_1'' = \frac{1}{(1-f)}\{\frac{h_d\Theta D\delta(1-f)KC_e}{(D+h_d\delta)(D+(1-f)K\delta)-D^2} -$$

$$- h_d\Theta C_\infty(1 - \frac{h_d\delta C_\infty(D+(1-f)K\delta)}{(D+h_d\delta)(D+(1-f)K\delta)-D^2})\} \quad (B8)$$

The final equation in the text is obtained when C_∞ is considered zero in Eq. B8 and the simplifying Eq. 41 is obtained.

$$\dot{m}_1'' = \frac{C_e\Theta}{\frac{1}{K} + (1-f)(\frac{1}{h_d} + \frac{\delta}{D})} , \quad (41)$$

B.2. Derivation of the Equation for the Concentration of Hydrogen at the Metal-Oxide Interface.

According to the reaction

$$Fe + 2H_2O \rightarrow Fe(OH)_2 + 2H_2 , \quad (B9)$$

which is the result of the following three equations:

$$Fe \rightarrow Fe^{++} + 2e^{-} \quad , \tag{B10}$$

$$2H_2O \rightarrow 2H^{+} + 2OH^{-} \quad , \tag{B11}$$

$$2H^{+} + 2e^{-} \rightarrow H_2 \quad , \tag{B12}$$

for every mole of $Fe(OH)_2$ formed there will be one mole of H_2 generated.

Since it has been considered that a fraction f of the hydroxide formed gets converted into magnetite according to:

$$3Fe(OH)_2 \rightarrow Fe_3O_4 + 2H_2O + H_2 \quad , \tag{B13}$$

the equation suggests that additional hydrogen is generated. For every mol of $Fe(OH)_2$ converted into magnetite, 1/3 mole of H_2 is produced.

The total generation of hydroxide at the metal-oxide interface is:

$$\dot{m}''_{1_H} = \dot{m}''_1 + \tfrac{1}{3}f\dot{m}''_1 \quad ,$$

$$\dot{m}''_{1_H} = (1 + \tfrac{1}{3}f)\dot{m}''_1 \quad , \tag{B14}$$

Other equations representing the diffusion through the layer and the removal of H_2 by the water are:

$$\dot{m}''_{2_H} = \dot{m}''_{1_H} = \frac{D_{H_2O}}{\delta}(H_{2_o} - H_{2_1}), \tag{B15}$$

$$\dot{m}_3'' = h_{d_{H_2}} (H_{2_1} - H_{2_\infty}), \qquad \text{(B16)}$$

where: D_{H_2} = diffusion coefficient of hydrogen

δ = oxide layer thickness

Θ = porosity

$h_{d_{H_2}}$ = mass transfer coefficient for hydrogen

H_{2_o} = hydrogen concentration at the metal base.

H_{2_1} = hydrogen concentration at the oxide-water interface

H_{2_∞} = hydrogen concentration in the bulk of the water.

At the oxide water interface it is necessary to consider that the amount of hydrogen removed is the result of the diffusion of hydrogen from the inside of the oxide layer minus the hydrogen consumed during the dissolution of the oxide at the oxide-water interface; therefore,

$$\dot{m}_3'' = \dot{m}_{2_h}'' - \tfrac{1}{3} f \dot{m}_1'' , \qquad \text{(B17)}$$

Figure B2 represents the processes included in the derivation of the equation for the hydrogen concentration at the meta-oxide interface.

From the assumptions made above, it follows that:

$$\dot{m}_{2_H}'' = \dot{m}_{1_H}'',$$

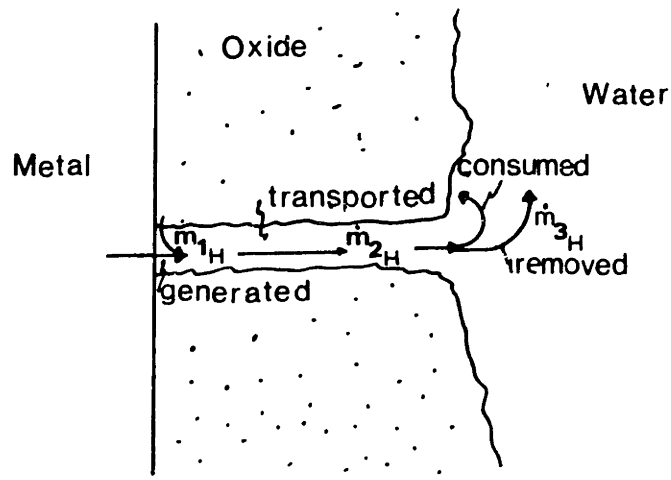

Figure B2. Processes included in the derivation of the expression for H_2 concentration at the metal-oxide interface.

which with Eqs. B14 and B15 above become:

$$(1+\tfrac{1}{3}f)\dot{m}_1'' = \frac{D_H\Theta}{\delta}(H_{2_o} - H_{2_1}),$$

$$H_{2_o} = \frac{\delta}{D_H\Theta}(1+\tfrac{1}{3}f)\dot{m}_1'' + H_{2_1}, \qquad \text{(B18)}$$

With Eqs. B15 and B16 in Eq. B17, the following relation is obtained:

$$h_{d_{H_2}}(H_{2_1} - H_{2_\infty}) = \frac{D_{H\Theta}}{\delta}(H_{2_o} - H_{2_1}) - \tfrac{1}{3}f\dot{m}_1''.$$

Solving for H_{2_1} the next relation is obtained:

$$H_{2_1} = \frac{D_H\Theta H_{2_o} + \delta^{h_{d_{H_2}}} H_{2_\infty} - \frac{1}{3}\delta f \dot{m}''_1}{\delta h_{d_{H_2}} + D_H\Theta}, \qquad (B19)$$

Combining Eq. B19 with Eq. B18, solving for H_{2_o} and simplifying the relation for the hydrogen concentration at the boundary metal-oxide is obtained:

$$H_{2_o} = \dot{m}''_1 \left(\frac{\delta}{D_H\Theta}\left(1+\frac{1}{3}f\right) + \frac{1}{h_{d_{H_2}}}\right) + H_{2_\infty}. \qquad (B20)$$

If the concentration H_{2_∞} is given in atm. and not in mole/cm^3, the factor RT (universal gas constant and temperature in degrees K) needs to multiply the first term of the right hand side of the above equation for a dimensionally correct relation to be obtained, that is the equation included in the text as Eq.42.

B.3. Derivation of the Hydrogen Ion Concentration at the Metal-Oxide Interface

The main assumption in the derivation of the expression for H^+_o is the consideration that the dissociation of water is very fast and thus the equilibrium concentration of H^+ exists through the layer.

The conditions of H^+ and hydroxyl radicals (OH^-) in the

bulk of the water are given by

$$|H^+|_\infty |OH^-|_\infty = K_W, \qquad \text{(B21)}$$

where: $|H^+|$ = hydrogen ion concentration in the bulk of the water

$|OH^-|$ = hydroxyl concentration in the bulk of the water

K_W = dissociation product of water

From Eqs. B9 to B12 it is evident that for every hydroxide formed there will be a consumption of 2 hydrogen ions. If C_o is the concentration of hydroxides at the metal-oxide interface, it can then be considered that there is a decrease in the number of hydrogen ions equal to $2C_o$.

In order to satisfy the equilibrium condition, water will dissociate according to Eq. B11. For every water molecule dissociated there will be one hydrox 1 radical and one hydrogen ion formed.

If X is defined as the number of water molecules dissociated, the hydrogen ion concentration at the metal-oxide interface will be given by:

$$H_o^+ = |H_\infty^+| - 2C_o + X, \qquad \text{(B22)}$$

while the number of hydroxyl radicals will increase by X, and therefore its concentration at the metal-oxide interface is given by:

$$OH_o^- = |OH_\infty^-| + X. \qquad \text{(B23)}$$

To obtain the value of X, reference is made to Eq. B21 which needs to be modified for the conditions at the metal-oxide interface, i.e.

$$(H_o^+)(OH_o^-) = K_w. \qquad \text{(B24)}$$

Equation B22 and B23 in Eq. B24 yield:

$$(H_\infty^+ - 2C_o + X)(OH_\infty^- + X) = K_w . \qquad \text{(B25)}$$

Equation B25 leads to a quadratic equation for X with the following relation as a solution:

$$X = \frac{-A + \sqrt{A^2 - B}}{2}, \qquad \text{(B26)}$$

where $A = H_\infty^+ - 2C_o + K_w/H_\infty^+$

$$B = 4\{(H_\infty^+ - 2C_o)\frac{K_w}{H_\infty^+} - K_w\}$$

Equation B26 in Eq. B22 results in Eq. 43 in the text.

APPENDIX C

DESCRIPTION OF THE COMPONENTS OF THE SYSTEM

In this appendix the characteristics of each component of the system are included. The calculations used in the design method have been omitted, but the design procedure is briefly described.

C.1. The Test Section

As described in the text, the requirements of simple hydrodynamic conditions around the specimen led us to choose an annular geometry for the test section. The specimen was machined according to the dimensions in Fig. C1. These dimensions allowed the specimen to be machined by making use of standard size lathe collars. The teflon pieces in the front and back of the specimen serve two purposes. One, they electrically isolate the specimen from any stray currents that may promote or retard the wear rate; and two, they serve as developers of the flow. The hydrodynamic conditions at the entrance of the actual specimen can be considered well developed. The length of the initial teflon piece is well over 20 L/D's, the distance required to have fully developed flow (White, 1979).

Tests were run at high and low velocities simultaneously

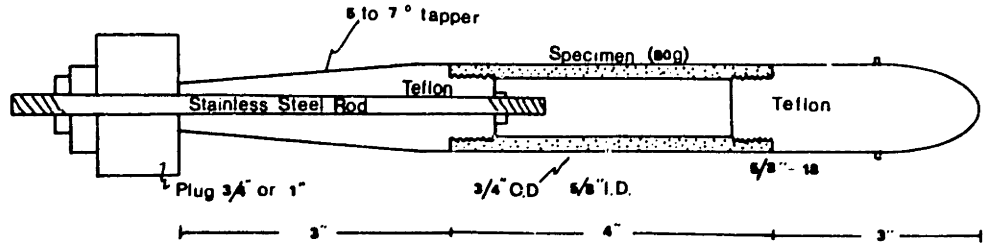

Figure C1. Corrosion-erosion specimen dimensions.

Low velocity tests were carried out by fitting the assembly of Fig. C1 to a 1" pipe, while in the high velocity test the assembly was placed in a 3/4" pipe. The arrangement for each section is shown in Fig. C2 and C3. Both assemblies were placed in series, and experimental data showed that this characteristic of the system does not influence the determination of the wear rate.

C.2 The Cooler

To purify 10 % of the flow, it was necessary to cool the water. The original design condition for this and the rest of the system was that the maximum operating temperature

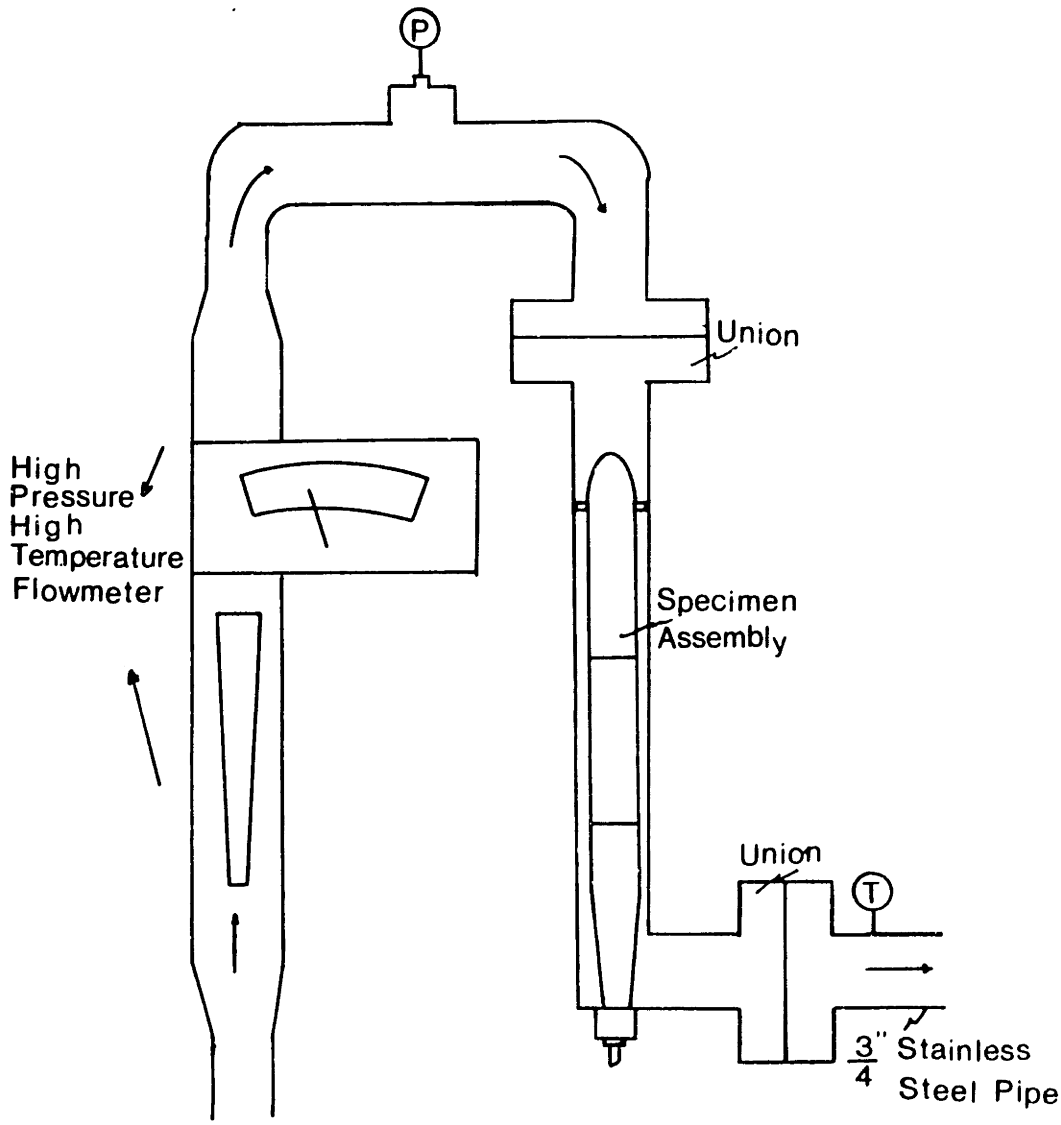

Figure C2. Test section arrangement.

Figure C3. Photograph of the test section.

would be 320 F, since at the time the rig was originally designed it was expected to find a peak in the wear rate vs. temperature curve around 270 F.

The wear rate data obtained showed the need to expand the range of temperature conditions to 360 F. The ion-exchanger and filter sections were modified to withstand the high pressures associated with 360 F, but the rest of the components were left as in the original design.

The cooler was designed to lower the temperature of 0.55

gpm from 320 F to 120 F. This component was a counterflow heat exhanger water-water made of 304-stainless steel pipe 3/8" in 3/4". Its total length was about 16 ft. Figure C4 shows a schematic of the cooler.

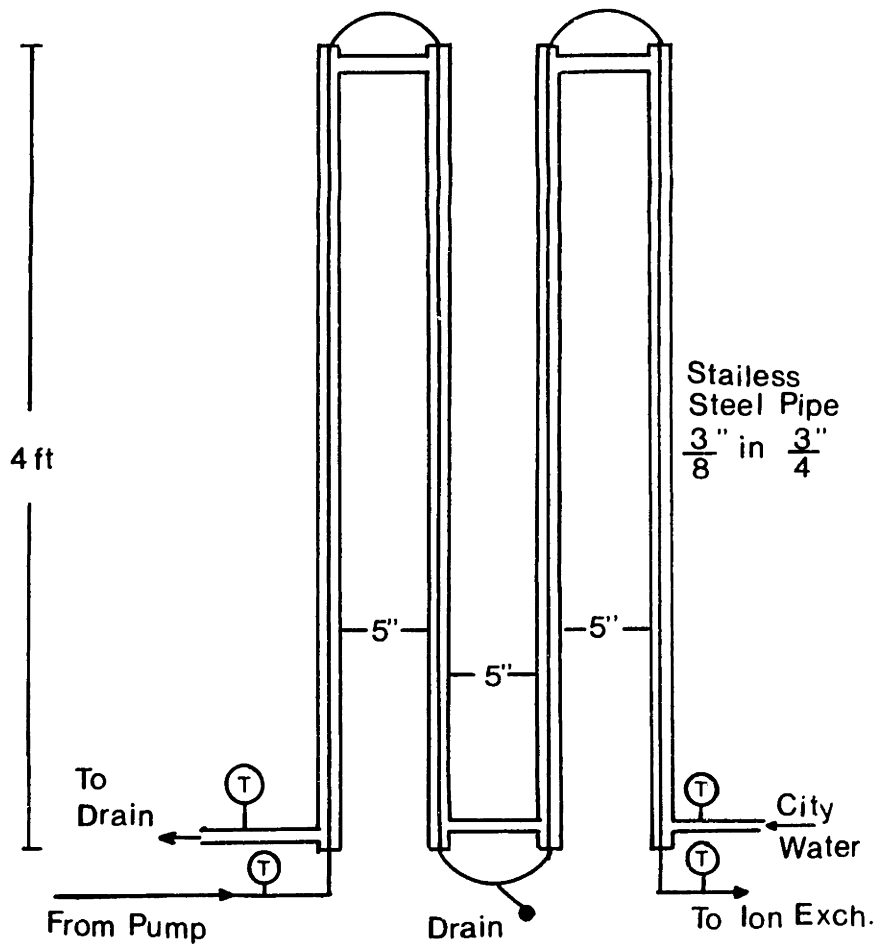

Figure C4. The cooler as a counter-flow heat exchanger.

C.3. The Purification System

The cleaning process includes a filter and an ion exchanger. The filter and resin to handle 0.55 gpm were housed inside a teflon vessel capable of withstanding 100 psi. Both, the filter and the ion-exchanger, were bought from Barnstead (Company Catalog numbers 15840, D 0700).

The original arrangement of the filter and ion-exchanger is shown in Fig. C5. The arrangement allowed for a pH-meter (Beckman number 900) to be installed in line to indicate continuously the pH of the water. The location of the pH meter probe is shown in Fig. C5. This probe was isolated from the loop. A PVC 1 foot long 1" pipe was used to make the connection. This arrangement prevented the flow of stray currents to the probe and allowed for measurement of a slowly renewing flow of water. Both recommendations, electrical isolation and low flow velocity (less than 0.025 gpm), were made by Jones (1981).

As mentioned previously this original arrangement had to be modified to allow operation at higher temperatures.

The maximum pressure level admitted by the casings of the filter and the ion exhanger and the pH probe was 100 psi. To overcome this limitation, the filter and ion exchanger tanks were each placed inside another vessel as shown in Fig. C6 and the pH probe was removed from the system.

The new arrangement is able to withstand up to 400 psi.

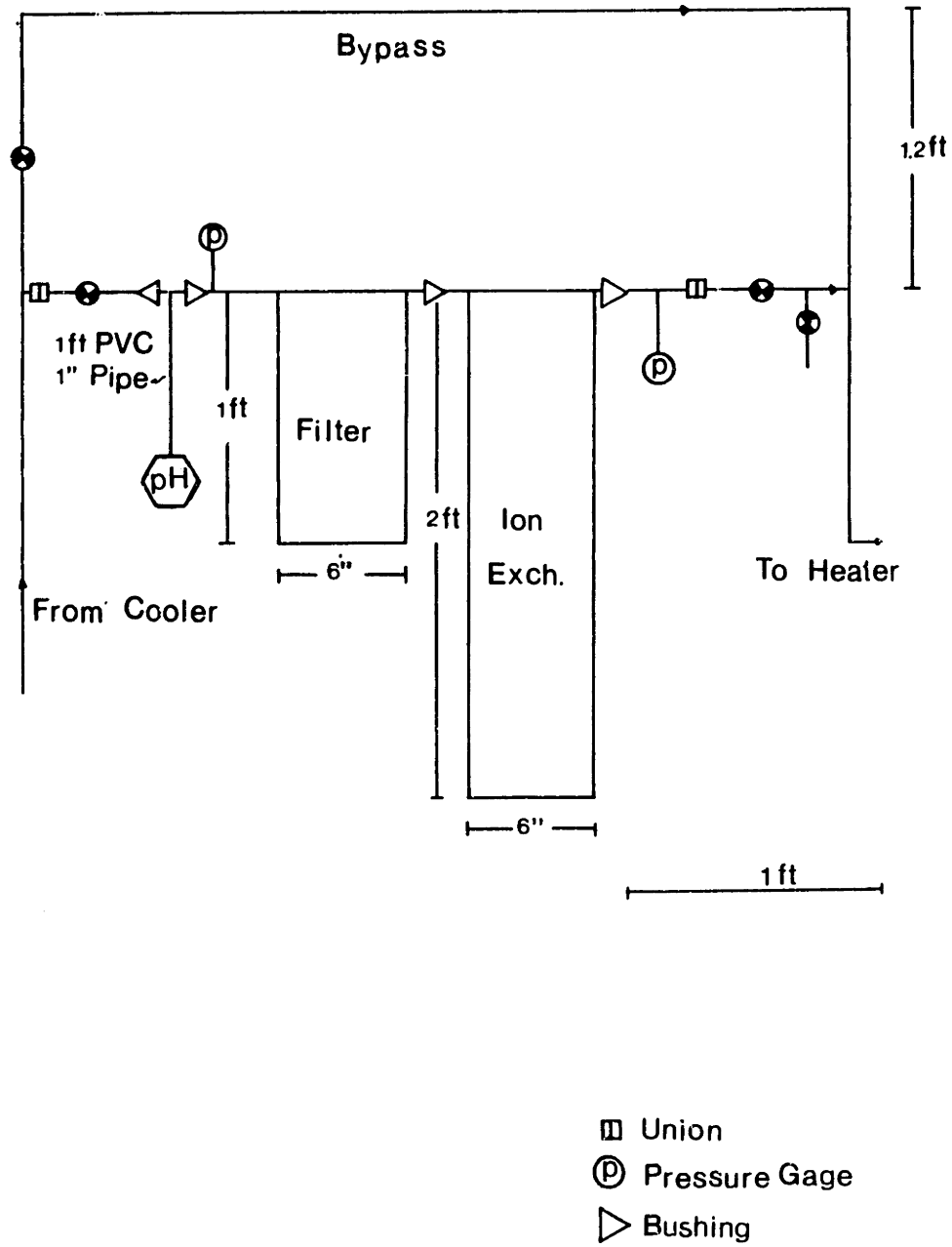

Figure C5. The original arrangement of the piping around the ion-exchanger. The pH pipe forms a 45 degree angle with the plane of the diagram.

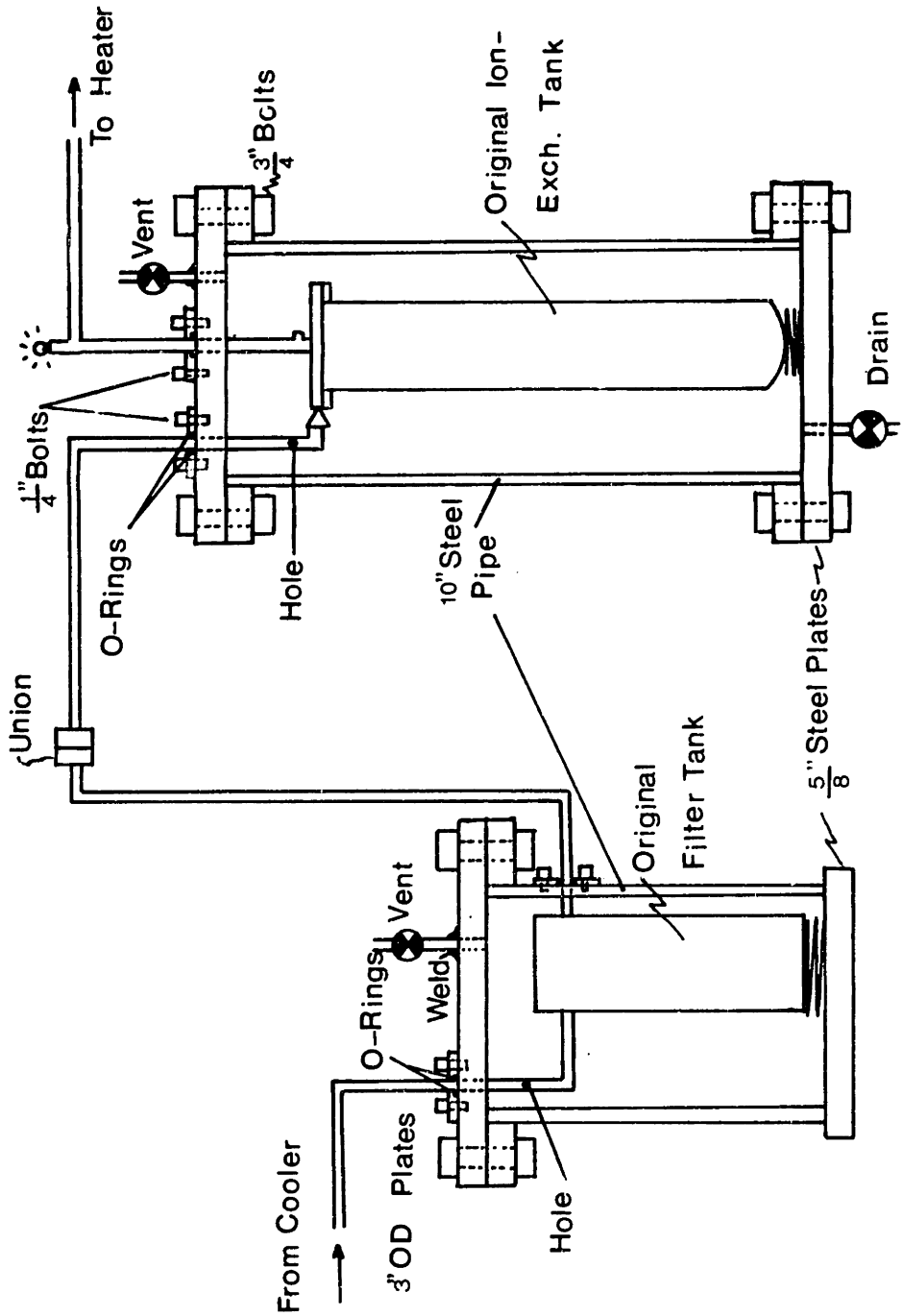

Figure C6. The modified arrangement of the filter and ion-exchanger. The steel tanks made out of a 10" steel pipe withstand the pressure, up to 400 psi.

C.4 The Heater

Once the water is purified, it needs to be reheated to the original temperature or even somewhat higher to compensate for heat losses in the rest of the loop.

The heater was designed as a condenser according to the method of Rohsenow (1982).

High pressure steam (400 psi) was used to heat 0.55 gpm of water from 120 F to 325 F. The heater was made as a counter-flow heat exchanger with 10 ft of 3/8" in 3/4" stainless steel pipe. To help the drainage and to increase the heat transfer coefficients, the pipes were placed on a 10 degree slope. Fig. C7 shows a sketch of the heater.

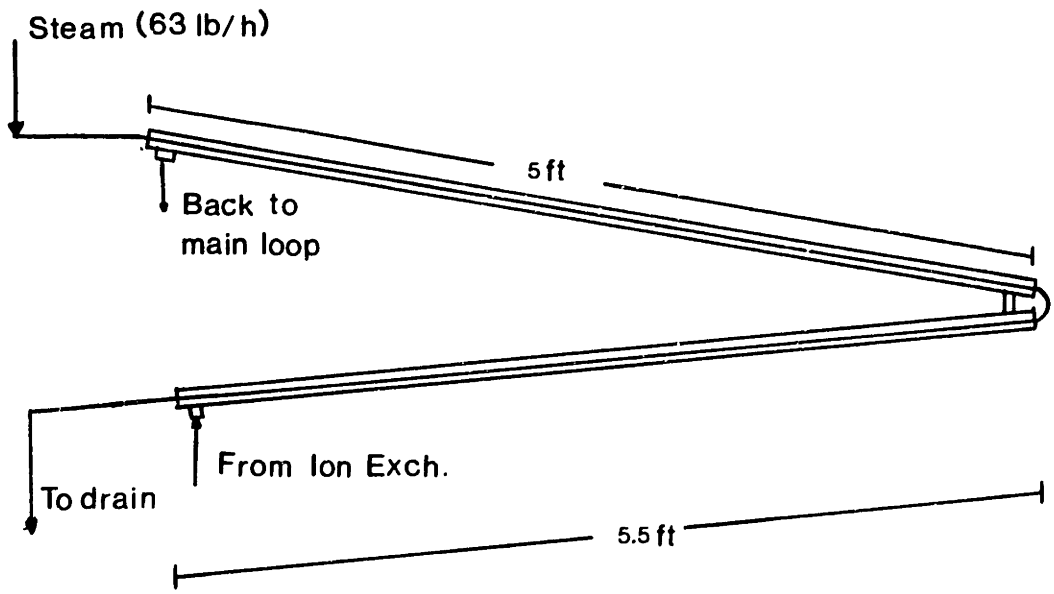

Figure C7. The heater as a counter flow heat-exchanger.

C.5. The Recirculating Pump

For each of the components already mentioned it was possible to calculate the pressure drop. The results of the calculations showed that the pump to be used would have to be capable of circulating 5.7 gpm through a total pressure drop of about 30 psi.

A Westinghouse model 30-A centrifugal pump was available in the laboratory. This unit is a single stage, high temperature (600 F), high pressure level (2000 psi), low head (25 psi) pump. The unit is totally enclosed and its parts are either cast or machined from a variety of stainless steels. This pump was first used by Henry (1953) and it was proven to be highly reliable.

The pump requires cooling by oil. In this case, a 5 gal kerosine tank was connected to a 0.5 hp Marathon Electric Co. pump. This smaller pump recirculated the kerosine through the motor windings of the Westinghouse pump, to a 5 galons reservoir tank and to a heat exhanger (Young Radiator Co. SSF-502-HR-1P) which uses city water to cool the oil.

Figure C8 shows the specifications of the stainless steel pump. From the information in the figure it can be seen that the pump was able to more than satisfy the flow and pressure drop requirements. Furthermore the pump was made of stainless steel and therefore provided a corrosion resistant material in contact with the water of the loop.

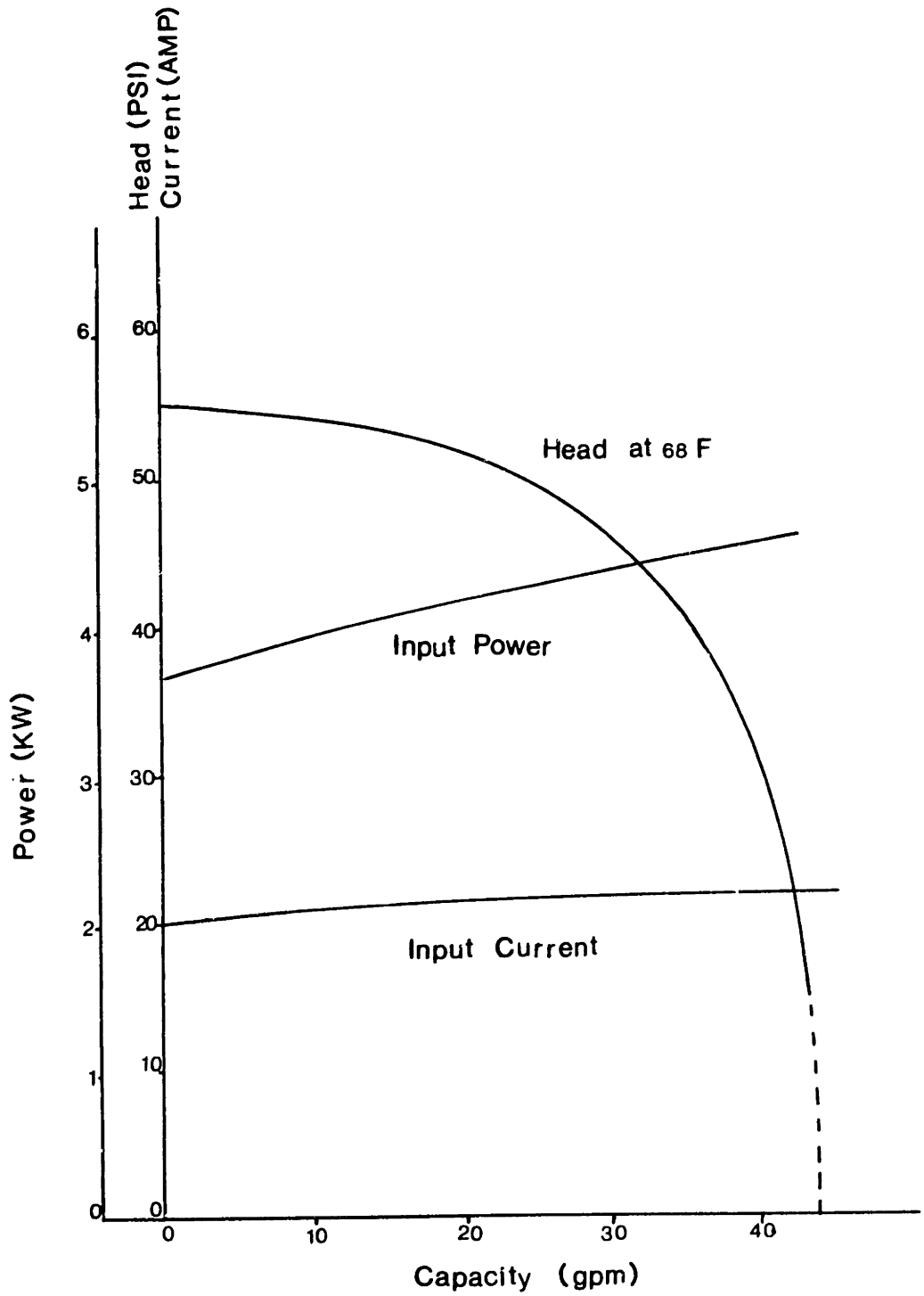

Figure C8. Performance curves for Model 30 - A Westinghouse centrifugal pump.

C.6. The Pressure Vessel

The pressure vessel, used as a water storage and as a damper of pump fluctuations, was a tank made out of a stainless steel 5" diameter pipe. The design method was the one used by Henry (1953) where the thickness of the vessel was determined by considering the stress at the center of the cover plate together with the radial and tangential stresses on the edge of the cover plate. The height of the tank (3 ft) did not follow any restriction but to have a good water storage capability. The characteristics of the vessel are included in Fig. C9.

From the figure it will be noticed that the vessel had a vent, a connection to a nitrogen tank, a location for a relief valve to be placed, and a glass water level gauge.

C.7. Other Characteristics of the System

C.7.1. Injector Tank -

Following the same design as the pressure vessel already described, a tank 1.5 ft. in lenth was designed and connected to the main loop. This vessel was only used to inject make up water, but it can also replenish the chemicals that were removed by the ion-exchanger during tests where the pH differs from the original water pH.

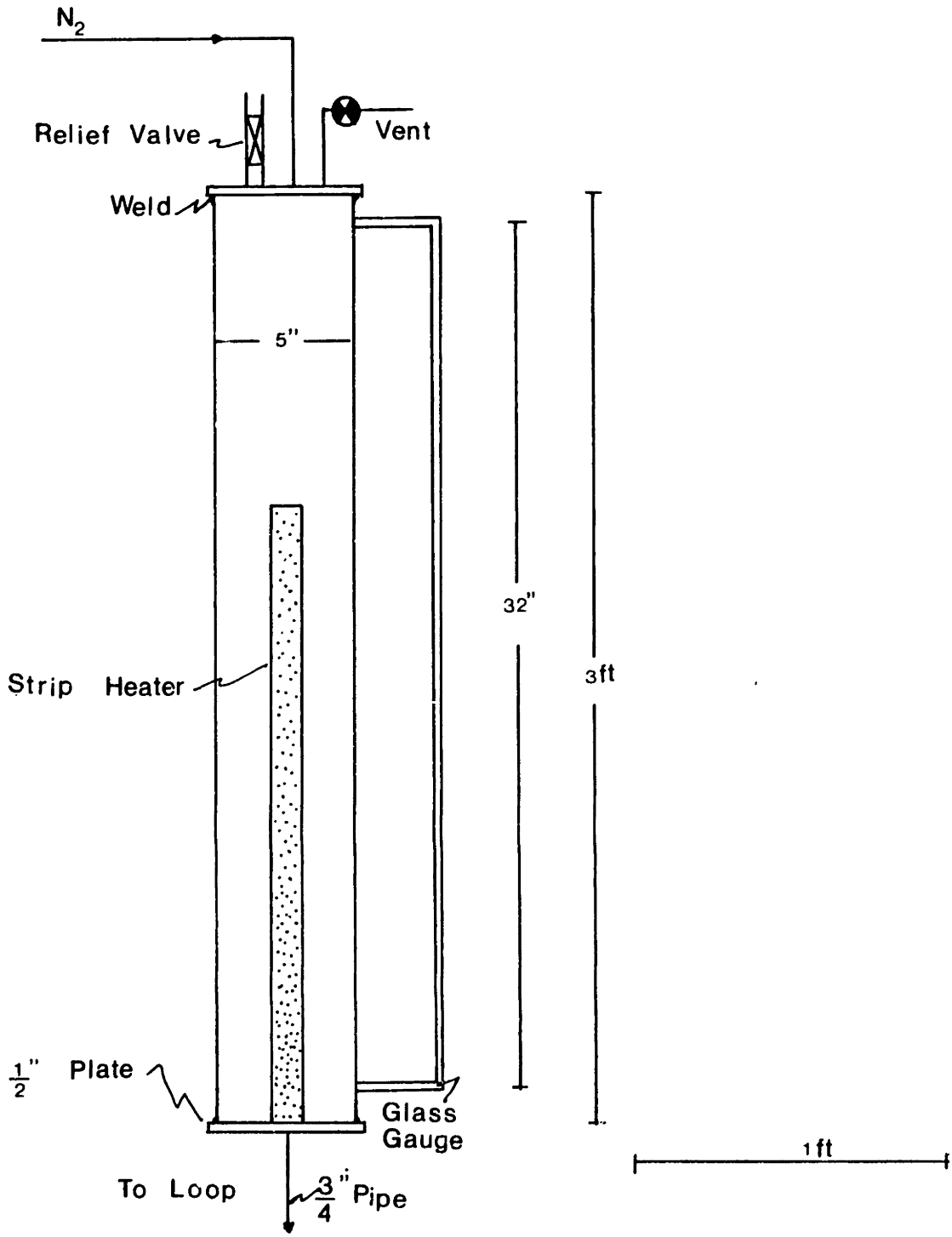

Figure C9. Dimensions of the pressure vessel.

C.7.1. Strip Heaters

Extra heat to the loop was provided by two 270 watt strip heaters. These heaters were wrapped around two sections of pipe in the main loop. One of the heaters was connected to a variac. This connection allowed for more control over the test section temperature.

C.7.3. Others

The loop has thermocouples, pressure gauges and flow meters that allow velocity and temperature conditions to be controlled.

The loop has several places where the water can be sampled. An oxygen monitor (Beckman 715) was connected to one of these sampling lines to determine the dissolved oxygen contents in the water. Unfortunately, the operation of this instrument was not reliable.

For the purpose of isolating different parts of the system there are bypasses around the test section, the ion-exchanger and the whole cleaning loop.

C.8. Recapitulation of the Main Features of the Design

The following list summarizes the main characteristics of the loop:

Temperature Range	200 to 350 F
Velocity Range	0 to 30 ft/s
Design Pressure	400 psi
Heat Requirements (Steam)	9 KW (63 lb/h)
City Water Requirements	68 gallons/h

The material of the loop is stainless steel (grades 304, 308, or 316). Figure 19 in the text shows the arrangement in which the different components were placed.

APPENDIX D

MACHINING PROCESS FOR MAKING SPECIMENS

Having cut the 2" plate down to a bar of 1" x 1" x 4" in the Johnson machine, the lathe was used for the rest of the process.

D.1. Conversion of the Square Bar to a 7/8" Diameter Rod

After placing the square bar in the four jaw chuck, it was turned at medium speed. The bar was then cut with the automatic feed at the rate of 46 threads per inch. At the beginning of the process, the cut was 0.060" in depth, but when the bar was round, the depths of the cuts were decreased to 0.030" until the diameter was 7/8".

When the specimens of the same run were round on one end, the 4 jaw chuck was removed and it was replaced with a 7/8" collar. Holding the specimens by the round end and following the same steps as described above, a round bar of 7/8" was obtained.

At low speed and cutting just as much as was necessary, both ends of the specimen were smoothened.

The time consumed in this first part for two specimens was close to 2.5 hours. During the process, the tool was kept sharp and machine oil was used to keep it cool.

D.2. Drilling the Center Hole

With the specimen in the 7/8" collar and well centered the following drills were used: 3/16,1/4,5/16,3/8,7/16,1/2, and 37/64. Drilling as far as the length of the drill allowed lead to subsequently bigger and longer holes. Around the 3/8" drill the specimen had a hole throughout.

At the end of these steps, it was useful to remove the edge of the hole with a file. This facilitated the use of the tap for making the threads.

This part of the process took about 2 hours.

D.3. Making the Threads

To make threads at the end of the specimens a 5/8" x 18 tap was used.

The total threads were about 3/4" in length. About midway the tap was brought out and cleaned.

These steps took close to 1 hour.

D.4. Reduction to the Final Diameter

At the speed of 56 threads per inch cuts of 0.020" in depth were made until the diameter was around .760".

Finally at the rate of 224 thread per inch a diameter close to 0.751" was obtained.

With one side of the specimen done, the other side was

also reduced in diameter by following the above steps in this section.

This part took about 1.75 hours.

D.5. Final Polishing

With the specimen turning on the lathe, the scratches were removed by using a fine file.

The following sand papers were subsequently used until the previous scratches had disappeared: 250, 320, and 600.

At the end when the specimen was well polished, it was washed with soap and water. It was quickly dried with air and stored in a desiccator.

The final polishing took about 45 minutes.

The total machining process for 2 specimens took about 8 hours (non-stop). It is suggested that it not be done in a single session.

Times indicated in this appendix are the required number of hours when tools and machines are readily available and when the user is familiar with the machining process.

APPENDIX E

GUIDELINES FOR THE OPERATION OF THE CORROSION-EROSION RIG

The following notes describe the procedure used to operate the corrosion-erosion apparatus. To aid in the explanation, the diagram of Fig. E1 will be used throughout this appendix. The figure shows a flow diagram of the experimental rig. It shows the location of the valves as well as the points where the temperature and pressure were recorded.

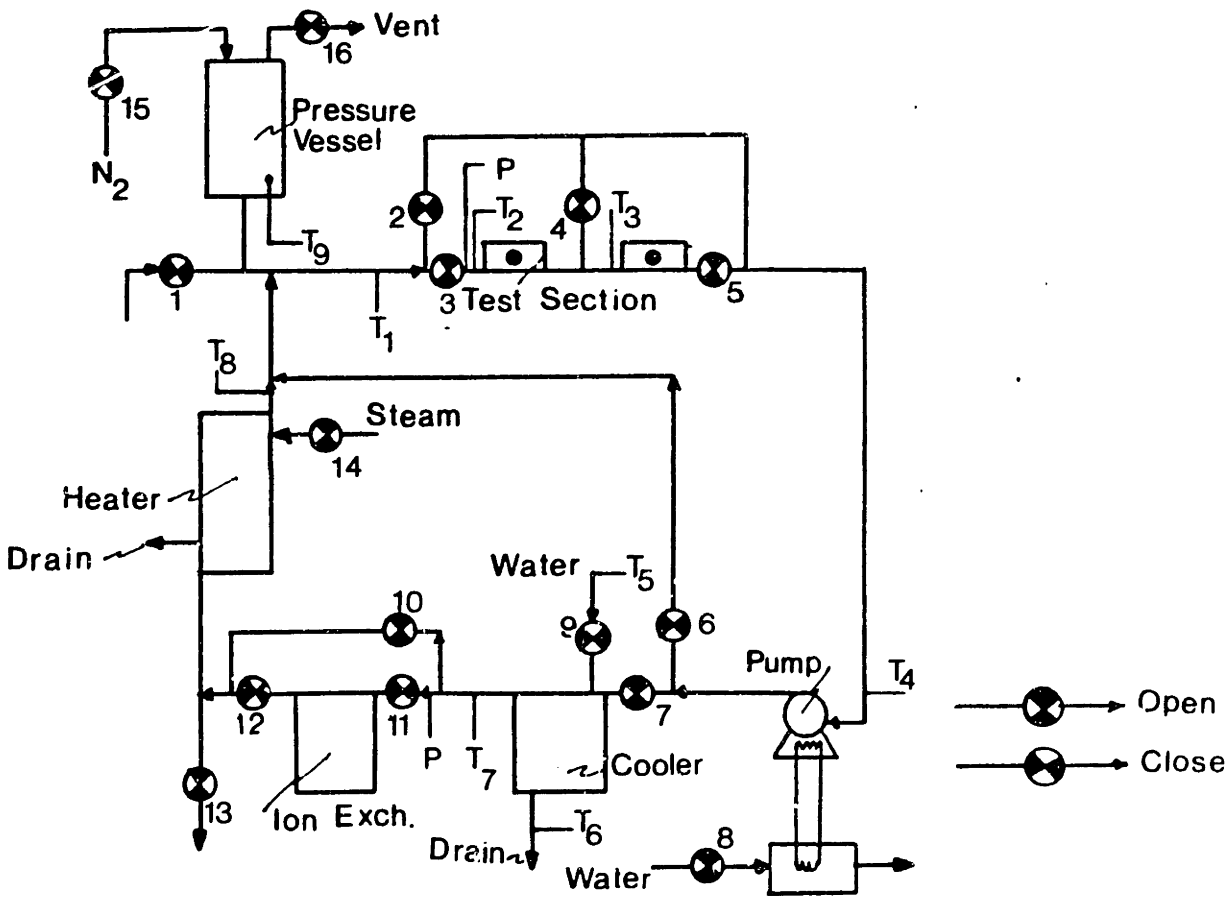

Figure E1. Temperature and pressure measurement locations in the experimental rig.

E.1. Filling the Loop

After long periods of non-operation of the system it is convenient to drain it throughly. Most of the sections of the loop have a drain near by; but, in any case to prevent any pockets of water, it is recommended to blow air through the supply pipe entrance (i.e., the air supply would be connected to the line of valve 1, this valve would be open during the blow down process).

After all the water has been drained, and only then, the vacuum that can be connected to the sampling line (valve 13) can be operated for around 15 min.

With the vacuum obtained and all valves open, the system is filled with distilled water by connecting the supply line to a bag of Belmont Co. distilled. The water supply line should be shut off when the level of water in the pressure vessel reaches the top of the glass gauge. To reach this level it is necessary to open the vent (valve 16).

E.2. Warm Up Period

This period which lasts a couple of hours before the the beginning of a test prepares the whole loop for degassing.

The warm up period consists of turning on all the electrical heaters (the one on the pressure vessel and the 2 strip heaters). By monitoring the value of the temperature on the pressure vessel wall (T_9) one can determine the moment

in which the water will start boiling. During this first part of the warm up period, the vent is opened and the valves that are closed are those that connect to the exterior (valves 1, 13, and 15), the ones around the ion exchanger (valves 11 and 12) and the providers of cold water and steam (valves 9 and 14).

Once the water is boiling, the vent is closed, the pressure vessel heater is shut off, and the water to cool the pumps is turned on (in the actual system there are two valves that provide the cold water to the pumps; in the figures in this appendix they are both represented as valve number 8). These last steps are extremely important and should not be forgotten.

The system was then pressurized by N_2 (Valve 15) up to 70 psi. Making sure that the valves around the ion exchanger are closed, and opening the valve for the city water to the cooler (valve 9), the pumps are turned on and the steam valve supply (valve 14) is opened. The condition aimed at is a temperature above 212 F. A temperature close to 220 F is adequate. Figure E2 shows the valves that would be open during this period.

E.3. Venting Period

Half an hour to 20 minutes prior to the beginning of the test, the warm up period ends. The pump is shut off, but its coolant is left on (valve 8 open). The city water and the steam

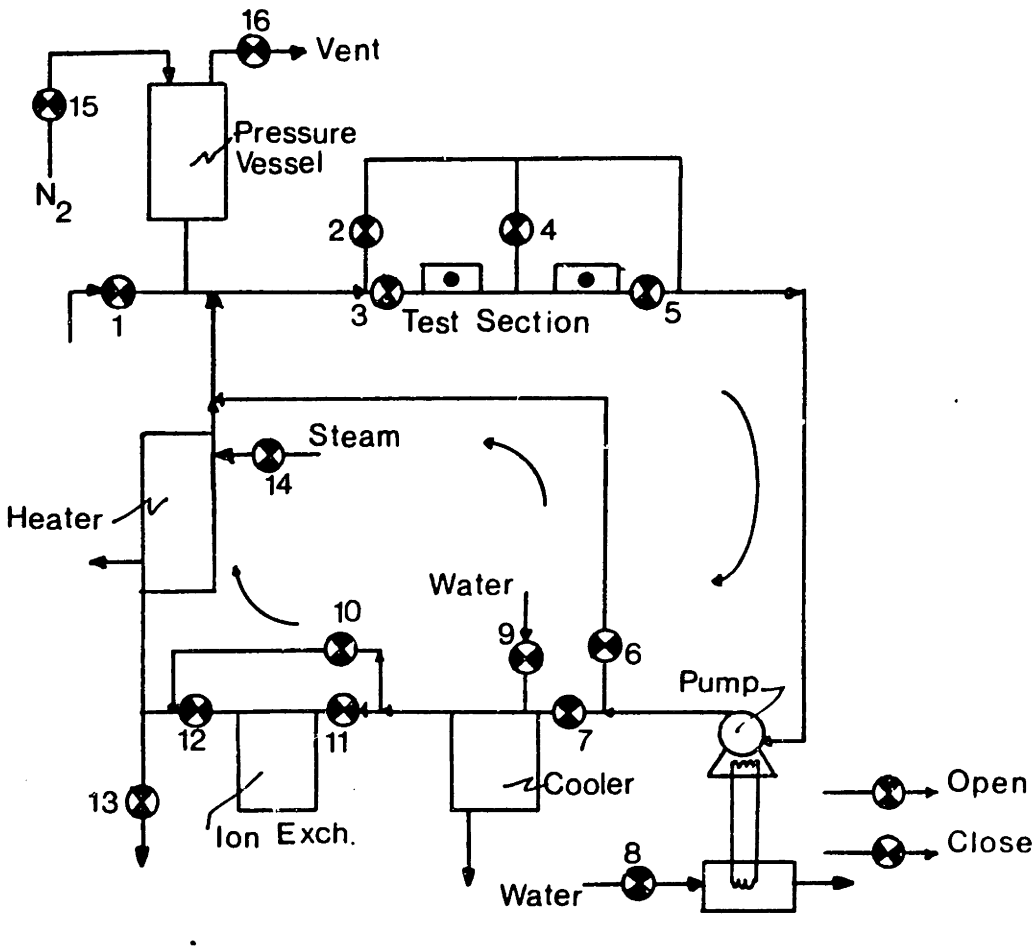

Figure E2. Diagram showing open valves during the warm up period.

supplies are closed (valves 9 and 14). The connection to the nitrogen tank (valve 15) is closed and the heater on the pressure vessel is turned on.

During the 20 minutes prior to starting the experiment the vent stays open (valve 16). The vent valve should not be opened all the way, since the steam leaving the vessel may carry considerable amount of water.

It would be convenient to recirculate the water in this condition (with the vent open), this is not possible because the pump needs about 25 psi head to operate properly.

E.4. Start Up Procedure

With the specimen assemblies ready, the valves that isolate the test section are closed (valves 3, 4, and 5). The temporary plugs on the test section are removed to allow for the specimen assembly to be put in place. With the specimens in place, the vent valve is closed and valve 4 is opened to allow the pressure gauge to be used. The heater on the pressure vessel is shut off.

The system is then pressurized and with conditions the same as during the warm up period, see Fig. E2, i.e. with the ion exchanger and the test section isolated, the pump is turned on. This first period of the start up is continued until the temperature close to the test section (T_1) is within 20 F of the desired test temperature. At this stage, valve

10 is gradually closed until the temperature of the water before the ion exchanger (T_7) is less than 120 F. When T_7 is less than 120 F valve 10 is closed, valve 12 is opened all the way and valve 11 is opened very little, just enough to maintain T_7 at less than 120 F and more than 100 F. Valve number 9 during all these steps should be at a position that maintains the flow of city water at 90 % of the flow meter scale (90 % of 1.19 GPM).

It is important to maintain T_7 between 100 and 120 F. If T_7 is greater than 120 F the risk of injuring the ion exchanger resin increases; if T_7 is much smaller than 100 F at 90 % of 1.19 GPM of city water to the cooler,it means that not enough water is circulating through the purification loop.

After T_7 is close to 120 F, the test section is opened. Valve 4 is closed and valve 5 is opened. Valve 3 is opened slowly and just enough to reach the flow conditions necessary to achieve the velocity required in the test section.

During the initial start up period, the temperature at the inlet of the Ion Exch. (T_7) and the temperature at the outlet of the heater (T_8) must be kept at the desired levels by constant regulation of valves 11 and 14.

At this stage the test is underway. Figure E3 shows the position of the valves that are open during normal operation.

E.5. Control of Conditions During and at the End of a Test

Throughout the test the variable that requires constant monitoring is the flow of city water (valve 9). The water flow will often go to values as low as 40 to 50 % of 1.19 GPM which puts the ion exchanger resin at risk.

It is also convenient to monitor the level of water in the pressure vessel. If the level comes down too fast, it may suggest the presence of large leaks which develop as a result of thermal stresses. The leaks should be found and repaired, if possible, at the end of the test.

Often during the course of the test, pressure levels decrease and cause a reduction in the flow of water to the test section. The solution to this problem most of the time involves opening valve 3 more and subsequently control temperatures T_7 and T_8 through the appropriate movement of the valves 11 and 14. In other occasions and when the pressure level is not near the limit of operation (250 psi) the pressure can be increased by inputing more nitrogen into the system (valve 15).

During a "good run" no major problems will occur and the last day of the test can be reached. To stop the experiment, simply close the steam supply (valve 14), the nitrogen supply (valve 15) and shut off the pump. The vent (valve 16) should then be opened to relieve the pressure.

To take the specimens out of the rig, the test section should be isolated (close valves 3, 4, and 5) when atmospheric pressure is reached.

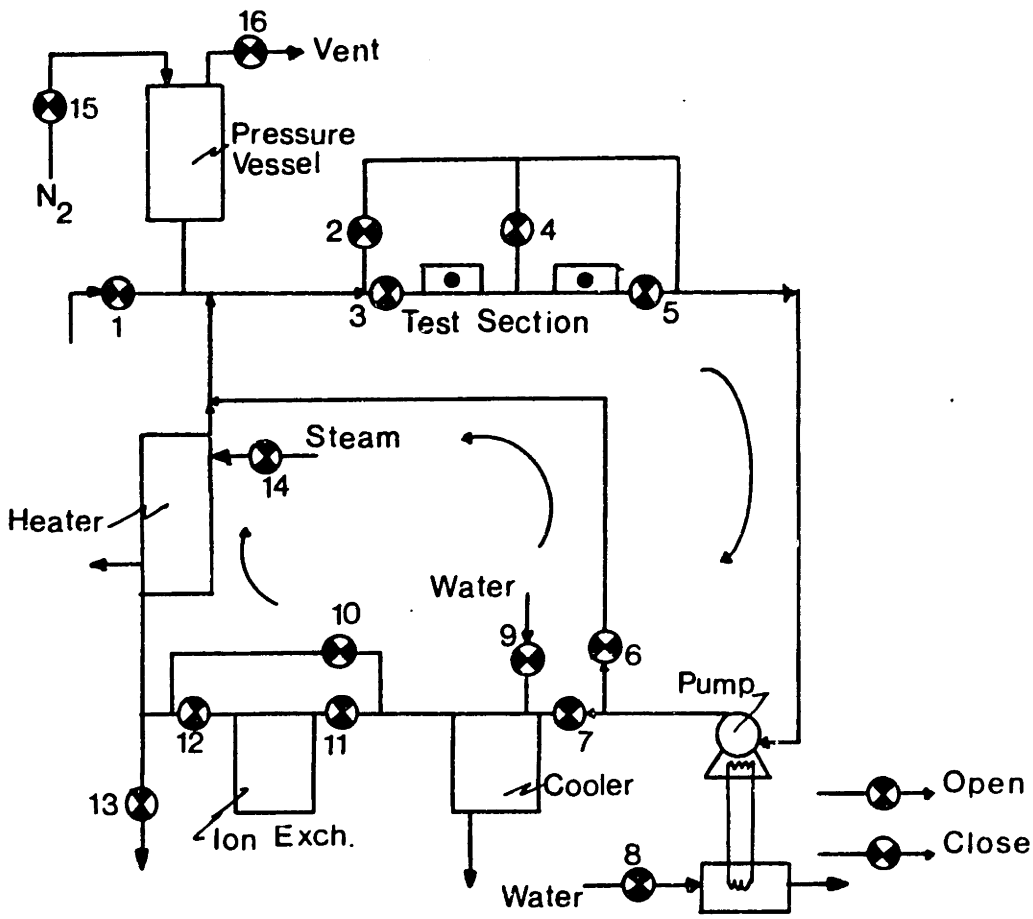

Figure E3. Diagram showing valve conditions during the normal course of a test.

Having taken the specimens out of the loop, the specimen chambers can be temporarily sealed with plugs which will allow the rig to be ready for the following warm up period.

After an hour from the moment the test was stopped, the city water supplies (valves 9 and 8) can be closed and the main power switch can be shut off.

E.6. Some Possible Problems

E.6.1. Lack of Flow Through the Test Section -

This situation often occurs. It may be caused by clogging of the test section or the accumulation of non-condensible gases in the system.

Before increasing the pressure of the system, it is convenient to stop the loop (close the steam supply, nitrogen tank and open the vent for a short time).

Often it is very helpful to purge the pump after a few minutes of venting. The pump has two valves. Both of them can be opened to allow for some gases to go out.

If the test section is clogged, it requires that the specimen is brought out of the loop and with the test section open, drain some water out.

E.6.2. Discovering that the pumps have ceased operating -

Under conditions of poor cooling of the kerosine that cools the motor windings of the stainless steel pump, a temperature controller (recording the kerosine temperature)

will shut the system off to prevent from burning the pump-motor.

If the system is found to be at a halt, it is convenient to check whether the 1/2 hp pump is capable of working. Also it is important to check that the flow of city water has not been restricted. Several other experiments in the laboratory are connected to the same water line and it has happened that their owners have shut off the wrong valves.

If none of the above cases seem to be the explanation for why the experiment may have stopped, it is advised to call Physical Plant. There may have been a power outage during the period when the failure is expected to have occurred. If electricity fails for an instant, the system is not able to come back to line on its own (due to the arrangement of the controller).

If frequent checkings to record temperature and flow rate conditions through the test section are made, a couple of hours during which the test was not running - in a 260 h test - should not influence the results.

E.6.3. Finding the Level of the Water in the Pressure Vessel Low

If the rig loses water at the rate of 2" per day (measured on the glass column of the pressure vessel) the performance of the system will deteriorate as the level decreases. If the

leaks are not very large, the test can be continued as planned as long as make-up water is put into the system. In order to imput make-up water, it is recommended that the rig be stopped and some pressure released. By making use of the injector tank it is possible to inject water into the system that is already degassed. With the pressure vessel full of water and with its vent closed, the system can be brought back to its operating conditions following the procedure in Section E.4.

The injector tank should be filled with water prior to the moment of injection. This tank has strip heaters which allow for the water to boil and to be vented prior to its injection into the rig. During the actual water injection the injector tank is capped and nitrogen is supplied to raise its pressure at slightly higher value than the remainder of the rig.

E.6.4. Emergency Procedure

In case a huge leak develops and high pressure water starts jetting out of the loop, the main power switch should be shut off, the steam valve (valve 14) should be closed and the vent should be opened to help relieve the pressure. If the electric heater on the pressure vessel is never left on, major accidents should never occur. However, if the heater is left on, the pressure could rise to the maximum pressure of 400 psi, leaks would develop throughout the system and the risk of breaking the glass gauge on the water tank is high. It is thus recommended that the glass always be covered by a clear PVC pipe.

It is convenient to provide a safety valve on the system. Originally the system had a safety relief valve but it was removed because it leaked.

E.6.5. Post Test Problems

At times it was found that specimens had gained instead of losing weight. The only reasons that have been found to explain these happenings are: poor cleaning, and specimens in water at zero velocities for long periods of time.

Care must be taken not to touch the specimen either with bare hands of with gloves once it has been cleaned. Not following this instruction may cause sites where oxide conglomerations occur, see Fig. E4.

When performing experiments that require specimens to be taken out of the loop every other day (See Section 5.1) it is necessary to take both the high and low velocity specimens out of the rig. Zero velocity conditions allow for a more protective layer of magnetite to be formed and this impedes further wear.

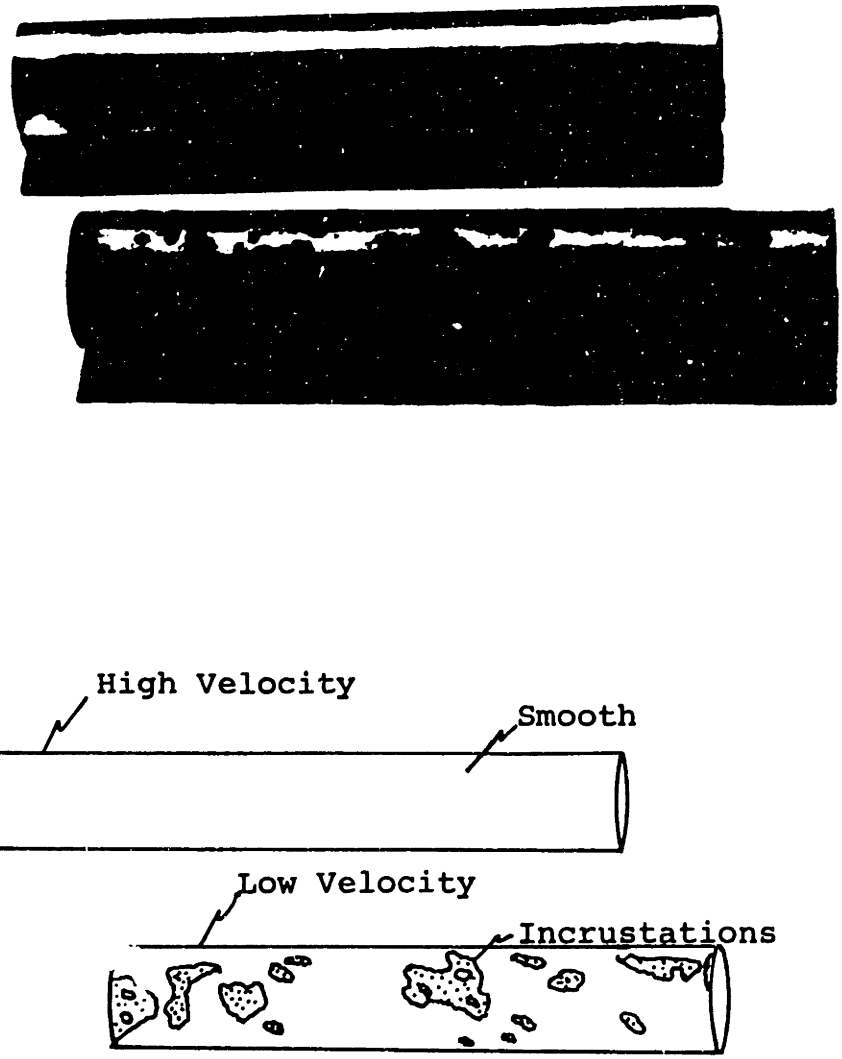

Figure E4. Photograph of specimens at 250 F. The front specimen corresponds to the test at low velocity (1.9 ft/s); this specimen was handled with gloves after cleaning was performed.

APPENDIX F

RAW DATA USED IN THE CALCULATION OF THE WEAR RATE

F.1. Determination of the Wear Rate from Eq. 47

Table F1 shows the data used to calculate the wear rate from Eq. 47 i.e.,

$$\dot{\delta} = \frac{87600\Delta W}{\rho_{met} t A_w}, \qquad (47)$$

where: $\dot{\delta}$ = wear rate in mm/y

ΔW = weight change of the specimen

t = length of test

A_w = available area for wear

ρ_{met} = density of the metal (7.84 g/cm^3)

The reader may notice that there are two specimens for which the weight change is negative, that is, the specimen gained weight instead of losing it. In the first case, (the high velocity specimen at 250 F), it is believed that the reason for not losing weight is related to the fact that it remained in the water under static conditions for a period of about 11 h, the accumulated time that was invested in taking the low velocity sample out of the rig and weighing it in order to determine weight loss as a function of time, see Fig. 22 in the text. The second case corresponds to the specimen

Table F1

Data Used in Equation 47

T (F)	V (ft/s)	ΔW (g)	t (h)	A_w (cm^2)	$\dot{\delta}$ (mm/y)
250	10.30	-.0125	231.0	61.25	0.0000
250	1.94	0.0093	231.0	60.47	0.0070
250	10.34	0.0191	243.6	60.04	0.0130
250	1.92	-.0766	243.6	61.42	0.0000
270	8.60	0.0467	240.0	61.40	0.0350
285	10.10	0.0420	191.2	59.71	0.0520
285	1.80	0.0186	191.2	58.52	0.0180
293	9.80	0.0621	235.0	60.00	0.0480
293	1.50	0.0188	235.0	59.29	0.0150
299	9.70	0.2414	240.0	59.23	0.1897
300	9.51	0.0939	233.6	60.62	0.0730
300	1.46	0.0554	233.6	59.81	0.0440
300	9.72	0.0567	238.9	56.23	0.0470
300	1.54	0.0337	238.9	57.19	0.0270
305	9.27	0.0824	264.0	59.50	0.0580
305	1.92	0.0666	264.0	59.19	0.0480
310	8.51	0.0896	236.6	57.90	0.0730
310	1.69	0.0533	236.6	60.12	0.0420
320	9.61	0.1508	344.5	59.52	0.0821
320	1.61	0.0868	344.5	58.65	0.0475
335	9.51	0.0619	264.4	60.47	0.0432
335	1.65	0.0443	264.4	57.66	0.0300
350	9.81	0.0283	228.3	59.21	0.0234
350	2.01	0.0098	228.3	58.90	0.0080

which picture was shown in Appendix E as an example of inadequate cleaning process. To this specimen, incrustation patches appeared on the surface.

Another point of interest is that of the high velocity point at 299 F. This was the first run of the corrosion-erosion rig. As can be seen the wear rate was excessive when compared to the rest of the runs. A value of wear as high as this was never obtained again. Although one can theorize on an explanation for this behaviour, it appears that the high wear rate was linked to the fact that it was the first run; however, no definite conclusion has been reached.

Neither of these specimens were considered in the analysis to determine the value of the reaction rate constant.

F.2. Determination of the Wear Rate from Eq. 48

As mentioned in the text, a section of each specimen was descaled. From the weight of the oxide the value of a descaled wear rate was obtained by using Eq. 48 ,

$$\dot{m}'' = (\Delta W + \{\Delta W_o + \Delta W_i * .276\}\frac{L}{L_s})\frac{10^6}{A_w t} , \quad (48)$$

where: $\dot{m}''$ = wear rate ($\mu g/cm^2 h$)

ΔW = weight loss during the length of the test

ΔW_o = weight of the outside oxide

ΔW_i = weight of the inside oxide

L = original length of the specimen

L_s = length of section of the specimen that was descaled

A_w = available area for wear

t = length of test.

Table F2 lists all the raw data used in evaluating $\dot{m}''$ from Eq. 47 .

The reader will notice that out of the two specimens that in Table F1 were shown to have gained weight, one of them (the high velocity specimen at 250 F) shows a positive wear rate; indeed, the removal of the oxide allows for such determination. For the other specimen, (the one that developed incrustations) the oxide could not be removed completely and therefore it was not possible to calculate the wear rate.

Table F2

Raw Data to Evaluate Wear Rate from Eq. 48

T (F)	V (ft/s)	L_s (cm)	L (cm)	ΔW_o (g)	ΔW_i (g)	ΔW (g)	t (h)	A_w (cm^2)	Oxid. Rate ($\mu g/cm^2 h$) - (mm/y)
250	10.30	4.79	10.27	0.0043	0.0235	-.0125	231.0	61.25	0.75 - 0.008
250	1.94	4.85	10.21	0.0078	0.0193	0.0093	231.0	60.47	2.64 - 0.008
250	10.30	4.20	10.07	0.0083	0.0015	0.0191	316.3	60.04	2.57 - 0.028
250	1.92	3.69	10.34	0.0105	0.0235	-.0766	316.3	61.42	0.00 - 0.000
270	8.64	2.51	10.30	0.0039	0.0136	0.0467	240.0	61.40	5.30 - 0.059
286	10.14	2.71	9.95	0.0061	0.0099	0.0420	191.2	59.71	6.51 - 0.073
286	1.78	4.42	9.83	0.0073	0.0055	0.0186	191.2	58.52	3.41 - 0.038
293	9.78	3.08	10.04	0.0059	0.0103	0.0621	235.0	60.00	6.60 - 0.074
293	1.49	4.40	9.92	0.0072	0.0182	0.0188	235.0	59.29	3.32 - 0.037
299	9.70	3.09	9.85	0.0090	0.0025	0.2414	240.0	59.23	19.16 - 0.214
300	9.51	2.86	10.13	0.0083	0.0073	0.0939	233.7	60.62	9.42 - 0.105
300	1.46	4.20	10.04	0.0086	0.0075	0.0554	233.7	59.81	5.79 - 0.065
300	9.72	3.01	9.40	0.0045	0.0091	0.0567	238.9	56.23	5.85 - 0.065
300	1.54	3.63	9.57	0.0072	0.0134	0.0337	238.9	57.19	4.57 - 0.051
305	9.27	3.88	9.98	0.0065	0.0124	0.0824	264.3	59.50	6.72 - 0.075
305	1.92	3.92	9.90	0.0100	0.0120	0.0666	264.3	59.19	6.42 - 0.071
310	8.51	3.30	9.70	0.0103	0.0034	0.0896	236.6	57.90	8.98 - 0.100
310	1.69	3.58	10.10	0.0147	0.0042	0.0533	236.6	60.10	6.89 - 0.077
320	9.61	3.21	9.91	0.0014	0.0247	0.1508	344.5	59.52	8.59 - 0.096
320	1.60	2.24	9.80	0.0055	0.0073	0.0868	344.5	58.65	5.92 - 0.066
335	9.51	3.40	10.09	0.0101	0.0108	0.0619	264.4	60.47	6.29 - 0.070
335	1.66	3.48	9.67	0.0077	0.0140	0.0443	264.4	57.66	5.01 - 0.056
350	9.81	3.40	9.90	0.0079	0.0080	0.0283	228.3	59.21	4.27 - 0.048
350	2.01	3.40	9.84	0.0052	0.0093	0.0098	228.3	58.90	2.40 - 0.027

APPENDIX G

COMPUTER PROGRAMS WEARR4 AND CORERO

This appendix provides the listings of the programs used in the calculation of the reaction rate constant K (in the program WEARR4.FOR, K0 represents K) and the wear rate $\dot{m}_1''$ (in the computer program CORERO.FOR, WEAR stands for $\dot{m}_1''$. The appendix also provides the formats in which the data was provided and typical outputs showing the results of the calculations.

The listings that will be found in this appendix are:

1) Program WEARR4.FOR
2) Input data to WEARR4.FOR
3) The results from the calculations in WEARR4.FOR
4) Program CORERO.FOR
5) Input data to CORERO.FOR
6) The results from the calculations in CORERO.FOR.

1) Program WEARR4.FOR

```
c**********************************************************************
c
c   THIS PROGRAM USES WEAR RATE DATA TO CALCULATE THE REACTION
C                      RATE CONSTANT KO
C
C**********************************************************************
C
C
C      PRELIMINARIES
C
C       IN THE FOLLOWING PROGRAM THE SUBINDEX 1 STANDS FOR Fe  ,
C       THE SUBINDEX 2 FOR Fe(OH) , THE SUBINDEX 3 FOR Fe(OH) ,
c       AND THE SUBINDEX 4 FOR Fe(OH) .

        DIMENSION A(5),B(5),D(5),DI(5),DIS(5),FE(5),R(5),V(10),
       1WEAR(30),WEARL(30),T(30)
        REAL K(5),MFE(5),MU,NU,KO(30),K1(30),ITK(30)
C
C
C     REQUIRED INFORMATION
C
C      THERMODYNAMIC DATA TO EVALUATE EUILIBRIUM CONSTANT K(I)
C      (SWEETON AND BAES, 1970)
C
        DATA (A(I),I=1,4)/-26876.,-11733.,4615.,9045./
        DATA (B(I),I=1,4)/9.81,3.35,0.,0./
        DATA (D(I),I=1,4)/-81.21,-42.72,-23.57,-49.37/
C
C      UNIVERSAL GAS CONSTANT  AND MOLECULAR WEIGHT OF VARIOUS
C      SPECIES.
C
        DATA R1,R2/1.987,82.05/
        DATA (MFE(I),I=1,4)/55.847,72.854,89.862,106.869/
C
C      ATOMIC VOLUME OF VARIOUS SPECIES
C
        DATA (V(I),I=1,6)/270.32,281.42,292.52,303.62,14.3,11.496/
C
C
C     VARIABLES SPECIFIC FOR EACH CASE
C
C      THE SPECIFICS FOR EACH CASE INCLUDE: FACTOR=A CONSTANT
C      USED IN THE CALCULATION OF HYDROGEN CONCENTRATION IN THE
C      BULK OF THE WATER (H2INF=H2SAT/FACTOR), NCASE=NUMBER
C      OF CASES, ITMAX= MAXIMUM NUMBER OF ITERATIONS, DLT=OXIDE
C      LAYER THICKNESS, THETA=POROSITY, ERR=ERROR ALLOWED IN THE
C      CONVERGENCE CRITERION, F=FRACTION OF OXIDIZED MATERIAL
C      THAT BECOMES MAGNETITE AT THE OXIDE-METAL INTERFACE,
C      WEAR=WEAR RATE, OTHER VARIABLES ARE SELF EXPLAINED.
C
        DATA M/4/
        READ (5,101) FACTOR
101     FORMAT(E10.4)
        WRITE(6,102)FACTOR
102     FORMAT(//,3X,'FACTOR = ',E10.4)
        READ (5,103) EX
103     FORMAT (F6.2)
```

```
      READ (5,631) NCASE,ITMAX,DLT,THETA,ERR,F
      WRITE(6,520) THETA,DLT,F
C
C
      DO 2000 N=1,NCASE
C
      READ(5,645)WEAR(N)
      WRITE(6,645)WEAR(N)
      READ(5,630) T(N),PH2SAT,PH,MU,RHO,D1,D2,U
C
C   CALCULATION OF KW(CWATER) THE EUILIBRIUM CONSTANT
C   OF WATER (IT SHOULD HAVE BEEN A FUNCTION OF
C   TEMPERATURE, HERE IT HAS ONLY BEEN CONSIDERED
C   AN AVERAGE VALUE)
C
      CWATER=1.94E-12
C
C     TEMPERATURE IN DEGREES KELVIN
C
        TK=((T(N)-32.)*5./9.)+273.
C
        ITK(N)=1./TK
C
C     CALCULATION OF EQUIVALENT DIAMETER AND REYNOLDS NO.
C
C
        DEQ=((D2**2.)-(D1**2.))/D1
        NU=MU/RHO
        RE=U*DEQ*3600./NU

C
C
C
C     CALCULATION OF H2 DIFFUSION AND MASS TRANSF. COEFS. (EQ.42 )
C
C      SUBROUTINE DIFCOR CALCULATES DIFFUSION COEFFIENTS WHILE
C      SUBROUTINE TRACOR CALCULATES MASS TRANSFER COEFFICIENTS.
C
        CALL DIFCOF(T(N),MU,V(5),DH2,DH2S)
        SCH=NU/DH2
        CALL TRACOF(SCH,DEQ,RE,DH2,HDH2)
        RESULTA=(HDH2*DLT+DH2S*THETA)/(HDH2*THETA*DH2S)
        RESULTB=R2*TK*WEAR(N)*(1+.333*F)*1.E-6/(MFE(1)*3600.)
        RESULTC=F*WEAR(N)*R2*TK*1.E-6/(MFE(1)*3600*HDH2*3.)
        PH2=(RESULTA*RESULTB)-RESULTC+PH2SAT/FACTOR
        IF(PH2.GE.PH2SAT) PH2=PH2SAT

C
C      CALCULATION OF H+ CONCENTRATION AT INFINITY
C
        HINF=(10.**(-PH))
        HINF=HINF*CWATER/(10.**(-13.262))
        H=HINF
C
C     CALCULATION OF EQUILIBRIUM CONSTANT K
C
C      EQUILIBRIUM CONSTANT (EQ.54 )
C
       DO 1000 I=1,M
```

```
        K(I)=EXP(((-A(I)/TK)+B(I)*(ALOG(TK)-1.0)+D(I))/RI)
 1000   CONTINUE
C
C
C
C  START ITERATIVE  LOOP FOR H+
C
C
        DO 999 L=1,ITMAX
C
C     CALCULATION OF EQUILIBRIUM CONCENTRATION (EQ.53).
C
C
        FESUM=0.
C
        DO 1010 I=1,M
         FE(I)=(K(I)*(PH2**(1./3.))*(H**(3-I)))/1000.
         FESUM=FESUM+FE(I)
 1010   CONTINUE
C
Ccc
C     CALCULATION OF RATIOS OF INDIVIDUAL CONCENTRATION TO TOTAL
C
        DO 1011 I=1,M
         R(I)=FE(I)/FESUM
 1011   CONTINUE
C
        IF(FESUM.GT.0.) GO TO 1012
        WRITE(6,498)L,N
C
C
C     CALCULATION OF DIFFUSION COEFFICIENT FOR IRON SPECIES
C
1012    DIAV=0.
        DISAV=0.
        DO 1020 I=1,M
         CALL DIFCOF(T(N),MU,V(I),DI(I),DIS(I))
         DIAV=DIAV+DI(I)*R(I)
         DISAV=DISAV+DIS(I)*R(I)
 1020   CONTINUE
C

C
C
C     CALCULATION OF SCHMIDT NOS. FOR IRON SPECIES
C
        SCH=NU/DIAV
C

C
C
C     CALCULATION OF MASS TRANSFER COEFFICIENT FOR IRON SPECIES
C
        CALL TRACOF(SCH,DEQ,RE,DIAV,HDAV)
C
C
C       CALCULATION OF TERMS FOR THE WEAR EQUATION
C
        TERM1=(1/HDAV+(DLT/DISAV))
        TERM2=THETA*FESUM*1.E6*MFE(1)*3600./WEAR(N)
```

```
C
C
C       CALCULATION OF REACTION RATE CONSTANT KO
C
        KO(N)=1./(TERM2-((1.-F)*TERM1))
C
C
CC
C
C   CALCULATION OF NEW H+ (EQ.43)
C
          TERMX=WEAR(N)*1.E-6/(MFE(1)*3600.*THETA*KO(N))
          CO=FESUM-TERMX
          OHA=CWATER/HINF
          HC=HINF-2.*CO
          TERMA=HC+OHA
          TERMB=4*(HC*OHA-CWATER)
          X=(-TERMA+SQRT(TERMA**2.-TERMB))/2.
          HF=HC+X
C
C   CONVERGENCE CRITERION
C
          ER1=(ABS(HF-H))/H
          IF(ER1.LE.ERR) GO TO 998
          H=HF
999       CONTINUE
C
998       IF(KO(N).LE.0.)GO TO 997
C
C   CALCULATION OF LN OF REACTION RATE CONSTANT
C
          K1(N)=ALOG(KO(N))
C
C     WRITING STATEMENTS
C
C      CONDITIONS
C
997       WRITE(6.620) T(N),U,HINF,PH2SAT,RHO,MU,L
C
C      EQUIVALENT DIAMETER
C
          WRITE (6,560)
          WRITE (6,610) DEQ
C
C      RYNOLDS NUMBER
C
          WRITE (6,545)
          WRITE (6,610) RE
C
C      EQUILIBRIUM CONSTANTS
C
         WRITE (6,590)
         WRITE (6,600) (K(I),I=1,M)
C
C      EQUILIBRIUM CONCENTRATION
C
         WRITE (6,580)
         WRITE (6,600) (FE(I),I=1,M)
         WRITE(6,610) FESUM
C
```

```
C       CONCENTRATION PERCENTAGE OF EACH SPECIES
C
        WRITE (6,614)
        WRITE (6,600) (R(I),I=1,M)
C
C       DIFFUSION COEFFICIENT FOR EACH SPECIES
C       AND AVERAGE DIFFUSION COEFFICENT
C
        WRITE (6,570)
C       WRITE (6,600) (DI(I),I=1,M)
        WRITE (6,610) DISAV
C
C      SCHMIDT NO. AND MASS TRANSFER COEF. OF IRON
C      SPECIES
C
C       WRITE (6,550)
C       WRITE (6,610) SCH
        WRITE (6,540)
        WRITE (6,610) HDAV
        WRITE (6,616) HF,PH2
        WRITE (6,499) RESULTA,RESULTB,CO
2000    CONTINUE
CC
C
C     LEAST SQUARE CALCULATION OF THE SLOPE AND Y-INTERCEPT
C     OF DATA POINTS IN A PLOT LN KO VS. 1/T
C
        WRITE(6,506)
C
        SX=0.
        SY=0.
        SXX=0.
        SXY=0.
C
        DO 4000 N=1,NCASE
C
        WRITE(6,505)N,T(N),KO(N),ITK(N),K1(N)
C
 4000   CONTINUE
C
C
        Read (5, 200) NSLOPE
200     FORMAT (I3)
        IN=NSLOPE-1
        DO 4001 N=IN,NCASE
        write(6,850)itk(n),K1(N)
850        format (e10.4,3X,E10.4)
        SX=SX+ITK(N)
        SY=SY+K1(N)
        SXY=SXY+(K1(N)*ITK(N))
        SXX=SXX+(ITK(N)**2.)
 4001   CONTINUE
        NCASN=NCASE-NSLOPE+2
        TERM3=NCASN*SXX-(SX**2)
        SLOPE=(NCASN*SXY-(SX*SY))/TERM3
        YINT=(SY*SXX-(SXY*SX))/TERM3
        E1=(-SLOPE)*1.98
        A11=EXP(YINT)
        WRITE(6,503)SLOPE,YINT,E1,A11
C
```

```
C      FORMATS
C
C
  645   FORMAT (F9.4)
  640   FORMAT (//,3X,'WEAR RATES;',2X,E10.5,2X,'G/CM2*H',3X,E10.5,
        12X,'MM/Y')
  631   FORMAT (2I3,3F9.6,F5.1)
  630   FORMAT (8F9.5)
  620   FORMAT (//,3X,'THIS CASE IS FOR: T= ',F10.4,' F',3X,'U= ',F10.4,
        1'FT/S',3X,'H+=',E10.4,/,3X,'WHERE THE VALUE OF PH2S, RHO, AND MU
        2 ARE RESPECTIVELY:',/,2X,F10.8,' ATM',3X,F10.4,' LB/FT3',3X,F10.
        34,'LB/FT*HR',2X,I3)
  616   FORMAT (//,3X,' THE HYDROGEN ION CONCENTRATION IS: ',E15.4,2X,
        1'MOL/CM3',/,3X,' THE HYDROGEN PRESSURE IS: ',E15.4,2X,'ATM')
  615   FORMAT (/,3X,4(E15.4,2X))
  614   FORMAT (/,3X,'RATIOS OF EACH SPECIES CONCENTRATION TO
        1 TOTAL:')
  610   FORMAT (3X,E15.4)
  600   FORMAT (3X,4E15.4)
  590   FORMAT (//,23H EQUILIBRIUM CONSTANTS:)
  580   FORMAT (/'IRON SPECIES CONCENTRATION AT EQUILIBRIUM (MOL/CM3:')
  570   FORMAT (//,33H DIFFUSION COEFFICIENT (CM**2/S):)
  560   FORMAT (//,'    EQUIVALENT DIAMETER (FT):')
  550   FORMAT (//,'    SCHMIDT NUMBER:')
  545   FORMAT (//,'    REYNOLDS NUMBER:')
  540   FORMAT (//,'    AVERAGE MASS TRANSFER COEFFICIENT (CM/S): ')
  530   FORMAT (//,'    RATIO OF THE TOTAL MASS REMOVE TO IRON MASSES
        1 REMOVED:',E15.4)
  520   FORMAT (//,'    POROSITY=',E15.4,2X,'DLT= ',E15.4,2X,'F= ',F5.2)
  510   FORMAT (//,'    TERM1 = ',E15.4,3X,'TERM2 = ',E15.4)
  508   FORMAT (///,'   RESULT = ',E15.4)
  506   FORMAT (//,4X,'N',7X,'T',9X,'KO',7X,'ITK',7X,'K1',//)
  505   FORMAT (/,3X,I3,1X,4(E10.4,1X))
  504   FORMAT (//,3X,'CO= ',E15.4,'MOLS/CM3')
  503   FORMAT(//,3X,'SLOPE = ',E15.4,2X,'YINT = ',E15.4,/,3X,'E1 = ',
     1  E10.4,2X,'A11 = ',E10.4)
  502   FORMAT (//,3X,'FOR THIS CONDITIONS NO CONVERGENCE',2X,2F5.3)
  501   FORMAT (2E10.4)
  499   FORMAT (6E10.4)
  500   FORMAT (//////)
  498   FORMAT (//,3X,'STOP FESUM=0. AND L= ',I3,2X,'N= ',I3)
    1   FORMAT (A40)
C
C
        STOP
        END


        SUBROUTINE DIFCOF(TT,TMU,VV,DIF,DIFS)
C
C
C
C        ***** THIS SUBROUTINE CALCULATES DIFFUSION COEFICENTS *****
C        *****          AT DIFFERENT TEMPERATURES (EQ.  )       *****
C
C
C
        DIF=4.E-7*(TT+459.4)/(TMU*((VV)**(1./3.)-2.))
        DIFS=DIF*0.25806
        RETURN
        END
```

```
      SUBROUTINE TRACOF(TSCH,TDEQ,TRE,DIFF,HCOF)
C
C
C
C     ***** THIS SUBROUTINE CALCULATES MASS TRANSFER *******
C     ***** COEFFICIENTS FROM EQ.51                  *******
C
C
C
      AA=0.86-(10./((4.7+TSCH)**3.))
      C=0.0165+(0.011*TSCH*EXP(-TSCH))
      CONV=30.48/3600.
      HCOF=(CONV*DIFF/TDEQ)*(2.+(C*(TRE**AA)*(TSCH**(1./3.))))
      RETURN
      END
```

```
**********************************************************************
Input data required by the program WEARR4.FOR.  It includes in order
of appearance: FACTOR, EX, NCASE, ITMAX, DLT, THETA, ERR, F, WEAR,
T, PH2SAT, PH (at room temperature), water density, water viscosity,
inside and outside diameters of the annulus, velocity and NSLOPE.
**********************************************************************

  2.0000E3
  0.0
 21 30 0.0001    0.0005  0.10      0.5
   4.27
350.        0.5872    5.6       0.3772  55.56      0.06246  0.06810  9.81
   2.40
350.        0.5872    5.6       0.3772  55.56      0.06254  0.0878   2.01
   6.29
335.        0.6262    5.6       0.3985  56.12      0.0625   0.06810  9.52
   5.01
335.        0.6262    5.6       0.3985  56.12      0.0623   0.08780  1.66
   8.59
320.        0.6652    5.6       0.4060  56.65      0.06275  0.06810  9.61
   5.92
320.        0.6652    5.6       0.4060  56.65      0.06250  0.08780  1.61
   8.98
310.        0.6912    5.6       0.4299  56.96      0.0623   0.06810  8.51
   6.89
310.        0.6912    5.6       0.4299  56.96      0.0622   0.0878   1.69
   6.72
305.        0.705     5.6       0.433   57.1       0.06229  0.06810  9.27
   6.42
305.        0.705     5.6       0.433   57.1       0.0625   0.0878   1.92
   9.42
300.        0.713     5.6       0.4378  57.34      0.06279  0.06810  9.51
   5.79
300.        0.713     5.6       0.4378  57.34      0.06250  0.0878   1.46
   5.85
300.        0.713     5.6       0.4378  57.34      0.0625   0.06810  9.72
   4.57
300.        0.713     5.6       0.4378  57.34      0.0624   0.0878   1.54
   6.6
293.        0.7359    5.6       0.462   57.54      0.0624   0.06810  9.78
   3.32
293.        0.7359    5.6       0.462   57.54      0.0624   0.0878   1.49
   6.5
286.        0.754     5.6       0.480   57.76      0.06266  0.06810 10.14
   3.414
286.        0.754     5.6       0.480   57.76      0.0622   0.08780  1.78
   5.3
270.        0.79      5.6       0.500   58.23      0.0622   0.06810  8.64
   1.63
250.        0.85      5.6       0.5748  58.79      0.0619   0.0878   1.94
   2.577
250.        0.85      5.6       0.5748  58.79      0.0623   0.06810 10.34
  4
```

****

Typical listing of the results of WEARR4.FOR

****

```
  FACTOR = 0.2000E+04

  POROSITY =      0.5000E-03  DLT=      0.1000E-03  F=  0.50
  4.2700

  THIS CASE IS FOR: T=   350.0000 F   U=     9.8100FT/S   H+=0.6908E-04
  WHERE THE VALUE OF PH2S, RHO, AND MU ARE RESPECTIVELY:
 0.58719999 ATM       55.5600 LB/FT3       0.3772LB/FT*HR    1

  EQUIVALENT DIAMETER (FT):
       0.1179E-01

  REYNOLDS NUMBER:
       0.6133E+05

EQUILIBRIUM CONSTANTS:
       0.1849E+07     0.1277E+01     0.4029E-07     0.6499E-15

RON SPECIES CONCENTRATION AT EQUILIBRIUM (MOL/CM3:
       0.1270E-05     0.9846E-08     0.3486E-11     0.6313E-15
       0.1280E-05

  RATIOS OF EACH SPECIES CONCENTRATION TO TOTAL:
       0.9923E+00     0.7692E-02     0.2724E-05     0.4932E-09

DIFFUSION COEFFICIENT (CM**2/S):
       0.4959E-04

  AVERAGE MASS TRANSFER COEFFICIENT (CM/S):
       0.9801E-01

   THE HYDROGEN ION CONCENTRATION IS:      0.8857E-04  MOL/CM3
   THE HYDROGEN PRESSURE IS:      0.6481E-03  ATM

.3882E+030.9141E-060.2595E-06
  2.4000
```

N	T	KO	ITK	K1
1	0.3500E+03	0.4162E-01	0.2224E-02	-.3179E+01
2	0.3500E+03	0.4352E-01	0.2224E-02	-.3135E+01
3	0.3350E+03	0.3394E-01	0.2266E-02	-.3383E+01
4	0.3350E+03	0.9384E-01	0.2266E-02	-.2366E+01
5	0.3200E+03	0.2486E-01	0.2309E-02	-.3694E+01
6	0.3200E+03	0.3507E-01	0.2309E-02	-.3350E+01
7	0.3100E+03	0.1754E-01	0.2339E-02	-.4043E+01
8	0.3100E+03	0.2257E-01	0.2339E-02	-.3791E+01
9	0.3050E+03	0.1115E-01	0.2355E-02	-.4496E+01
10	0.3050E+03	0.1456E-01	0.2355E-02	-.4229E+01
11	0.3000E+03	0.1216E-01	0.2370E-02	-.4410E+01
12	0.3000E+03	0.1107E-01	0.2370E-02	-.4503E+01
13	0.3000E+03	0.8155E-02	0.2370E-02	-.4809E+01
14	0.3000E+03	0.8355E-02	0.2370E-02	-.4785E+01
15	0.2930E+03	0.6824E-02	0.2392E-02	-.4987E+01
16	0.2930E+03	0.4398E-02	0.2392E-02	-.5427E+01
17	0.2860E+03	0.5091E-02	0.2415E-02	-.5280E+01
18	0.2860E+03	0.3265E-02	0.2415E-02	-.5724E+01
19	0.2700E+03	0.2279E-02	0.2468E-02	-.6084E+01
20	0.2500E+03	0.3606E-03	0.2537E-02	-.7928E+01
21	0.2500E+03	0.5332E-03	0.2537E-02	-.7537E+01

.2266E-02 -.3383E+01

.2266E-02 -.2366E+01

```
.2309E-02   -.3694E+01
.2309E-02   -.3350E+01
.2339E-02   -.4043E+01
.2339E-02   -.3791E+01
.2355E-02   -.4496E+01
.2355E-02   -.4229E+01
.2370E-02   -.4410E+01
.2370E-02   -.4503E+01
.2370E-02   -.4809E+01
.2370E-02   -.4785E+01
.2392E-02   -.4987E+01
.2392E-02   -.5427E+01
.2415E-02   -.5280E+01
.2415E-02   -.5724E+01
.2468E-02   -.6084E+01
.2537E-02   -.7928E+01
.2537E-02   -.7537E+01

 SLOPE =     -0.1799E+05  YINT =      0.3800E+02
 E1 = 0.3562E+05  A11 = 0.3184E+17
```

```
C
C
C
C
C       " PROGRAM TO ESTIMATE THE WEAR RATE BY CORROSION-EROSION "
C
C
C         PRELIMINARIES
C
        DIMENSION A(5),B(5),D(5),DI(5),DIS(5),FE(5),R(5),V(10),
       1TERM1(30),TERM2(30),WEAR(30),WEARL(30),T(30),TERM3(30)
        REAL K(5),MFE(5),MU,NU,K0(30),K1(30)
C
C
C         REQUIRED INFORMATION
C
        DATA (A(I),I=1,4)/-26876.,-11733.,4615.,9045./
        DATA (B(I),I=1,4)/9.81,3.35,0.,0./
        DATA (D(I),I=1,4)/-81.21,-42.72,-23.57,-49.37/
C
        DATA R1,R2/1.987,82.05/
        DATA (MFE(I),I=1,4)/55.847,72.854,89.862,106.869/
        DATA (V(I),I=1,6)/270.32,281.42,292.52,303.62,14.3,11.496/
C
C
C         VARIABLES SPECIFIC FOR EACH CASE
C
        DATA M/4/
        READ (5,631) NCASE,ITMAX,DLT,THETA,ERR,DELTT
        READ (5,101) FACTOR,F
101      FORMAT(2E10.4)
        WRITE (6,103) FACTOR,F
103      FORMAT(//,3X,'FACTOR = ',E10.4,2X,'F = ',E10.4)
C

C
        READ (5,630) T(1),PH,U,D1,D2
        READ (5,501) A11,E1
        WRITE (6,503)E1,A11,DLT
C
        DO 2000 N=1,NCASE
C
C
C CALCULATION OF SATURATED CONDITION FOR H2
C
         PH2SAT=0.6
         IF(T(N).LE.335.) PH2SAT=0.66
         IF(T(N).LE.310.) PH2SAT=0.7
         IF(T(N).LE.295.) PH2SAT=0.75
         IF(T(N).LE.270.) PH2SAT=0.8
         IF(T(N).LE.255.) PH2SAT=0.85
C
C        TEMPERATURE IN DEGREES KELVIN
```

```
C
          TK=((T(N)-32.)*5./9.)+273.
C
C CALCULATION OF DENSITY

C
          IF(T(N).LE.370.)RHO=55.56
          IF(T(N).LE.340.)RHO=56.12
          IF(T(N).LE.315.)RHO=56.96
          IF(T(N).LE.295.)RHO=57.50
          IF(T(N).LE.275.)RHO=58.23
          IF(T(N).LE.255.)RHO=58.79
C
C CALCULATION OF VISCOSITY
C
          IF(T(N).LE.370.)MU=0.3772
          IF(T(N).LE.340.)MU=0.3985
          IF(T(N).LE.315.)MU=0.434
          IF(T(N).LE.295.)MU=0.462
          IF(T(N).LE.275.)MU=0.5
          IF(T(N).LE.255.)MU=0.5748
C
C
C CALCULATION OF KW (CWATER)
C
        CWATER=1.94E-12
C
C CALCULATION OF EQUIVALENT DIAMETER AND REYNOLDS NO.
C
C
                  DEQ=((D2**2.)-(D1**2.))/D1
          NU=MU/RHO
          RE=U*DEQ*3600./NU

C
C
C
C CALCULATION OF H2 DIFFUSION AND MASS TRANSF. COEFS.
C
C
          CALL DIFCOF(T(N),MU,V(5),DH2,DH2S)
                SCH=NU/DH2
          CALL TRACOF(SCH,DEQ,RE,DH2,HDH2)

C
C  CALCULATION OF H+ DIFFUSION AND MASS TRANSF. COEFS.
C
C
          CALL DIFCOF(T(N),MU,V(6),DHION,DHIONS)
          SCH=NU/DHION
          CALL TRACOF(SCH,DEQ,RE,DHION,HDION)
          RESULT=(10.**(-PH))
          HINF=RESULT*CWATER/(10.**(-13.262))
```

```
C
C CALCULATION OF EQUILIBRIUM CONSTANT K
C
C          EQUILIBRIUM CONSTANT
C
        DO 1000 I=1,M
         K(I)=EXP(((-A(I)/TK)+B(I)*(ALOG(TK)-1.0)+D(I))/R1)
 1000   CONTINUE
C


C
C
C  START LOOP
C
C
        PH2=PH2SAT/FACTOR
        H=HINF
        DO 999 L=1,ITMAX
C
C CALCULATION OF EQUILIBRIUM CONCENTRATION
C
C
        FESUM=0.
C
        DO 1010 I=1,M
         FE(I)=(K(I)*(PH2**(1./3.))*(H**(3-I)))/1000.
         FESUM=FESUM+FE(I)
 1010   CONTINUE
C
Ccc
C CALCULATION OF RATIOS OF INDIVIDUAL CONCENTRATION TO TOTAL
C
    .   DO 1011 I=1,M
         R(I)=FE(I)/FESUM
 1011   CONTINUE
C
        IF(FESUM.GT.0.) GO TO 1012
        WRITE(6,498)L,N
C
C
C CALCULATION OF DIFFUSION COEFFICIENT
C
1012    DIAV=0.
        DISAV=0.
        DO 1020 I=1,M
         CALL DIFCOF(T(N),MU,V(I),DI(I),DIS(I))
         DIAV=DIAV+DI(I)*R(I)
         DISAV=DISAV+DIS(I)*R(I)
 1020   CONTINUE
C

C
C
```

```
C CALCULATION OF SCHMIDT NOS. FOR IRON SPECIES
C
        SCH=NU/DIAV
C

C
C
C CALCULATION OF MASS TRANSFER COEFFICIENTS
C
        CALL TRACOF(SCH,DEQ,RE,DIAV,HDAV)
C
CCALCULATION OF POROSITY
C
        IF(T(N).GE.300.)THETA=(-6.66667E-6)*(T(N)-300.)+.0005
        IF(T(N).GE.355.)THETA=0.0001
CC
C
C
C
C       CALCULATION OF TERMS FOR THE WEAR EQUATION
C
        KO(N)=A11*EXP(-E1/(R1*TK))
        TERM1(N)=3600.*(10.**6.)*MFE(1)*DISAV*THETA*FESUM*KO(N)
        TERM2(N)=KO(N)*DISAV*(1.-F)/HDAV
        TERM3(N)=DISAV+(KO(N)*DLT*(1.-F))
C
C
C CALCULATION OF WEAR RATE
C
        WEAR(N)=TERM1(N)/(TERM2(N)+TERM3(N))
C
C
C CALCULATION OF NEW H2 AND H+ CONCENTRATIONS
C
C
C        NEW H2
C

C CALCULATION OF HYDROGEN PRESSURE
C
C
         RESULTA=(HDH2*DLT+DH2S*THETA)/(HDH2*THETA*DH2S)
         RESULTB=R2*TK*WEAR(N)*(1+.333*F)*1.E-6/(MFE(1)*3600.)
         RESULTC=F*WEAR(N)*R2*TK*1.E-6/(MFE(1)*3600*HDH2*3.)
         PH2F=(RESULTA*RESULTB)-RESULTC+PH2SAT/FACTOR
                 IF(PH2F.GE.PH2SAT) PH2F=PH2SAT

C

C        NEW H+
C
C
         TERMX=WEAR(N)*1.E-6/(MFE(1)*3600.*THETA*KO(N))
         CO=FESUM-TERMX
```

```
          OHA=CWATER/HINF
          HC=HINF-2.*C0
          TERMA=CH+OHA
          TERMB=4*(HC*OHA-CWATER)
          X=(-TERMA+SQRT(TERMA**2.-TERMB))/2.
          HF=HC+X
C
C    CONVERGENCE CRITERION
C
          ER1=(ABS(PH2F-PH2))/PH2
          ER2=(ABS(HF-H))/H
          IF(ER1.GT.ERR) GO TO 998
          IF(ER2.LE.ERR) GO TO 1999
998        PH2=PH2F
          H=HF
999      CONTINUE
C


          WRITE (6,502)ER1,ER2
          GO TO 2000
C
1999     CONTINUE
C
C         WRITING STATEMENTS
C
C   CONDITIONS
C
           WRITE(6,620) T(N),U,HF,PH2F,RHO,MU,L
           WRITE(6,520) THETA
C
C          EQUIVALENT DIAMETER
C
          WRITE (6,560)
          WRITE (6,610) DEQ
C
C         REYNOLDS NUMBER
C
          WRITE (6,545)
          WRITE (6,610) RE
C
C          EQUILIBRIUM CONSTANTS
C
          WRITE (6,590)
          WRITE (6,600) (K(I),I=1,M)
C
C          EQUILIBRIUM CONCENTRATION
C
         WRITE (6,580)
         WRITE (6,600) (FE(I),I=1,M)
         WRITE(6,610) FESUM
C
C   CONCENTRATION PERCENTAGE OF EACH SPECIES
C
```

```
      WRITE (6,614)
      WRITE (6,600) (R(I),I=1,M)
      WRITE (6,570)
C     WRITE (6,600) (DI(I),I=1,M)
      WRITE (6,610) DISAV
C
C      SCHMIDT NO. AND MASS TRANSFER COEF. OF IRON
C      SPECIES
C
C        WRITE (6,550)
C     WRITE (6,610) SCH
      WRITE (6,540)
      WRITE (6,610) HDAV
      WRITE(6,616)HF,PH2
      T(N+1)=T(N)+DELTT
2000  CONTINUE
CC
C


      DO 3000 N=1,NCASE
      WRITE (6,505) N,T(N),WEAR(N)
3000  CONTINUE
C
C


C
C      FORMATS
C
C
  645 FORMAT (F9.4)
  640 FORMAT (//,3X,'WEAR RATES:',2X,E10.5,2X,'G/CM2*H',3X,E10.5,
      12X,'MM/Y')
  631 FORMAT (2I3,3F9.6,F5.1)
  630 FORMAT (3F6.2,2F9.5)
  620 FORMAT (//,3X,'THIS CASE IS FOR: T= ',F10.4,' F',3X,'U= ',F10.4,
      1'FT/S',3X,'H+=',E10.4,/,3X,'WHERE THE VALUE OF PH2S, RHO, AND MU
      2 ARE RESPECTIVELY:',/,2X,F10.8,' ATM',3X,F10.4,' LB/FT3',3X,F10.
      34,'LB/FT*HR',2X,I3)
  616 FORMAT (//,3X,' THE HYDROGEN ION CONCENTRATION IS: ',E15.4,2X,
      1'MOL/CM3',/,3X,' THE HYDROGEN PRESSURE IS: ',E15.4,2X,'ATM')
  615 FORMAT (/,3X,4(E15.4,2X))
  614 FORMAT (/,3X,'RATIOS OF EACH SPECIES CONCENTRATION TO
      1 TOTAL:')
  610 FORMAT (3X,E15.4)
  600 FORMAT (3X,4E15.4)
  590 FORMAT (//,23H EQUILIBRIUM CONSTANTS:)
  580 FORMAT (//,2X,' IRON SPECIES CONCENTRATION AT EQUILIBRIUM
      1  (MOL/CM3)')
  570 FORMAT (//,33H DIFFUSION COEFFICIENT (CM**2/S):)
  560 FORMAT (//,'   EQUIVALENT DIAMETER (FT):')
  550 FORMAT (//,'   SCHMIDT NUMBER:')
  545 FORMAT (//,'   REYNOLDS NUMBER:')
```

```
  560   FORMAT (//,'   EQUIVALENT DIAMETER (FT):')
  550   FORMAT (//,'   SCHMIDT NUMBER:')
  545   FORMAT (//,'   REYNOLDS NUMBER:')
  540   FORMAT (//,'   AVERAGE MASS TRANSFER COEFFICIENT (CM/S): ')
  530   FORMAT (//,'   RATIO OF THE TOTAL MASS REMOVE TO IRON MASSES
        1 REMOVED:',E15.4)
  520   FORMAT (//,'   POROSITY: ',E15.4)
  510   FORMAT (//,'   TERM1 = ',E15.4,3X,'TERM2 = ',E15.4)
  508   FORMAT (///,'  RESULT = ',E15.4)
  505   FORMAT (/,5X,I3,2X,'T= ',F10.6,'WEAR = ',E15.4,3X,'MIGR/C2*H')
  504   FORMAT (//,3X,'CO= ',E15.4,'MOLS/CM3')
  503   FORMAT (//,3X,'E1 = ',E10.4,2X,'A11 = ',E10.4,2X,'DLT = ',
        1  E10.4)
  502   FORMAT (//,3X,'FOR THIS CONDITIONS NO CONVERGENCE',2X,2F5.3)
  501   FORMAT (2E10.4)
  499   FORMAT (6E10.4)
  500   FORMAT (//////)
  498   FORMAT (//,3X,'STOP FESUM=0. AND L= ',I3,2X,'N= ',I3)
1       FORMAT (A40)
C
C
        STOP
        END


        SUBROUTINE DIFCOF(TT,TMU,VV,DIF,DIFS)
C
C
C
C        ***** THIS SUBROUTINE CALCULATES DIFFUSION COEFICENTS *****
C        *****          AT DIFFERENT TEMPERATURES (EQ.  )       *****
C
C
C
        DIF=4.E-7*(TT+459.4)/(TMU*((VV)**(1./3.)-2.))
        DIFS=DIF*0.25806
        RETURN
        END


        SUBROUTINE TRACOF(TSCH,TDEQ,TRE,DIFF,HCOF)
C
C
C
C       ***** THIS SUBROUTINE CALCULATES MASS TRANSFER *******
C       ***** COEFFICIENTS FROM EQ.                    *******
C
C
C
C
        AA=0.86-(10./((4.7+TSCH)**3.))
        C=0.0165+(0.011*TSCH*EXP(-TSCH))
        CONV=30.48/3600.
        HCOF=(CONV*DIFF/TDEQ)*(2.+(C*(TRE**AA)*(TSCH**(1./3.))))
        RETURN
```

```
**************************************************************************

Typical listing of the input data for the program CORERO.FOR
The data uses the case of the high velocity specimens and
where the slope was obtained from the least square linear
regression to 19 points.

The data includes in order of appearance: NCASE, ITMAX, DLT, ER1, ER2,
increment in temperature, F, T, PH (at room temperature), V, inside
and outside diameters of annulus, pre-exponential term and activation
energy of the reaction rate constant.

**************************************************************************

 12 20 0.0001   0.0005   0.1      10.0
  2.0000E3  0.5000E0
250.00  5.60  9.63  0.06247  0.06810
 0.3184E17  0.3562E5
```

```
**************************************************************************

 Typical listing of the results of CORERO.FOR for high velocity specimens

**************************************************************************

  FACTOR = 0.2000E+04   F = 0.5000E+00

  E1 = 0.3562E+05  All = 0.3184E+17  DLT = 0.1000E-03

  THIS CASE IS FOR: T=    250.0000 F    U=      9.6300FT/S    H+=0.8862E-04
  WHERE THE VALUE OF PH2S, RHO, AND MU    ARE RESPECTIVELY:
 0.00075800 ATM       58.7900 LB/FT3        0.5748LB/FT*HR     2

  POROSITY:       0.5000E-03

  EQUIVALENT DIAMETER (FT):
       0.1177E-01

  REYNOLDS NUMBER:
       0.4172E+05

EQUILIBRIUM CONSTANTS:
       0.6595E+08      0.6511E+01      0.1945E-07      0.1560E-15

  IRON SPECIES CONCENTRATION AT EQUILIBRIUM      (MOL/CM3)
       0.4695E-04      0.5148E-07      0.1734E-11      0.1568E-15
       0.4700E-04

  RATIOS OF EACH SPECIES CONCENTRATION TO    TOTAL:
       0.9989E+00      0.1095E-02      0.3689E-07      0.3335E-11

DIFFUSION COEFFICIENT (CM**2/S):
       0.2853E-04

  AVERAGE MASS TRANSFER COEFFICIENT (CM/S):
       0.5517E-01

   THE HYDROGEN ION CONCENTRATION IS:       0.8862E-04  MOL/CM3
   THE HYDROGEN PRESSURE IS:        0.7083E-03  ATM
```

1	T= 250.000000WEAR =	0.2633E+01	MIGR/C2*H
2	T= 260.000000WEAR =	0.3272E+01	MIGR/C2*H
3	T= 270.000000WEAR =	0.4302E+01	MIGR/C2*H
4	T= 280.000000WEAR =	0.5340E+01	MIGR/C2*H
5	T= 290.000000WEAR =	0.6710E+01	MIGR/C2*H
6	T= 300.000000WEAR =	0.8117E+01	MIGR/C2*H
7	T= 310.000000WEAR =	0.8439E+01	MIGR/C2*H
8	T= 320.000000WEAR =	0.8159E+01	MIGR/C2*H
9	T= 330.000000WEAR =	0.7347E+01	MIGR/C2*H
10	T= 340.000000WEAR =	0.5825E+01	MIGR/C2*H
11	T= 350.000000WEAR =	0.4089E+01	MIGR/C2*H
12	T= 360.000000WEAR =	0.2216E+01	MIGR/C2*H

```
**************************************************************************

  Typical listing of the results of CORERO.FOR for low velocity specimens

**************************************************************************

  FACTOR = 0.2000E+04  F = 0.5000E+00

  E1 = 0.3562E+05  A11 = 0.3184E+17  DLT = 0.1000E-03

  THIS CASE IS FOR: T=   250.0000 F   U=     1.7100FT/S   H+=0.8674E-04
  WHERE THE VALUE OF PH2S, RHO, AND MU   ARE RESPECTIVELY:
 0.0007455? ATM       58.7900 LB/FT3        0.5748LB/FT*HR    2

  POROSITY:       0.5000E-03

  EQUIVALENT DIAMETER (FT):
       0.6147E-01

  REYNOLDS NUMBER:
       0.3870E+05

EQUILIBRIUM CONSTANTS:
       0.6695E+08      0.6511E+01      0.1945E-07      0.1560E-15

  IRON SPECIES CONCENTRATION AT EQUILIBRIUM      (MOL/CM3)
       0.4519E-04      0.5050E-07      0.1734E-11      0.1598E-15
       0.4524E-04

  RATIOS OF EACH SPECIES CONCENTRATION TO    TOTAL:
       0.9989E+00      0.1116E-02      0.3832E-07      0.3532E-11

DIFFUSION COEFFICIENT (CM**2/S):
       0.2853E-04

  AVERAGE MASS TRANSFER COEFFICIENT (CM/S):
       0.9901E-02

   THE HYDROGEN ION CONCENTRATION IS:       0.8674E-04  MOL/CM3
   THE HYDROGEN PRESSURE IS:       0.7083E-03  ATM
```

1	T= 250.000000WEAR =	0.2477E+01	MIGR/C2*H
2	T= 260.000000WEAR =	0.3032E+01	MIGR/C2*H
3	T= 270.000000WEAR =	0.3706E+01	MIGR/C2*H
4	T= 280.000000WEAR =	0.4354E+01	MIGR/C2*H
5	T= 290.000000WEAR =	0.5066E+01	MIGR/C2*H
6	T= 300.000000WEAR =	0.5489E+01	MIGR/C2*H
7	T= 310.000000WEAR =	0.4817E+01	MIGR/C2*H
8	T= 320.000000WEAR =	0.3968E+01	MIGR/C2*H
9	T= 330.000000WEAR =	0.2871E+01	MIGR/C2*H
10	T= 340.000000WEAR =	0.1785E+01	MIGR/C2*H
11	T= 350.000000WEAR =	0.1067E+01	MIGR/C2*H
12	T= 360.000000WEAR =	0.4983E+00	MIGR/C2*H